1-22-2024 1:15 PM

Luminescent Group 11 Metal (I) Chalcogen Clusters with a Conjugated Diphosphine Ligand

Kai Yu Jeffrey Li, *Western University*

Supervisor: Corrigan, John F., *The University of Western Ontario*

A thesis submitted in partial fulfillment of the requirements for the Master of Science degree in Chemistry

Abstract

Polynuclear Au (I) complexes exhibit rich photochemical properties and have the potential to find applications as molecular sensors, switches, or energy storage devices. Although dinuclear Au (I) complexes with bridging diphosphines have been extensively examined, most of those reported do not contain rigid-diphosphine ligands.

This thesis examines how the rigid diphosphine, 4,6-*bis*(diphenylphosphino)dibenzofuran (DBFDP) can be incorporated for the controlled assembly of photoluminescent gold (I) metal – chalcogenolate (chalcogenolate = RS^-, RSe^-; R = organic moiety) and gold (I) chalcogenide (chalcogenide = S^{2-}, Se^{2-}) bimetallic complexes. In these studies, the chalcogen reagents $E(SiMe_3)_2$ or $RESiMe_3$ are reacted with the gold coordination complex $[(AuOAc)_2(\mu\text{-dbfdp})]$ to yield $[Au_2E(\mu\text{-dbfdp})]$ and $[(AuER)_2(\mu\text{-dbfdp})]$, respectively, via the formation and elimination of $AcOSiMe_3$. Further reaction of the $[Au_2E(dbfdp)]$ with AuOTf yields higher nuclearity clusters ranging from 4-6, namely $[Au_4(\mu_4\text{-E})(\mu\text{-dbfdp})_2](OTf)_2$ and $[Au_6(\mu_3\text{-E})_2(\mu\text{-dbfdp})_3](OTf)_2$. A common feature among these di-gold complexes is the bridging nature of the DBFDP ligand.

The preparation, characterization, and photophysical properties of several of these and related gold-chalcogen assemblies clusters are presented.

Keywords: metal chalcogenides, metal chalcogenolates, phosphine ligands, luminescence, emission, gold coordination

Summary for Lay Audience

Group 11 coinage metals copper, silver, and gold in combination with group 16 elements, also known as chalcogens, such as oxygen, sulfur, selenium, and tellurium can form assemblies known as “group 11 metal chalcogenolate/chalcogenide clusters”. These clusters often have interesting physical properties such as photoluminescence, referring to the emission of light when excited with light of a higher energy. Phosphorus containing organic compounds (phosphine ligands) can provide stability to these chalcogenolate and chalcogenide clusters as well as introduce an additional method for changing their physical properties (e.g. luminescence). Chalcogenolates (RE^-, R = organic substituent, E = O, S, Se, Te) have the ability to bond these group 11 metals which result in a M-E-R (M = Cu, Ag, Au) interaction. These R groups can be altered to provide kinetic control in the assembly of these compounds. Chalcogenides (E^{2-}) can also be reacted with group 11 coinage metals and generally result in M_2E core with a 2:1 ratio between M and E. Chalcogenides form the core alongside the group 11 metals which, are protected by the mentioned phosphine ligands. These clusters can have potential applications in light emitting materials, optical sensors, and bioimaging.

This thesis focuses on the incorporation of a custom phosphine ligand which has the ability to bridge two metal centres (here, Cu or Au). The incorporation of this phosphine ligand leads to chalcogenide complexes with the number of metal atoms ranging from 2-6. Additionally, different chalcogenolate ligands were also incorporated to study the effect of various R groups (Ph, C_6F_5).

Co-Authorship Statement

The work in this thesis contains contributions from the author as well as Dr. Jalil Assoud, Kenneth Chu, Dr. Tim Goldhawk, Dr. Aruni Pulukkody, Nils Vogeler, and Dr. John F. Corrigan. The contributions are described below.

Chapter 1 was written by the author and edited by Dr. Corrigan.

Chapter 2 reports compounds synthesized by the author. The crystallography experiments as well as structure resolution and refinement were performed with the assistance of Dr. Jalil Assoud, Nils Vogeler, and Dr. Corrigan. Kenneth Chu performed emission and excitation measurements and conducted excitation and emission spectrofluorometer training to collect future measurements of the complexes. Dr. Tim Goldhawk provided energy-dispersive X-ray (EDX) analysis on the complexes. Dr. Aruni Pulukkody provided mass-spectrometry measurements on the synthesized complexes. The chapter was written by the author and edited by Dr. Corrigan.

Chapter 3 reports compounds synthesized by the author. The crystallography experiments as well as structure resolution and refinement were performed with the assistance of Dr. Jalil Assoud, Nils Vogeler and Dr. Corrigan. The emission and excitation measurements were conducted by the author. The chapter was written by the author and edited by Dr. Corrigan.

Chapter 4 provides a conclusion and future outlooks for Chapters 2 and 3. The chapter was written by the author and edited by Dr. Corrigan.

To Grandpa,

李啟裕敬上

Acknowledgements

I would like to first thank the Department of Chemistry at the University of Western Ontario for making the past 3 years of my academic journey unforgettable. I was able to achieve what I have done thanks to the contribution of the staff and faculty in the department, and I am forever indebted.

I am extremely grateful to my supervisor Dr. John F. Corrigan who has taught me to be a better scientist and a better critical thinker. Over the past few years working together, Dr. Corrigan has taught me to think deeper and look beyond the surface. I owe it to him of who I am today. I am also grateful for my colleagues, old and new. Thank you, Nils for being there when the going gets tough, and when I need someone to grill me in terms of knowledge. Thank you, Andy for always bringing laughs to the lab and crazy ideas such as the baby monitor and the glovebox contraption. Thank you, Alex, for always being the rock and the solid one in the lab and being a great listener. Thank you, Ted, for allowing me to grow as a mentor and grow my teaching skills as a teacher in the lab. Thank you, Mansha. Once my mentor, colleague and now a dear friend, for the laughs, the jokes, the discussions and the (semi-) intellectual ideas that you have.

I would like to thank Dr. Kenneth Chu, Dr. Jalil Assoud and Dr. Aruni Pulukkody for helping me out with excitation, emission spectra, X-ray data and mass spec data. Thank you for Dr. Mat Wilans for helping me out with NMR and everyone in the department who has helped me gather data for my thesis.

I want to thank my friends for their help and support along the way of obtaining this degree. I want to extend my warmest thank you to my partner and best friend, Haley Marier for helping me out with everything from my undergrad to being the most supportive partner someone could ask for. To Mansha, thank you for treating me as an older brother. I will never forget the Tim Hortons runs and late-night lab sessions when neither of our chemistry was working. To Zahra, thank you for your constant support and your push of motivation to obtain this degree. To Arad, thank you for

being such a great friend and I'm sure we will continue to grow our collection of matching socks. Without all of you, I would not have been able to do this.

To my family, Mom, Dad, Andrea and my pup Buddy, you guys have been the greatest support system someone can have. From the Uber Eats you've sent me to the meals you've cooked and packed for me; I could not have done this degree without you. I am the luckiest son / brother in the world. Last, thank you to my grandparents. Without them I would not be able to pursue the career and education that I wanted. Although many of you couldn't see me graduate, I know that you are there in spirit with me. This degree is not only mine, but it's ours.

Thank you.

Table of Contents

List of Figures

List of Schemes

List of Tables

List of Compounds

2.1 [(AuOAc)$_2$(μ-dbfdp)]** <u>Same as (3.1)</u>

2.2 [(AuOTF)$_2$(μ-dbfdp)]

2.3 S [(Au$_2$S)(μ-dbfdp)]

2.3 Se [(Au$_2$Se)(μ-dbfdp)]

2.4 S [Au$_4$(μ$_4$-S)(μ-dbfdp)$_2$](OTf$_2$)

2.4 Se [Au$_4$(μ$_4$-Se)(μ-dbfdp)$_2$](OTf$_2$)

2.5 S [Au$_6$(μ$_3$-S)$_2$(μ-dbfdp)$_3$](OTf)$_2$

2.5 Se [Au$_6$(μ$_3$-eS)$_2$(μ-dbfdp)$_3$](OTf)$_2$

3.1 [(AuOAc)$_2$(dbfdp)]** <u>Same as (2.1)</u>

3.2 [(AuSPh)$_2$(dbfdp)]

3.3 [(AuSePh)$_2$(dbfdp)]

3.4 [(AuSC$_6$F$_5$)$_2$(dbfdp)]

3.5 [Cu$_4$(SC$_6$F$_5$)$_4$(dbfdp)$_2$]

List of Abbreviations

Å	Angstrom
μ	Bridging
δ	Chemical shift
κ	Kappa (coordination)
ε	Molar absorptivity coefficient
λ_{em}	Wavelength of emission
λ_{exc}	Wavelength of excitation
λ_{max}	Wavelength maximum
°	Degrees
°C	Degrees Celsius
$°C_{decomp}$	Decomposition temperature
ΔE	Difference in energy
μm	Micrometres
a.u.	Arbitrary units
ATR-IR	Attenuated Total Reflectance Infrared
CC	Cluster centered
DBF	Dibenzofuran
DBFDP	4,6-*bis*(diphenylphosphino)dibenzofuran
DCM	Dichloromethane
DFT	Density functional theory
Dipp	2,6-diisopropylphenyl
dpP	Diphenylphosphine
dppm	*bis*(diphenylphosphino)methane
dppo	1,8-*bis*(diphenylphosphino)octane
dpppt	1,2-*bis*(diphenylphosphino)pentane
E	Chalcogen: S, Se, Te

ER	Chalcogenolate
Et	Ethyl
EtDBP	2,8-diethyl-dibenzofuran
EtDBFDP	2,8-diethyl-(4,6-*bis*(diphenylphosphino))dibenzofuran
equiv.	Equivalents
eV	Electron Volt (-1.6022 x 10^{-19} J)
g	Grams
HOMO	Highest occupied molecular orbital
HSAB	Hard soft acid base
K	Kelvin
LMCT	Ligand to metal charge transfer
LUMO	Lowest unoccupied molecular orbital
Me	Methyl
meV	Millielectron volt
MHz	Megahertz
mL	Milliliter
M	Group 11 metal
MLCT	Metal to ligand charge transfer
(M+X)LCT	Metal + halide to ligand charge transfer
mmol	Millimole
MOAc	Metal acetate
m.p.	Melting point
N_{abs}	Number of photons absorbed
N_{em}	Number of photons emitted
nm	Nanometers
NMR	Nuclear Magnetic Resonance
$^{-}$OAc	Acetate
OLED	Organic Light Emitting Diodes

Ph	Phenyl
PH	Phosphorescence
PLQY	Photoluminescence Quantum Yield
ppm	Parts per million
PR_3	Tertiary phosphine
QY	Quantum Yield
R	Organic group
RT	Room temperature
S_0	Singlet ground state
S_1	Singlet excited state
SOC	Spin orbit coupling
T_1	Triplet excited state
TADF	Thermally activated delayed fluorescence
THF	Tetrahydrofuran
TMEDA	Tetramethylethylenediamine
UV-Vis	Ultraviolet-Visible
$W_{1/2}$	Full width half maximum

Chapter 1

1.0 Introduction

1.1 Group 11 Metal Chalcogen Clusters

Metal chalcogen complexes have been previously researched on account of their wide range of structural, chemical, and physical properties.[1–4] The field of coinage metal (copper, silver and gold) polynuclear (cluster) chemistry with chalcogenides (E^{2-}) and chalcogenolates (RE^{-}) ligands has gained much interest, spurred in part by the ability to control size and functionality of the assemblies by varying organic substituents on the surface. Possible organic moieties that can be added allows for changes in the electronic and steric properties affecting the overall size, shape and electronic structure of the cluster. Such metal chalcogen clusters can be incorporated into organic light emitting diodes due to their easily tunable emission and excitation properties.[5–7]

1.1.1 Group 11 Metal Chalcogenide Clusters (M_2E)

Group 11 metal chalcogenide clusters have a 2:1, M:E ratio core with protective ligands attached at the periphery. Chalcogenides in the clusters can bridge in a μ_2, μ_3, μ_4 or even higher fashion and metal atoms generally follow a linear, trigonal planar or tetrahedral geometry. The bonding modes of the chalcogenide and metal result in a cluster with the metal atoms in the corners of the core bonded to organic ligands and chalcogenides, while metal atoms within the centre of the core can be bridged and stabilized by chalcogenides exclusively, as shown by Fenske, Yam and several others.[1,2,8,9] Such clusters have been demonstrated to have different nuclearities and different dimensions yet with a consistent metal to chalcogen ratio of 2:1.

The solid materials of group 11 metal chalcogenide clusters have been extensively examined on account of their ability to exhibit high ionic and electric conductivity in their solid state[1,2] with rich photophysical properties which can be implemented into application such as medicine, catalysis and electronics.[3,7,8] X-ray crystallography acts as an exceptional method of characterization for these metal (I) chalcogenide clusters and complexes largely due to its usefulness in providing structural and molecular information of these clusters.[10]

Metallophillic interactions are weak attractive forces between metal atoms within a cluster. These metallophilic interactions, weak bonds often regarded as 'secondary bonds', are most often observed with group 11 metal complexes containing univalent d^{10} coinage metals such as Cu (I), Ag (I), and Au (I).[11] A heavily investigated metallophilic interaction is the aurophilic interaction which involves interactions between Au centres at characteristic distances of 2.5-3.5 Å. Compared to Van der Waals forces, these Au (I)···Au (I) interactions are slightly stronger and considered unique due to these coinage metals having a closed shell configuration.[12,13] Due to the linear coordination geometry of the Au atoms, there is an overlap of the d-orbitals which, results in aurophilic interactions (7-12 kcal mol^{-1}).[11] These aurophilic interactions form perpendicular to the linearly coordinated structural moieties – this linear coordination likely provides optimal overlapping of the d-orbitals of the Au (I) centres.[13] The most widely accepted theory for said aurophilic interactions is the relativistic contraction of the valence electrons – an effect which is more pronounced in heavier atoms such as gold.

Argentophilic interactions are less investigated than aurophilic interactions since linear coordination geometry is observed more commonly in Au compounds compared to Ag (I).[11] Argentophilic interactions are presumed to be present when the Ag···Ag distance is shorter than 2.5-3.5 Å with an estimated binding energy of ~5 kcal mol^{-1}.[11,14]

Even less researched are the copper counterparts, the cuprophilic interactions; d^{10} – d^{10} Cu (I) – Cu (I) interactions (up to 4 kcal mol^{-1}) which are weaker than aurophilic and argentophilic interactions and are equivalent to Van der Waals forces.[11,15,16] Due to the relativistic effects being more pronounced in heavier elements such as gold, the tendency for Cu (I) to adopt trigonal planar / tetrahedral geometry, the presence of cuprophilic interactions has been discussed as controversial. The primary method of determining if an interaction is cuprophilic is a short distance between the two Cu (I) centres. The distance of the interaction or bond must be shorter than the sum of the Van der Waals radii of the two Cu (I) atoms (3.92 Å); and commonly observed at a distance of 2.4 A-2.8 Å.[11]

When comparing cuprophilic, argentophilic and aurophilic interactions, all have similar structural characteristics. However, with the cuprophilic and argentophilic interactions, Cu (I) and Ag (I) are more likely to adopt trigonal planar / tetrahedral coordination geometry which result in higher

coordination modes.[11] Copper and silver are also lighter elements which in turn have weaker relativistic effects than gold. As cuprophilic interactions are relatively weak compared to their silver and gold counterparts, it can be difficult to differentiate between other stronger forces such as crystal packing, hydrogen bonding, and $\pi - \pi$ interactions. However, one of the primary methods for determining if there are metallophilic interactions is through single crystal X-ray diffraction.[11]

Copper (I) chalcogenide compounds have recently grown of interest due to their diverse structural chemistry and their useful chemical and physical properties. Various copper (I) chalcogenide clusters have been discovered over the past decade and generally employ a core of Cu_2E (E = S, Se, Te) with supporting ligands at the periphery (usually phosphines, NHCs, CAACs, etc.).[1,2,17–19] Two prime examples of stable copper chalcogenide clusters are $[Cu_{12}S_6(P^nPr_3)_8]$ **(I.I)** and $[Cu_{20}S_{10}(P^nBu^tBu_2)_8]$ **(I.II)** shown in *Figure 1.1a* and *Figure 1.1b.* Both clusters are composed of Cu (I) and S^{2-} with a 2:1 ratio in the core and protective phosphine ligands on the periphery.[17] The phosphine ligands act as protective ligands bonded to copper, while the sulfide is in a μ_4 coordination.[17] The core forms a cubooctohedron, with the copper atoms in the corners exhibiting a trigonal planar geometry bonded to two S^{2-} and a PR_3 ligand, whereas the copper atoms in the middle (copper centres not bonded to a phosphorus centre) exhibit a tetrahedral coordination geometry and each stabilized by two S^{2-} which results in a linear (S-Cu-S angles 171.59(10) ° and 172.46(9) ° in (**I.I)**) coordination geometry.[17] The short copper-copper distances (2.533(2) – 2.950(2) Å) in **I.I** and **I.II** are indicative for the presence of cuprophilic interactions.[17]

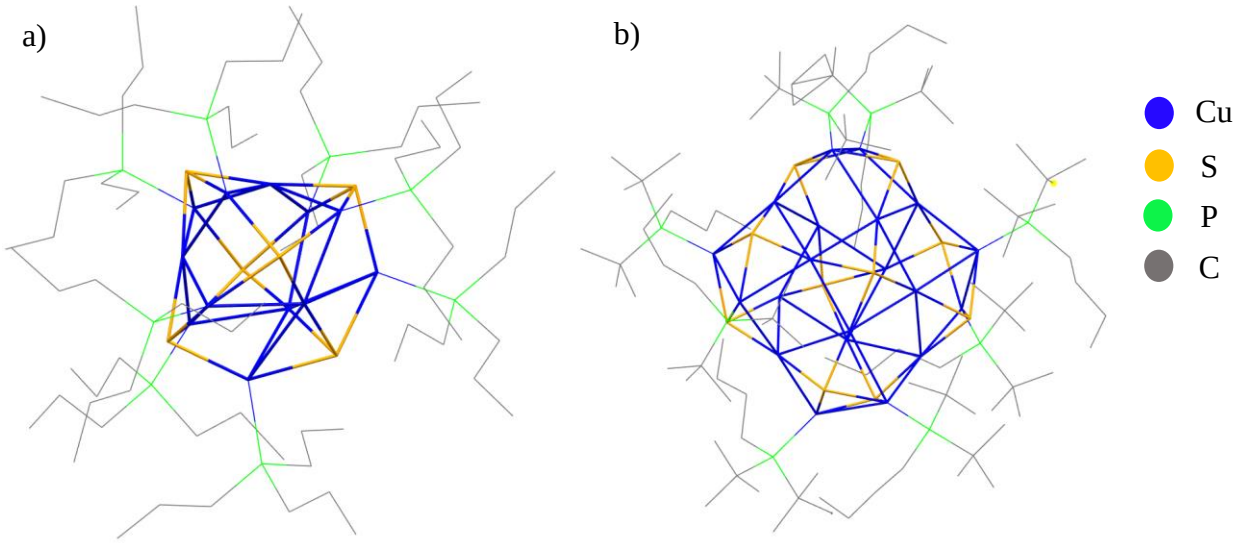

Figure 1.1: (a) Molecular structure of $[Cu_{12}S_6(P^nPr_3)_8]$ ***(I.I)*** *and (b) Molecular structure of* $[Cu_{20}S_{10}(P^nBu^tBu_2)_8]$ ***(I.II)*** *(H atoms are omitted for clarity).*[17]

Two clusters in which act as prime examples of how the chalcogen affects the cluster size and dimensionality are $[Cu_{12}S_6(dppo)_4]$ (**I.III)** (dppo = diphenylphosphineoctane) and its selenium counterpart, $[Cu_{12}Se_6(dppo)_4]$ (**I.IV).**[20,21] Both clusters have a metal to chalcogen ratio of 2:1 (Cu:E; E = S, Se) which conforms to the 2:1 rule mentioned earlier.[20,21] Although isostructural in nature, there are slight geometric differences between the two clusters. The bond lengths for Cu – Se in (**I.IV**) range from 2.295(1) – 2.458(2) Å, whereas the bond lengths for Cu – S in (**I.III**) range from 2.155(1) – 2.3781(9) Å, indicating a larger bond length on average with a larger chalcogen.[20,21]

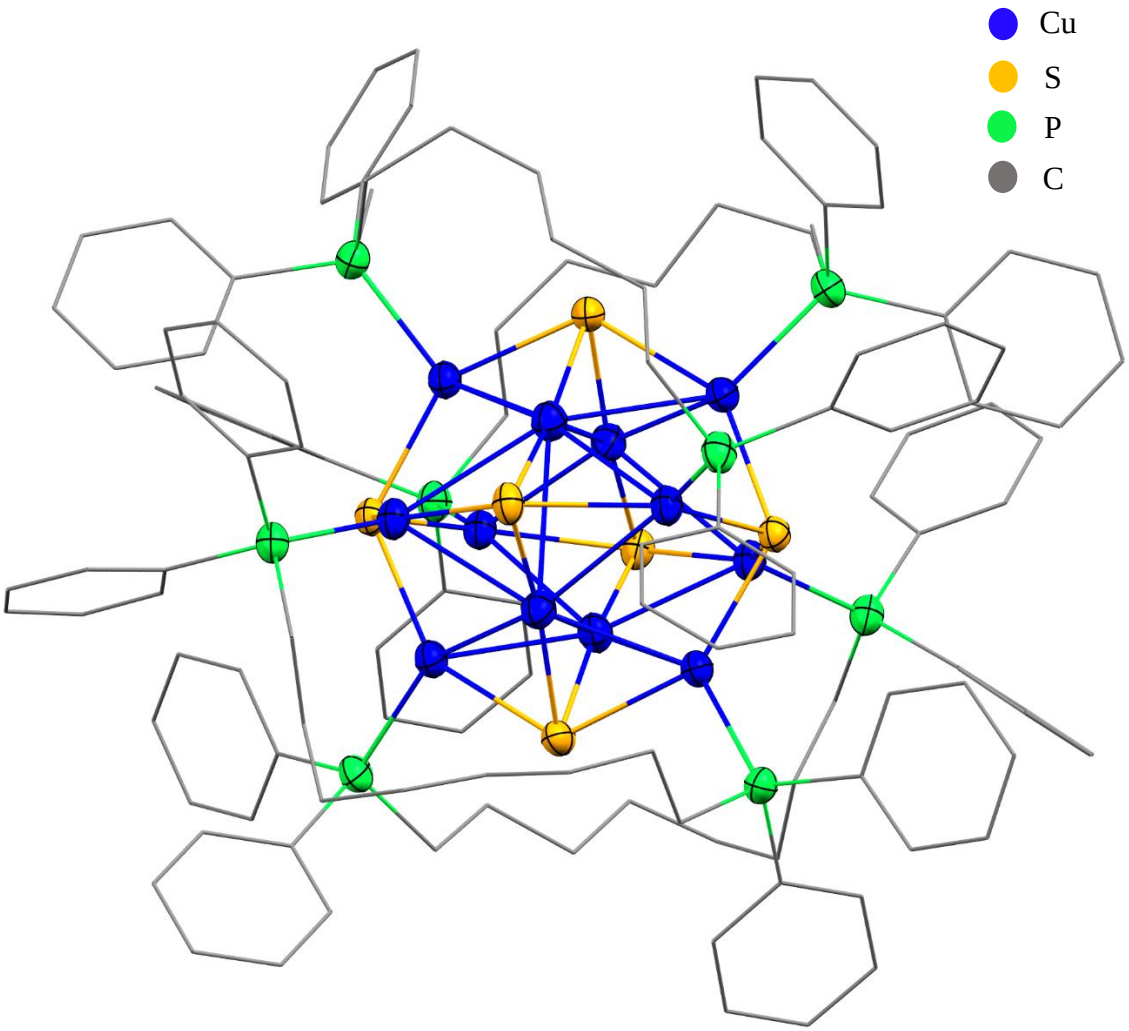

*Figure 1.2: Molecular structure of [$Cu_{12}S_6(dppo)_4$] (**I.III**) (H atoms omitted for clarity).*[20]

Given their difficulty to synthesize and limited thermal and photo- sensitivity, silver chalcogenide clusters are much less discussed and not as extensively researched. There are not many reports on silver chalcogenide clusters with the core consisting of solely Ag and E^{2-} – due to the tendency for these syntheses to run thermodynamically downhill forming the bulk Ag_2E. However, there are many Ag clusters with a mixture of both chalcogenides (E^{2-}) and chalcogenolate (RE^-) periphery protective ligands.[22]

$[Ag_{188}S_{94}(P^nPr_3)_{30}]$ (**I.V**), reported by Fenske and co-workers, acts as a good example for a silver chalcogenide complex which possesses an Ag_2S core.[23] This cluster possesses a unique framework as the Ag (I) is stabilized by S^{2-} with the periphery phosphine ligands protecting the core.[23] Most

silver chalcogenide clusters are core-shell clusters where a $(Ag_2S)_x$ core is protected by silver thiolates and organic periphery ligands such as N-heterocyclic carbenes or phosphines.[10,24] Such core-shell clusters can be highlighted by the $[Ag_{58}S_{13}(SAd)_{32}]$ (SAd = 1-adamantanethiolate) (**I.VI**) reported by Fenske and co-workers and can be seen in *Figure 1.3*.[24] The icosahedral core is neutral and formed from 13 (Ag_2S) subunits and is encapsulated by the shell which is made up of 32 AgSAd. Moreover, within the core, the Ag (I) centres are stabilized by S^{2-} as compared to the Ag (I) which are stabilized by AdS^- moieties. The Ag (I) atoms exhibit different bonding geometries (linear, trigonal planar and tetrahedral) and the sulfide also exhibits different coordination geometries (μ_2 - μ_7).[24] Given the close distance between neighboring silver atoms, the presence of argentophilic interactions is suggested.[24]

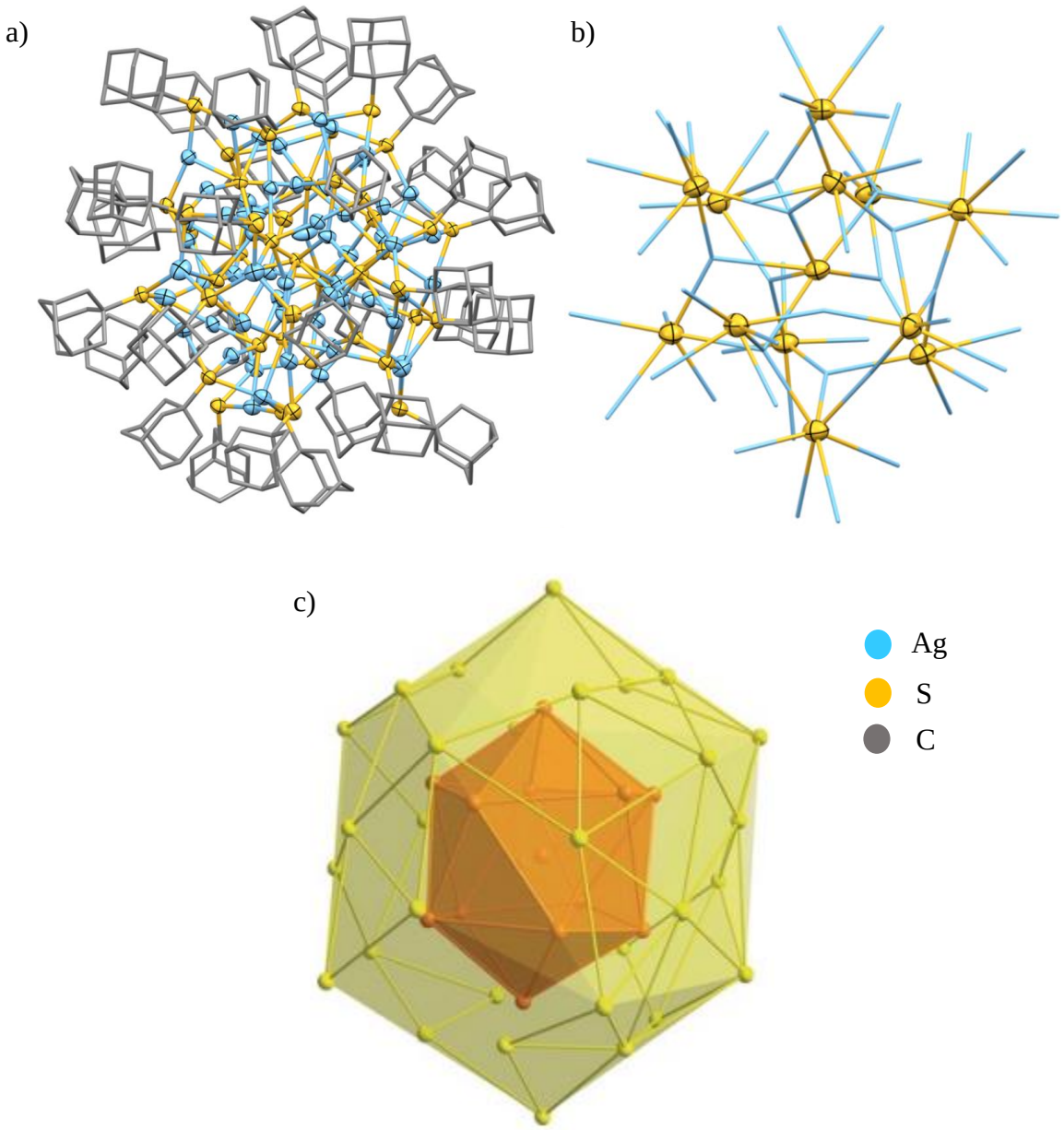

*Figure 1.3: (a) Molecular structure of $[Ag_{58}S_{13}(SAd)_{32}]$ (**I.VI**) (b) $(Ag_2S)_{13}$ core (only core sulfide atoms are included for clarity) (c) S_{13} distorted icosahedral core made of S^{2-} surrounded by 32 thiolate ligands. Lines between S atoms are non-bonding and only indicate geometric arrangement (H atoms omitted for clarity) (figure adapted from literature).*[24]

Gold (I) chalcogenide clusters have been extensively developed due to their luminescent properties and their known ability to form aurophilic interactions.[12,13] Gold chalcogenide clusters are different than the silver and copper counterparts as these clusters are generally formed by multiple [$Au_3(\mu_3$-

S)]$^{+}$ subunits.[25–28] This can lead to many of the formed clusters being charged requiring one or multiple anions as a counterion. $[Au_{18}(\mu\text{-dpepp})_6(\mu_3\text{-S})_6]^{6+}$ (depepp = *bis*(2-diphenylphosphinoethyl)phenylphosphine) **(I.VII)** acts as a good example of a complex cation of a gold (I) chalcogenide complex that clearly highlights these $Au_3(\mu_3\text{-S})$ subunits.[26] The sulfide bridges three Au (I) centres with each Au (I) connected to the phosphine ligand. There are clear indications of aurophilic interactions which form the supramolecular 'macrocycle' and can be seen in *Figure 1.4a* and *b*.

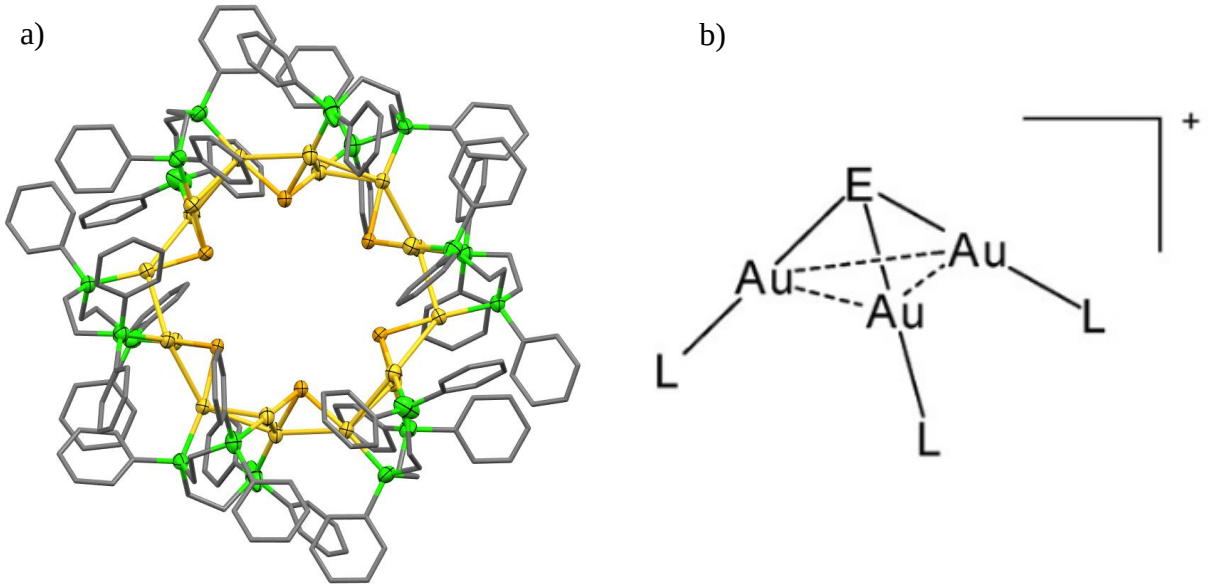

Figure 1.4: (a) Supramolecular structure of $[Au_{18}(\mu\text{-dpepp})_6(\mu_3\text{-S})_6]^{6+}$ cation. ***(I.VII)*** *(A water molecule sitting inside the cavity has been omitted for clarity) (b) $Au_3(\mu_3\text{-S})$ subunit of $[Au_{18}(\mu\text{-dpepp})_6(\mu_3\text{-S})_6]^{6+}$ (six subunits come together to form the supramolecular structure by aurophilic interactions (figure adapted from literature).*[26]

1.1.2 Group 11 Metal Chalcogenolate Clusters (M-ER)

Group 11 metal chalcogenolate complexes have been extensively studied and explored and were shown to form clusters with different nuclearities and dimensionalities. Cu, Ag, and Au have been shown to form these clusters with protective μ_2, μ_3, or μ_4 bridging chalcogenolate and organic ligands bonded to the metal centre. Higher nuclearity coinage metal clusters can exhibit indications of metallophilic interactions ultimately reducing vibrations within the cluster reducing energy loss

through vibrations. This factor is important in the stability of the cluster as well as playing a role in photoemission.

There have been extensive studies on coinage metal (Cu, Ag, Au) coordination clusters in combination with chalcogenolates. These clusters are commonly highly modifiable in terms of the dimensionality of their structure and functionality of the organic moiety (on the chalcogenolate). This ultimately changes the electronic properties of the material.[5,6] The metal-chalcogen bond is favoured due to the soft base-soft acid interaction between these atoms. By adding organic moieties of different sizes on the chalcogenolate (M-ER; M = Cu, Ag, Au, R = organic substituent) and taking advantage of this favourability of the M-ER bond, metal clusters of different dimensionalities can be achieved.[5,6] These chalcogenolate complexes generally have a centre composed of M (I) and RE^- which results in $(ME)_x$ at the centre and the R group bound to the chalcogen. Due to the instability of these cluster cores and their tendencies to form the bulk M_2E, peripheral organic ligands are generally bound to the metal (phosphines, NHCs etc.). Chalcogenolates (RE^-, E = S, Se) have been observed to coordinate in different modes with group 11 metals, which results in differences in structure and photophysical properties.[6,29]

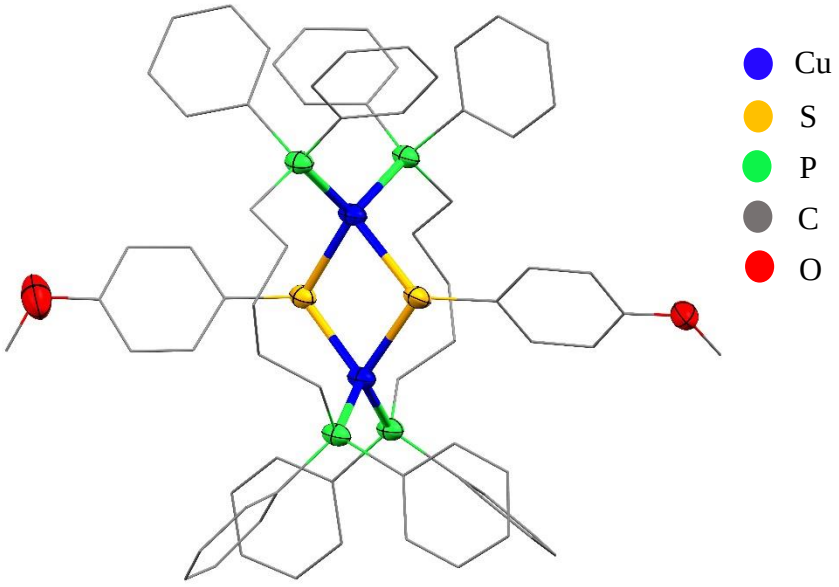

Figure 1.5: Molecular structure of $[Cu_2(\mu_2\text{-}S\text{-}C_6H_4\text{-}OMe)_2(dpppt)_2]$ ***(I.VIII)*** *(H atoms are omitted for clarity).*[6]

[$Cu_2(\mu_2\text{-}S\text{-}C_6H_4\text{-}OMe)_2(dpppt)_2$] (dppt = diphenylphosphinopentane) (**I.VIII**) and [$Cu_7(p\text{-}S\text{-}C_6H_4\text{-}NMe_2)_7(PPh_3)_4$] (**I.IX**) both act as good examples of copper thiolate clusters that highlight the differences in dimensions and nuclearity size in copper thiolate clusters, and were both reported by Fuhr and co-workers.[6,29] As seen in *Figure 1.5*, (**I.VIII)** is a binuclear copper compound with a copper-thiolate core, with organic moieties attached to the chalcogen present at the periphery and protective phosphine ligands.[6] Both copper atoms (**I.VIII)** assume a tetrahedral geometry and are bound to two thiolates, where both adopt a μ_2 coordination mode, and two phosphines.[6] In (**I.IX**) which can be seen in *Figure 1.6*, three Cu centres have a trigonal planar geometry, being bound to three thiolate ligands, with the remaining having a tetrahedral geometry being additionally bound to a phosphine ligand as well.[29] As seen with previous clusters, (**I.IX**) demonstrates evidence of cuprophilic interactions as shown with the short distances between copper atoms.[29]

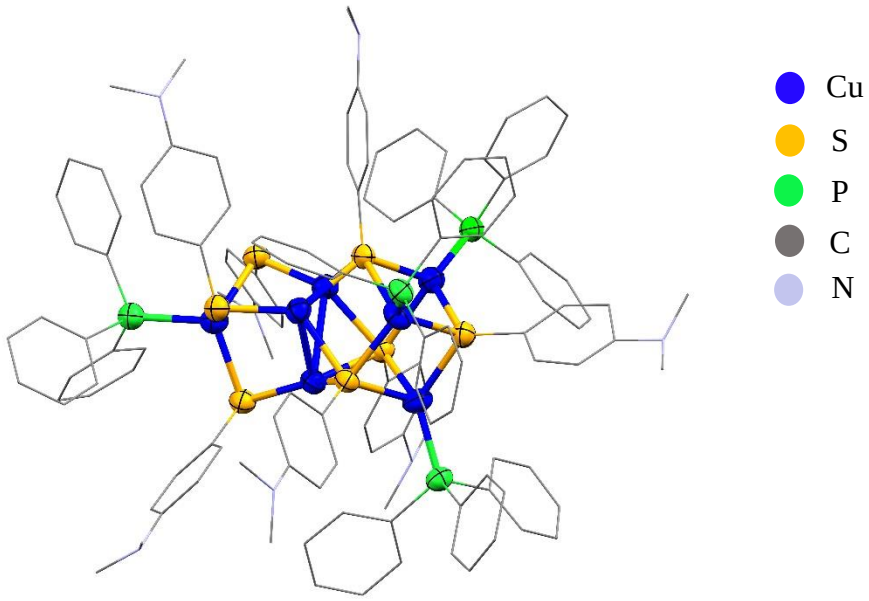

*Figure 1.6: Molecular structure of [$Cu_7(p\text{-}S\text{-}C_6H_4\text{-}NMe_2)_7(PPh_3)_4$] **(I.IX)** (H atoms are omitted for clarity).*[29]

Silver chalcogenolate clusters demonstrate interesting emission properties as well as a wide range of structural diversity.[30] However, silver chalcogen complexes are often unstable under light and moisture, which causes decomposition, and acts as a hurdle for in depth analysis on such

clusters.[31,32] $[Ag_{12}(SCH_2C_6H_5)_6(CF_3COO)_6(pyridine)_6]$ (**I.X**), as seen in *Figure 1.7*, is an example of a stable silver chalcogenolate cluster, which has silver atoms bridged by μ_4 thiolates resulting in a Ag_{12} cuboctahedron.[33] This cluster contains both tetrahedral and trigonal planar coordinated Ag (I) atoms – this molecule contains two thiolates and a pyridine or CF_3COO^- bonded to Ag (I) whereas the distorted tetrahedral arise from a bridging CF_3COO^-.[33] The presence of argentophilic interactions can be assumed in this cluster due to the close proximity of Ag (I) centres with distances ranging from 2.935(1) Å to 3.218(2) Å.[33]

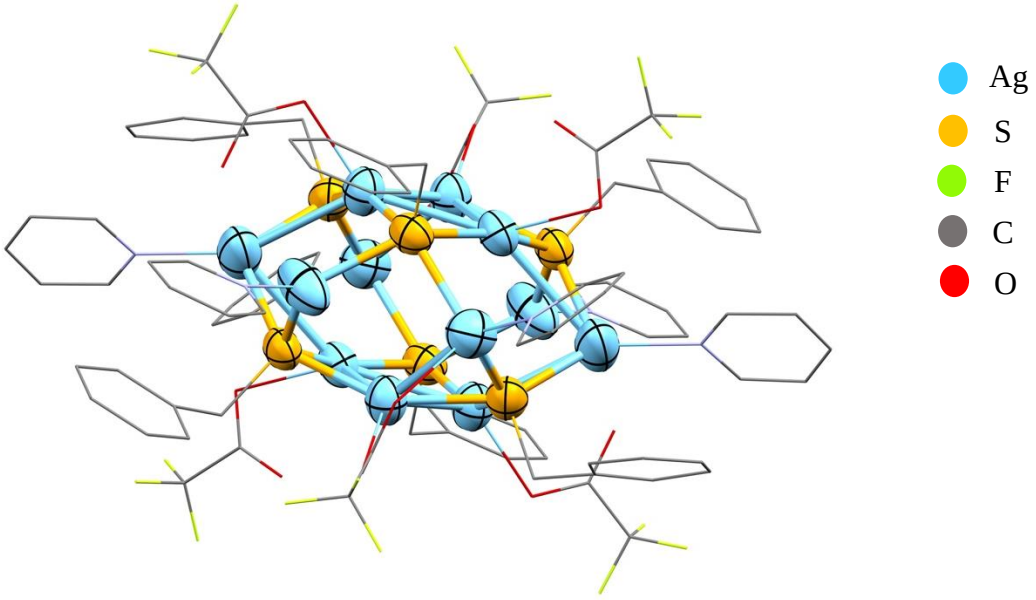

*Figure 1.7: Molecular structure of $[Ag_{12}(SCH_2C_6H_5)_6(CF_3COO)_6(pyridine)_6]$ (**I.X**) (H atoms are omitted for clarity).*[33]

Gold chalcogenolate clusters differ from silver and copper chalcogenolate clusters as Au (I) prefers to exist in a linear coordination geometry.[34] $[\{Au(PMe_3)\}_2(\mu_2\text{-}SMe)]O_3SCF_3$ (**I.XI**) acts as a prime example of a gold (I) thiolate complex where the gold (I) centre has a linear coordination geometry.[35] As seen in *Figure 1.8*, the Au (I) atoms exhibit a linear bonding geometry, as they are bonded to the peripheral phosphine ligand and the CH_3S^- thiolate ligand. With this cluster, two $[Au(PMe_3)(SMe)]$ monomers are associated into centrosymmetrical dimers which are stabilized by aurophilic interactions.[35] Moreover, *Figure 1.7* demonstrates indication of aurophilic interactions are seen with the short bond distance between the Au (I) centres.[35]

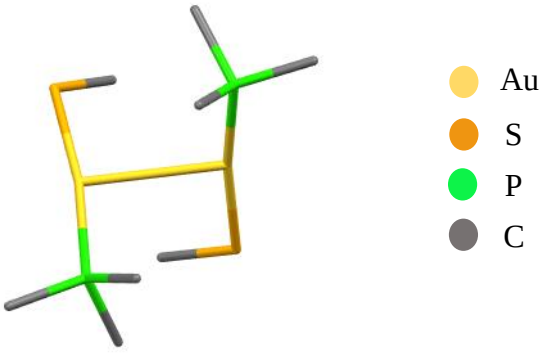

*Figure 1.8: Molecular structure of [{Au(PMe$_3$)}$_2$(μ$_2$-SMe)] (**I.XI**) in the crystal (H atoms and OTf anion are omitted for clarity).*[35]

1.2 Synthesis Methods for Group 11 Metal Chalcogen Clusters

Historically, there have been many ways to synthesize metal chalcogen clusters. The use of H_2S is one of the oldest techniques to synthesize coinage metal sulfide clusters.[36] There are two general synthetic pathways for the use of H_2S: i) it can either be used in a condensation reaction displacing the metal oxide or ii) by bubbling into an aqueous base, which results in sulfide which can then be further reacted with a metal salt to form the metal sulfide complex as highlights in *Scheme 1.1*.[36]

$$H_2S + OH^- \longrightarrow S_n^{2-}$$

$$S_n^{2-} + Cu(OAc)_2{\cdot}H_2O \longrightarrow [Cu_3S_4)_4]^{3-}$$

Scheme 1.1: Synthesis of a copper sulfide complex using deprotonated sulfide (scheme adapted from literature).[36]

However, the selenide and telluride analogues of H_2S are less commonly used due to the tendency to form impure products.[36] Moreover, H_2Te also suffers from disproportionation to H_2 and Te at room temperature rendering it an unsuitable approach.[36] Given these hydrogen chalcogen reagents are highly toxic and lethal, safer ways of incorporating chalcogens into metal clusters have thus been investigated.[36,37] Another method of synthesis is by incorporating alkali metals instead of hydrogen. Yam and co-workers have reported the use of Na_2S in the synthesis of [Cu$_4$(μ-dppm)$_4$(μ$_4$-S)](PF$_6$)$_2$] (dppm = diphenylphopshinomethane) (**I.XII**).[38] A series of Cu (I) and Ag (I) with μ$_4$ chalcogenides were also reported with Li$_2$E.[38]

Similarly, chalcogenol reagents (REH, E = S, Se, Te, R = organic moiety) can be used to synthesize said metal chalcogenolate clusters.[39–42] Generally a weak base such as NEt_3 is added as a proton scavenger to remove the proton from the chalcogenol to form the chalcogenolate.[40,43] Chalcogenols can also be added directly without a base in some cases.[44,45] The addition of the thiolate proceeded under relatively mild conditions and resulted in products with high yields. An example of this is the $[CuSAr^{iPr}{}_4]_2$ (**I.XIII**) which is synthesized by stirring the thiol ($Ar^{iPr}{}_4$ = C_6H_3-2,6-(C_6H_3-2,6-iPr_2)$_2$) with a mesityl copper complex in THF. This can be seen in *Scheme 1.2*.[44]

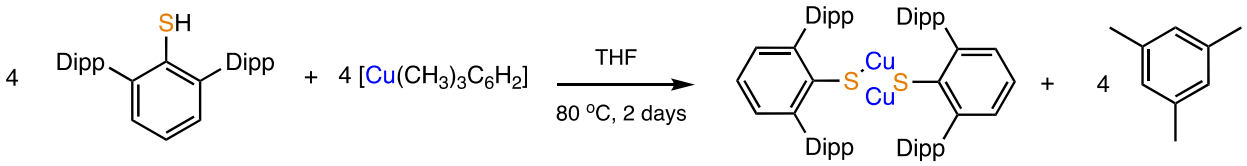

*Scheme 1.2: Reaction scheme for synthesis of $[CuSAr^{i}Pr_4]_2$ (**I.XIII**) (Dipp = -C_6H_3-2,6-(C_6H_3-2,6-$^{i}Pr_2$).*[44]

Given the tendency for chalcogenols to be unstable in air (especially chalcogenols with small R groups), another method for synthesis of these metal chalcogenolate complexes is the reaction with the akali metal chalcogenolate (REA; A = alkali metal: Na, Li), which is initially formed by reactions between an akali metal and the chalcogenol. The alkali metal increases nucleophilic reactivity due to the A-E bond. Yam and co-workers recently discussed the synthesis of $[Cu_3(\mu$-$dppm)_3(\mu_3$-$SC_6H_4CH_3$-4)(μ_3-Cl))]PF_6 (**I.XIV**) using the sodium salt of the thiol.[46]

1.2.1 Silylated Chalcogen Reagents for Synthesis of Group 11 Metal Chalcogen Clusters

Another method of introducing chalcogen to group 11 metals is with the use of trimethylsilyl chalcogen reagents, $E(SiMe_3)_2$ and $RE(SiMe_3)$ where E = S, Se, Te and R = organic substituent.[2,47] Silylated chalcogen reagents are of interest due to their solubility, the inert byproduct they form, and act as an easily handled chalcogen source.[48] Two examples of clusters synthesized using trimethylsilyl protected chalcogen reagents are $[Cu_{12}S_6(dppo)_4]$ (**I.III**)[20] and $[Ag_{188}S_{94}(P^{n}Pr_3)_{30}]$ (**I.V**)[23]. Several metal chalcogenolate clusters were also highlighted using this trimethylsilyl chalcogen reagent synthesis such as $[Cu_2(\mu_2$-S-C_6H_4-OMe)$_2$(dpppt)$_2$] **(I.VIII)**[6] and $[Cu_2(SePh)_2(dpppt)_2]$ (**I.XV**)[6].

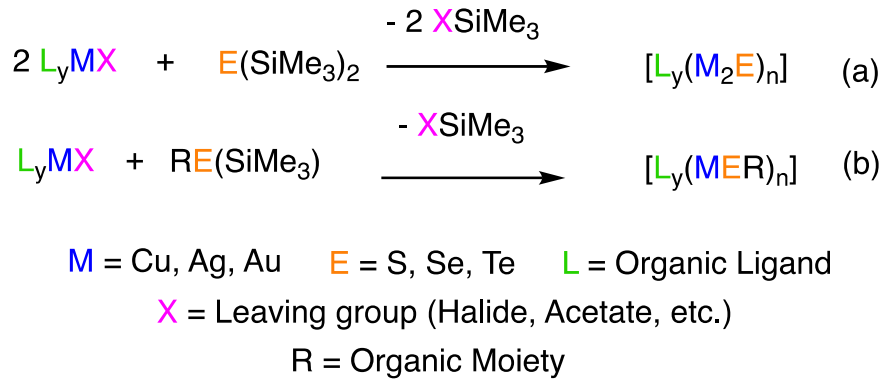

Scheme 1.3: General reaction scheme for synthesis of (a) metal chalcogenide clusters (b) metal chalcogenolate clusters (n = 1,2,3 … y = 1,2,3 …) (Metal bound to ligand in metal salt).[1,9,47–49]

As depicted in *Scheme 1.3*, these chalcogen reagents can readily react with metal salts (MX_n) (X = leaving group = Cl, Br, OAc, OTf, etc.) to form the M-E bond and the silane (X-$SiMe_3$) byproduct.[1,9,47,48] The reactivity of the metal salt with the trimethylsilyl chalcogen reagent depends on the nature of X – the thermodynamic formation of the X-$SiMe_3$ is the driving force behind the reaction thus the reactivity depends largely on the bond strength of the Si-X bond.[1,9,50] The silylated chalcogen reagents are also extremely soluble in common organic solvents, even at cold temperature, and the silane byproduct does not hinder the crystallization of the desired metal cluster.[51]

1.3 Phosphine Stabilized Group 11 Metal Chalcogen Clusters

With d^{10} metal chalcogen clusters, there is a tendency to form the thermodynamic stable product (M_2E), thus requiring the need for a kinetically stabilizing ligand.[1,2,9,50] There are several types of protective ligands, from N-heterocyclic carbenes to the more common monodentate/bidentate phosphines.[1,2,9,52] Several metal chalcogen clusters with phosphine ligands highlight the use of these monodentate/bidentate PR_3 such as $[Ag_{188}S_{94}(P^nPr_3)_{30}]$ (**I.V**)[23], $[Cu_{146}Se_{73}(PPh_3)_{30}]$ (**I.XVI**)[53], $[Cu_2(SePh)_2(PPh_3)_3]$ (**I.XVII**)[1] and $[Ag_7(SPh)_7(dppm)]$ (**I.XVIII**)[23] were reported by Fenske and co-workers. The organic moiety within metal chalcogenolate clusters, meanwhile providing kinetic stability, can also include different functional groups to change structural and electronic properties to fine tune photophysical properties.

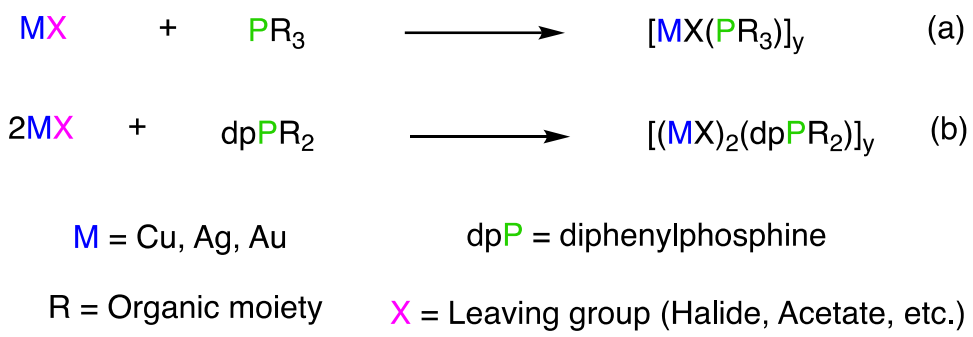

Scheme 1.4: General reaction scheme for the synthesis of phosphine stabilized metal complexes (x = 1,2,3 … y = 1,2,3 …).[2,6,9]

Although the major driving force behind the formation of the metal cluster depends on the formation of the Si-X bond, the phosphine ligand also plays a huge factor in the formation.[1,2,49,51] As shown in *Scheme 1.4*, the metal salt is first stirred with the free phosphine to synthesize the metal complex.[2,9,18] This then acts as an excellent handle/entry point to introduce the chalcogen with the trimethylsilyl protected chalcogen reagent. Generally, the introduction of chalcogen leads to polynuclear metal complexes which have the ability to be incorporated into light emitting applications such as bio-labelling or organic light emitting diodes (OLEDs). This can be attributed to their typically high rigidity from metallophilic interactions which result in high photostability.[20]

1.4 Luminescence, Photoluminescence, Fluorescence, and Phosphorescence

Luminescence is defined as "spontaneous emission of radiation from electrically excited species or from vibronically excited species which are not in thermal equilibrium with the environment".[54] There are multiple ways that luminescence can be classified, and is dependent on the method of excitation. When a photon is emitted after absorption of energy from an electromagnetic radiation source, this optical phenomenon can be classified as photoluminescence.[54] This optical phenomenon arises from the absorption of photons that leads to the excitation of an electron – when the electron relaxes back to ground state, the molecule then emits at a wavelength of light which is inversely proportional to the energy difference between the ground and the excited state.[55] Charge transfers can also happen between ligands attached to the metal core, when one of them is a Lewis base (electron donating) and the other is a Lewis acid (electron accepting). When electrons of the ligand are excited, absorption occurs due to a charge transfer between the ligand to the metal centre – this is referred to as a LMCT (ligand to metal charge transfer).[56] A MLCT (metal to ligand

charge transfer) occurs when the metal is a donor, and the ligand is the acceptor.[56] Such transitions have high molar absorptivity values and can be seen in the visible region.[56]

Excited states for classical transition metal complexes can be categorized into 3 main types. Ligand-field (LF) or d-d states involve promotion of an electron from an occupied d-orbital to an unoccupied orbital. Intraligand transitions (IL) are generally localized within the ligand sphere and involve the promotion of an electron from the π orbital into the antibonding π* of an aromatic system (π-π* transition). Last, charge transfers (CT) involve the movement of an electron from one d-orbital to the π* orbital of a ligand (MLCT; metal-to-ligand charge transfer). Alternatively, transfer of an electron from π orbital to the unoccupied unfilled d orbital (LMCT; ligand-to-metal charge transfer) can also exist. Metal complexes with multiple metals can also experience a charge transfer known as metal-to-metal-ligand charge transfer (MMLCT). Spin orbit coupling is a phenomenon in which the orbit of the electron couples with the orbit of the nucleus, which increases the rate of intersystem crossing (S_n to T_n). This increased rate of intersystem crossing (ISC) can lead to phosphorescence, thus increasing the lifetime of emission. The efficiency of spin orbit coupling increases with larger atomic numbers, with heavy atoms such as Au and Pt.

There are two principal types of photoluminescence – fluorescence and phosphorescence.[57] One of the main differences between fluorescence and phosphorescence is the time for the excited electron to return to the ground state.[58] In fluorescence, the electron is excited from the S_0 ground state into the S_1 excited state and emissions can last from picoseconds to nanoseconds.[54] In phosphorescence, the excited state lifetime is longer lived as the excited state undergoes a spin forbidden transition resulting in a different spin state multiplicity due to intersystem crossing.[55] Intersystem crossing is considered a spin forbidden process which leads to a slower rate for phosphorescence. However, this process can become more probable with a phenomenon known as spin orbit coupling, a relativistic interaction of an electron's spin with the orbital motion around its nucleus. For transition metal complexes, the central metal core can display significant spin orbit coupling and results in efficient intersystem crossing which results in phosphorescence (*Figure 1.8).*[59]

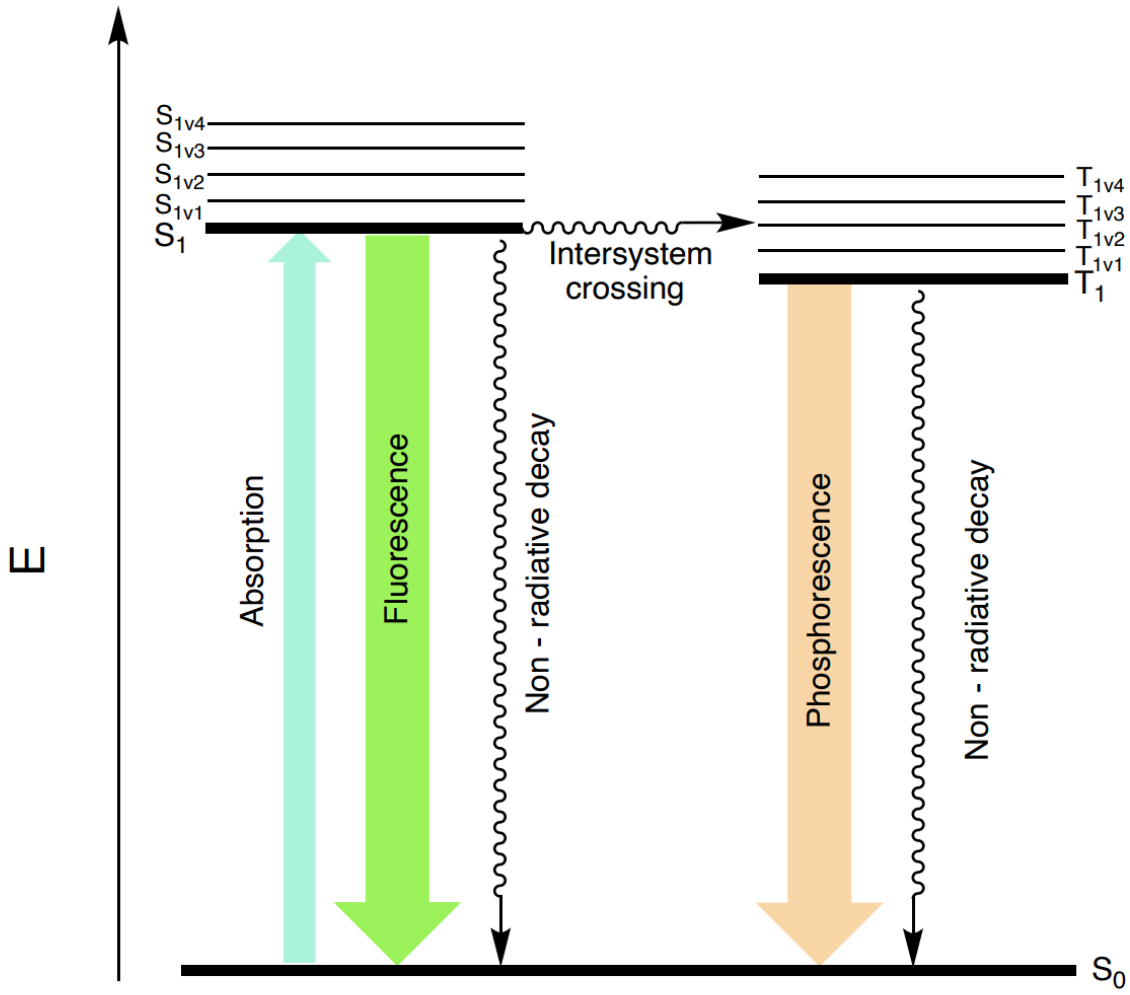

Figure 1.9: Simplified Jablonski diagram depicting differences between fluorescence and phosphorescence. (figure adapted from literature)[59]

Photoluminescent transition metal complexes make suitable candidates for organic light emitting diodes (OLEDs) due to the process of intersystem crossing which enables mechanisms such as thermally activated delayed fluorescence (TADF) and phosphorescence (PH).[59,60] In TADF, thermal energy is used for the excited electron to undergo reverse intersystem crossing back into the singlet state (S_1) due to the small $\Delta E(S1\text{-}T1)$, resulting in efficient light emission which gives rise to adequate photoluminescence quantum yields (PLQYs). In PH, the excited electron undergoes an intersystem crossing and has efficient light emissions from triplet states with high PLQYs.[60] These PLQY values are calculated using the ratio between number of emitted photons

(N_{em}) to the number of absorbed photons (N_{abs}). Thus, the calculation is indicative of whether a material is exhibiting fluorescence or phosphorescence.[61]

1.5 Luminescent Group 11 Metal Chalcogen Complexes Incorporating Phosphine Ligands

Previously, Eichhöfer and co-workers have investigated the use of σ donating phosphine ligands with copper (I) chalcogenide clusters and their effects on modulating the photophysical properties. Several copper chalcogenide clusters were synthesized with different phosphine ligands, however several had similar core structure.[20] It was observed that not only the type of phosphine ligand influences the PLQY, however, the crystal packing also plays a factor.[20] *Figure 1.10* below depicts the general structure of the aforementioned clusters:

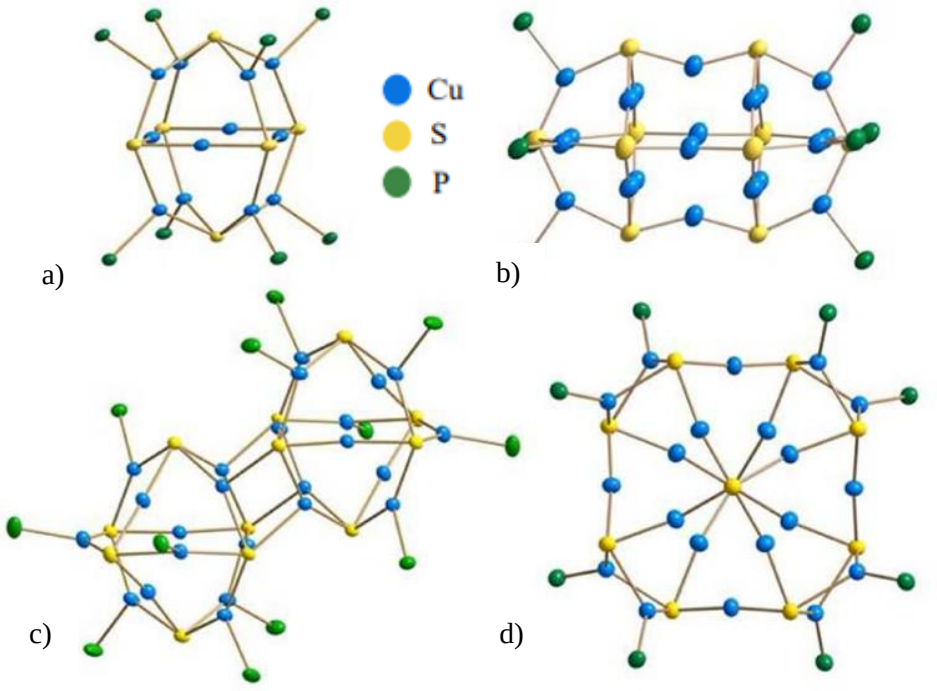

*Figure 1.10: General core structures of copper (I) sulfide clusters with phosphine ligands (a)[$Cu_{12}S_6(dpppt)_4$] **(I.XIX)** (b)[$Cu_{20}S_{10}(PPh_3)_8$] **(I.XX)** (c)[$Cu_{24}S_{12}(PEt_3Ph)_{12}$]**(I.XXI)** (d)[$Cu_{20}S_{10}(P^tBu_3)_8$] **(I.XXII)** (C and H atoms are omitted for clarity).*[20]

For complexes which contained the core $Cu_{12}E_6$ (E = S, Se), a bright red phosphorescent emission was observed at ambient temperature – with high photoluminescent quantum yields between 21 % and 63 %.[20] Surprisingly, with these observations, not only does the type of phosphine ligand affect the PLQYs, but also the crystal packing (triclinic vs. tetragonal) also plays a role.

Due to the highly emissive nature of gold (I) chalcogenide clusters, there has fortunately been much work conducted on gold (I) sulfido clusters. Yam and co-workers have previously discussed the role of a more electron-donating substituent on a ligand and how it would affect the emission characteristics of a gold chalcogenide cluster. Incorporating small differences in the backbone (H, Me, F, CN) of the 1,3-*bis*(diphenylphosphino)benzene ligand (L^{H}, L^{Me}, L^{F}, L^{CN}) can yield formation of different structure of a polynuclear gold (I)-sulfido complexes being [L^{H}-Au_5]Cl (**I.XXIII**), [L^{Me}-Au_5]Cl (**I.XXIV**), [L^{F}-Au_5]Cl (**I.XXV**), [L^{CN}-Au_5]Cl (**I.XXVI**), [L^{F}-Au_{18}] (**I.XXVII**) and [L^{CN}-Au_{18}] (**I.XXVIII**) (L = R-(diphenylphosphino)benzene).[62] Interestingly, the substitution of fluorine and cyanide on the ligand of these clusters would increase the cluster nuclearity to 18 Au (I) atoms by introduction of H_2S gas in dichloromethane-pyridine. At ambient temperatures, as the substitution on the (diphenylphosino)benzene ligand increased in electron-donating character, the emission wavelength would experience a bathochromic shift.[62] *Figure 1.11a* and *b* demonstrate the bathochromic in the emission spectra at ambient temperatures and 77 K.[62]

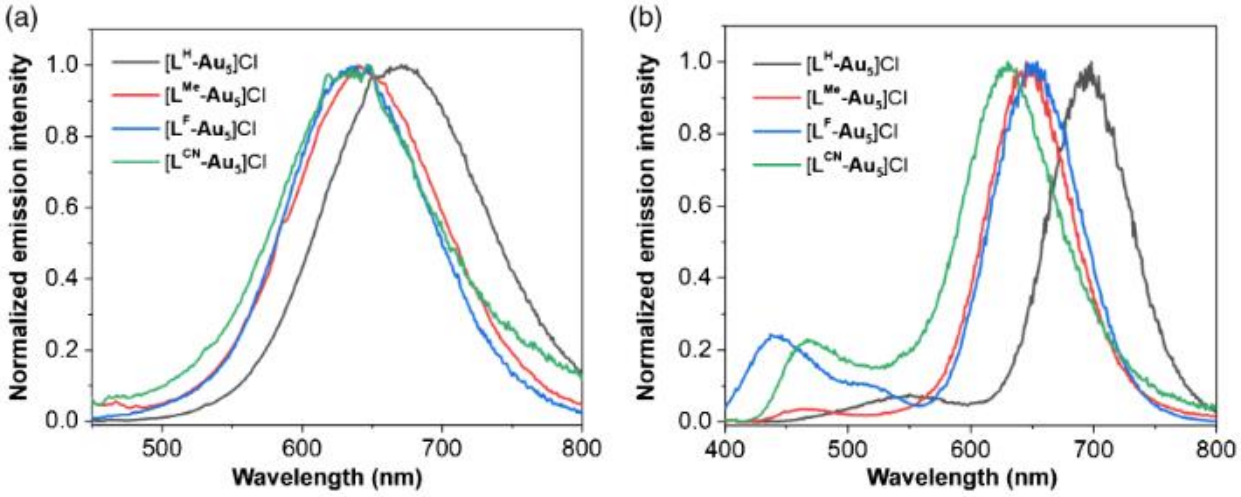

*Figure 1.11: Solid-state emission spectra of [L^{H}-Au_5]Cl (**I.XXIII**), [L^{Me}-Au_5]Cl (**I.XXIV**), [L^{F}-Au_5]Cl (**I.XXV**), [L^{CN}-Au_5]Cl (**I.XXVI**), [L^{F}-Au_{18}] (**I.XXVII**) and [L^{CN}-Au_{18}](**I.XXVIII**) (a) at ambient temperature and (b) low temperature (77K).[62] This figure has been published in CCS Chemistry 2021 ; Substituent-Mediated Transformation of Polynuclear Gold (I)-Sulfido Complexes-From Pentanuclear to Octadecanuclear Cluster-to-Cluster Transformation is available online at [https://doi.org/10.31635/ccschem.021.202000662].*

A good example of a luminescent metal chalcogenolate is $[Cu_2(\mu_2\text{-}S\text{-}C_6H_4\text{-}OMe)_2(dpppt)_2]$ (**I.VIII**) which was previously discussed *(Figure 1.5)* – this cluster displays emissions in the solid state at ambient temperatures (λ_{em} = 465 nm).[6] A good comparison to this cluster is reported by Zhu and co-workers, $[Cu_{13}(SePh)_{13}(PPh_3)_4]$ (**I.XXIX**). This cluster exhibits red luminescence (λ_{em} = 727 nm) in the solid state, which is a stark difference compared to the high energy emission of (**I.VIII**).[63] (**I.XXIX**) does not display high emission intensity at room temperature, however, reducing the temperature to 80 K increases the emission intensity and causes a hypsochromic shift (λ_{em} = 680 nm). Despite their differences, (**I.VIII**) and (**I.XXIX**) show a MLCT where the highest occupied molecular orbital (HOMO) is composed of the metal chalcogenolate core and the lowest unoccupied molecular orbital (LUMO) is composed of the phosphine ligands.[63]

Silver chalcogenolates can also see potential as OLEDs or other photofunctional materials, however, instability due to light as well as poor luminescence at room temperature pose as a major obstacle.[31] One of the limited examples of an emissive silver chalcogenolate cluster is $[Ag_{14}(SC_6H_3F_2)_3PPh_3]$ (**I.XXX**). This cluster possesses an Ag_6^{4+} core which is encased by a cube of $[Ag(SC_6H_3F_2)_3PPh_3$ which share a peripheral ($SC_6H_3F_2^-$). In this cluster, there are silvers of both oxidation state (I) and (0) which results in the Ag_6^{4+} core – very rarely seen in thiolate protected Ag clusters.[64] All thiolates have a μ_3 coordination geometry and are bound to three Ag atoms. (**I.XXXI**) displays an emission in solid state at room temperature, however, only has a PLQY of 0.1 %. This cluster is also unstable in solution for extended periods of time, is photosensitive, and loses emission in the presence of O_2.[64]

An example of a gold chalcogenolate cluster is $[Au_9(\mu\text{-}dppm)_4(\mu\text{-}p\text{-}tc)_6](PF_6)_3$ (p-tc = p-thiocresolate) (**I.XXXII**) reported by Bruce and co-workers.[65] As seen in *Figure 1.12*, two gold display distorted trigonal planar geometries and the remaining gold atoms exhibit near linear coordination. The thiolate ligands are bridging two gold atoms and each Au_2S unit is bridged by the phosphine ligand, except for the central AuS_2.[65] This cluster displays a weak yellow emission at ambient temperature, and at 77 K a brilliant yellow (λ_{em} = 540 nm) emission, with a long lifetime – indicative of triplet involvement (phosphorescence) in the emission pathway.[65]

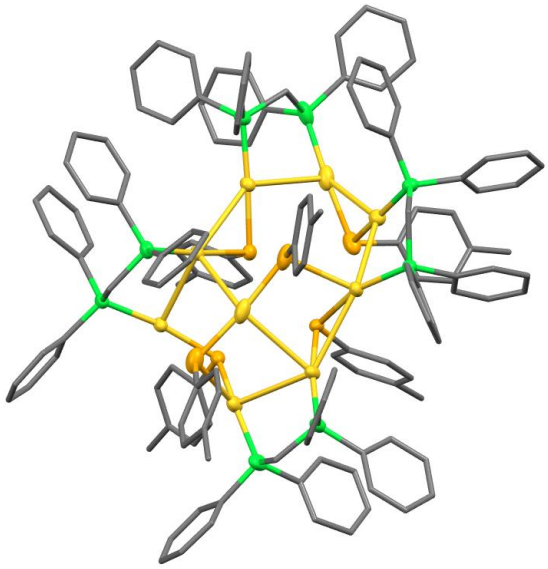

Figure 1.12: Molecular structure of the complex cation $[Au_9(\mu\text{-dppm})_4(\mu\text{-p-tc})_6]^{3+}$ ***(I.XXXII)*** *(H atoms and* PF_6 *anions were omitted for clarity).*[65]

1.6 The Phosphine Ligand: 4,6-bis(diphenylphosphino)dibenzofuran (DBFDP)

Copper (I) iodide clusters have been widely studied as luminescent materials for an extended period.[66] However, given their weak electroactivity and poor solution processability, copper (I) iodide clusters have not yet been incorporated into surface coating of OLEDs. The *Xie* group has recently reported that with the addition of 4,6-*bis*(diphenylphosphino)dibenzofuran (DBFDP), the solution processability and electroactivity of said copper (I) iodide clusters have greatly improved.[66]

More recently, Nayyar showed that the addition of 4,6-*bis*(diphenylphosphino)dibenzofuran (DBFDP) to copper and silver chalcogenido clusters have modified and enhanced their luminescent properties.[67] An example of such is $[Cu_4(SePh)_4(\mu\text{-dbfdp})_2]$ (**I.XXXIII**), where the λ_{em} was observed at 560 nm with a PLQY of 33.8 % at room temperature.[67]

DBFDP, as shown in *Figure 1.13a*, was chosen with considerations due to two characteristics (i) the distance between the two phosphorus atoms and (ii) the rigidity promoted in the cluster due to the DBF backbone.[66] The distance between the phosphorus atoms can provide excellent coordination ability and appropriate space to bridge two metal centres in the metal cluster. Additionally, the DBF ring acts as a high-energy-gap chromophore with functions such as energy

level modulation, electron transport enhancement, and solubilizing the metal centre.[66] The large energy gap between the HOMO and LUMO results in the aforementioned high-energy-gap chromophore and allows the ligand to coordinate with metal clusters with efficient luminescence.[66]

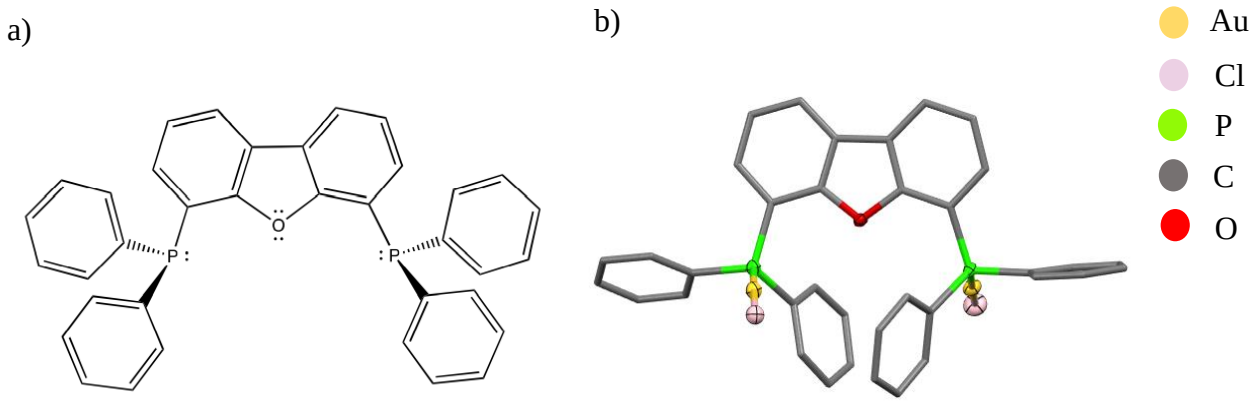

*Figure 1.13(a) 4,6-bis(diphenylphosphino)dibenzofuran ligand (DBFDP)[66] (b) [(AuCl)$_2$(μ-dbfdp)] (**I.XXXIV**) (H atoms omitted for clarity).[68]*

Lagunas and co-workers have reported the complex [(AuCl)$_2$(μ-DBFDP)] (**I.XXXIV**).[68] This complex however, does not display indications of aurophilic interactions between the two gold atoms. In terms of photophysical properties, there is a strong absorption that occurs in (**I.XXXIV**) in the 250-300 nm range which can be assigned to the $\pi \rightarrow \pi^*$ transition localized on the aromatic groups – shifting to slightly higher energy upon coordination. (**I.XXXIV**) emits at 429 nm and 458 nm at room temperature upon photoexcitation with a shoulder at 488 nm which can be attributed to an intraligand charge transfer ($\sigma \rightarrow a_\pi$).[68] The low energy emissions seen in aromatic diphosphine gold analogues, [(AuCl$_2$)(μ-dpephos)] (dpephos = [*bis*(2-diphenylphosphino)phenyl ether]) (**I.XXXV**) and [(AuCl$_2$)(μ-xantphos)] (xantphos = 9,9-dimethyl-4,5-*bis*(diphenylphosphino)-xanthene)) (**I.XXXVI**), were not observed with (**I.XXXVII**), and can be attributed to the lack of aurophilic interactions in the Se complex.[68] The structure of (**I.XXXIV**) can be seen in *Figure 1.12b.*

1.7 Scope of Thesis

This thesis highlights the work conducted on incorporating the ligand 4,6-*bis*(diphenylphosphino)dibenzofuran (DBFDP) onto Au (I) chalcogen cluster to examine the effect of the phosphine on structure, electronic and photophysical properties. Moreover, an investigation on how the organic moieties on the chalcogenolate reagents (M-ER; M = metal, E= S, Se, R = organic moiety) affect the structure of these assemblies was conducted on group 11 metals (Cu (I) and Au (I)). Chapter 2 focuses on incorporation of DBFDP onto gold chalcogenide clusters with the analysis of their molecular, electronic and luminescent properties; it also discusses the effect of the chalcogen on the size of the complex and effect on structure. Chapter 3 focuses on the incorporation of DBFDP onto gold chalcogenolate clusters with the analysis of their molecular, electronic and luminescent properties. Moreover, different chalcogenolate ligands and group d^{10} metals were investigated to explore the effect on structural and photophysical properties. Chapter 4 summarizes the results from Chapters 2 and 3 and suggests future work that can be conducted involving the DBFDP ligand.

1.8 References

(1) Fuhr, O.; Dehnen, S.; Fenske, D. Chalcogenide Clusters of Copper and Silver from Silylated Chalcogenide Sources. *Chem. Soc. Rev.* **2013**, *42* (4), 1871–1906. https://doi.org/10.1039/C2CS35252D.

(2) Dehnen, S.; Eichhöfer, A.; Fenske, D. Chalcogen-Bridged Copper Clusters. *Eur. J. Inorg. Chem.* **2002**, *2002* (2), 279–317. https://doi.org/10.1002/1099-0682(20022)2002:2<279::AID-EJIC279>3.0.CO;2-H.

(3) Yam, V. W.-W.; Lo, K. K.-W. Luminescent Polynuclear d 10 Metal Complexes. *Chem. Soc. Rev.* **1999**, *28* (5), 323–334. https://doi.org/10.1039/A804249G.

(4) Lo, W.-Y.; Lam, C.-H.; Yam, V. W.-W.; Zhu, N.; Cheung, K.-K.; Fathallah, S.; Messaoudi, S.; Le Guennic, B.; Kahlal, S.; Halet, J.-F. Synthesis, Photophysics, Electrochemistry, Theoretical, and Transient Absorption Studies of Luminescent Copper(I) and Silver(I) Diynyl Complexes. X-Ray Crystal Structures of [Cu3(μ-Dppm)3(M3-H1-C⁝CC⁝CPh)2]PF6 and [Cu3(μ-Dppm)3(M3-H1-C⁝CC⁝CH)2]PF6. *J. Am. Chem. Soc.* **2004**, *126* (23), 7300–7310. https://doi.org/10.1021/ja049300x.

(5) Veselska, O.; Demessence, A. D10 Coinage Metal Organic Chalcogenolates: From Oligomers to Coordination Polymers. *Coord. Chem. Rev.* **2018**, *355*, 240–270. https://doi.org/10.1016/j.ccr.2017.08.014.

(6) Hu, B.; Su, C. Y.; Fenske, D.; Fuhr, O. Synthesis, characterization and optical properties of a series of binuclear copper chalcogenolato complexes. *Inorganica Chim. Acta* **2014**, *419* (August), 118. https://doi.org/10.1016/j.ica.2014.05.009.

(7) Yam, V. W.-W. Molecular Design of Luminescent Metal-Based Materials. *Pure Appl. Chem.* **2001**, *73* (3), 543–548.

(8) Yam, V. W.-W.; Cheng, E. C.-C.; Zhu, N. A Novel Polynuclear Gold–Sulfur Cube with an Unusually Large Stokes Shift. *Angew. Chem. Int. Ed.* **2001**, *40* (9), 1763–1765. https://doi.org/10.1002/1521-3773(20010504)40:9<1763::AID-ANIE17630>3.0.CO;2-O.

(9) Dehnen, S.; Eichhöfer, A.; Corrigan, J. F.; Fuhr, O.; Fenske, D. *Synthesis and characterization of Ib-VI nanoclusters*. https://publikationen.bibliothek.kit.edu/150081429 (accessed 2023-06-12).

(10) Bestgen, S.; Fuhr, O.; Breitung, B.; Chakravadhanula, V. S. K.; Guthausen, G.; Hennrich, F.; Yu, W.; Kappes, M. M.; Roesky, P. W.; Fenske, D. [Ag115S34(SCH2C6H4tBu)47(Dpph)6]: Synthesis, Crystal Structure and NMR Investigations of a Soluble Silver Chalcogenide Nanocluster. *Chem. Sci.* **2017**, *8* (3), 2235–2240. https://doi.org/10.1039/C6SC04578B.

(11) Harisomayajula, N. V. S.; Makovetskyi, S.; Tsai, Y. Cuprophilic Interactions in and between Molecular Entities. *Chem. – Eur. J.* **2019**, *25* (38), 8936–8954. https://doi.org/10.1002/chem.201900332.

(12) Schmidbaur, H. Is Gold Chemistry a Topical Field of Study? *Angew. Chem. Int. Ed. Engl.* **1976**, *15* (12), 728–740. https://doi.org/10.1002/anie.197607281.

(13) Schmidbaur, H.; Graf, W.; Müller, G. Weak Intramolecular Bonding Relationships: The Conformation-Determining Attractive Interaction between Gold(I) Centers. *Angew. Chem. Int. Ed. Engl.* **1988**, *27* (3), 417–419. https://doi.org/10.1002/anie.198804171.

(14) Schmidbaur, H.; Schier, A. Argentophilic Interactions. *Angew. Chem. Int. Ed.* **2015**, *54* (3), 746–784. https://doi.org/10.1002/anie.201405936.

(15) Carvajal, M. A.; Alvarez, S.; Novoa, J. J. The Nature of Intermolecular $Cu^{I} \cdots Cu^{I}$ Interactions: A Combined Theoretical and Structural Database Analysis. *Chem. – Eur. J.* **2004**, *10* (9), 2117–2132. https://doi.org/10.1002/chem.200305249.
(16) Hermann, H. L.; Boche, G.; Schwerdtfeger, P. Metallophilic Interactions in Closed-Shell Copper(I) Compounds—A Theoretical Study. *Chem. – Eur. J.* **2001**, *7* (24), 5333–5342. https://doi.org/10.1002/1521-3765(20011217)7:24<5333::AID-CHEM5333>3.0.CO;2-1.
(17) Dehnen, S.; Fenske, D.; Deveson, A. C. [Cu12S6(PnPr3)8] and [Cu20S10(PnBu1Bu2)8]: Two Sulfur Bridged Copper Clusters with Cu-s Cluster Cores of Known Compositions but New Structures. *J. Clust. Sci.* **1996**, *7* (3), 351–369. https://doi.org/10.1007/BF01171188.
(18) Deveson, A.; Dehnen, S.; Fenske, D. Syntheses and Structures of Four New Copper(I)–Selenium Clusters: Size Dependence of the Cluster on the Reaction Conditions. *J. Chem. Soc. Dalton Trans.* **1997**, *0* (23), 4491–4498. https://doi.org/10.1039/A705750D.
(19) Khadka, C. B.; Najafabadi, B. K.; Hesari, M.; Workentin, M. S.; Corrigan, J. F. Copper Chalcogenide Clusters Stabilized with Ferrocene-Based Diphosphine Ligands. *Inorg. Chem.* **2013**, *52* (12), 6798–6805. https://doi.org/10.1021/ic3021854.
(20) Eichhöfer, A.; Buth, G.; Lebedkin, S.; Kühn, M.; Weigend, F. Luminescence in Phosphine-Stabilized Copper Chalcogenide Cluster Molecules—A Comparative Study. *Inorg. Chem.* **2015**, *54* (19), 9413–9422. https://doi.org/10.1021/acs.inorgchem.5b01146.
(21) Yang, X.-X.; Issac, I.; Lebedkin, S.; Kühn, M.; Weigend, F.; Fenske, D.; Fuhr, O.; Eichhöfer, A. Red-Luminescent Biphosphine Stabilized '$Cu_{12}S_6$' Cluster Molecules. *Chem. Commun.* **2014**, *50* (75), 11043. https://doi.org/10.1039/C4CC04702H.
(22) Zhang, S.-S.; Liu, R.-C.; Zhang, X.-C.; Feng, L.; Xue, Q.-W.; Gao, Z.-Y.; Tung, C.-H.; Sun, D. Core Engineering of Paired Core-Shell Silver Nanoclusters. *Sci. China Chem.* **2021**, *64* (12), 2118–2124. https://doi.org/10.1007/s11426-021-1060-3.
(23) Wang, X.-J.; Langetepe, T.; Persau, C.; Kang, B.-S.; Sheldrick, G. M.; Fenske, D. Syntheses and Crystal Structures of the New Ag-S Clusters [Ag70S16(SPh)34(PhCO2)4(Triphos)4] and [Ag188S94(PR3)30]. *Angew. Chem. Int. Ed Engl.* **2002**, *41* (20), 3818–3822. https://doi.org/10.1002/1521-3773(20021018)41:20<3818::AID-ANIE3818>3.0.CO;2-R.
(24) Bestgen, S.; Yang, X.; Issac, I.; Fuhr, O.; Roesky, P. W.; Fenske, D. Adamantyl- and Furanyl-Protected Nanoscale Silver Sulfide Clusters. *Chem. – Eur. J.* **2016**, *22* (29), 9933–9937. https://doi.org/10.1002/chem.201602158.
(25) Yao, L.-Y.; Yam, V. W.-W. Photoinduced Isomerization-Driven Structural Transformation Between Decanuclear and Octadecanuclear Gold(I) Sulfido Clusters. *J. Am. Chem. Soc.* **2015**, *137* (10), 3506–3509. https://doi.org/10.1021/jacs.5b01676.
(26) Lee, T. K.-M.; Zhu, N.; Yam, V. W.-W. An Unprecedented Luminescent Polynuclear Gold(I) M3-Sulfido Cluster With a Thiacrown-like Architecture. *J. Am. Chem. Soc.* **2010**, *132* (50), 17646–17648. https://doi.org/10.1021/ja1055017.
(27) Yan, L.-L.; Yao, L.-Y.; Yam, V. W.-W. Concentration- and Solvation-Induced Reversible Structural Transformation and Assembly of Polynuclear Gold(I) Sulfido Complexes. *J. Am. Chem. Soc.* **2020**, *142* (26), 11560–11568. https://doi.org/10.1021/jacs.0c04677.
(28) Cheng, E. C.-C.; Lo, W.-Y.; Lee, T. K.-M.; Zhu, N.; Yam, V. W.-W. Synthesis, Characterization, and Luminescence Studies of Discrete Polynuclear Gold(I) Sulfido and Selenido Complexes with Intramolecular Aurophilic Contacts. *Inorg. Chem.* **2014**, *53* (7), 3854–3863. https://doi.org/10.1021/ic500215d.

(29) Langer, R.; Yadav, M.; Weinert, B.; Fenske, D.; Fuhr, O. Luminescence in Functionalized Copper Thiolate Clusters – Synthesis and Structural Effects. *Eur. J. Inorg. Chem.* **2013**, *2013* (21), 3623–3631. https://doi.org/10.1002/ejic.201300155.
(30) Wang, J.; Li, Y.-L.; Wang, Z.-Y.; Zang, S.-Q. A Robust Wave-like Silver–Thiolate Chain Based Metal–Organic Network: Synthesis, Structure and Luminescence. *CrystEngComm* **2019**, *21* (14), 2264–2267. https://doi.org/10.1039/C9CE00054B.
(31) Wang, Y.-M.; Zhang, J.-W.; Wang, Q.-Y.; Li, H.-Y.; Dong, X.-Y.; Wang, S.; Zang, S.-Q. Fabrication of Silver Chalcogenolate Cluster Hybrid Membranes with Enhanced Structural Stability and Luminescence Efficiency. *Chem. Commun.* **2019**, *55* (97), 14677–14680. https://doi.org/10.1039/C9CC07797A.
(32) Li, Y.-H.; Wang, Z.-Y.; Ma, B.; Xu, H.; Zang, S.-Q.; Mak, T. C. W. Self-Assembly of Thiolate-Protected Silver Coordination Polymers Regulated by POMs. *Nanoscale* **2020**, *12* (20), 10944–10948. https://doi.org/10.1039/D0NR00342E.
(33) Li, Y.-L.; Zhang, W.-M.; Wang, J.; Tian, Y.; Wang, Z.-Y.; Du, C.-X.; Zang, S.-Q.; Mak, T. C. W. Photoluminescence Modulation of an Atomically Precise Silver(I)–Thiolate Cluster via Site-Specific Surface Engineering. *Dalton Trans.* **2018**, *47* (42), 14884–14888. https://doi.org/10.1039/C8DT03165G.
(34) Vittal, J.; Puddephatt, R. Gold: Inorganic & Coordination Chemistry; 2011. https://doi.org/10.1002/9781119951438.eibc0076.
(35) Sladek, A.; Angermaier, K.; Schmidbaur, H. Gold Clustering at the Methylthiolate Anion. *Chem. Commun.* **1996**, No. 16, 1959. https://doi.org/10.1039/cc9960001959.
(36) Roof, L. C.; Kolis, J. W. New Developments in the Coordination Chemistry of Inorganic Selenide and Telluride Ligands. *Chem. Rev.* **1993**, *93* (3), 1037–1080. https://doi.org/10.1021/cr00019a010.
(37) Legator, M. S.; Singleton, C. R.; Morris, D. L.; Philips, D. L. Health Effects from Chronic Low-Level Exposure to Hydrogen Sulfide. *Arch. Environ. Health Int. J.* **2001**, *56* (2), 123–131. https://doi.org/10.1080/00039890109604063.
(38) Yam, V. W.-W.; Wong, K. M.-C. From Simple Molecules to Molecular Functional Materials and Nanoscience. In *Nanoscale Phenomena: Basic Science to Device Applications*; Tang, Z., Sheng, P., Eds.; Lecture Notes in Nanoscale Science and Technology; Springer: New York, NY, 2008; pp 217–234. https://doi.org/10.1007/978-0-387-73048-6_19.
(39) Ananikov, V. P.; Orlov, N. V.; Beletskaya, I. P. Highly Efficient Nickel-Based Heterogeneous Catalytic System with Nanosized Structural Organization for Selective Se−H Bond Addition to Terminal and Internal Alkynes. *Organometallics* **2007**, *26* (3), 740–750. https://doi.org/10.1021/om061033b.
(40) Forward, J. M.; Bohmann, D.; Fackler, J. P.; Staples, R. J. Luminescence Studies of Gold(I) Thiolate Complexes. *Inorg. Chem.* **1995**, *34* (25), 6330–6336. https://doi.org/10.1021/ic00129a019.
(41) Seligson, A. L.; Arnold, J. Synthesis, Structure, and Reactivity of Homoleptic Tin(II) and Lead(II) Chalcogenolates and Conversion to Metal Chalcogenides. X-Ray Crystal Structures of {Sn[TeSi(SiMe3)3]2}2 and (PMe3)Sn[TeSi(SiMe3)3]2. *J. Am. Chem. Soc.* **1993**, *115* (18), 8214–8220. https://doi.org/10.1021/ja00071a034.
(42) Bochmann, M.; Song, X.; Hursthouse, M. B.; Karaulov, A. Chalcogenolato Complexes of Bismuth and Antimony. Syntheses, Thermolysis Reactions, and Crystal Structure of Sb(SC6H2Pri 3-2,4,6)3. *J. Chem. Soc. Dalton Trans.* **1995**, No. 10, 1649. https://doi.org/10.1039/dt9950001649.

(43) Yam, V. W.-W.; Chan, C.-L.; Li, C.-K.; Wong, K. M.-C. Molecular Design of Luminescent Dinuclear Gold(I) Thiolate Complexes: From Fundamentals to Chemosensing. *Coord. Chem. Rev.* **2001**, *216–217*, 173–194. https://doi.org/10.1016/S0010-8545(01)00310-1.
(44) Zou, W.; Zhu, Q.; Fettinger, J. C.; Power, P. P. Dimeric Copper and Lithium Thiolates: Comparison of Copper Thiolates with Their Lithium Congeners. *Inorg. Chem.* **2021**, *60* (23), 17641–17648. https://doi.org/10.1021/acs.inorgchem.1c02226.
(45) Gunawardene, P. N.; Corrigan, J. F.; Workentin, M. S. Golden Opportunity: A Clickable Azide-Functionalized [Au25(SR)18]− Nanocluster Platform for Interfacial Surface Modifications. *J. Am. Chem. Soc.* **2019**, *141* (30), 11781–11785. https://doi.org/10.1021/jacs.9b05182.
(46) Yam, V. W.-W.; Lam, C.-H.; Fung, W. K.-M.; Cheung, K.-K. Syntheses, Photophysics, and Photochemistry of Trinuclear Copper(I) Thiolate and Hexanuclear Copper(I) Selenolate Complexes: X-Ray Crystal Structures of [Cu6(μ-Dppm)4(M3-SePh)4](BF4)2 and [Cu6{μ-(Ph2P)2NH}4(M3-SePh)4](BF4)2. *Inorg. Chem.* **2001**, *40* (14), 3435–3442. https://doi.org/10.1021/ic0012322.
(47) DeGroot, M. W.; Corrigan, J. F. Coordination Complexes of Zinc with Reactive ESiMe3 (E = S, Se, Te) Ligands. *Organometallics* **2005**, *24* (14), 3378–3385. https://doi.org/10.1021/om050088v.
(48) DeGroot, M. W.; Corrigan, J. F. Polynuclear Bismuth Selenolates: Rings En Route to Clusters. *J. Chem. Soc. Dalton Trans.* **2000**, No. 8, 1235–1236. https://doi.org/10.1039/B001417F.
(49) Duan, T.; Zhang, X.-Z.; Zhang, Q.-F. Synthesis and Crystal Structure of a Polynuclear Copper-Selenide Cluster [CuI36(CuIICl)2Se13(SePh)12(Dppe)6] · 3EtOH. *Z. Für Naturforschung B* **2008**, *63* (8), 941–944. https://doi.org/10.1515/znb-2008-0804.
(50) MacDonald, D. G.; Corrigan, J. F. Metal Chalcogenide Nanoclusters with 'Tailored' Surfaces via 'Designer' Silylated Chalcogen Reagents. *Philos. Trans. R. Soc. Math. Phys. Eng. Sci.* **2010**, *368* (1915), 1455–1472. https://doi.org/10.1098/rsta.2009.0276.
(51) DeGroot, M. W.; Corrigan, J. F. Metal-Chalcogenolate Complexes with Silyl Functionalities: Synthesis and Reaction Chemistry. *Z. Für Anorg. Allg. Chem.* **2006**, *632* (1), 19–29. https://doi.org/10.1002/zaac.200500314.
(52) Polgar, A. M.; Weigend, F.; Zhang, A.; Stillman, M. J.; Corrigan, J. F. A *N* -Heterocyclic Carbene-Stabilized Coinage Metal-Chalcogenide Framework with Tunable Optical Properties. *J. Am. Chem. Soc.* **2017**, *139* (40), 14045–14048. https://doi.org/10.1021/jacs.7b09025.
(53) Krautscheid, H.; Fenske, D.; Baum, G.; Semmelmann, M. A New Copper Selenide Cluster with PPh3 Ligands: [Cu146Se73(PPh3)30]. *Angew. Chem. Int. Ed. Engl.* **1993**, *32* (9), 1303–1305. https://doi.org/10.1002/anie.199313031.
(54) Valeur, B.; Berberan-Santos, M. N. A Brief History of Fluorescence and Phosphorescence before the Emergence of Quantum Theory. *J. Chem. Educ.* **2011**, *88* (6), 731–738. https://doi.org/10.1021/ed100182h.
(55) Munson, C. A.; Gottfried, J. L.; De Lucia, Jr.; Frank C., M.; Kevin L., M.; Andrzej W. *Laser-Based Detection Methods for Explosives:*; Defense Technical Information Center: Fort Belvoir, VA, 2007. https://doi.org/10.21236/ADA474060.
(56) Gonzalez-Moraga, G. *Cluster Chemistry: Introduction to the Chemistry of Transition Metal and Main Group Element Molecular Clusters*; Springer Science & Business Media, 2013.

(57) Bravo, J. A.; Valdivieso, F.; Quiróz, N.; Vila, J. L. Compuestos luminiscentes:: Gingerol, sulfato de quinina y fluoresceína, revisión abreviada. *Rev. Boliv. Quím.* **2018**, *35* (4), 108–116.
(58) Powell, A. L. The Fundamentals of Fluorescence. *J. Chem. Educ.* **1947**, *24* (9), 423. https://doi.org/10.1021/ed024p423.
(59) Ravaro, L. P.; Zanoni, K. P. S.; de Camargo, A. S. S. Luminescent Copper(I) Complexes as Promising Materials for the next Generation of Energy-Saving OLED Devices. *Energy Rep.* **2020**, *6*, 37–45. https://doi.org/10.1016/j.egyr.2019.10.044.
(60) Seo, S.; Shitagaki, S.; Ohsawa, N.; Inoue, H.; Suzuki, K.; Nowatari, H.; Takahashi, T.; Hamada, T.; Watabe, T.; Yamada, Y.; Mitsumori, S. Recent Development of Organic Light-Emitting Diode Utilizing Energy Transfer from Exciplex to Phosphorescent Emitter. In *Organic Light Emitting Materials and Devices XX*; SPIE, 2016; Vol. 9941, pp 44–60. https://doi.org/10.1117/12.2236191.
(61) Resch-Genger, U.; Rurack, K. Determination of the Photoluminescence Quantum Yield of Dilute Dye Solutions (IUPAC Technical Report). *Pure Appl. Chem.* **2013**, *85* (10), 2005–2013. https://doi.org/10.1351/pac-rep-12-03-03.
(62) Yan, L.-L.; Yao, L.-Y.; Leung, M.-Y.; Yam, V. W.-W. Substituent-Mediated Transformation of Polynuclear Gold(I)-Sulfido Complexes—From Pentanuclear to Octadecanuclear Cluster-to-Cluster Transformation. *CCS Chem.* **2021**, *3* (8), 326–337. https://doi.org/10.31635/ccschem.021.202000662.
(63) Ke, F.; Song, Y.; Li, H.; Zhou, C.; Du, Y.; Zhu, M. Sub-Nanometer Cu(I) Clusters: Coordination-Modulated (Se vs. S) Atom-Packing Mode and Emission. *Dalton Trans.* **2019**, *48* (37), 13921–13924. https://doi.org/10.1039/C9DT02908G.
(64) Huang, R.-W.; Wei, Y.-S.; Dong, X.-Y.; Wu, X.-H.; Du, C.-X.; Zang, S.-Q.; Mak, T. C. W. Hypersensitive Dual-Function Luminescence Switching of a Silver-Chalcogenolate Cluster-Based Metal-Organic Framework. *Nat. Chem.* **2017**, *9* (7), 689–697. https://doi.org/10.1038/nchem.2718.
(65) Chen, J.; Mohamed, A. A.; Abdou, H. E.; Krause Bauer, J. A.; Fackler, Jr., J. P.; Bruce, A. E.; Bruce, M. R. M. Novel Metallamacrocyclic Gold(I) Thiolate Cluster Complex: Structure and Luminescence of [Au $_9$ (μ-Dppm) $_4$ (μ-p-Tc) $_6$](PF $_6$) $_3$. *Chem Commun* **2005**, No. 12, 1575–1577. https://doi.org/10.1039/B415488F.
(66) Xie, M.; Han, C.; Zhang, J.; Xie, G.; Xu, H. White Electroluminescent Phosphine-Chelated Copper Iodide Nanoclusters. *Chem. Mater.* **2017**, *29* (16), 6606–6610. https://doi.org/10.1021/acs.chemmater.7b01443.
(67) Nayyar, M. Luminescent Group 11 Metal Chalcogen Clusters with Bidentate Phosphine Ligands, The University of Western Ontario, London, 2021.
(68) Pintado-Alba, A.; De La Riva, H.; Nieuwhuyzen, M.; Bautista, D.; Raithby, P. R.; Sparkes, H. A.; Teat, S. J.; López-de-Luzuriaga, J. M.; Lagunas, M. C. Effects of Diphosphine Structure on Aurophilicity and Luminescence in Au(I) Complexes. *Dalton Trans* **2004**, No. 21, 3459–3467. https://doi.org/10.1039/B410619A.

Chapter 2

2.0 Luminescent Gold (I) Chalcogenide Clusters with a Conjugated Diphosphine Ligand

2.1 Introduction

Group 11 metal chalcogenide clusters have been extensively studied due to their diverse dimensionalities, varying metal core sizes in addition to their photophysical properties. These properties allow such clusters to be incorporated into a myriad of applications from optoelectronics, bioimaging and light emitting materials.[1,2] Due to their long-lived excited states, their capacity to form clusters of varying nuclearities, and varying emission and excitation properties attributable to the protecting ligand, these complexes have generated an intense amount of interest.

By altering the organic ligand, the electronic structure of these compounds can be modified which leads to HOMO-LUMO energy gap differences.[3] This property makes these group 11 metal chalcogenide clusters attractive targets for incorporation into everyday electronics in the form of organic light emitting diodes (OLEDs).[4,5]

Structural trends for Cu (I), Ag (I) and Au (I) differ drastically due to their individual preferences for various coordination modes and ability to form metallophilic interactions. For the lighter d^{10} metals, copper (I) and silver (I), a coordination number of four can be achieved with different ligands, whereas for heavier metals such as gold (I), the coordination geometry is usually two. Given this two-coordination propensity, Au (I) chalcogenides form low-nuclearity clusters more often than Ag(I) or Cu(I).[6] For Au(I) clusters with a single chalcogenide ligand, they can form clusters of nuclearities of 2-6 (i.e. $[(\mu\text{-E})(AuPR_3)_2]$ to $[(\mu_6\text{-E})(AuPR_3)_6]^{4+}$] (E = S, Se).[7–9] By first starting with the $[(AuCl)_x(PR_3)_x]$ (x = 1 for monodentate, 2 for bidentate), an E^{2-} source can be used with sources such as Li_2E or silylated chalcogen reagents ($E(SiMe_3)_2$ or $RESiMe_3$). The reaction is driven forward by the formation of $X\text{-}SiMe_3$ and as a result, forms the metal chalcogenide core.[10–12] Starting from $[(\mu\text{-E})(AuPR_3)_2]$, a cluster can be grown with sequential addition of 1-4 equivalents of $[R_3PAu(OTf)]$. With larger electron deficient clusters, stability is enhanced by previously mentioned strong metallophilic interactions of Au (I).

Phosphine ligands are one of the most common organic ligands in coordination chemistry and can be incorporated into d^{10} metal clusters in order to prevent formation of thermodynamically driven binary phase of bulk M_2E (M = Cu, Ag, Au; E = S, Se). The structure of the cluster and its physical properties can all change depending on the type of phosphine used. Recent studies by Eichhöfer and co-workers have synthesized numerous copper chalcogenide clusters with different phosphine ligands containing a Cu_2E (E = S, Se) core structure. These clusters display bright red phosphorescent emissions at ambient temperature with a $Cu_{12}S_6$ core: such complexes show high PLQYs with values ranging from 21 % to 63 %.[13] It was observed that not only the type of phosphine ligand influences the PLQY, however the crystal packing also plays a factor.[13]

Gold (I) complexes have gained recent interest due to their ability to exhibit secondary bonds such as aurophilic interactions, which are similar in strength to hydrogen bonds.[14,15] Several gold (I) chalcogenide clusters have demonstrated interesting luminescence properties and can form cluster with nuclearities ranging from 2 to higher than 6, forming electron-deficient complexes.[8,9] Examples of bridging phosphine stabilized gold clusters include $[Au_6(\mu\text{-dppf})_3(\mu_3\text{-S})_2](OTf)_2$ (**II.I**) (dppf = 1,1'-*bis*(diphenylphosphanyl)ferrocene), $[Au_6(\mu\text{-}Ph_2PN(p\text{-}CH_3C_6H_4)PPh_2\}_3(\mu_3\text{-S})_2](ClO_4)_2$ (**II.II**), both of which include different phosphine ligands which change their respective photophysical characteristics as reported by Yam and Jones.[8,16]

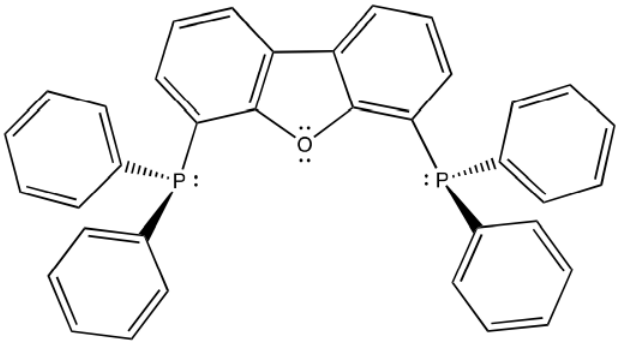

Figure 2.1: 4,6-bis(diphenylphosphino)dibenzofuran (DBFDP)[17]

Recent studies have been conducted and have demonstrated that the reaction between 4,6-*bis*(diphenylphosphino)dibenzofuran (DBFDP) *(Figure 2.1)* and copper (I) acetate leads to $[\{Cu(\mu\text{-}\kappa O\text{-}OAc)(\mu\text{-dbfdp})\}_2]$ whereas reactions with silver acetate leads to $[\{Ag(\mu\text{-}\kappa O\text{-}OAc)(\mu\text{-dbfdp})\}_2]$.[18,19] Following characterization by single crystal X-ray diffraction, it was observed the

copper/silver centre takes on a distorted tetrahedral conformation with two phosphorus atoms and bridging O atoms from the acetate ligand. Acetates have 4 bonding modes, however, since symmetry of the free ion is low, there is no large difference in the infrared spectrum of each type.

With the addition of 1.0 equivalent of $E(SiMe_3)_2$ (E = S, Se), a double displacement reaction occurs to generate a $[(M_2E)_x(dbfdp)_y]$ complex. Previous attempts for synthesizing luminescent copper chalcogenide clusters were also made in the Corrigan group.[18] However, due to unsuitable crystal size, these copper chalcogenide clusters could not be characterized. The incorporation of ethyl groups on the backbone was successful and suitable sized crystals of $[(Cu_{12}Se_6)(etdbfdp)_4]$ **(II.III)** were obtained. The $[(Ag_2S)_x(\mu\text{-}dbfdp)_y]$ and $[(Ag_2Se)_x(\mu\text{-}dbfdp)_y]$ products were unable to be crystallized due to decomposition due to light or the reaction proceeded to decompose to Ag_2S and Ag_2Se. Logically, incorporating DBFDP into gold (I) chalcogenide clusters would allow for a more in depth understanding of the structure-property relationship and how the size of the metal atom affects emission, excitation and other photophysical properties.

Previously, research has demonstrated that the reaction between 4,6-*bis*(diphenylphosphino)dibenzofuran (DBFDP) and chloro(tetrahydrothiophene) gold (I) leads to $[(AuCl)_2(\mu\text{-}dbfdp)_2]$ **(I.XXXI)**.[20] Similar to the copper and silver analogues, addition of 1.0 equivalent of $E(SiMe_3)_2$ (E = S, Se) results in a double displacement reaction to generate $[(Au_2E)(\mu\text{-}dbfdp)]$ complexes. These complexes confirmed the expectation that the diphopshine bridges the two metal centres and the molecule demonstrates a potential aurophilic interaction. Though the $[(Au_2E)(\mu\text{-}dbfdp)]$ complexes were able to be obtained from reactions between $[(AuCl)_2(\mu\text{-}dbfdp)_2]$ **(I.XXXI)** and the silylated chalcogen reagents *(Figure 2.2)*, the reaction was determined to be unselective due to different crystal morphologies and $^{31}P\{^1H\}$ data that indicated an additional, unknown species.[19]

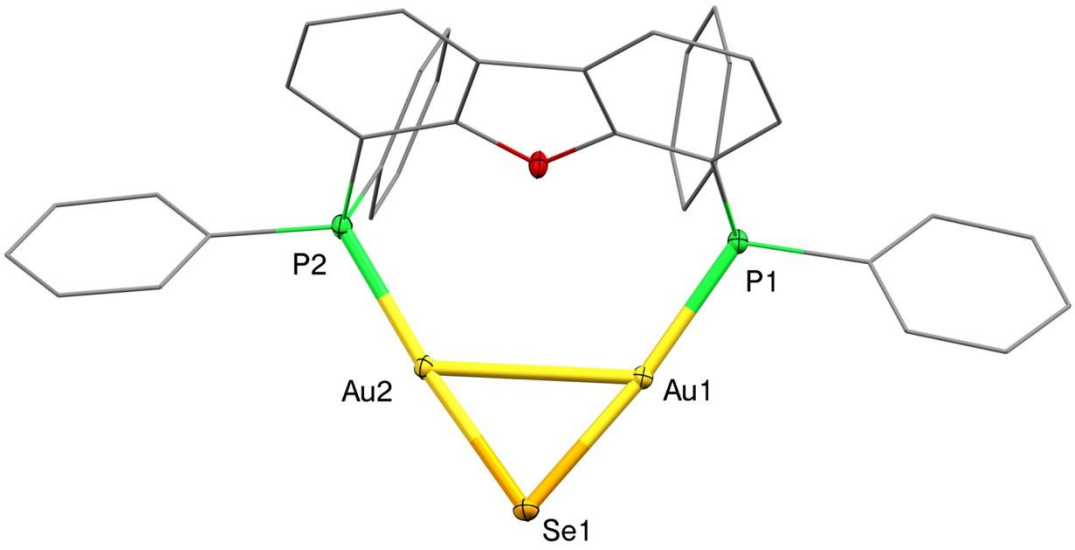

Figure 2.2: Molecular structure of [(Au_2Se)(dbfdp)] ***(2.3 Se)*** *in the crystal (H atoms omitted for clarity)*[19]

Herein, the incorporation of the bidentate phosphine 4,6-*bis*(diphenylphosphino)dibenzofuran (DBFDP) into gold (I) chalcogen complexes and clusters is reported. Phosphine protected M(I)Cl and M(I)OAc (M = Cu, Ag, Au) salts and chalcogen reagents with $SiMe_3$ moieties have been well documented and intensively investigated.[10–12] Thus, [$(AuOAc)_2$(μ-dbfdp)] **(2.1)** and the related $(AuOTf)_2$(μ-dbfdp)] (2.2) represents an excellent starting point for the preparation of gold (I) chalcogenido- clusters which contain the DBFDP ligand. [$(AuOAc)_2$(μ-dbfdp)] **(2.1)** was synthesized by stirring 1.0 equivalent of [$(AuCl)_2$(μ-dbfdp)] **(I.XXXI)** with 2.2 equivalents of AgOAc to result in the formation of the phosphine metal acetate complex. *Bis*(trimethylsilyl)sulfide and *bis*(trimethylsilyl)selenide were subsequently introduced to the solutions of [$(AuOAc)_2$(μ-dbfdp)] **(2.1)** resulting in [(Au_2S)(μ-dbfdp)] **(2.3 S)** and [(Au_2Se)(μ-dbfdp)] **(2.3 Se)**. Addition of the triflouromethanesulfonate (triflate or OTf) sources (Cu(I)OTf or [$(AuOTf)_2$(μ-dbfdp)]) **(2.2)** resulted in larger homometallic gold clusters with nuclearities ranging from 4-6: [Au_4(μ_4-S)(μ-dbfdp)$_2$](OTf)$_2$ (**2.4 S)**, [Au_4(μ_4-Se)(μ-dbfdp)$_2$](OTf)$_2$ **(2.4 Se)**, [Au_6(μ_3-S)$_2$(μ-dbfdp)$_3$ **(2.5 S)** and [Au_6(μ_3-Se)$_2$(μ-dbfdp)$_3$] **(2.5 Se)**. A full analysis of their molecular structure and their photophysical properties was conducted.

2.2 Results and Discussion

2.2.1 Synthesis and Characterization of [(Au$_2$S)(μ-dbfdp)] (2.3 S), [(Au$_2$Se)(μ-dbfdp)] (2.3 Se)

Given that phosphine ligated metal salts react with chalcogen with -SiMe$_3$ moieties, [(AuOAc)$_2$(μ-dbfdp)] **(2.1)** and [(AuOTf)$_2$(μ-dbfdp)] **(2.2)** represent excellent starting points for the preparation of gold chalcogenido- complexes which contain the DBFDP ligand. The synthesis of complexes **(2.3 S)** and **(2.3 Se)** were carried out by adding 1.0 equivalent of E(SiMe$_3$)$_2$ (E = S, Se) to solutions of [(AuOAc)$_2$(μ-dbfdp)] **(2.1)** in DCM.

The syntheses of compounds **(2.4 S)** and **(2.5 S)** were initially carried out by adding 0.3 equivalents of [Cu(NCCH$_3$)$_4$]OTf to solutions of **(2.3 S)** in DCM. Synthesis of **(2.4 Se)** and **(2.5 Se)** were carried out in a similar fashion with **(2.3 Se)**. Aside from generating the bulk material (Cu$_2$E) during the reaction, it was hypothesized that the copper (I) atom does not play a large role in this reaction; thus, to confirm such, the previously mentioned synthesis of **(2.4 S)**, **(2.5 S)**, **(2.4 Se)** and **(2.5 Se)** were performed by adding 0.5 equivalents of [(AuOTf)$_2$(μ-dbfdp)] **(2.2)** as the source of OTf$^-$. In both methods, the Au$_4$E and Au$_6$E (E = S, Se) clusters were obtained as a mixture as crystalline material. These syntheses are depicted in *Scheme 2.1*.

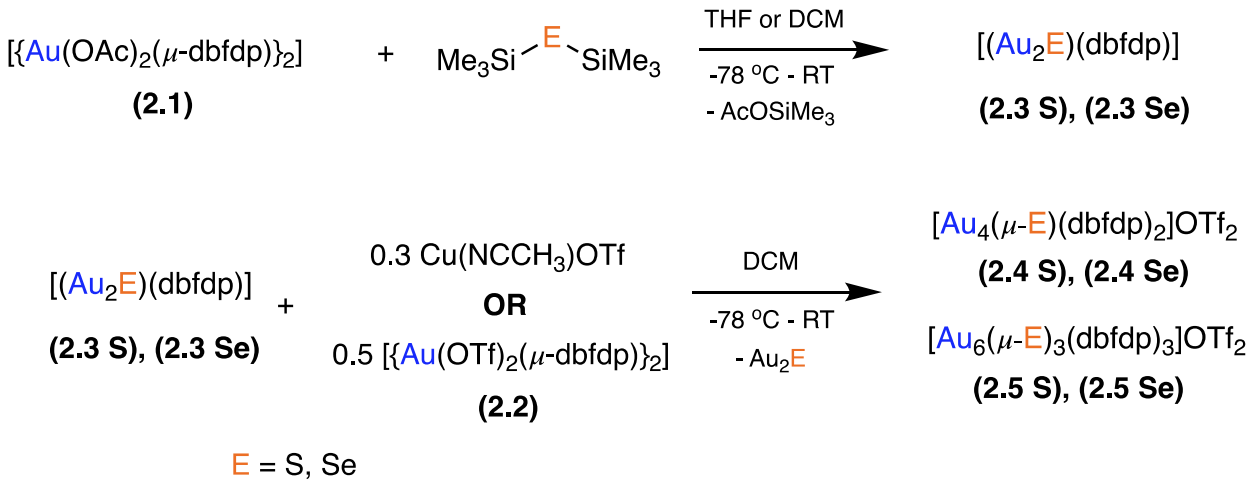

*Scheme 2.1: General synthetic schematic of group 11 metal chalcogenide clusters **(2.3 S/Se), (2.4 S/Se)** and **(2.5 S/Se).***

As previously mentioned, the reactions between [(AuCl)$_2$(μ-dbfdp)$_2$] **(I.XXXI)** and E(SiMe$_3$)$_2$, though generated the desired products, was determined to be unselective as another species was formed.[19] The next logical step was to attempt to have a more selective reaction with [(AuOAc)$_2$(μ-

dbfdp)] **(2.1)**. The addition of AgOAc to [(AuCl)$_2$(μ-dbfdp)$_2$] **(I.XXXI)**, results in a metathesis reaction yielding AgCl and the desired [(AuOAc)$_2$(μ-dbfdp)] **(2.1)**.[20] The resulting solution was filtered over Celite® to remove the precipitated AgCl. The solution was concentrated in *vacuo*, then layered with heptane as a counter solvent. This resulted in **(2.1)** being isolated as slightly orange-coloured plates in 47 % yield.

The $^{31}P\{^{1}H\}$ NMR spectrum of [(AuOAc)$_2$(μ-dbfdp)] **(2.1)** shows a chemical shift to lower frequency to 18.9 ppm as compared to [(AuCl)$_2$(μ-dbfdp)$_2$] **(I.XXXI)** at 24.0 ppm. The low frequency shift could be attributed to the presence of a lower density electron cloud when going from chloride to acetate in **(2.1)**.

The molecular structure of **(2.1)** was determined by single crystal X-ray diffraction as seen in *Figure 2.3*. Complex **(2.1)** crystallizes in the triclinic space group $P\bar{1}$ and a Z of 2. Complex **(2.1)** contains the bridging DBFDP phosphine ligands attached to 2 AuOAc moieties. When compared to [{Cu(μ-κO-OAc)(μ-dbfdp)}$_2$] **(II.VI)** and [{Ag(μ-κO-OAc)(μ-dbfdp)}$_2$] **(II.VII)**, in which the acetates has a bridging bonding mode, the acetates in complex **(2.1)** exhibit a terminal coordination.[18,19]

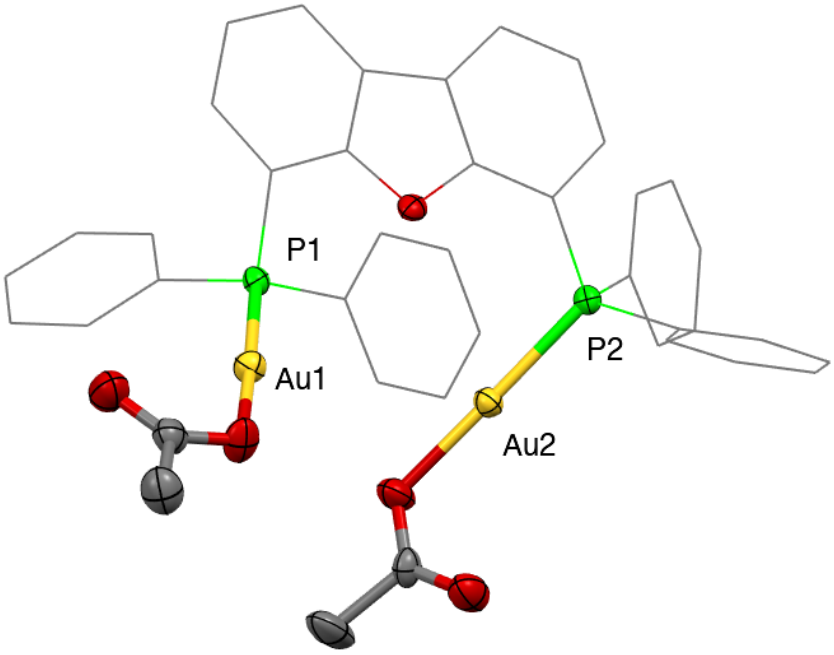

*Figure 2.3: Molecular structure of [(AuOAc)$_2$(μ-dbfdp)] (**2.1**) in the crystal.*

The synthesis of complex **(2.3 S)** occurs in a similar fashion when using either [$(AuCl)_2$(μ-dbfdp)$_2$] **(I.XXXI)** or [$(AuOAc)_2$(μ-dbfdp)] **(2.1)**. The addition of 1.0 equivalent of $S(SiMe_3)_2$ was carried out at -78 °C in THF; the reaction proceeded from a clear colourless solution to a cloudy, colourless solution. The progression of the reaction was monitored using the change in luminescence with a handheld UV lamp. Interestingly, following the addition of the chalcogen reagent, a significant change in luminescence occured, turning bright green then proceeding to a teal colour as the reaction warmed from -78 °C. The THF was subsequently removed *in vacuo*, and all contents of the reaction flask were solubilized in DCM. The reaction was then layered with heptane as a counter solvent and colourless block crystals of **(2.3 S)** formed after 3 days (yield: 41 %). Single crystal X-ray diffraction was used to confirm the formation of [(Au_2S)(μ-dbfdp)] **(2.3 S)**.

The $^{31}P\{^1H\}$ NMR spectrum of the crystals of **(2.3 S)** in CD_2Cl_2 shows a chemical shift at 19.9 ppm ($W_{1/2}$ = 10 Hz), indicating most phosphorus atoms in the sample were in the same environment. However, a small impurity peak at 18.0 ppm is identified which likely results from the phosphorus sulfide side product, resulting in a higher frequency shift when compared to the free phosphine. This shift is also characteristic in PPh_3 when it forms the phosphorus sulfide.[21] This is consistent with the ^1H NMR spectrum as there are small unknown impurities at 8.05 ppm, 7.04 ppm, and 1.58 ppm. Compared to **(2.1)**, the ^1H NMR spectrum of **(2.3 S)** both have a doublet at approximately 8.17 ppm. However, the multiplet of **(2.3 S)** (*δ*: 7.21-7.53) and the doublet of doublets (*δ*: 6.90) is shifted to a lower frequency likely due to the higher electron density from the sulfur in the molecule.

The single crystal X-ray diffraction analysis confirmed the molecular structure of **(2.3 S)** which contains the DBFDP phosphine bridging the two gold (I) atoms *(Figure 2.4)*. Compound **(2.3 S)** crystallizes in the space group C2/c with a Z of 8. Notably, the Au···Au distance (2.9558(7) Å) falls within the acceptable range of aurophilic interactions which may indicate the possibility of a metallophilic 'bond'. Compared to $[S(AuPPh_3)_2]\cdot CH_2Cl_2$ **(II.VIII)** reported by Lensch and co-workers, the Au-S-Au bonds in a bent fashion with an angle of 88.7 °, similar to 80.03 ° in compound **(2.3 S)**.[22] The smaller distance between Au (I) atoms in compound **(2.3 S)** may be due to a more rigid ligand as compared to 2 separate PPh_3 ligands in the literature compound.[22] Furthermore, in **(2.3 S)**, the Au···Au distance falls within the range predicted for aurophilic

interactions at 2.9558(7) Å compared to [S(AuPPh$_3$)$_2$] **(II.VIII)** which has a Au···Au distance of 3.018(1) Å.

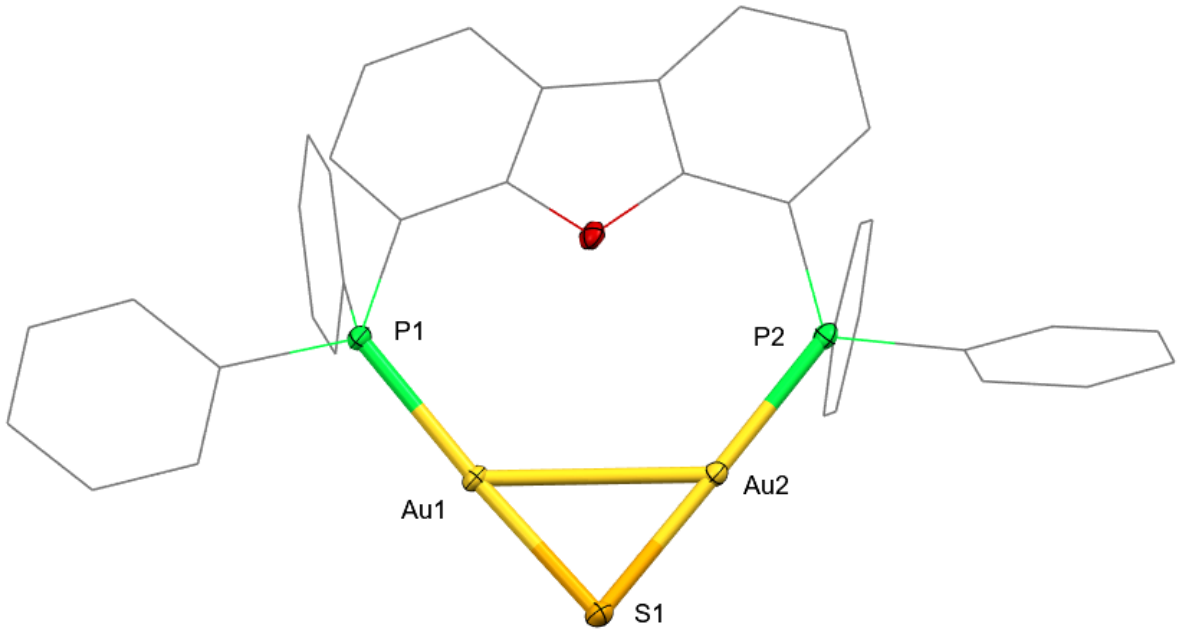

*Figure 2.4: Molecular structure of [(Au$_2$S)(μ-dbfdp)] (**2.3 S**) in the crystal (Au – S: 2.298(2) – 2.299(1) Å, Au – P: 2.253(2) – 2.254(1) Å, Au···Au: 2.9558(7) Å) (H atoms are omitted for clarity).*

Complex **(2.3 Se)** was synthesized by adding 1.0 equivalent of Se(SiMe$_3$)$_2$ to [(AuOAc)$_2$(μ-dbfdp)] **(2.1)** at -78 °C in THF. As the reaction warmed to room temperature, there was no change in the colour of the solution, however the presence of a blue emitting solid was observed. THF was removed *in vacuo*, the contents of the flask were solubilized in DCM and the solution of **(2.3 Se)** in CH_2Cl_2 displayed a yellow luminescence. The reaction solution was layered with heptane which led to crystallization of colourless needles and colourless blocks (which was an issue discussed in previously conducted research).[19] Both crystal morphologies were attempted to be solubilized in $CDCl_3$, however, a colourless, orange emissive, amorphous solid precipitated upon addition of solvent. Thus, $^{31}P\{^1H\}$ NMR and ^1H NMR spectra were obtained using CD_2Cl_2.

Through single crystal X-ray diffraction analysis, it was determined that the blocks were compound **(2.3 Se)** which crystallized in the space group $P\bar{1}$ with a Z of 2. Similar to compound **(2.3 S)**, the two Au (I) centres are bridged by the DBFDP phosphine ligands as well as the chalcogen atom *(Figure 2.5)*. The gold centres exhibit linear geometry with the selenium having

an Au-Se-Au angle of 76.15(1) ° as compared to the 79.35(5) ° as seen in compound **(2.3 S)**. Again, there is an indication of aurophilic interactions between the two gold (I) atoms present in the molecule with a Au···Au distance of 2.9748(4) Å which falls into the acceptable range of aurophilic interactions.[14] Unfortunately, the needles in the sample were too small to be analyzed via single crystal X-ray diffraction, thus to confirm synthesis of a singular product, NMR analysis was conducted.

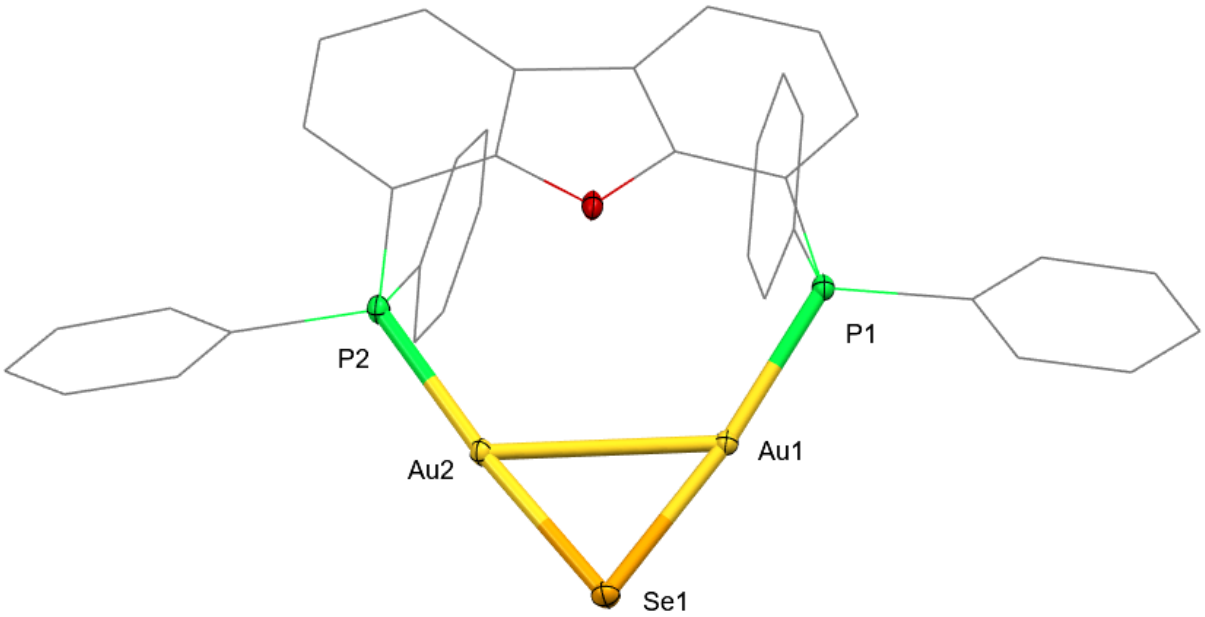

Figure 2.5: Molecular structure of [(Au_2Se)(μ-dbfdp)] ***(2.3 S)*** *in the crystal (Au – Se: 2.4086(3) – 2.4152(5) Å, Au – P: 2.2638(8) – 2.2647(6) Å, Au···Au: 2.9748(4) Å) (H atoms are omitted for clarity).*

Given the unexpected observation of two different crystal types, it was hypothesized that two distinct signals would be observed in the $^{31}P\{^{1}H\}$ NMR spectrum if there were indeed two different compounds (blocks and needles). However, the mixture of needles and blocks of compounds **(2.3 Se)** showed a single chemical shift at 22.7 ppm, which is a shift to higher frequency when compared to the chemical shift of **(2.1)** at 18.9 ppm. This high frequency chemical shift is likely due to the presence of the chalcogen in the compound and indicates that in solution, there is a homogenous [(Au_2Se)(μ-dbfdp)] product. A similar trend observed in compound **(2.3 S)** is also observed in the ^{1}H NMR spectrum of compound **(2.3 Se),** where the doublet at 8.18 ppm and the

multiplet and doublet of doublet is shifted to a lower frequency. This is likely due to the chalcogenide present in the complex.

As compared to chloride moieties of $[(AuCl)_2(\mu\text{-dbfdp})_2]$ **(I.XXXI)** discussed by Laguna, the acetate groups of compound **(2.1)** also coordinates terminally.[20] Additionally, the molecule also adopts an anion (e.g. chloride/acetate) to gold ratio of 1:1. However, the acetate interestingly does not possess emission properties at ambient temperatures in the visible range, whereas $[(AuCl)_2(\mu\text{-dbfdp})_2]$ **(I.XXXI)** is reported to be weakly emissive at 420 nm.[20]

In regard to structure, compounds **(2.3 S)** and **(2.3 Se)** resemble general frameworks proposed in previously known gold – chalcogenide complexes with a gold:chalcogen ratio of 2:1.[6] The compounds **(2.3 S**) and **(2.3 Se)** adopt a two-dimensional triangular shape with a bridging chalcogenide similar to previously discussed frameworks. The DBFDP ligand provides additional structural rigidity to the compound and holds the two golds in place alongside the chalcogenide.

2.2.2 Synthesis and Characterization of $[(AuOTf)_2(\mu\text{-dbfdp})]$ (2.2), $[Au_4(\mu_4\text{-S})(\mu\text{-dbfdp})_2](OTf)_2$ (2.4 S), $[Au_4(\mu_4\text{-Se})(\mu\text{-dbfdp})_2](OTf)_2$ (2.4 Se), $[Au_6(\mu_3\text{-S})_2(\mu\text{-dbfdp})_3](OTf)_2$ (2.5 S) $[Au_6(\mu_3\text{-Se})_2(\mu\text{-dbfdp})_3](OTf)_2$ (2.5 Se)

As an attempt to synthesize a higher nuclearity gold (I) homometallic or heterometallic Cu (I)/Au (I) cluster, $[Cu(NCCH_3)_4]OTf$ was added as a possible soluble metal source (without the involvement of a second phosphine). To synthesize $[Au_4(\mu_4\text{-S})(\mu\text{-dbfdp})_2](OTf)_2$ **(2.4 S)** and $[Au_6(\mu_3\text{-Se})_2(\mu\text{-dbfdp})_3](OTf)_2$ **(2.5 Se)**, $[Cu(NCCH_3)_4]OTf$ was added respectively to compounds **(2.3 S)** and **(2.3 Se)** in a 1:3 ratio. For **(2.4 S)**, compound **(2.3 S)** was solubilized in DCM and cooled to -78 °C, which yielded a clear, colourless solution with a teal emission when examined with a handheld UV lamp. Subsequent addition of $[Cu(NCCH_3)_4]OTf$ resulted in a clear, red, non-emissive solution. This clear, red solution was layered with hexanes which yielded pale yellow crystals. Similarly, compound **(2.5 Se)** was synthesized by adding **(2.3 Se)** to $[Cu(NCCH_3)_4]OTf$ at a 3:1 ratio. The reaction solution proceeded from a yellow emissive, clear, colourless solution to a dark red, clear solution which was also non-emissive. The resulting clear solution was layered and this yielded pale yellow/orange-coloured crystals. With the addition of a triflate source, it is hypothesized that 1 equivalent of Au_2E (E = S, Se) is eliminated. The elimination of the Au_2E results in the formation of a cationic cluster core which requires the OTf^- counterion.

Compound **(2.2)** was synthesized as an alternative triflate source and method to target the Au_4S **(2.4 S)** and Au_6Se **(2.5 Se)** clusters without the use of CuOTf. Similar to the synthesis of $[(AuOAc)_2(\mu\text{-dbfdp})]$ **(2.1)**, $[(AuCl)_2(\mu\text{-dbfdp})]$ **(I.XXXI)** was stirred with 2.0 equivalents of AgOTf. This resulted in a colourless solid which displayed a chemical shift of 15.7 ppm in the $^{31}P\{^1H\}$ NMR spectrum and -77.2 ppm in the $^{19}F\{^1H\}$ NMR spectrum. Addition of compound **(2.2)** to **(2.3 S)** resulted in a clear colourless solution which slowly resulted in a red solution and a loss of emissive properties. Similarly, addition of **(2.2)** to **(2.3 Se)** also resulted in a clear, non-emissive dark red solution. These solutions were layered with hexanes respectively to yield pale yellow **(2.5 S)** and colourless crystals **(2.4 Se)**.

As determined by single crystal X-ray diffraction, compound **(2.4 S)** crystallizes in the space group $P\bar{1}$ and has a Z of 2. The sulfide atom possesses a μ_4 coordination geometry and bridges 4 gold atoms. The four gold atoms are ligated by two DBFDP ligands which act as a bridge between two individual gold (I) centres. Two OTf^- moieties act as anions for the cationic cluster shown in *Figure 2.6*. The core of **(2.4 S)** can be viewed as a distorted square based pyramid formed by the 4 gold (I) centres and the sulfur centre at the apex. All gold atoms exhibit near-linear coordination geometry which ranges from 166.6(2) ° to 177.7(2) °. Additionally, the gold (I) atoms within the cluster indicate evidence for aurophilicity with bond distances ranging from 2.777(4) Å - 2.935(2) Å with distances between two gold atoms all falling under 3.5 Å, the accepted range for an aurophilic interaction.[14,15] However, it is to be noted that crystals of **(2.4 S)** were highly twinned and weakly diffracting, which may explain the disorder on the Au(4) centre.

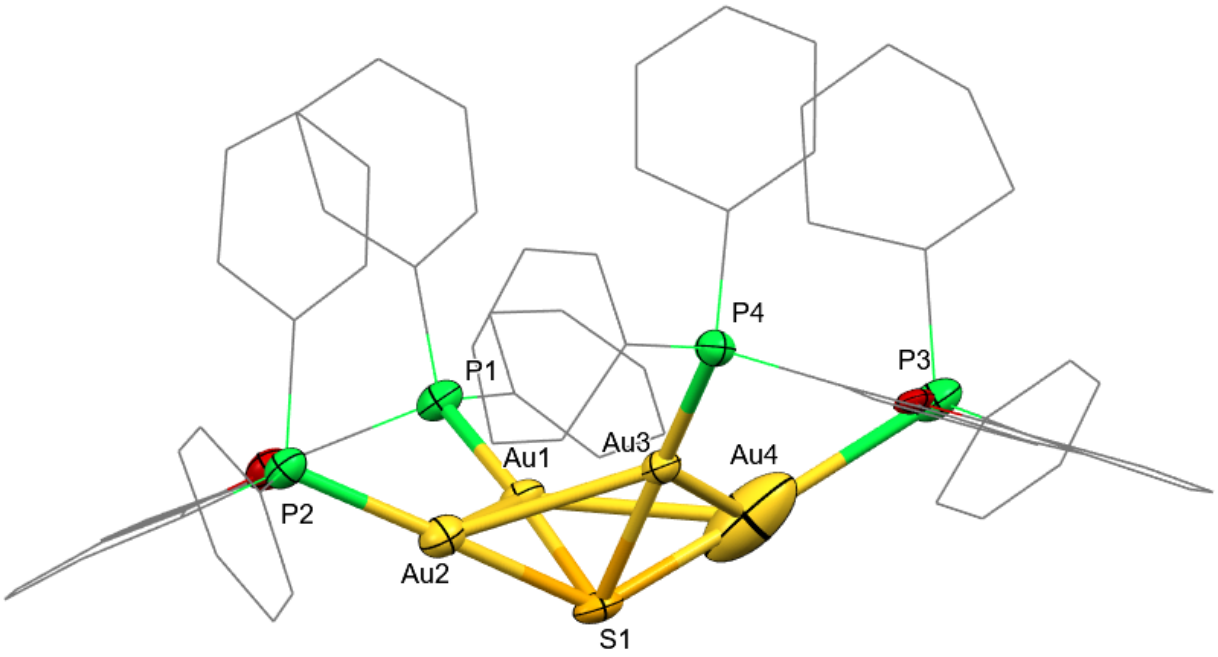

*Figure 2.6: Molecular structure of $[Au_4(\mu_4\text{-}S)(\mu\text{-}dbfdp)_2]^{2+}$unit in (**2.4 S**) in the crystal (Au – S: 2.353(5) – 2.426(6) Å, Au – P: 2.257(6) – 2.871(7) Å, Au···Au: 2.777(4) – 2.935(3) Å) (H atoms and OTf^- anions omitted for clarity).*

Compound **(2.5 Se)** crystallizes in the space group C 2/c and has a Z of 8. The selenide atoms within the cluster bridges 3 gold centres per selenide. This $(Au_3E)^+$ subunit has been well documented in many clusters such as $[E(AuPPh_2CH_2\text{-}CH_2py)_3]BF_4$ **(II.IX)**[23], $[(E(AuPPh_2py)_3]BF_4$ **(II.X)**[23] and $[Au_6(Ph_2PN(CH_3)PPh_2)(\mu_3\text{-}S)]Cl_2$ **(II.XI)**[24] as reported by Villacampa and Yam. The two individual $(Au_3E)^+$ are bridged by suggested aurophilic interactions between Au(1) and Au(1) as well as the two P3 atoms in the DBFDP ligand (*Figure 2.7)*, which links two gold (I) centres (Au(3) and Au(3)), one each from the individual $(Au_3E)^+$ subunits. The molecule resides about a crystallographic inversion centre with each $(Au_3E)^+$ subunit taking shape of a triangular based pyramid.

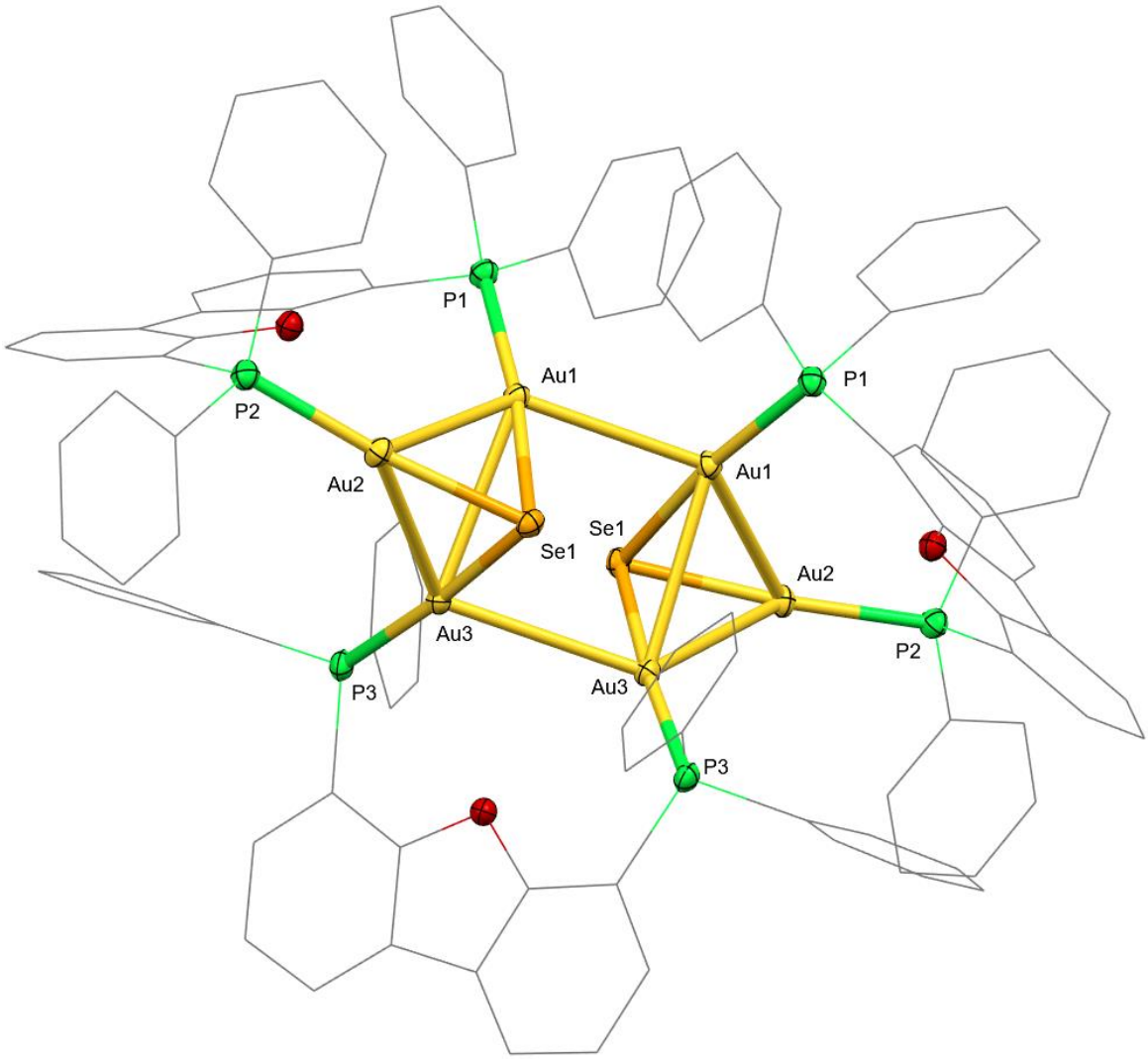

*Figure 2.7: Molecular structure of $[Au_6(\mu_3\text{-}Se)_2(\mu\text{-}dbfdp)_3]^{2+}$ unit in (**2.5 Se**) in the crystal (Au – Se: 2.432(1) Å – 2.477(1) Å, Au···Au: 3.0473(8) Å – 3.1844(9) Å) (H atoms and OTf^- anions omitted for clarity). (The molecule resides about a 2-fold rotation axis which bisects Au(1)/Au(1')/Au(3)/Au(3')).*

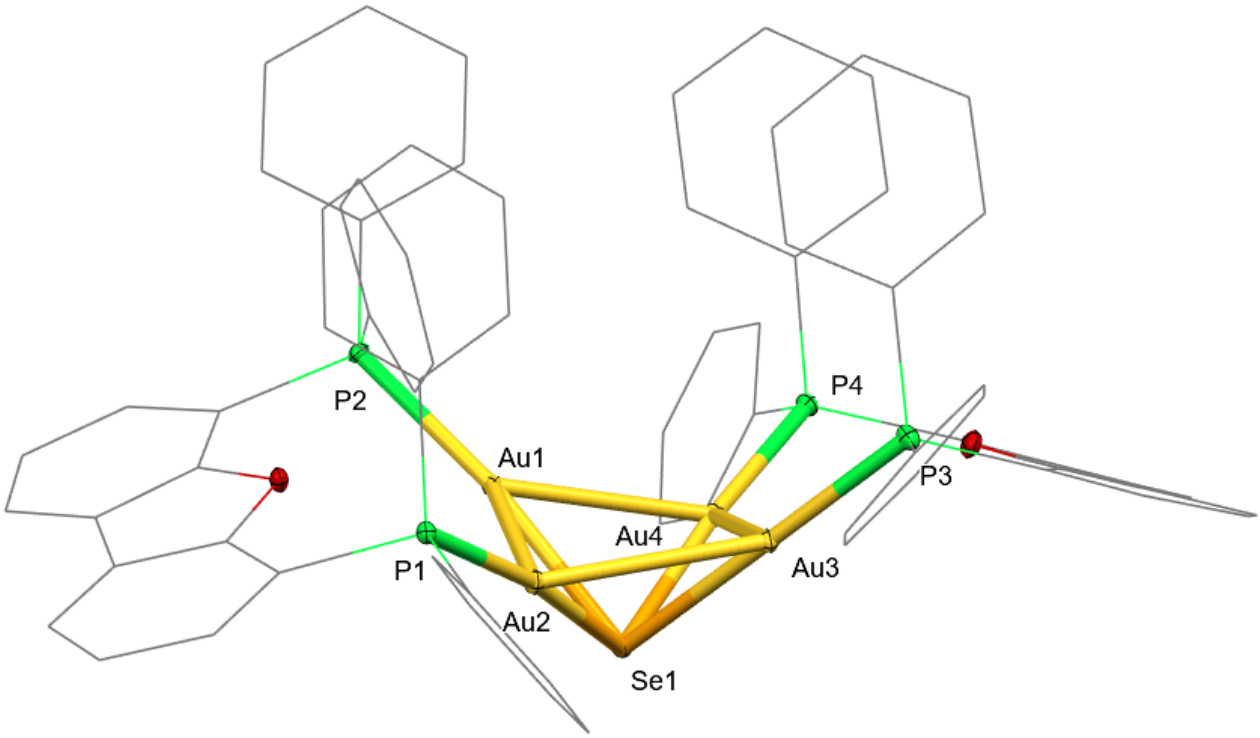

*Figure 2.8: Molecular structure of $[Au_4(\mu_4\text{-}Se)(\mu\text{-}dbfdp)_2]^{2+}$ unit in (**2.4 Se**) in the crystal (Au - Se: 2.353(5) – 2.426(6) Å, Au – P: 2.257(6) – 2.871(7) Å, Au···Au: 2.777(4) – 2.935(3) Å) (H atoms and OTf^- anions and omitted for clarity).*

The molecular structure of **(2.4 Se)** very closely resembles the molecular structure of **(2.4 S)**, with the same square based pyramid structure (*Figure 2.8).* Compound **(2.4 Se)** crystallizes in the space group $P\bar{1}$. All gold (I) atoms have a linear coordination geometry and form a square based pyramid with the chalcogen at the apex. It is composed of 2 DBFDP-Au_2 units linked together by one Se atom.

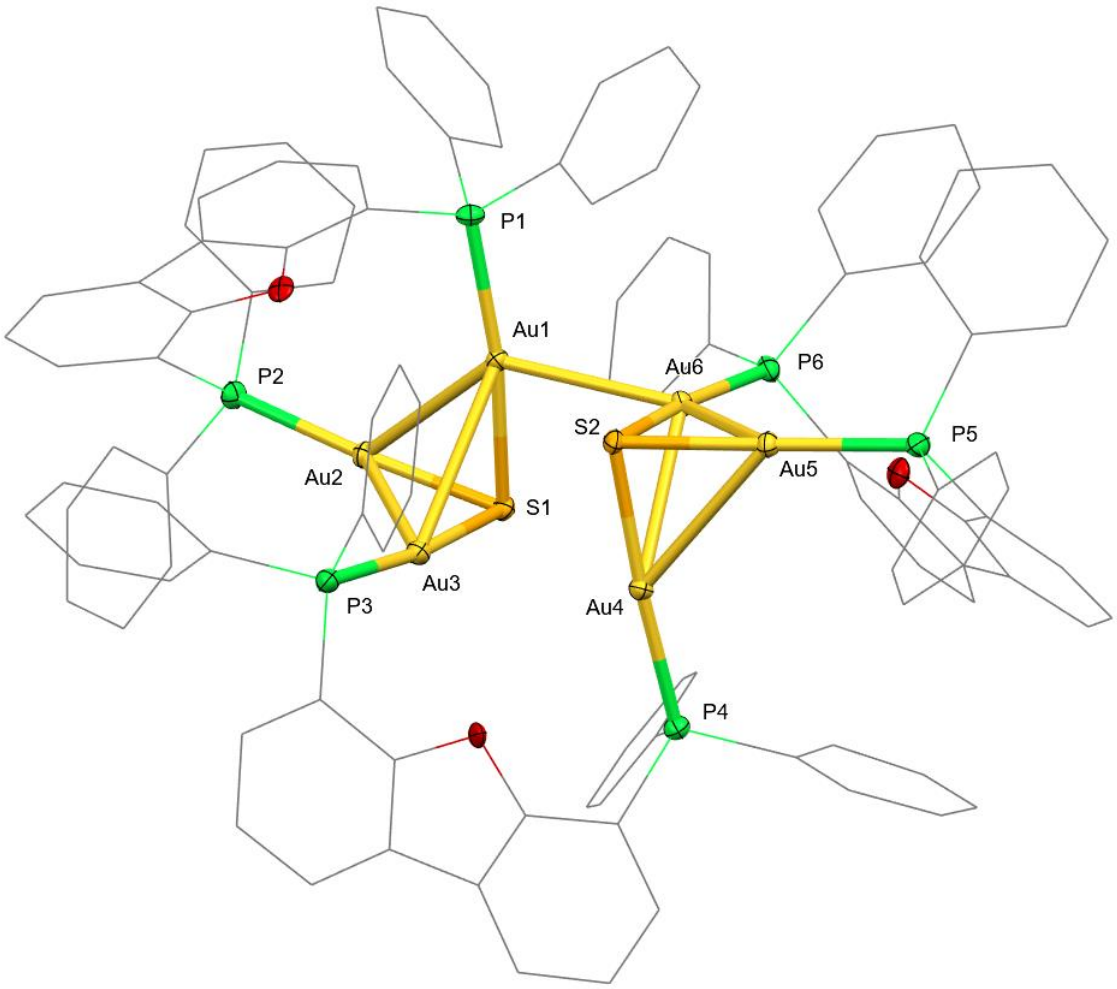

*Figure 2.9: Molecular structure of $[Au_6(\mu_3\text{-}Se)_2(\mu\text{-}dbfdp)_3]^{2+}$ unit in (**2.5 S**) in the crystal (Au – S: 2.316(4) – 2.363(4) Å, Au Au: 2.9241(7) – 3.577(1) Å) (H atoms and OTf^- anions and omitted for clarity).*

Compound **(2.5 S)** was synthesized by reacting **(2.2)** with **(2.3 S)**. It was initially hypothesized that cluster **(2.4 S)** could be targeted with a triflate source other than CuOTf. However, the molecular structure of **(2.5 S)** showed a structure similar to **(2.5 Se)** with 2 $(Au_3Se)^+$ subunits being bridged by a DBFDP phosphine and a potential aurophilic interaction (*Figure 2.9)*. Compound **(2.5 S)** crystallizes in the space group $P2_1/c$ with a Z of 4. When comparing the metal-chalcogen core of compounds **(2.5 S)** and **(2.5 Se)** (*Figure 2.10)*, although they are generally similar, there are key differences which are present. For **(2.5 Se)**, the Au···Au distances fall between 3.051 Å – 3.213 Å

which is within the threshold for aurophilic interactions. In compound **(2.5 S)**, one of the gold-gold distances between the two $(Au_3Se)^+$ subunits fall within range of the aurophilic interactions at 2.924 Å and the other falling outside the range at 3.577 Å. It is interesting to note that Au(4) and Au(5) in compound **(2.5 S)** are distorted compared to the analogous Au(3) and Au(3') in compound **(2.5 Se)**. This may be due difference in sizes between the chalcogens.

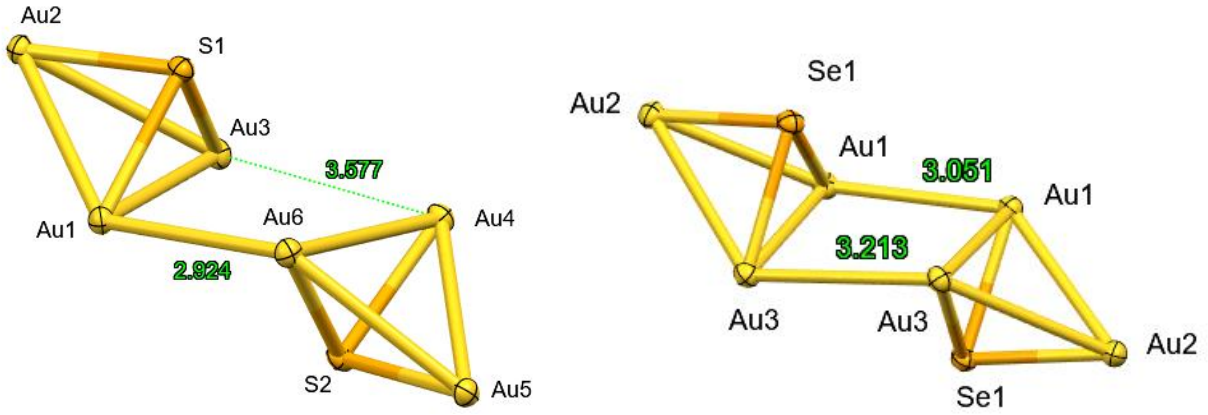

Figure 2.10: Cluster core of $[Au_6(\mu_3\text{-}S)_2(\mu\text{-}dbfdp)_3]^{2+}$ ***(2.5 S)*** *(left) and $[Au_6(\mu_3\text{-}Se)_2(\mu\text{-}dbfdp)_3]^{2+}$* ***(2.5 Se)*** *(right) in the crystal. The core of compound* ***(2.5 S)*** *is distorted which may explain the reason behind the absence of a potential aurophilic interaction seen in* ***(2.5 Se)****.*

From energy-dispersive X-ray analysis as well as mass spectrometry, it was confirmed compounds **(2.4 S)** and (**2.5 S)** both co-crystallized. This was also confirmed to be the case for **(2.4 Se)** and **(2.5 Se)**. When examining the crystalline samples of the reaction between $[Cu(NCCH_3)_4]OTf$ and **(2.3 S**), the mass spectrum displayed m/z peaks at 1429.1005 and a small m/z at 946.0741. When the mass spectrum was deconvoluted, both peaks indicated a 2+ charge which is characteristic of both $[Au_4(\mu_4\text{-}S)(\mu\text{-}dbfdp)_2]^{2+}$ **(2.4 S)** and $[Au_6(\mu_3\text{-}S)_2(\mu\text{-}dbfdp)_3]^{2+}$ **(2.5 S)**. Other peaks in the spectrum are fragments of either cluster (m/z = 1687: $[(DBFDP)_2(Au_3S)]^+$ m/z = 2042: $[M\text{-}OTf]^+$; m/z = 2122: $[M\text{-}IO_3]^+$) (*Figure 2.11 a and b*). From the energy-dispersive X-ray analysis, it was confirmed that there were different species with various Au:S ratios (characteristic of both **(2.4 S)** and the higher nuclearity **(2.5 S)**. Consequently, when examining the $^{31}P\{^1H\}$ NMR spectrum of the crystalline sample, 4 signals at 23.3 ppm, 19.9 ppm, 18.1 ppm and 14.2 ppm were observed. The peak at 19.9 ppm could be attributed to starting material **(2.3 S)**, which may indicate that the reaction did not proceed to completion. The chemical shifts at 19.9 ppm and 18.1 are attributed to compound **(2.4 S)** and **(2.5 S)**, however, these signals could not be individually assigned as these

compounds co-crystallized and proved difficult to separate (*Figure 2.12 a and b)*. Similar observations were obtained when the crystalline material of the reaction between [$(AuOTf)_2$(μ-dbfdp)] **(2.2)** and **(2.3 Se)** were obtained where the $^{31}P\{^1H\}$ NMR spectrum, mass spectrometry and EDX analysis all show a mixture of products **(2.4 S)** and **(2.5 S)**.

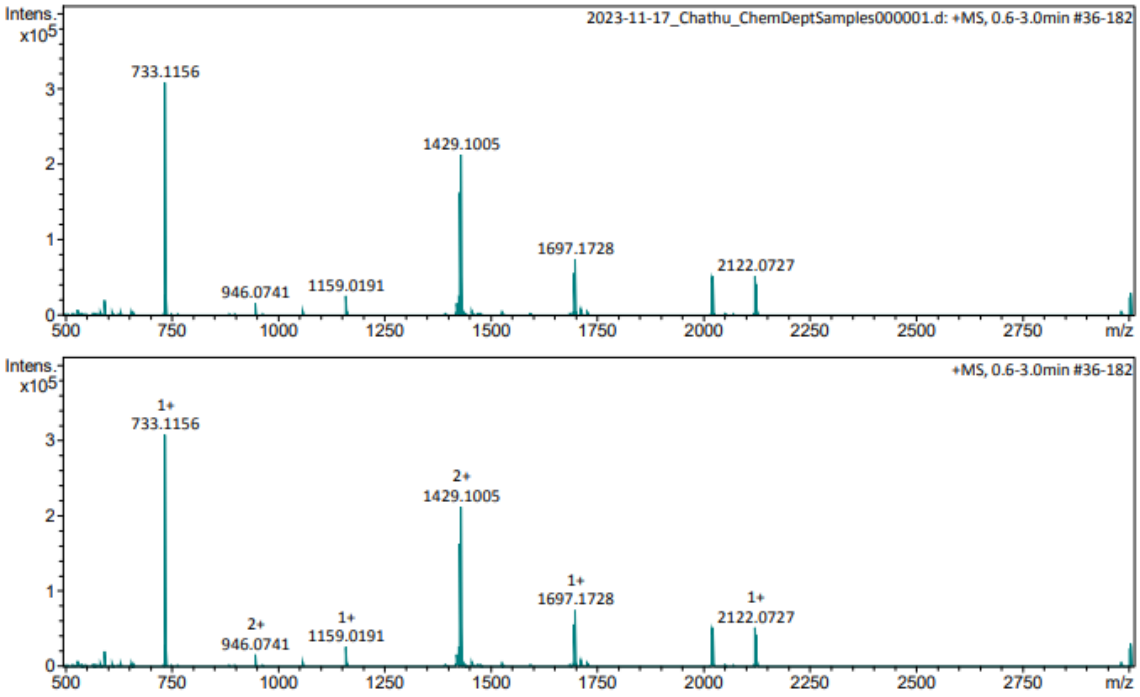

*Figure 2.11: a) Mass spectrum of crystalline material obtained from reaction between [$(Cu(NCCH_3)_4]OTf$ and (**2.3 S**). b) Deconvoluted mass spectrum of crystalline material obtained from reaction between [$(Cu(NCCH_3)_4]OTf$ and (**2.3 S**). Comparison of experimental spectra and predicted spectra indicate evidence of an unknown 3rd impurity. This impurity may contribute to the experimental m/z of 1429.1005 vs. calculated m/z of 1427.5922.*

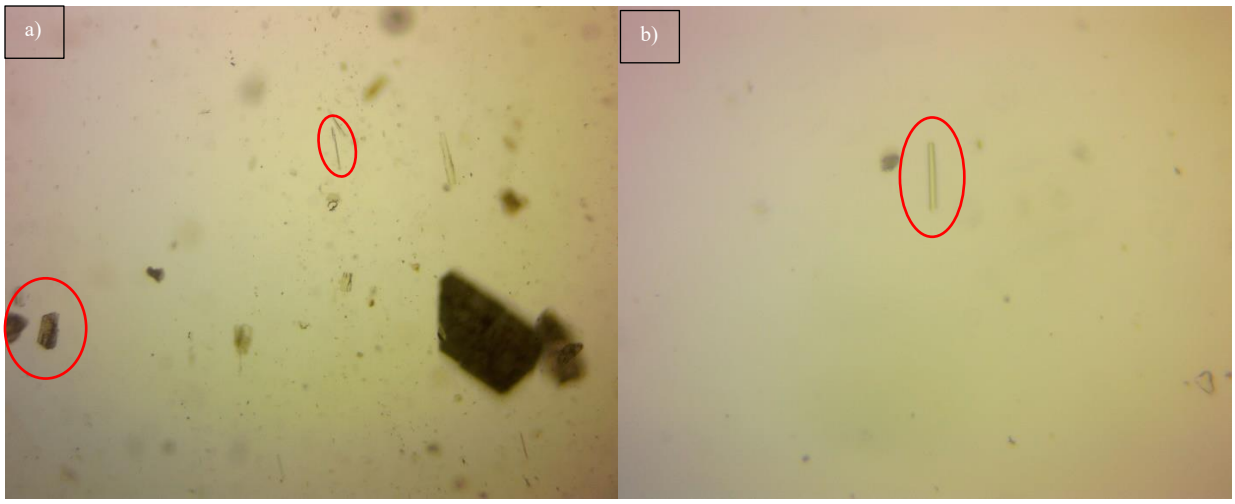

*Figure 2.12: a) Crystalline sample of mixture of **(2.4 S)** and **(2.5 S)** depicting different crystal morphologies within the sample with magnification 40x. b) Magnified picture of one of the crystal morphologies found in the sample mixture of **(2.4 S)** and **(2.5 S)** at 125x.*

Similarly, there was evidence that compounds **(2.4 Se)** and **(2.5 Se)** also co-crystallized. The mass spectrum of crystalline samples of the reaction between $[(Cu(NCCH_3)_4]OTf$ and **(2.3 Se)** indicated a mixture of the compounds **(2.4 Se)** and **(2.5 Se)**. Peaks indicate fragments of clusters $[Au_4(\mu_4\text{-}Se)(\mu\text{-}dbfdp)_2]^{2+}$ **(2.4 Se)** (m/z = 907.0425) and $[Au_6(\mu_3\text{-}Se)_2(\mu\text{-}dbfdp)_3]^{2+}$ **(2.5 Se)** (m/z = 1476.5450) as well as other fragments (m/z = 1743: $[(DBFDP)_2(Au_3Se)]^+$; m/z = $[M\text{-}I]^+$) *(Figure 2.13 a* and *b)*. Additionally, examining the electron-dispersive X-ray analysis confirms the existence of a mixture species with Au:S ratio of (3:1 and 4:1; i.e. compounds **(2.4 Se** and **2.5 Se)**. The $^{31}P\{^1H\}$ NMR spectrum of the crystalline sample acquired from the reaction between $[Cu(NCCH_3)_4]OTf$ and **(2.3 Se**), displays 2 signals at 22.6 ppm and 19.9 ppm. These two peaks could be attributed to both compounds **(2.4 Se)** and **(2.5 Se)**, however these signals were not able to be individually assigned due to co-crystallization. Similar observations were obtained when the crystalline material of the reaction between $[(AuOTf)_2(\mu\text{-}dbfdp)]$ **(2.2)** and **(2.3 Se)** were obtained where the $^{31}P\{^1H\}$ NMR spectrum, mass spectrometry and EDX analysis all show a mixture of products **(2.4 Se)** and **(2.5 Se)**.

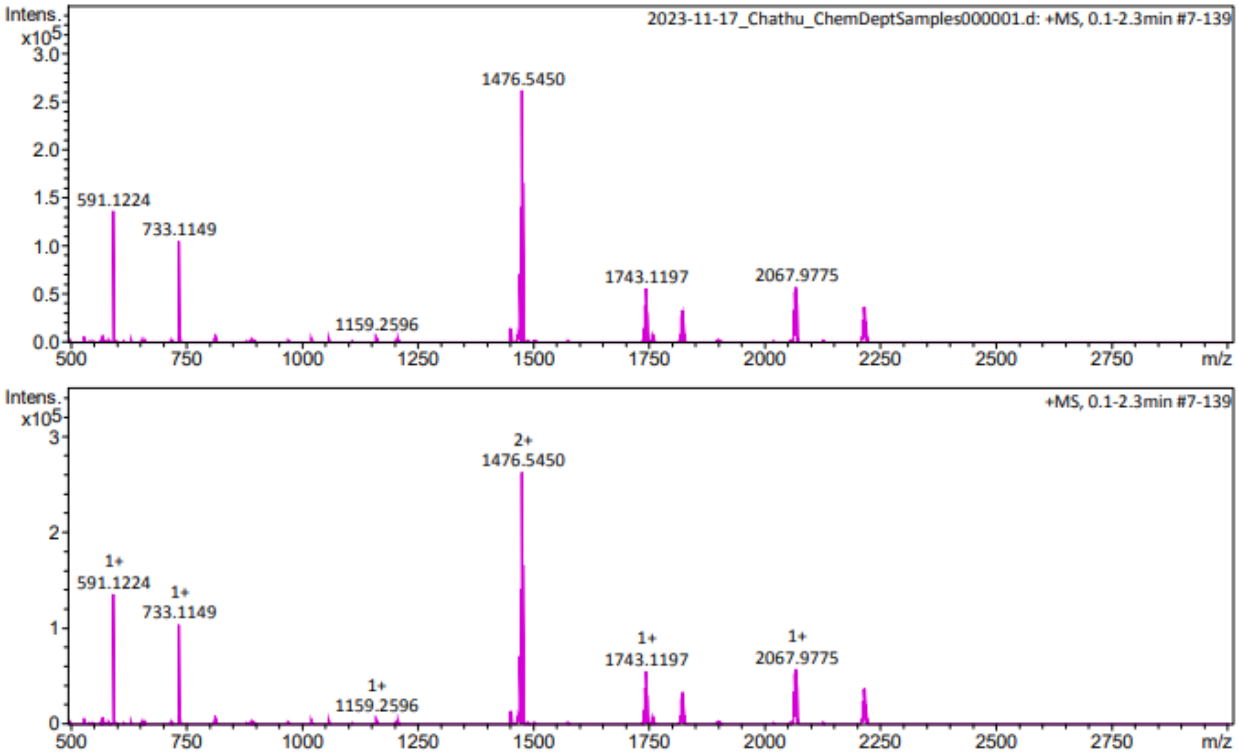

Figure 2.13: a) Mass spectrum of crystalline material obtained from reaction between [(Cu(NCCH$_3$)$_4$]OTf and ***(2.3 Se)****. b) Deconvoluted mass spectrum of crystalline material obtained from reaction between [(Cu(NCCH$_3$)$_4$]OTf and* ***(2.3 Se)****. Comparison of experimental spectra and predicted spectra indicate evidence of an unknown 3rd impurity. This impurity may contribute to the experimental m/z of 1476.5450 vs. calculated m/z of 1475.5363.*

2.2.3 Photophysical Properties of [(Au$_2$S)(μ-dbfdp)] (2.3 S), [(Au$_2$Se)(μ-dbfdp)] (2.3 Se), [Au$_4$(μ$_4$-S)(μ-dbfdp)$_2$](OTf)$_2$ (2.4 S), [Au$_4$(μ$_4$-Se)(μ-dbfdp)$_2$](OTf)$_2$ (2.4 Se), [Au$_6$(μ$_3$-S)$_2$(μ-dbfdp)$_3$](OTf)$_2$ (2.5 S) and [Au$_6$(μ$_3$-Se)$_2$(μ-dbfdp)$_3$](OTf)$_2$ (2.5 Se)

It is well documented that DBFDP plays a role in enhancing luminescent properties of stable group 11 metal chalcogenide clusters.[18,19] DBFDP demonstrates the ability to bridge two d^{10} metal centres and results in efficient PLQY's of copper and silver chalcogenide clusters. In this vein of research, Corrigan and co-workers have observed the reaction solution of [(Au$_2$S)(μ-dbfdp)] **(2.3 S)** and [(Au$_2$Se)(μ-dbfdp)] **(2.3 Se)** to be emissive, however were not able to produce the complexes purely.[19] Therefore, during the synthesis of **(2.3 S/Se)**, **(2.4 S/Se)** and **(2.5 S/Se)**, reactions were irradiated with a handheld UV lamp (λ = 254 nm and 365 nm) to inspect for luminescent behaviours displayed during the reaction. It was observed that compounds **(2.1)** and

(2.2) were not emissive when irradiated with the UV lamp. Interestingly, upon addition of the chalcogen ($E(SiMe_3)_2$) reagents, compounds **(2.3 S)** and **(2.3 Se)** exhibited luminescent behaviour. It is important to note that compounds **(2.3 S)** and **(2.3 Se)** were briefly studied in previous work done by Corrigan and co-workers, and UV-visible absorption data were collected. Herein, the emission data for compounds **(2.3 S/Se), (2.4 S/Se)** and **(2.5 S/Se)** are presented below.

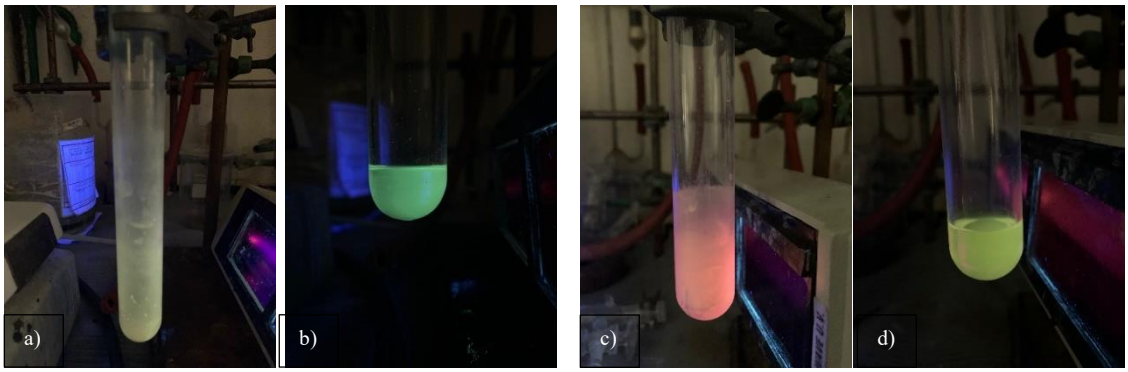

*Figure 2.14: Solid state luminescence of **(2.3 S)** after (a) removal of $CDCl_3$ and (b) solution state luminescence of **(2.3 S)** in DCM (c) solid state luminescence of **(2.3 Se)** after removal of $CDCl_3$ and (d) solution state luminescence of **(2.3 Se)** in DCM (irradiated with a UV lamp at 365 nm)*

A notable point of discussion for compounds **(2.3 S)** and **(2.3 Se)** are their different luminescent properties when their crystals interact with different solvents. Following addition and subsequent removal of $CDCl_3$ (due to insolubility), **(2.3 S)** and **(2.3 Se)** precipitated as colourless precipitates and were yellow and orange emissive, respectively as seen *in Figure 2.15*. Subsequent dissolution of **(2.3 S)** and **(2.3 Se)** yielded a yellow-green emissive, slightly orange, clear solution (S) and clear, colourless, yellow emissive clear solution (Se).

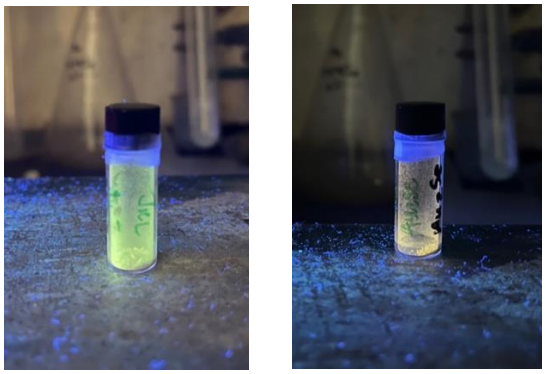

Figure 2.15: (a) Emission of [(Au_2S)(μ-dbfdp)] ***(2.3 S)*** *(b) Emission of [(Au_2Se)(μ-dbfdp)]* ***(2.3 Se)****. (Qualitative observation of the emission of solid-state samples at room temperature when irradiated with handheld UV lamp at 365 nm).*

The emission and excitation spectra of compounds **(2.3 S)**, **(2.3 Se)**, **(2.4 Se)** and **(2.5 S)** were obtained in solid state. In the solid state, compounds **(2.3 S)** and **(2.3 Se)** are seen to visually have green and orange emission *(Figure 2.16)* when irradiated with a handheld UV lamp (λ = 254 nm and 365 nm). When comparing clusters to each other, the differences in λ_{exc} and λ_{em} are notable. It can be observed in compounds **(2.3 S)** and **(2.3 Se)**, that by changing the chalcogen, the emission experiences a hypsochromic shift. The emission and excitation spectra are shown in *Figure 2.16, Figure 2.17* and *Figure S2.16* in **Appendix**.

λ_{exc} was determined to be 358 nm and λ_{em} was determined to be 514 nm for compound **(2.3 S)**. The λ_{em} is within the yellow-green region which also what is seen from the solid in *Figure 2.15*. To study the effect that changing the chalcogen would have, the λ_{exc} and λ_{em} of [(Au_2S)(μ-dbfdp)] **(2.3 S)** can be compared to [(Au_2Se)(μ-dbfdp)] **(2.3 Se)**. It is interesting to note that compound **(2.3 Se)** visually appears orange, but upon conducting photoluminescent excitation and emission studies, it is found that λ_{em} is 438 nm with λ_{exc} at 346 nm. By changing the chalcogen to Se, it can be seen that the emission experiences a hypsochromic shift, or a shift to lower wavelength. As compared to the literature [$(AuCl)_2$(μ-dbfdp)$_2$] **(I.XXXI)** which has an emission maximum at 420 nm, both **(2.3 S)** and **(2.3 Se)** have a bathochromic shift in emission when a chalcogen is introduced.[20]

To compare the effects of an increasing nuclearity in a gold (I) chalcogenide cluster, compound **(2.3 S)** and compound **(2.4 Se)** can be compared. Compound **(2.4 Se)** has a nuclearity of 4 whereas

(2.3 S) has a nuclearity of 2, which may play a role in altering the HOMO and LUMO of this compound.

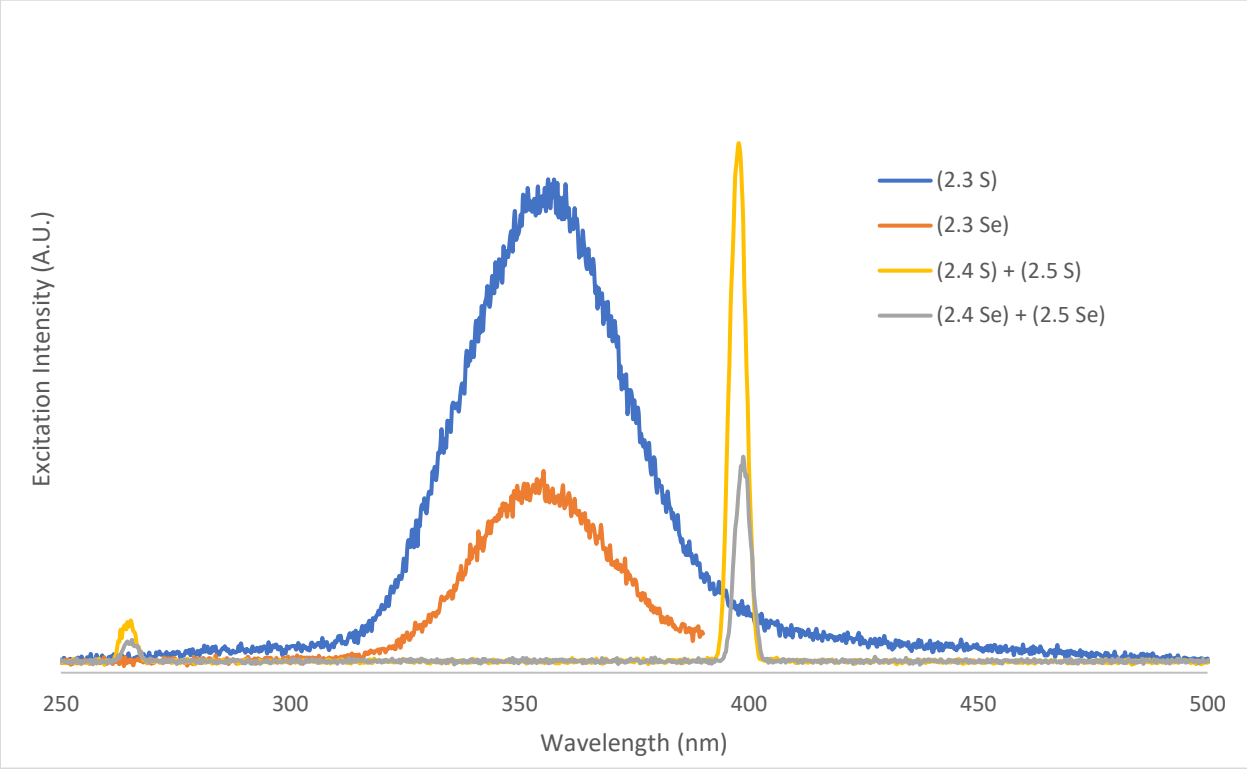

*Figure 2.16: Excitation spectra of **(2.3 S)**, **(2.3 Se)**, **(2.4 Se)** and **(2.5 S)** in the solid state at room temperature. The selected $\lambda_{exc(max)}$ for these cluster/complexes range between 250 and 450 nm. The maxima at 398 nm for **(2.4 Se)** and **(2.5 S)** are attributed to an artifact.*

However, the mixture of compounds **(2.4 S)** and **(2.5 S)** were visually not shown to have luminescent properties. It was previously noted that the solution of starting material **(2.3 S)** displayed teal luminescence. Upon addition of $[Cu(NCCH_3)_4]OTf$, it resulted in the immediate disappearance of the luminescent properties when examined with a handheld UV lamp (254 nm and 365 nm). The reaction was layered at room temperature with hexanes and yielded colourless crystalline material which was later determined to be a mixture of **(2.4 S)** and **(2.5 S)**. Excitation and emission analysis of the crystalline sample confirmed no excitation and emission maxima in the visible region (*Figure S2.16* in **Appendix**). It can be thus confirmed that neither **(2.4 S)** or **(2.5 S)** is emissive. The crystalline solids obtained from the reaction between compounds **(2.2)** and **(2.3 S)**, also was confirmed to be not visually emissive.

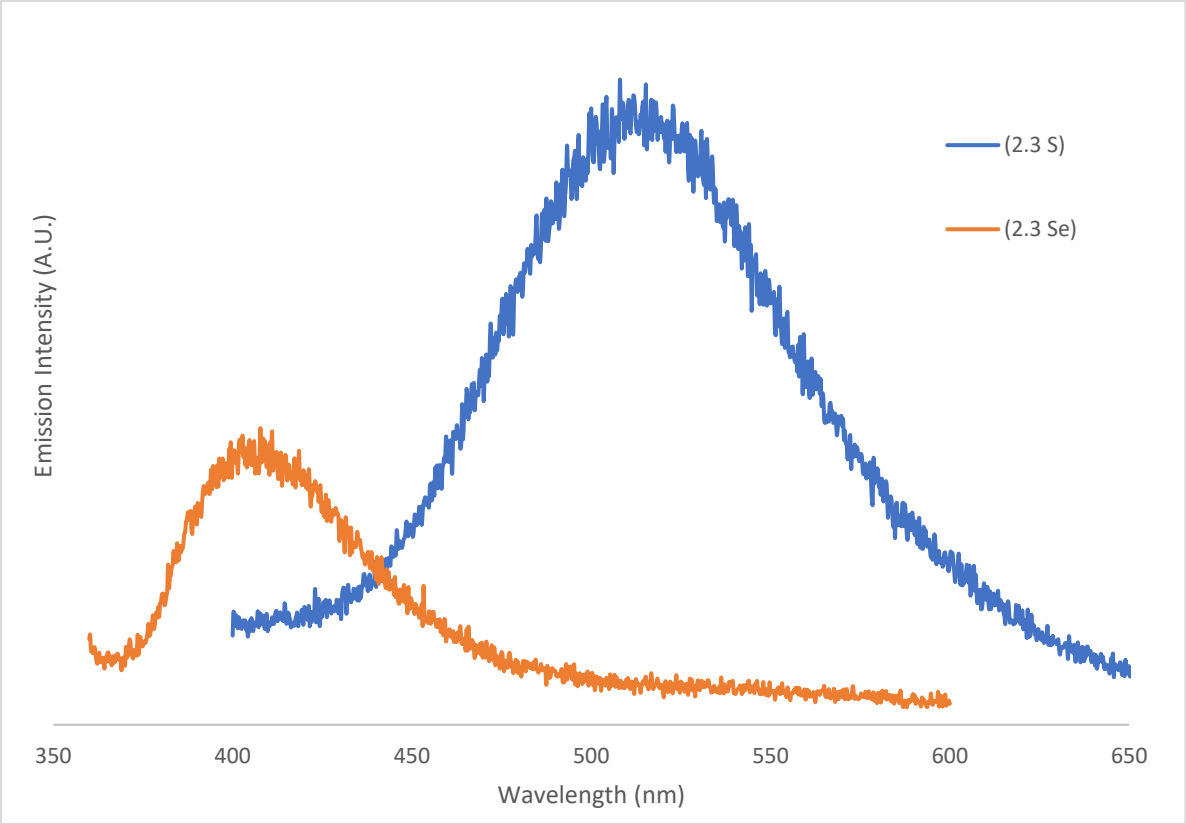

*Figure 2.17: Emission spectra of **(2.3 S)** and **(2.3 Se)** in the solid state at room temperature. (λ_{exc} = 358 nm **(2.3 S)**, λ_{exc} = 346 nm **(2.3 Se)**).*

Similarly, the mixture of compounds **(2.4 Se)** and **(2.5 Se)** were not visually emissive when irradiated with a handheld UV lamp. In CH_2Cl_2, compound **(2.3 Se)** displays a yellow luminescence. Upon addition of $[Cu(NCCH_3)_4]OTf$, the yellow emission disappears instantaneously. The reaction solution was allowed to warm to room temperature and consequently layered with hexanes and yielded crystalline material later determined to be **(2.4 Se)** and **(2.5 Se)** as a mixture. Analysis of the emission and excitation spectra of the mixture of **(2.4 Se)** and **(2.5 Se)** determined that neither compound is emissive in the visible region. The crystalline sample from the reaction between compounds **(2.2)** and **(2.3 Se)** was also confirmed to be not visually emissive.

2.3 Experimental

2.3.1 General Considerations

All experiments were carried out under an inert atmosphere of high purity, dried nitrogen using standard Schlenk line techniques on a double manifold vacuum line. All solvents used were either

distilled over the appropriate desiccant under nitrogen or were dried using a commercial MBraun MB-SP series solvent purification system. Celite® was dried under dynamic vacuum at 220 °C for 24 hours and stored under nitrogen in a sealed flask.

Dibenzofuran was purchased from TCI America and was used without further purifications. Silver acetate was purchased from Fisher Chemicals and used without further purification. *Tetrakis*(acetonitrile)copper(I) triflate was purchased from Sigma Aldrich and was used without further purification. Chlorodiphenylphosphine and n-butyllithium (1.6 M in hexanes) were purchased from Fischer Chemicals and used without further purification. Tetramethylethylenediamene (TMEDA) was refluxed with KOH pellets for three hours and distilled under nitrogen according to literature procedure.[31] *Bis*(trimethylsilyl)sulfide and *bis*(trimethylsilyl)selenide were synthesized by a colleague using literature procedures and used without further purification.[32] 4,6-*bis*(diphenylphosphino)dibenzofuran (DBFDP) was synthesized by incorporating two literature procedures with few modifications.[17,33] *Bis*(trimethylsilyl)chalcogenide reagents were diluted to a 10% stock solution by adding 0.50 mL to 4.50 mL of tetrahydrofuran.

^{1}H, $^{31}P\{^{1}H\}$, $^{13}C\{^{1}H\}$, ^{19}F NMR spectra were recorded on the Bruker AvanceIII HD 400 (B400) with frequencies of 400.130 MHz, 161.976 MHz, 100.613, and 56.76 MHz respectively. The ^{1}H NMR spectra were referenced to residual proton solvent in $CDCl_3$ and CD_2Cl_2. The $^{13}C\{^{1}H\}$ NMR spectra were referenced to the carbon atoms in $CDCl_3$ and CD_2Cl_2. The $^{31}P\{^{1}H\}$ NMR spectra were referenced to 85 % H_3PO_4. Attenuated Total Reflectance Infrared (ATR-IR) spectra of samples of **(2.3 S)**, **(2.3 Se)**, **(2.4 Se)** and **(2.5 S)** were obtained using Bruker Alpha II Spectrometer. The data were analyzed using OPUS-Operator Default Software. Melting points of samples **(2.1)**, **(2.3 S/Se)**, **(2.4 S/Se)** and **(2.5 S/Se)** were recorded on a Gallenkamp melting point apparatus under N_2 atmosphere. Samples for elemental analysis were prepared under N_2 atmosphere. Samples are currently awaiting elemental analysis at the Centre for Environmental Analysis and Remediation by Patricia Granados at Saint Mary's University in Halifax, Nova Scotia.

Single crystal X-ray data collection were completed by Dr. John F. Corrigan, Dr. Jalil Assoud and Nils Vogeler on a Bruker Kappa Axis Apex 2 diffractometer at a temperature of 110 K. The sample was placed on a MiTeGen polyimide micromount with a small amount of Paratone N oil. The raw data were scaled, and absorption corrected using SADABS and the frame integration was done by

SAINT.[34,35] SHELXT program was used to solve the structure.[36] All non-hydrogen atoms were obtained from the initial solution, introduced at idealized positions, and were allowed to ride on the parent atom. The structural model was fit to the data by full matrix least squares based on F2. The structure was further refined using the SHELXL program from the SHELXTL suite of crystallographic software.[37]

In the collection of the solid photoluminescence, crystalline powders of **(2.3 S)**, **(2.3 Se)**, **(2.4 Se)** and **(2.5 S)** were adhered to 2-sided Scotch tape (410B, 3M, Saint Paul, MN) on a custom-made platform with a 45-degree angle between the excitation beam and emission detector. The emission and excitation slit widths were optimized for the signal strength. The 2-sided tape was chosen due to its low PL signal. The powder was spread over the tape via spatula in a thin layer to prevent excitation of the tape via the excitation beam. The data was analyzed by the FelixGX version 2 software by Photon Technology International (PTI).

2.3.2 Synthesis of [(AuOAc)$_2$(dbfdp)] (2.1)

[(AuCl)$_2$(dbfdp)] was prepared with DBFDP (0.054 g, 0.098 mmol, 1 equiv.) and chloro(tetrahydrothiophene)gold(I) (AuTHTCl) (0.063 g, 0.190 mmol, 2 equiv.) by stirring for one hour in 20 mL of THF.[21] The reaction solution was then reduced to 5 mL *in vacuo* and precipitated with 15 mL of pentane to yield a colourless solid. The resulting precipitate was then washed thrice with 5 mL of pentane. AgOAc (0.033 g, 0.190 mmol, 2 equiv.) was added to the solution of [(AuCl)$_2$(dbfdp)] alongside 10 mL of THF and stirred overnight. The reaction mixture was filtered over Celite®, and volatiles were removed *in vacuo*. The resulting white solid was isolated and washed thrice with 5 mL of pentane and dried for 5-6 hours. Yield = 47 % $^{31}P\{^1H\}$ NMR (161 MHz, $CDCl_3$, 23.5 °C): δ = 18.9. ^1H NMR (400.130 MHz, $CDCl_3$, 23.5 °C): δ = 8.17 (2H, d, J = 7.4 Hz), 7.40 -7.56 (20H, m), 7.16 (2H, dd, J = 7.5, 14.1 Hz), 2.07 (6H, s). m.p. = 210 °C$_{decomp}$. Crystal structure data, bond angles and bond lengths are attached in the **Appendix** in *Tables S2.1, S2.2* and *S2.3.* $^{31}P\{^1H\}$ NMR and ^1H NMR spectra are attached in the **Appendix** in *Figures S2.1* and *S2.2.*

2.3.3 Synthesis of [(AuOTf)$_2$(μ-dbfdp)] (2.2)

[(AuCl)$_2$(dbfdp)] was prepared with DBFDP (0.054 g, 0.098 mmol, 1 equiv.) and chloro(tetrahydrothiophene)gold(I) (AuTHTCl) (0.063 g, 0.190 mmol, 2 equiv.) by stirring for one hour in 20 mL of THF.[21] The reaction solution was then reduced to 5 mL *in vacuo* and precipitated

in 15 mL of pentane yielded a colourless solid. The resulting precipitate was then washed thrice with 5 mL of pentane. AgOTf (0.049 g, 0.190 mmol, 2 equiv.) was added alongside 10 mL of THF and stirred overnight. The reaction mixture was filtered over Celite®, and volatiles were removed *in vacuo*. The resulting white paste was isolated and washed thrice with 5 mL of pentane and dried for 5-6 hours. Yield = 38 % $^{31}P\{^{1}H\}$ NMR (161 MHz, $CDCl_3$, 23.5 °C): δ = 15.6. ^{1}H NMR (400.130 MHz, $CDCl_3$, 23.5 °C): δ = 8.37 (2H, d, *J* = 7.2 Hz), 7.42 – 7.62 (20H, m), 6.98 (2H, dd, *J* = 7.3, 11.7 Hz). $^{19}F\{^{1}H\}$ NMR (56.76 MHz, $CDCl_3$, 23.5 °C): δ = -77.2. $^{31}P\{^{1}H\}$ NMR, ^{1}H NMR and $^{19}F\{^{1}H\}$ NMR spectra are attached in the **Appendix** in *Figures S2.3*, *S2.4* and *S2.5.*

2.3.4 Synthesis of [(Au₂S)(dbfdp)] (2.3 S)

Compound **(2.1)** (0.050 g, 0.048 mmol, 1 equiv.) was dissolved in 10 mL of THF and stirred for 15 minutes. *Bis*(trimethylsilyl)sulfide (0.04 mL of 10% stock solution, 0.048 mmol, 1.0 equiv.) was added while stirring at -78 °C. The solution was warmed slowly to room temperature and stirred overnight resulting in a cloudy colourless solution. THF was removed *in vacuo* and contents were solubilized in DCM. The solution was then layered with heptane and colourless crystals of **(2.3 S)** were observed after 2 days. The resulting crystals were isolated and washed twice with 20 mL of pentane and dried *in vacuo* for 5-6 hours. Yield = 41 % based on **(2.1)**. $^{31}P\{^{1}H\}$ NMR (161 MHz, CD_2Cl_2, 23.5 °C): δ = 19.9. ^{1}H NMR (400.130 MHz, CD_2Cl_2, 23.5 °C): δ = 8.18 (2H, d, *J* = 7.7 Hz), 7.23 – 7.54 (20H, m), 6.90 (2H, dd, *J* = 7.3, 11.4 Hz). ATR IR (cm^{-1}): TBD. m.p. = 240 $°C_{decomp}$. λ_{exc} = 350 nm, λ_{em} = 408 nm, Crystal structure data, bond angles and bond lengths are attached in **Appendix** in *Tables S2.4, S2.5* and *S2.6*. $^{31}P\{^{1}H\}$ NMR and ^{1}H NMR spectra are attached in the **Appendix** in *Figures S2.6* and *S2.7.*

2.3.5 Synthesis of [(Au₂Se)(dbfdp)] (2.3 Se)

Compound **(2.1)** (0.050 g, 0.048 mmol, 1 equiv.) was dissolved in 10 mL of THF and stirred for 15 minutes. *Bis*(trimethylsilyl)selenide (0.04 mL of 10% stock solution, 0.048 mmol, 1.0 equiv.) was added while stirring at -78 °C. The solution was warmed slowly to room temperature and stirred overnight resulting in a cloudy colourless solution. THF was removed *in vacuo* and contents were solubilized in DCM. The solution was then layered with heptane and colourless crystals of **(2.3 Se)** were observed after 2 days. The resulting crystals were isolated and washed twice with 20 mL of pentane and dried *in vacuo* for 5-6 hours. Yield = 37 % based on **(2.1)**. $^{31}P\{^{1}H\}$ NMR (161 MHZ, CD_2Cl_2, 23.5 °C): δ = 22.7. ^{1}H NMR (400.130 MHz, CD_2Cl_2, 23.5 °C): δ = 8.19 (2H, d, *J*

= 7.5 Hz), 7.24-7.54 (20H, m), 6.88 (2H, dd, *J* = 7.3, 11.7 Hz). ATR IR (cm^{-1}): TBD. m.p. = >260 °C_{decomp}. λ_{exc} = 350 nm, λ_{em} = 514 nm, Crystal structure data, bond angles and bond lengths are attached in the **Appendix** in *Tables S2.7, S2.8* and *S2.9.* $^{31}P\{^{1}H\}$ NMR and ^{1}H NMR spectra are attached in the **Appendix** in *Figures S2.8* and *S2.9.*

2.3.6 Synthesis of [Au₄(μ₄-S)(μ-dbfdp)₂](OTf₂) (2.4 S)

Compound **(2.3 S)** (0.024 g, 0.024 mmol, 3.0 equiv.) was dissolved in 10 mL DCM and stirred for 10 minutes and cooled to -78 °C. *Tetrakis*(acetonitrile)copper (I) triflate was solubilized in 5 mL DCM, stirred for 15 minutes and added dropwise to the solution of **(2.3 S)**. The clear colourless solution was warmed over 2 hours to room temperature and stirred overnight to yield a clear orange solution overnight. The solution was subsequently layered with hexanes and red-orange crystals of **(2.4 S)** were observed after 3 days. The resulting crystals were isolated and washed twice with 20 mL of pentane and dried *in vacuo* for 5-6 hours. Yield = 36 % $^{31}P\{^{1}H\}$ NMR (161 MHz, $CDCl_3$, 23.5 °C): δ = 18.1. ^{1}H NMR (400.130 MHz, CD_2Cl_2, 23.5 °C): δ = 8.13 (2H, d, *J* = 7.7 Hz), 6.78-7.61 (24H, m) $^{19}F\{^{1}H\}$ NMR (56.76 MHz, $CDCl_3$, 23.5 °C): δ = -78.9. Crystal structure data, bond angles and bond lengths are attached in the **Appendix** in *Tables S2.10*, *S2.11* and *S2.12*.

2.3.7 Synthesis of [Au₆(μ₃-S)₂(μ-dbfdp)₃](OTf)₂ (2.5 S)

Compound **(2.3 S)** (0.016 g, 0.016 mmol, 2.0 equiv) was dissolved in 10 mL of DCM, stirred for 10 minutes and cooled to -78 °C. A 5 mL DCM solution of **(2.2)** (0.010 g, 0.008 mmol, 1.0 equiv.) was prepared and also cooled to -78 °C. The 5 mL solution of **(2.2)** was added dropwise to the solution of **(2.3 S)** and allowed to warm to room temperature over 2 hours and stirred overnight. The slightly orange, clear solution was layered with hexanes and yielded pale orange-red crystals of **(2.4 Se)** after 3 days. The resulting crystals were isolated and washed thrice with 20 mL of pentane and dried *in vacuo* for 5-6 hours. Yield = 52 % $^{31}P\{^{1}H\}$ NMR (161 MHz, $CDCl_3$, 23.5 °C): δ = 18.1, 14.2. ^{1}H NMR (400.130 MHz, CD_2Cl_2, 23.5 °C): δ = 8.24 (2H, d, *J* = 7.7 Hz), 6.90-7.62 (24H, m) $^{19}F\{^{1}H\}$ NMR (56.76 MHz, $CDCl_3$, 23.5 °C): δ = -78.9. Crystal structure data, bond angles and bond lengths are attached in the **Appendix** in *Tables S2.16*, *S2.17* and *S2.18*.

2.3.8 Synthesis of [Au₄(μ₄-Se)(μ-dbfdp)₂](OTf)₂ (2.4 Se)

Compound **(2.3 Se)** (0.016 g, 0.016 mmol, 2.0 equiv.) was dissolved in 10 mL of DCM and stirred for 10 minutes and cooled to -78 °C. A 5 mL DCM solution of **(2.2)** (0.010 g, 0.008 mmol, 1.0

equiv.) was prepared and also cooled to -78 °C. The 5 mL solution of **(2.2)** was added dropwise to the solution of compound **(2.3 Se)**, thereafter was warmed to room temperature over 2 hours and stirred overnight. The slight orange, clear solution was layered with hexanes and yielded pale orange-red crystals of **(2.5 S)** were observed after 3 days. The resulting crystals were isolated and washed thrice with 20 mL of pentane and dried *in vacuo* for 5-6 hours. Yield = 34 % $^{31}P\{^{1}H\}$ NMR (161 MHz, $CDCl_3$, 23.5 °C): δ = 20.1. ^{1}H NMR (400.130 MHz, CD_2Cl_2, 23.5 °C): δ = 8.42 (2H, s), 6.90 – 7.62 (24H, m) 6.85 (2H, s). $^{19}F\{^{1}H\}$ NMR (56.76 MHz, $CDCl_3$, 23.5 °C): δ = -78.9. Crystal structure data, bond angles and bond lengths are attached in the **Appendix** in *Tables S2.13, S2.14* and *S2.15*.

2.3.9 Synthesis of $[Au_6(\mu_3\text{-}Se)_2(\mu\text{-}dbfdp)_3](OTf)_2$ (2.5 Se)

Compound **(2.3 Se)** (0.024 g, 0.024 mmol, 3.0 equiv.) was dissolved in 10 mL DCM and stirred for 10 minutes and cooled to -78 °C. *Tetrakis*(acetonitrile)copper (I) triflate was solubilized in 5 mL DCM and stirred for 15 minutes and added dropwise to the first solution. The clear colourless solution was warmed slowly to room temperature and stirred overnight. The solution had turned into a clear deep red solution overnight which was subsequently layered with hexanes and pale orange crystals of **(2.5 Se)** were observed after 3 days. The resulting crystals were isolated and washed twice with 20 mL of pentane and dried *in vacuo* for 5-6 hours. Yield = 26 % $^{31}P\{^{1}H\}$ NMR (161 MHz, $CDCl_3$, 23.5 °C): δ = 19.8, 17.2. ^{1}H NMR (400.130 MHz, CD_2Cl_2, 23.5 °C): δ = 8.18 (2H, s), 6.87 – 7. (24H, m) $^{19}F\{^{1}H\}$ NMR (56.76 MHz, $CDCl_3$, 23.5 °C): δ = -78.9. Crystal structure data, bond angles and bond lengths are attached in the **Appendix** in *Tables S2.19, S2.20* and *S2.21*.

2.4 Conclusion

In summary, the addition of $E(SiMe_3)_2$ (E = S, Se) to $[(AuOAc)_2(\mu\text{-dbfdp})]$ results in dinuclear gold chalcogenide complexes with a bridging chalcogen and DBFDP. When the generated dinuclear complexes $[(Au_2S)(dbfdp)]$ **(2.3 S)** and $[(Au_2Se)(dbfdp)]$ **(2.3)** were reacted with a OTf^- source, (*tetrakis*(acetonitrile)copper (I) triflate or $[(AuOTf)_2(\mu\text{-dbfdp})]$ (2.2)), a mixture of higher nuclearity gold (I) complexes were formed; namely $[Au_4(\mu_4\text{-S})(\mu\text{-dbfdp})_2]OTf_2$ (2.4 S), $[Au_6(\mu_3\text{-S})_2(\mu\text{-dbfdp})_3](OTf)_2$ (2.5 S) in one reaction mixture and $[Au_4(\mu_4\text{-Se})(\mu\text{-dbfdp})_2](OTf)_2$ (2.4 Se), $[Au_6(\mu_3\text{-Se})_2(\mu\text{-dbfdp})_3](OTf)_2$ (2.5 Se) in another. The dinuclear complexes were determined to be emissive with a λ_{em} of 514 nm for **(2.3 S)** and 438 nm **(2.3 Se)**. These complexes all displayed varying levels of aurophilicity with the shortest Au···Au distance at 2.777(4) Å (falling within the accepted 2.5 Å-3.5 Å range) and the longest Au Au distance at 3.577(1) Å.

2.5 References

(1) Latouche, C.; Liu, C. W.; Saillard, J.-Y. Encapsulating Hydrides and Main-Group Anions in D10-Metal Clusters Stabilized by 1,1-Dichalcogeno Ligands. *J. Clust. Sci.* **2014**, *25* (1), 147–171. https://doi.org/10.1007/s10876-013-0671-3.

(2) Arvizo, R. R.; Bhattacharyya, S.; Kudgus, R. A.; Giri, K.; Bhattacharya, R.; Mukherjee, P. Intrinsic Therapeutic Applications of Noble Metal Nanoparticles: Past, Present and Future. *Chem. Soc. Rev.* **2012**, *41* (7), 2943–2970. https://doi.org/10.1039/C2CS15355F.

(3) Chu, A.; Hau, F. K.-W.; Yao, L.-Y.; Yam, V. W.-W. Decanuclear Gold(I) Sulfido Pseudopolymorphs Displaying Stimuli-Responsive RGBY Luminescence Changes. *ACS Mater. Lett.* **2019**, *1* (2), 277–284. https://doi.org/10.1021/acsmaterialslett.9b00175.

(4) Yang, X.-X.; Issac, I.; Lebedkin, S.; Kühn, M.; Weigend, F.; Fenske, D.; Fuhr, O.; Eichhöfer, A. Red-Luminescent Biphosphine Stabilized 'Cu $_{12}$ S $_{6}$ ' Cluster Molecules. *Chem. Commun.* **2014**, *50* (75), 11043. https://doi.org/10.1039/C4CC04702H.

(5) Hu, B.; Su, C. Y.; Fenske, D.; Fuhr, O. Synthesis, characterization and optical properties of a series of binuclear copper chalcogenolato complexes. *Inorganica Chim. Acta* **2014**, *419* (August), 118. https://doi.org/10.1016/j.ica.2014.05.009.

(6) Gimeno, M. C.; Laguna, A. Chalcogenide Centred Gold Complexes. *Chem. Soc. Rev.* **2008**, *37* (9), 1952. https://doi.org/10.1039/b708618k.

(7) Canales, F.; Gimeno, C.; Laguna, A.; Villacampa, M. D. Aurophilicity at Sulfur Centers. Synthesis of the Polyaurated Species [S(AuPR3)n](N−2)+ (n = 2–6). *Inorganica Chim. Acta* **1996**, *244* (1), 95–103. https://doi.org/10.1016/0020-1693(95)04759-X.

(8) Canales, F.; Gimeno, M. C.; Laguna, A.; Jones, P. G. Aurophilicity at Sulfur Centers. Synthesis and Reactivity of the Complex [S(Au2dppf)]; Formation of Polynuclear Sulfur-Centered Complexes. Crystal Structures of [S(Au2dppf)]·2CHCl3, [(μ-Au2dppf){S(Au2dppf)}2](OTf)2· 8CHCl3, and [S(AuPPh2Me)2(Au2dppf)](ClO4)2·3CH2Cl2. *J. Am. Chem. Soc.* **1996**, *118* (20), 4839–4845. https://doi.org/10.1021/ja9517678.

(9) Canales, S.; Crespo, O.; Gimeno, M. C.; Jones, P. G.; Laguna, A.; Mendizabal, F. Polynuclear Gold Complexes with Bridging Selenido Ligands. Theoretical Studies of Gold−Gold Interactions. *Organometallics* **2000**, *19* (24), 4985–4994. https://doi.org/10.1021/om000119g.

(10) Fuhr, O.; Dehnen, S.; Fenske, D. Chalcogenide Clusters of Copper and Silver from Silylated Chalcogenide Sources. *Chem. Soc. Rev.* **2013**, *42* (4), 1871–1906. https://doi.org/10.1039/C2CS35252D.

(11) MacDonald, D. G.; Corrigan, J. F. Metal Chalcogenide Nanoclusters with 'Tailored' Surfaces via 'Designer' Silylated Chalcogen Reagents. *Philos. Trans. R. Soc. Math. Phys. Eng. Sci.* **2010**, *368* (1915), 1455–1472. https://doi.org/10.1098/rsta.2009.0276.

(12) Dehnen, S.; Eichhöfer, A.; Corrigan, J. F.; Fuhr, O.; Fenske, D. *Synthesis and characterization of Ib-VI nanoclusters*. https://publikationen.bibliothek.kit.edu/150081429 (accessed 2023-06-12).

(13) Eichhöfer, A.; Buth, G.; Lebedkin, S.; Kühn, M.; Weigend, F. Luminescence in Phosphine-Stabilized Copper Chalcogenide Cluster Molecules—A Comparative Study. *Inorg. Chem.* **2015**, *54* (19), 9413–9422. https://doi.org/10.1021/acs.inorgchem.5b01146.

(14) Schmidbaur, H.; Graf, W.; Müller, G. Weak Intramolecular Bonding Relationships: The Conformation-Determining Attractive Interaction between Gold(I) Centers. *Angew. Chem. Int. Ed. Engl.* **1988**, *27* (3), 417–419. https://doi.org/10.1002/anie.198804171.

(15) Schmidbaur, H. Is Gold Chemistry a Topical Field of Study? *Angew. Chem. Int. Ed. Engl.* **1976**, *15* (12), 728–740. https://doi.org/10.1002/anie.197607281.
(16) Yam, V. W.-W.; Cheng, E. C.-C.; Zhu, N. A Novel Polynuclear Gold–Sulfur Cube with an Unusually Large Stokes Shift. *Angew. Chem. Int. Ed.* **2001**, *40* (9), 1763–1765. https://doi.org/10.1002/1521-3773(20010504)40:9<1763::AID-ANIE17630>3.0.CO;2-O.
(17) Xie, M.; Han, C.; Zhang, J.; Xie, G.; Xu, H. White Electroluminescent Phosphine-Chelated Copper Iodide Nanoclusters. *Chem. Mater.* **2017**, *29* (16), 6606–6610. https://doi.org/10.1021/acs.chemmater.7b01443.
(18) Nayyar, M. Luminescent Group 11 Metal Chalcogen Clusters with Bidentate Phosphine Ligands, The University of Western Ontario, London, 2021.
(19) Li, J. Ligand Controlled Luminescence in Silver and Gold-Chalcogenide Clusters, University of Western Ontario, 2021.
(20) Pintado-Alba, A.; De La Riva, H.; Nieuwhuyzen, M.; Bautista, D.; Raithby, P. R.; Sparkes, H. A.; Teat, S. J.; López-de-Luzuriaga, J. M.; Lagunas, M. C. Effects of Diphosphine Structure on Aurophilicity and Luminescence in Au(I) Complexes. *Dalton Trans* **2004**, No. 21, 3459–3467. https://doi.org/10.1039/B410619A.
(21) Al-Maythalony, B. A.; Wazeer, M. I. M.; Isab, A. A. Synthesis of Aurocyanide and Auricyanide Complexes of Phosphines, Phosphine Sulfides and Phosphine Selenides, and Their Characterization by IR, Far-IR, UV Solution, and Solid-State NMR Spectroscopic Methods. *J. Coord. Chem.* **2010**, *63* (21), 3824–3832. https://doi.org/10.1080/00958972.2010.518759.
(22) Lensch, C.; Jones, P. G.; Sheldrick, G. M. Kristallstrukturen Der Selenid- Bzw. Sulfidverbrückten Gold(I)Verbindungen [Se(AuPPh3)+3]PF6- Und [S(AuPPh3)2] · CH2Cl2/Crystal Structures of the Selenide- and Sulphide-Bridged Gold(I) Complexes [Se(AuPPh3)3]+PF6- and [S(AuPPh3)2] · CH2Cl2. *Z. Für Naturforschung B* **1982**, *37* (8), 944–949. https://doi.org/10.1515/znb-1982-0803.
(23) Crespo, O.; Gimeno, M. C.; Laguna, A.; Larraz, C.; Villacampa, M. D. Highly Luminescent Gold(I)-Silver(I) and Gold(I)-Copper(I) Chalcogenide Clusters. *Chem. - Eur. J.* **2007**, *13* (1), 235–246. https://doi.org/10.1002/chem.200600566.
(24) Yan, L.-L.; Yao, L.-Y.; Yam, V. W.-W. Concentration- and Solvation-Induced Reversible Structural Transformation and Assembly of Polynuclear Gold(I) Sulfido Complexes. *J. Am. Chem. Soc.* **2020**, *142* (26), 11560–11568. https://doi.org/10.1021/jacs.0c04677.
(25) Olkowska-Oetzel, J.; Sevillano, P.; Eichhöfer, A.; Fenske, D. Binary and Ternary Cluster Complexes Containing Gold-Selenium, Gold-Indium-Selenium and Gold-Gallium-Tellurium − Synthesis and Structures of $[Au_5Se_2(PPh_3)_4]Cl$, $[(Au_3Se)_2\{Ph_2P(CH_2)_6PPh_2\}_3]Cl_2$, $[Au_{10}Se_4\{Ph_2P(CH_2)_5PPh_2\}_4]InCl_5$, $[Au_4(SeInCl_3)_2\{Ph_2P(CH_2)_5PPh_2\}_2]$, $[Au_2(TeGaCl_3)\{Ph_2P(CH_2)_6PPh_2\}]_2$ and $[Au_8Se_4In\{Ph_2P(CH_2)_2PPh_2\}_4](InCl_4)_3$. *Eur. J. Inorg. Chem.* **2004**, *2004* (5), 1100–1106. https://doi.org/10.1002/ejic.200300774.
(26) Eichhöfer, A.; Fenske, D. Syntheses and Structures of New Copper(I)–Indium(III)–Selenide Clusters. *J. Chem. Soc. Dalton Trans.* **2000**, No. 6, 941–944. https://doi.org/10.1039/A909737F.
(27) Eichhöfer, A.; Kühn, M.; Lebedkin, S.; Kehry, M.; Kappes, Manfred. M.; Weigend, F. Synthesis and Optical Properties of [Cu6E6(SnPh)2(PPh2Et)6] (E = S, Se, Te) Cluster Molecules. *Inorg. Chem.* **2017**, *56* (15), 9330–9336. https://doi.org/10.1021/acs.inorgchem.7b01495.

(28) DeGroot, M. W.; Corrigan, J. F. Coordination Complexes of Zinc with Reactive ESiMe3 (E = S, Se, Te) Ligands. *Organometallics* **2005**, *24* (14), 3378–3385. https://doi.org/10.1021/om050088v.
(29) Dehnen, S.; Eichhöfer, A.; Fenske, D. Chalcogen-Bridged Copper Clusters. *Eur. J. Inorg. Chem.* **2002**, *2002* (2), 279–317. https://doi.org/10.1002/1099-0682(20022)2002:2<279::AID-EJIC279>3.0.CO;2-H.
(30) DeGroot, M. W.; Corrigan, J. F. Polynuclear Bismuth Selenolates: Rings En Route to Clusters. *J. Chem. Soc. Dalton Trans.* **2000**, No. 8, 1235–1236. https://doi.org/10.1039/B001417F.
(31) Armarego, W. L. F. *Purification of Laboratory Chemicals: Part 2 Inorganic Chemicals, Catalysts, Biochemicals, Physiologically Active Chemicals, Nanomaterials*; Butterworth-Heinemann, 2022.
(32) So, J.-H.; Boudjouk, P. Convenient Syntheses of Hexamethyldisilathiane and Tetramethyldisilathiane. *Synthesis* **1989**, *1989* (04), 306–307. https://doi.org/10.1055/s-1989-27235.
(33) Kranenburg, M.; van der Burgt, Y. E. M.; Kamer, P. C. J.; van Leeuwen, P. W. N. M.; Goubitz, K.; Fraanje, J. New Diphosphine Ligands Based on Heterocyclic Aromatics Inducing Very High Regioselectivity in Rhodium-Catalyzed Hydroformylation: Effect of the Bite Angle. *Organometallics* **1995**, *14* (6), 3081–3089. https://doi.org/10.1021/om00006a057.
(34) Bruker-AXS, SADABS Version 2012.1, 2012, Bruker-AXS, Madison WI 53711, USA.
(35) Bruker-AXS, SAINT Version 2013.8, 2013, Bruker-AXS, Madison WI53711, USA.
(36) Sheldrick, G. M. SHELXT – Integrated Space-Group and Crystal-Structure Determination. *Acta Crystallogr. Sect. Found. Adv.* **2015**, *71* (1), 3–8. https://doi.org/10.1107/S2053273314026370.
(37) Sheldrick, G. M. Crystal Structure Refinement with SHELXL. *Acta Crystallogr. Sect. C Struct. Chem.* **2015**, *71* (1), 3–8. https://doi.org/10.1107/S2053229614024218.

Chapter 3

3.0 Luminescent Group 11 Metal (I) Chalcogenolate Clusters with a Conjugated Diphosphine Ligand

3.1 Introduction

Polynuclear group 11 d^{10} metal chalcogenolate complexes have been extensively investigated which can be attributed to their wide range of structural, chemical and photophysical properties such as emission, excitation and photoluimesence.[1] The combination of these group 11 coinage metals (copper, silver and gold) with chalcogenolates have been of heavy research importance due to the potential of their physical properties being modified. Their electronic and conductive properties can be modified via dimensionality of the structure as well as functionality of the organic substituent added.[2,3] Altering these organic moieties can lead to a variety of compounds, which can be used in light emitting materials due to their photophysical properties such as emission at room temperature.[2–4]

Similar to the metal chalcogenides, these chalcogenolate clusters can be readily synthesized using silylated chalcogen reagents ($RESiMe_3$, R = organic substituent, E = S, Se) with ligand protected metal complexes (LMX, L = organic protecting ligand, M = Cu, Ag, Au, X = leaving group: ex. OAc, OTf, Cl).[1,5–8] By use of these silylated reagents, the formation of $X\text{-}SiMe_3$ byproducts drives the reaction forward and results in a metal chalcogenolate core.[1,5,8] By altering the organic moiety attached on the chalcogenolate ligand or changing the steric hinderance of this organic moiety, the size and structure of the clusters can be selectively targeted. The presence of the R group attached to the chalcogen provides stability and prevents formation of undesirable bulk M_2E by products.[9–13] Organic ligands can also be introduced as a method to control optical properties such as luminescence.[4,10–12]

Two interesting examples that highlight the effect a different organic moiety can have on photophysical properties are [(TPA)AuS(C_6H_3-3,5-Cl_2)] **(III.I)** and [(TPA)AuS(C_6H_4-*o*-OMe)] **(III.II)** (TPA = 1,3,5-triaza-7-phosphaadamantanetriylphosphine) reported by Staples and co-workers.[11] The clusters luminesce at 77 K at 485 nm and 589 nm, respectively, and have their emissions assigned to a metal to ligand charge transfer (MLCT) with the excitation from an orbital associated with the sulfur to the metal-based orbital excited state.[11] **(III.I**) and **(III.II)** are very

similar in structure – both compounds contain 2 monomers linked by aurophilic interactions. However, a key difference between the two structures is the orientation of the monomers relatively to one another. In compound **(III.I)**, the thiolate ligands are aligned with one another such that the phenyl rings are partially overlapping. In comparison, compound **(III.II)** has the monomers rotated 180 ° (as compared to **(III.I)**) and has a mirror plane in between the monomers.[11] The bond lengths for Au-S in **(III.I)** are 2.291(6) Å to 2.304(5) Å. When an electron-withdrawing group is added to the phenyl rings of the thiolate ligand **(III.II)**, the bond lengths are slightly longer.

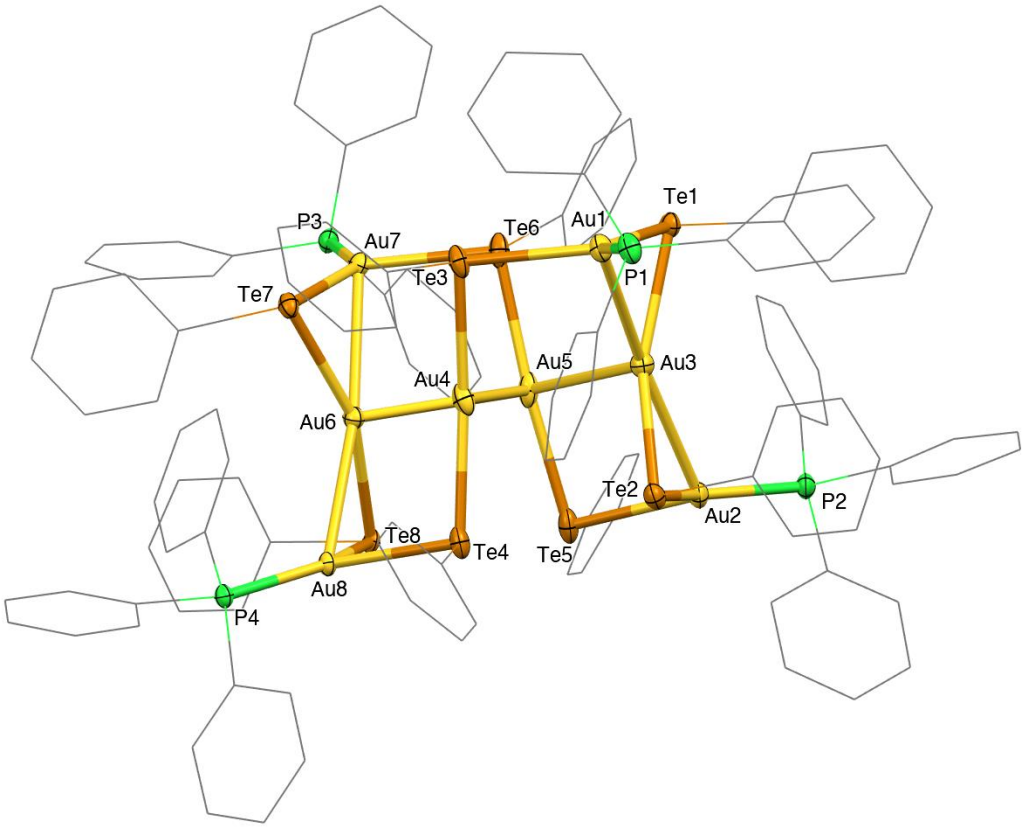

Figure 3.1: Molecular structure of [Au_8(μ-TePh)$_8$(PPh_3)$_4$] in the crystal ***(III.III)*** *(H atoms are omitted for clarity).*[14]

Reported by Villacampa and co-workers, [Au_8(μ-TePh)$_8$(PPh_3)$_4$] **(III.III)** *(Figure 3.1)* acts as another example to consider and has an emission band at 660 nm and a shoulder at 645 nm at room temperature upon photoexcitation at < 450 nm.[14] The observation of multiple bands indicate a complicated origin of emission with both metal-centered and MLCT transition involved.[14] Compound **(III.III)** has a AuTe core with μ_2 tellurolate ligands. The atoms are arranged such that

they form 3 layers of gold atoms and tellurium ligands; Au_3Te_2:Au_2Te_4:Au_3Te_2.[14] The Au···Au interactions range from 2.9462(7) Å to 3.3133(7) Å with the shortest aurophilic interactions being on the outside Au_3Te_2 'layer'.[14]

The 4,6-*bis*(diphenylphosphino)dibenzofuran (DBFDP) ligand has been recently incorporated in d^{10} copper and silver chalcogenolate clusters which demonstrated tuneable luminescent properties by changing the chalcogen or metal. These chalcogenolate ligands display bright luminescence with PLQY's ranging from 5 % to 73 % depending on which chalcogen and d^{10} metal is used.[15] Given the promising incorporation of this phosphine ligand to the smaller d^{10} metal counterparts, it is interesting to investigate the effect that DBFDP will have on gold (I) chalcogen clusters which are known to exhibit aurophilic interactions, which may influence the structural rigidity of these complexes, leading to more intense emissions.

Herein, the incorporation of the bidentate phosphine 4,6-*bis*(diphenylphosphino)dibenzofuran (DBFDP) in gold chalcogenolate complexes is reported. Additionally, during the syntheses of the gold (I) chalcogenolate complexes, a novel DBFDP copper (I) chalcogenolate cluster was synthesized as a comparison to the larger gold counterparts. Three different gold (I) chalcogenolate complexes, along with one copper (I) chalcogenolate cluster were synthesized. The compounds $[(AuSPh)_2(\mu\text{-dbfdp})]$ **(3.2)** and $[(AuSePh)_2(\mu\text{-dbfdp})]$ **(3.3)** were synthesized by adding 2 equivalents of $PhESiMe_3$ (E = S, Se) to solutions of $[(AuOAc)_2(dbfdp)]$ (**3.1**). $[(AuSC_6F_5)_2(\mu\text{-dbfdp})]$ **(3.4)** and $[Cu_4(\mu_2\text{-}SC_6F_5)(\mu\text{-dbfdp})_2]$ **(3.5)** were generated by reacting M(I)Cl (M = Cu, Au) with DBFDP resulting in $[(M(I)Cl)_2(dbfdp)]$. The chalcogenol (R-EH; E = S, Se, R = C_6F_5) was then added to the phosphine-solubilized metal complexes alongside a weak base (NEt_3). Complexes **(3.4)** and **(3.5)** displayed no visible luminescence at ambient temperature when irradiated with a handheld UV-lamp (λ = 254 nm and 265 nm). Their photophysical properties were nonetheless investigated in detail to examine the effect of the addition of the bidentate phosphine and how that affected the structural and electronic properties of these group 11 metal chalcogenolate complexes.

3.2 Results and Discussion

3.2.1 Synthesis and Characterization of [(AuSPh)$_2$(μ-dbfdp)] (3.2), [(AuSePh)$_2$(μ-dbfdp)] (3.3), [(AuSC$_6$F$_5$)$_2$(μ-dbfdp)] (3.4) and [Cu$_4$(μ$_2$-SC$_6$F$_5$)$_4$(μ-dbfdp)$_2$] (3.5)

As mentioned in prior sections, phosphine ligated group 11 metal complexes (OAc, OTf, Cl) react with chalcogen reagents with -SiMe$_3$ moieties.[1,4] [(AuOAc)$_2$(dbfdp)] (**3.1**) acts as an excellent entry point for the insertion of a chalcogen reagent with a tuneable organic moiety. Another known method of synthesis is the addition of a chalcogenol (RE-H; R = organic moiety, E = S, Se) with a base (ex. KOH, NEt$_3$) to the phosphine protected metal complexes to yield the chalcogenolate substituted metal cluster.[11,12,16] The synthesis of complexes **(3.2)** and **(3.3)** was carried out by adding 2 equivalents of PhESiMe$_3$ (E = S, Se) to solutions of [(AuOAc)$_2$(dbfdp)] **(3.1)** in DCM. The synthesis of **(3.4)** and **(3.5)** were conducted by the addition of two equivalents of (C$_6$F$_5$SH) and two equivalents of NEt$_3$ to one equivalent to [(MCl)$_2$(μ-dbfdp)] (M = Cu, Au). These reactions are highlighted in *Scheme 3.1* below.

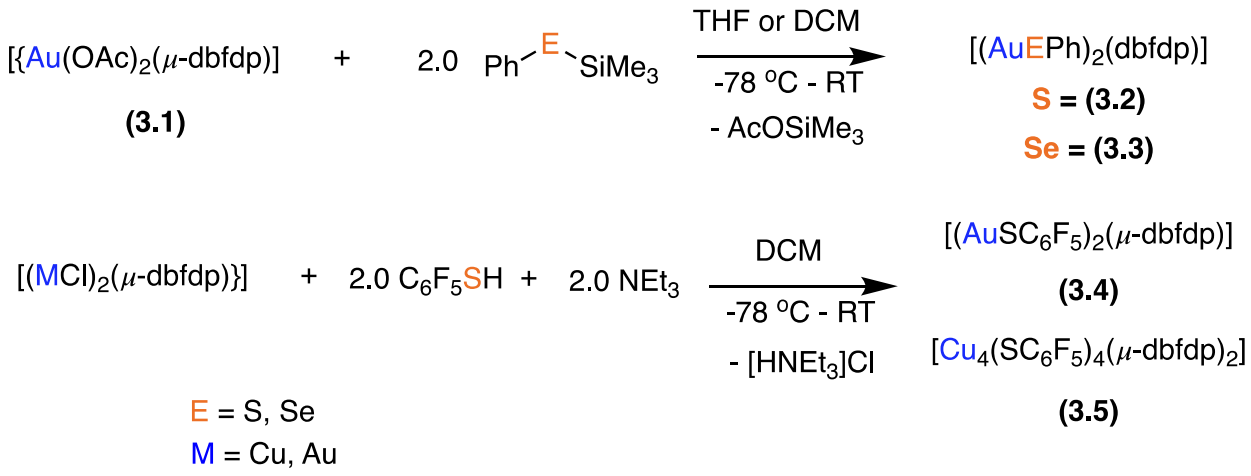

*Scheme 3.1: Synthetic schemes of group 11 metal chalcogenolate complexes **(3.2) - (3.5)**.*

Addition of PhESiMe$_3$ at -78 °C to solutions of **(3.1)** resulted in a reaction between the chloride and SiMe$_3$. This consequently resulted in the formation of the metal chalcogenolate complexes and the elimination of the SiMe$_3$-Cl product. The reactions were monitored with a handheld UV lamp as the temperature increased. For compound **(3.2)**, the reaction solution proceeds from a clear colourless solution to a clear light-yellow solution at -50 °C with no further change in colour observed. For compound **(3.3)**, the reaction solution proceeds from a clear colourless solution to a light yellow-green solution with no further change in colour observed.

The addition of the thiol (C_6F_5SH) to a DCM solution of [$(AuCl)_2$(μ-dbfdp)] **(III.IV)** results in no visible change in the colour of the solution for **(3.4)**. However, for the synthesis of **(3.5)**, upon addition of the thiol to a colourless solution of [$(CuCl)_2$(μ-dbfdp)] in DCM, the yellow emissive solution becomes a non-emissive clear, colourless solution as the reaction warmed to room temperature. To eliminate the [$HNEt_3$]Cl which is formed as a byproduct of the reaction, volatiles were removed *in vacuo*, and toluene was added to the solution. The resulting cloudy, colourless reaction mixtures of **(3.4)** and **(3.5)** are then individually filtered over Celite® and the filtrate was layered with hexanes to yield crystals of **(3.4)** and **(3.5)**.

The $^{31}P\{^1H\}$ NMR spectrum of crystals of **(3.2)** was in $CDCl_3$ shows a singular peak at 30.2 ppm ($W_{1/2}$ = 71 Hz) and shows a significant shift to higher frequency as compared to the **(3.1)** starting material. This is likely due to the presence of the chalcogen as seen in a similar cluster, [$Ag_4(SPh)_4(dbfdp)_2$] reported by Nayyar.[15]

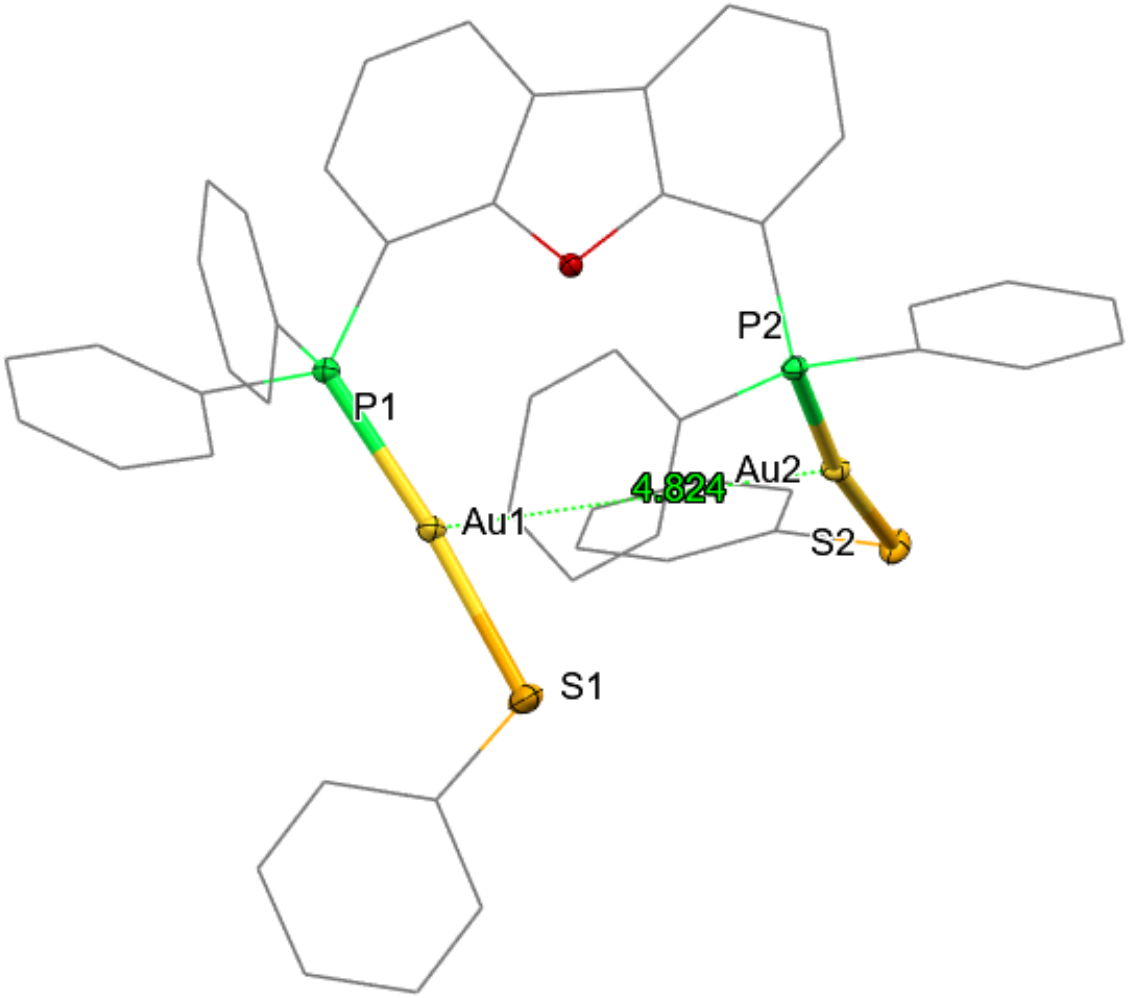

Figure 3.2: Molecular structure of [(AuSPh)$_2$(μ-dbfdp)] ***(3.2)*** *in the crystal (Au – S: 2.293(1) – 2.3044(8) Å, Au – P: 2.2496(9) – 2.2660(8) Å, Au Au distance: 4.824(8) Å) (H atoms are omitted for clarity).*

The molecular structure of **(3.2)** was determined by single crystal X-ray diffraction. Complex **(3.2)** crystallizes in the monoclinic space group $P2_1/c$ and contains four molecules per unit cell (Z = 4). The geometry of the gold (I) centres in compound **(3.2)** closely resembles the geometry of gold (I) centres in [(AuOAc)$_2$(dbfdp)] **(3.1)**, however the Au Au distance is even larger (4.824(8) Å in compound **(3.2)** vs. 3.723(2) Å in [(AuOAc)$_2$(dbfdp)] **(3.1)**). In compound **(3.2)**, the gold centres have a near-linear coordination geometry, bonding with one phosphorus and one sulfur centre. The P-Au-S angles in these compounds are near-linear with angles ranging from 170.68(3) ° to 175.32(4) °. A similar dinuclear gold (I) thiolate, [Au$_2${Ph$_2$PN(C$_6$H$_{11}$)PPh$_2$}(SC$_6$H$_4$F-*p*)$_2$] **(III.V)**

reported by Yam and co-workers, also demonstrates a near-linear gold geometry ranging from 165.41(7) ° to 172.38(7) °.[16] The bond distances between Au – S of **(III.V)** both sit at 2.290(2) Å, a very similar bond length to **(3.2)**, which range from 2.293(1) Å to 2.3044(8) Å. Surprisingly, **(III.V)** possesses an Au···Au length of 3.4379(4) Å which falls into the accepted aurophilic interaction range. This is likely the case due to the smaller phosphine-phosphine bite distance, which is 2.869(3) Å in $Ph_2PN(C_6H_{11})PPh_2$ and nearly double that at 5.813(1) Å in DBFDP.

The $^{31}P\{^1H\}$ NMR spectrum of the crystals of **(3.3)** showed a singular peak at 27.6 ppm ($W_{1/2}$ = 217 Hz). Compared to **(3.2)**, the chemical shift is lower frequency, likely due to the selenide donating more electron density than the sulfur. This is consistent with $[PPh_3Au(SC(SiMe_3)_3)]$ **(III.VI)** and $[(PPh_3Au(SeC(SiMe_3)_3)]$ **(III.VII)** reported by Arnold and co-workers.[17] The selenolate complex has a chemical shift of 37.6 ppm (lower frequency) compared to the 38.4 (higher frequency) of the thiolate.[17]

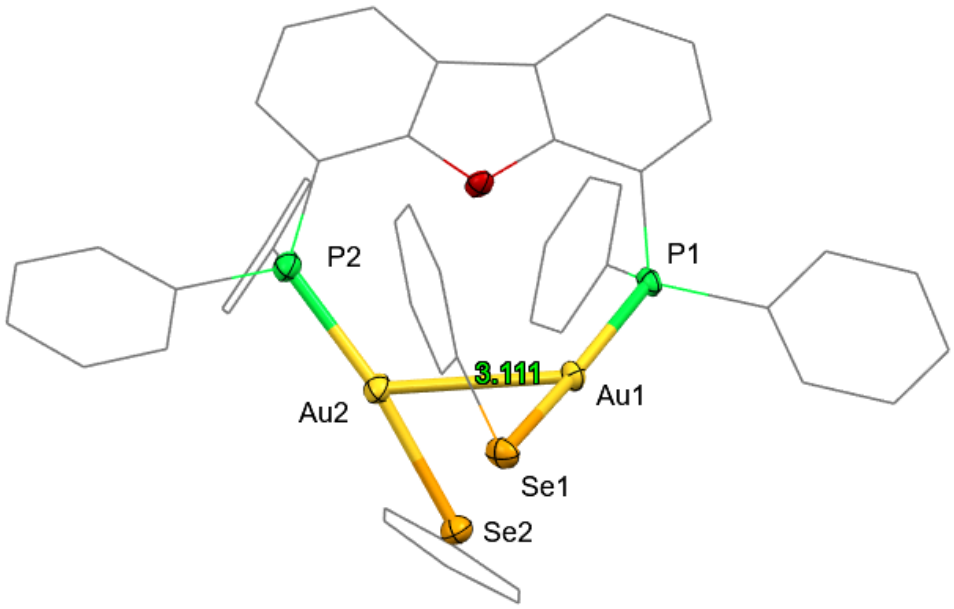

*Figure 3.3: Molecular structure of $[(AuSePh)_2(\mu\text{-dbfdp})]$ **(3.2)** in the crystal (Au – Se: 2.430(1) – 2.452(1) Å, Au – P: 2.267(2) – 2.284(2) Å, Au···Au: 3.111(1) Å) (H atoms are omitted for clarity).*

Compound **(3.3)** crystallizes in the space group $P\bar{1}$ and has two molecules per unit cell (Z = 2). The structure of compound **(3.3)** resembles closely to that of **(3.2)**, with the bridging DBFDP phosphine tethering two gold (I) atoms together. The P-Au-Se angle has a distorted-linear

geometry with angles ranging from 166.70(7) ° to 167.06(8) °. [(Ph_3P)AuSePh] **(III.VIII)** reported by Jones and co-workers acts as a good comparison for compound **(3.3)**.[18] As compared to compound **(3.3)**, **(III.VIII)** crystallizes as two independent molecules, which are linked by a gold-gold interaction of 3.118(1) Å which is of similar size to the gold-gold interactions linking the gold atoms in compound **(3.3)** (3.111(1) Å).[18] When comparing the coordination geometry of the gold (I) atoms in both complexes, **(III.VIII)** contains a more linear coordination geometry with angles ranging from 175.6(1) ° to 179.6(1) °. This is perhaps attributable to the incorporation of the DBFDP bidentate phosphine ligand forcing the gold atoms closer together in compound **(3.3)** (though in a side on fashion), creating a more distorted linear shape, as compared to the monodentate PPh_3 ligand which allows the P-Au-S angle to be less distorted in **(III.VIII)**.[18] The Au-Se length ranges from 2.422(1) Å to 2.415(1) Å in **(III.VIII)**, which resemble closely to the bond lengths in compound **(3.3)** which range from 2.430(1) Å to 2.452(1) Å.

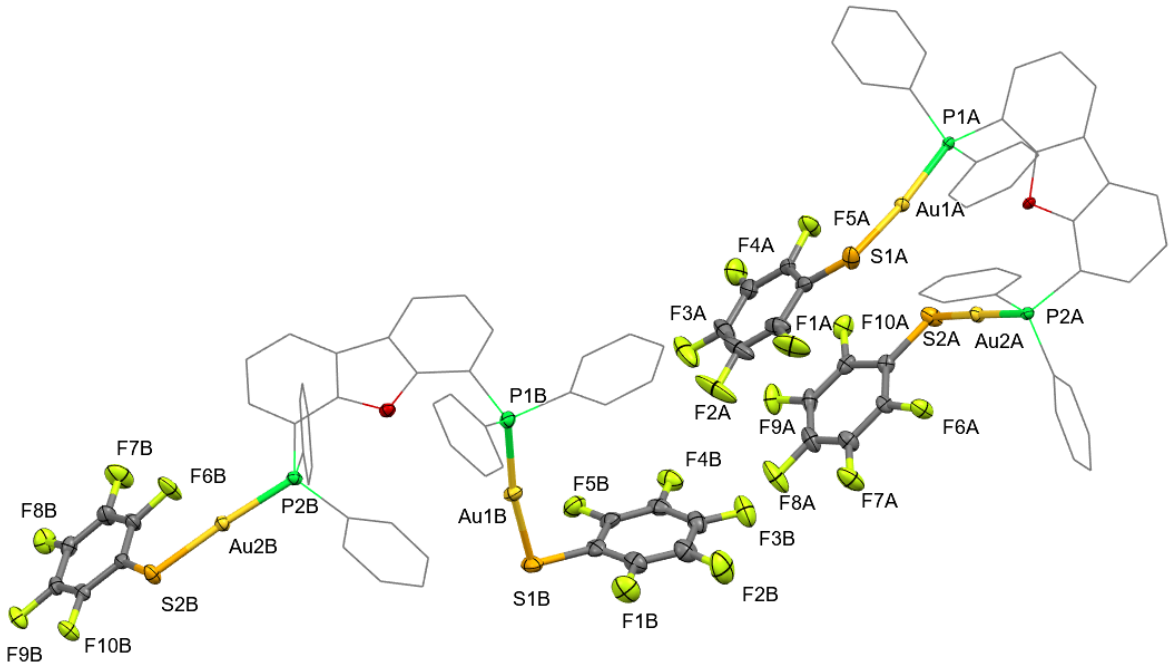

Figure 3.4: Molecular structure of [($AuSC_6F_5$)$_2$(μ-dbfdp)] ***(3.4)*** *in the crystal (Au – S: 2.302(3) – 2.314(2) Å, Au – P: 2.263(2) – 2.267(2) Å, Au Au distances: 3.53(1) – 7.941(2) Å) (H atoms are omitted for clarity).*

Following a different synthetic pathway than used for the preparation of **(3.2)** and **(3.3)**, compound **(3.4)** was obtained by the addition of 2,3,4,5-pentafluorothiolphenol and NEt_3 to [($AuCl$)$_2$(dbfdp)]

(III.IV) at -78 °C. The $^{31}P\{^{1}H\}$ NMR spectrum of compound **(3.4)** shows a peak at 25.9 ppm. However, a small peak of at 24.9 ppm indicates trace amounts of starting material remaining, $[(AuCl)_2(dbfdp)]$ **(III.IV)**.

The structures of compounds **(3.2)**, **(3.3)** and **(3.4)** resemble that reported by Forward.[11] The gold thiolates mentioned above all are dinuclear gold complexes with a bridging DBFDP ligand. Moreover, the chalcogenolates are coordinated in a terminal fashion with a ratio of 1:1 between chalcogenolate to gold centre similar to compounds that Forward discusses.[11]

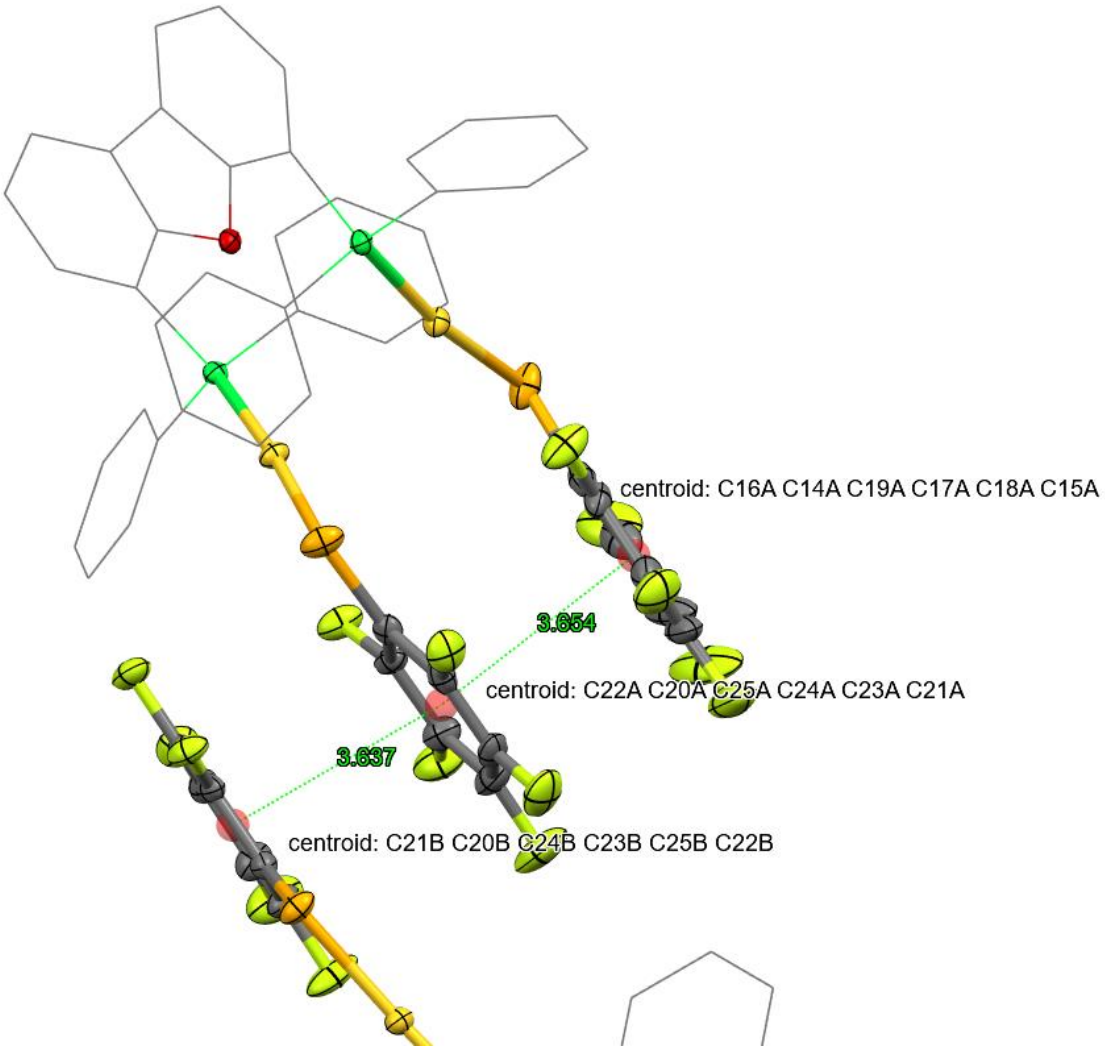

Figure 3.5: Crystal packing of $[(AuSC_6F_5)_2(\mu\text{-dbfdp})]$ ***(3.4)*** *depicting possible intramolecular and intermolecular π-π interactions and the distance between C_6F_5 aromatic rings.*

Compound **(3.4)** crystallizes in the space group $P\bar{1}$. **(3.4)** contains 2 molecules per asymmetric unit and has 4 molecules per unit cell (Z = 4). Similar to compounds **(3.2)** and **(3.3)**, the coordination geometries around the gold (I) atoms are close to linear. The angles of the P-Au-S bonds range from 170.61(8) ° to 176.20(7) °. Additionally, the Au-S bond distances range from 2.302(3) Å to 2.314(2) Å which are slightly longer than when compared to the Au-S distances for compound **(3.2)**. An interesting observation when examining the molecular structure of **(3.4)** is the perfluorinated phenyl rings of an individual asymmetrical unit (F1A – F5A vs F6A – F10A) – these C_6F_5 rings are in a 'parallel offset' orientation and are in the accepted distance (~3.8 Å) for π-π stacking.[19] With the addition of an electron withdrawing group, the dipoles of the perfluorinated rings invert. This could influence the potential π interactions between the two intramolecular rings, which appear to be in a parallel offset orientation. Interestingly, when examining the crystal packing of the molecule (*Figure 3.5* and *Figure 3.6)*, it appears that another C_6F_5 ring from another molecule of compound **(3.4)** participates in an intermolecular π-π interaction which could influence the crystal packing. However, to confirm if this arrangement of C_6F_5 rings result in a π interaction, computational studies are required.

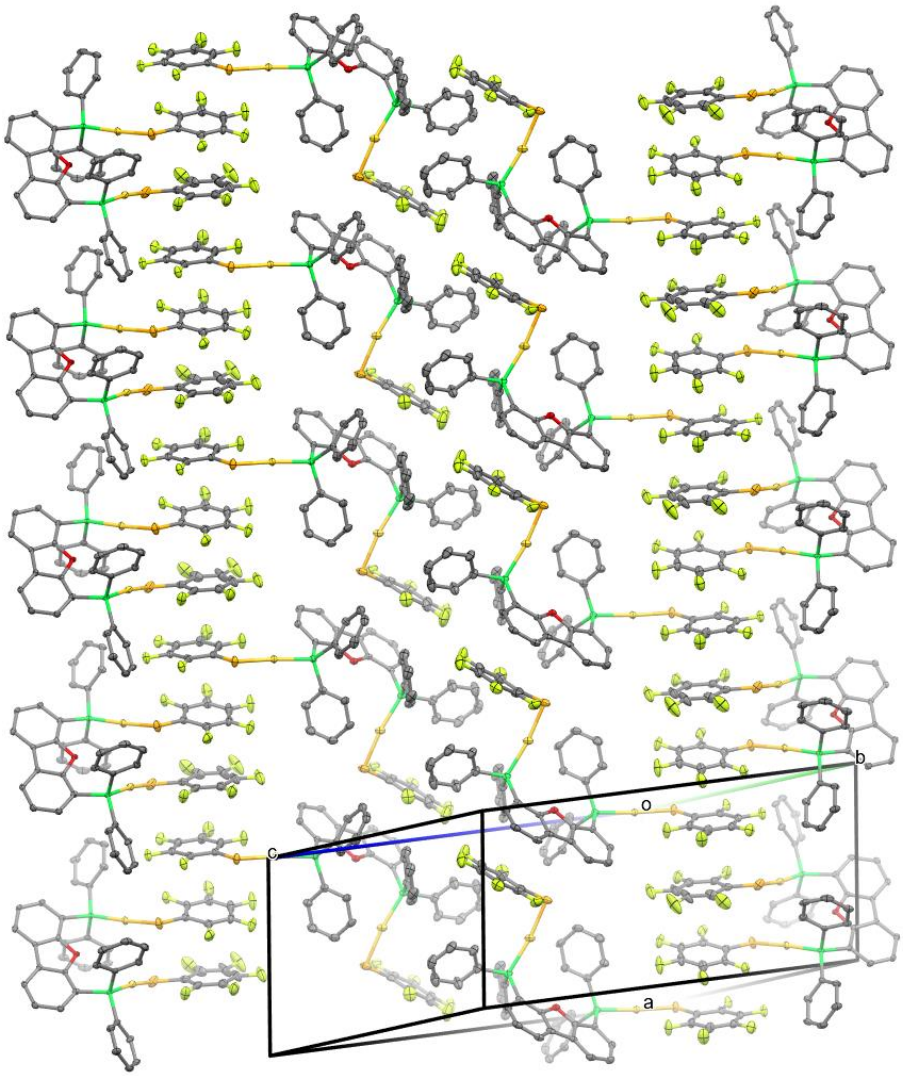

Figure 3.6: Crystal packing of [(AuSC$_6$F$_5$)$_2$(μ-dbfdp)] ***(3.4)*** *demonstrating possible long range intramolecular and intermolecular π interactions between C$_6$F$_5$ aromatic rings. (H atoms omitted for clarity)*

A $^{31}P\{^{1}H\}$ NMR spectrum was obtained for crystals of [Cu$_4$(μ$_2$-SC$_6$F$_5$)$_4$(μ-dbfdp)$_2$] **(3.5)** and showed a singular peak at -17.0 ppm ($W_{1/2}$ = 26.6 Hz). As compared to [(Cu$_5$(SPh)$_4$Cl(dbfdp)$_2$] **(III.IX),** which was previously synthesized by Nayyar, and shows a chemical shift at -15 ppm, compound **(3.5)** results in a similar chemical shift.[15]

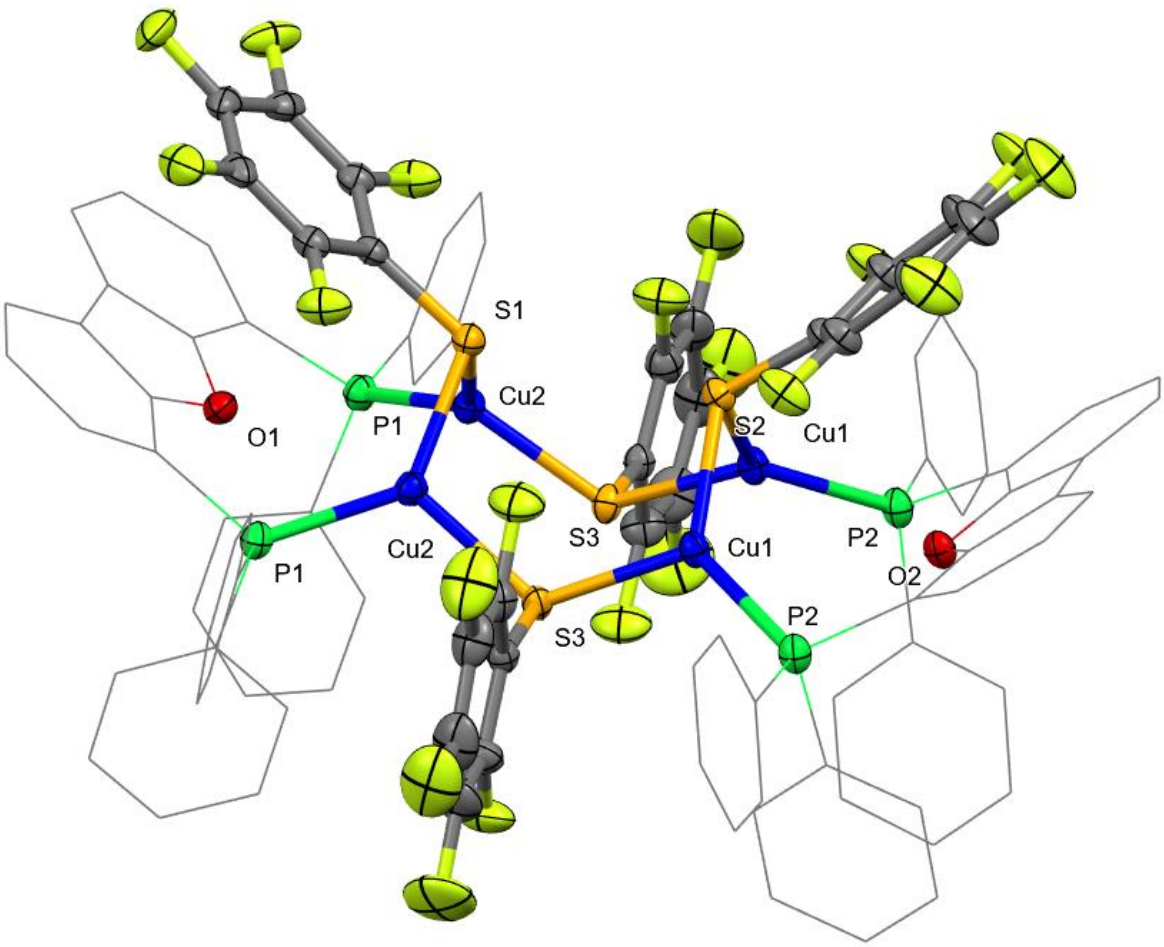

*Figure 3.7: Molecular structure of [($Cu_4(SC_6F_5)_4$(μ-dbfdp)$_2$] **(3.5)** in the crystal (Cu – S: 2.246 – 2.292(2) Å, Cu – P: 2.237(1) Å) (H atoms are omitted for clarity) (The molecule resides about a mirror plane O1/S1/S2/O2).*

Compound **(3.5)** crystallizes in the orthorhombic space group $Cmc2_1$ and contains 8 molecules per unit cell (Z of 8). There are four μ_2 thiolates that bridge two copper atoms. The four copper atoms within compound **(3.5)** have a trigonal planar coordination, bonded to one phosphorus and two sulfur centres as shown in *Figure 3.7.* The molecule contains a mirror plane through the two sulfur ligands (mirror plane passes through O1/S1/S2/O2 centres and the perfluorinated rings). Compound **(3.5)** is similar in structure to the previously discussed [($Cu_5(SPh)_4Cl$(dbfdp)$_2$] **(III.IX)**, aside from a chloride functionality between the analogous (S3 centres in **(3.5)**). This could be due to extra electron density from the fluorine as compared to the protons in **(III.IX).** No

evidence for cuprophilic interactions were observed (distances between copper atoms were larger than possible cuprophilic distances).[20] It can also be argued that there are π interactions between the two phenyl rings of the DBFDP and the C_6F_5 ring of the thiolate ligand (Ph-C_6F_5-Ph) on the periphery of the molecule. With the reversed dipole moment, the periphery of the C_6F_5 ring inverts in polarity which can interact with the slightly positive dipole of the phenyl ring.[19,21] The same π-interactions may also be argued with the C_6F_5 ring above the dibenzofuran backbone of the phosphine ligand.

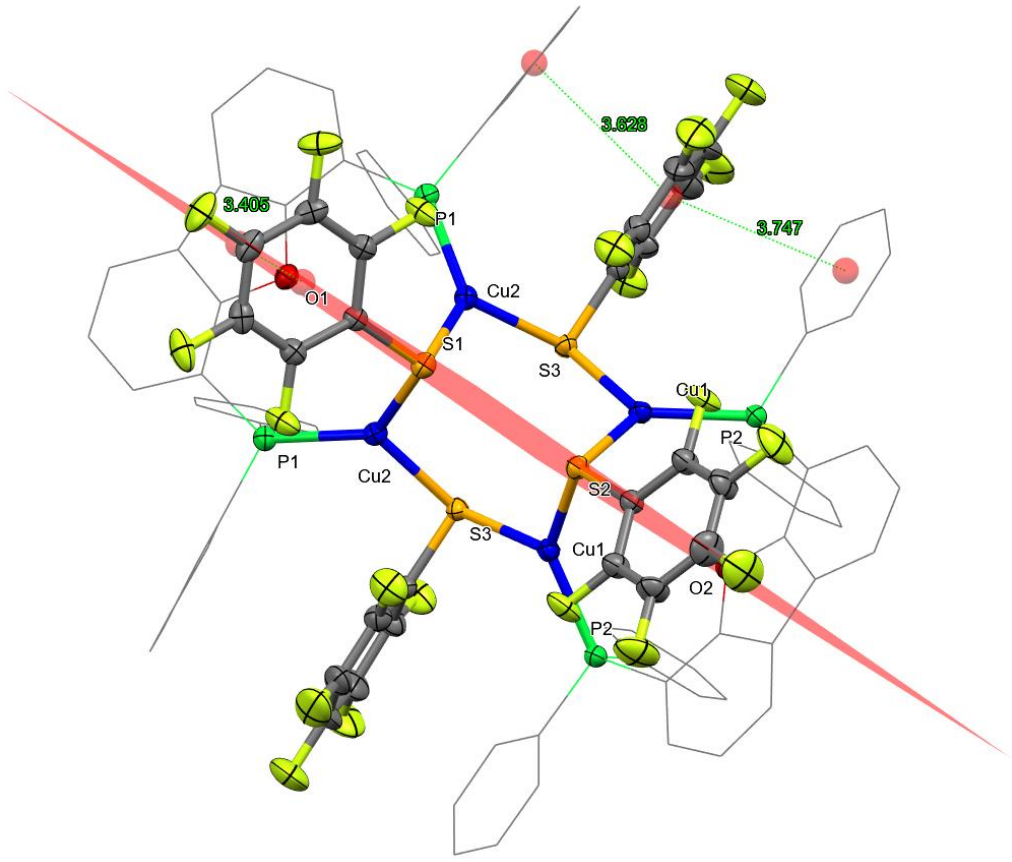

*Figure 3.8: Illustration of mirror planes in compound **(3.5)** from top-down perspective. Mirror plane passes through S1/S2/O1/O2. Distances between C_6F_5 distances range from 3.405 Å – 3.747 Å.*

3.2.2 Photophysical Properties of Metal Chalcogenolate Complexes (3.2) – (3.5)

It has previously been well documented that the use of DBFDP and group 11 metals results in highly luminescent materials. With the ability of DBFDP to bridge two metal centres and the

rigidity of the ligand due to its backbone, copper and silver chalcogenolate complexes with a wide range of PLQYs were documented by Nayyar.[15] Incorporation of DBFDP could result in different luminescence of the complexes prepared. Crystals of **(3.2) - (3.5)** were irradiated with a handheld UV lamp (λ = 254 nm and 365 nm) and it was observed that **(3.2)** and **(3.3)** were visually emissive. However, crystals of **(3.4)** and **(3.5)** did not seem emissive when irradiated. The emission and excitation spectra of **(3.2) - (3.5)** were obtained in the solid state. When compared to one another, the difference in λ_{exc} and λ_{em} can be observed in **(3.2)** and **(3.3)** likely as a result of the difference in electron density of the chalcogen (change from S to Se).

For compound **(3.2)**, λ_{exc} was observed to be 470 nm and λ_{em} was observed to be at 552 nm. With a λ_{em} of 552 nm, it is expected to be emissive in the green-yellow region which is what is observed at a weak intensity. As compared to $[Au_2\{Ph_2PN(Ph)PPh_2\}(SC_6H_4Me\text{-}p)_2]$ **(III.X)** reported by Yam and co-workers, the reported cluster has a λ_{em} of 506 nm which is similar in structure to **(3.2)**, as well as somewhat similar in emission wavelengths (552 nm vs 506 nm).[16]

The λ_{exc} of **(3.3)** was determined to be 447 nm and the λ_{em} was determined to be 513 nm. In terms of intensity, compound **(3.3)** was more emissive than compound **(3.2)** according to the emission spectra**.** This could be the case due to the structural rigidity of the complex when comparing **(3.2)** to **(3.3)**, as the selenolate analogue has a potential aurophilic interaction which makes the molecule more rigid as compared to the free thiolate moiety in **(3.2)**. As a comparison, the $[Cu_4(\mu_{2/3}\text{-}SePh)_4(\mu\text{-}dbfdp)_2]$ **(III.XI)** and $[Ag_6(\mu_{2/3}\text{-}SePh)_6(\mu\text{-}dbfdp)_2]$ **(III.XII)** clusters documented by Nayyar can be used to examine differences when using a larger d^{10} metal. $[Cu_4(\mu_{2/3}\text{-}SePh)_4(\mu\text{-}dbfdp)_2]$ **(III.XI)** was determined to have a λ_{em} of 560 nm and $[Ag_6(\mu_{2/3}\text{-}SePh)_6(\mu\text{-}dbfdp)_2]$ **(III.XII)** was determined to have a λ_{em} of 530 nm. Compound **(3.3)** has a λ_{em} of 513 nm, thus by changing the metal of increasing size, it appears the λ_{em} experiences a slight hypsochromic shift for the emission as seen in *Figure 3.9.*

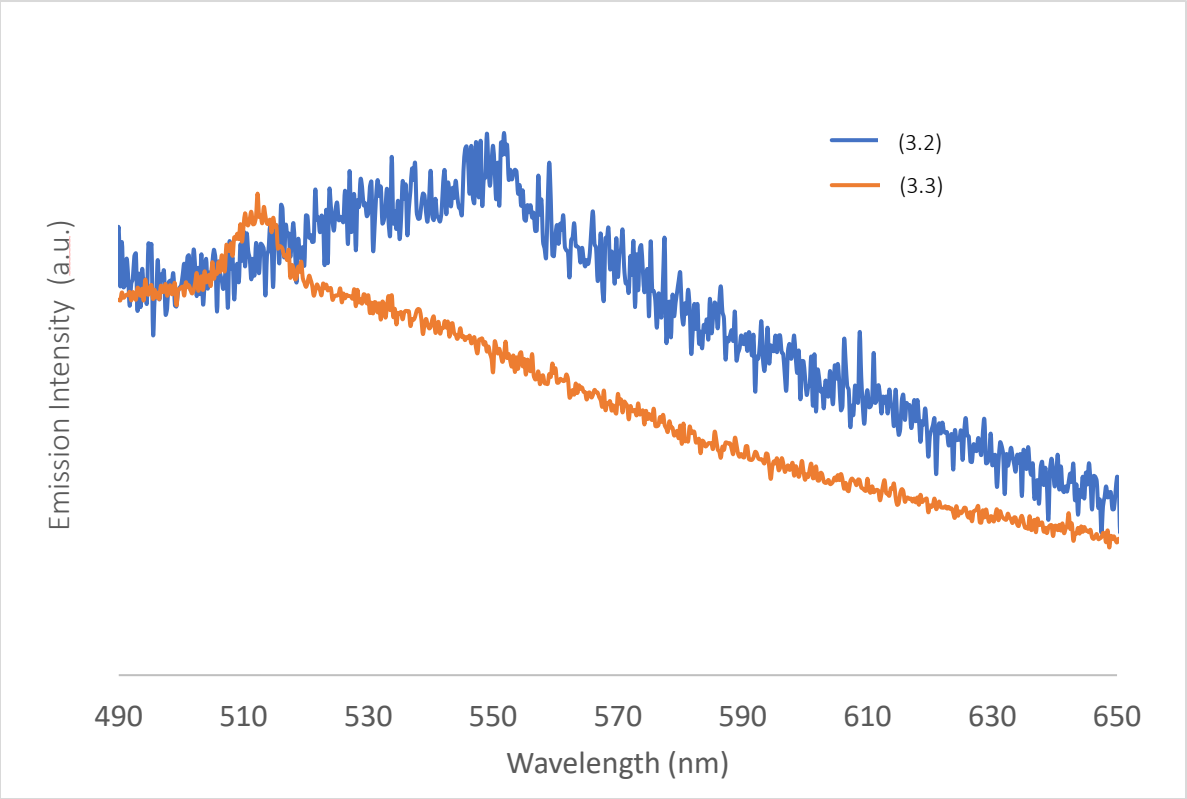

*Figure 3.9: Emission spectra of **(3.2), (3.3)** in the solid state at room temperature. (λ_{exc} = 470 nm **(3.2)**, λ_{exc} = 447 nm **(3.3)**).*

To understand the effect of the addition of an electron-withdrawing group to the gold (I) chalcogenolate clusters, $C_6F_5S^-$ was introduced. By addition of an electron-withdrawing group, it was hypothesized that the HOMO-LUMO gap would be altered, and a different emission profile could be observed. However, compounds **(3.4)** and **(3.5)** did not appear visually emissive – the absorption, emission and excitation spectra were gathered and reported below.

When the PL and PLE spectra of **(3.4)** are examined, the λ_{exc} is determined to be 293 nm. Aside from the artifact (which occurs at two times the excitation wavelength), **(3.4)** is determined to be non-emissive in the visible spectrum. As evidenced by Forward and co-workers, when an electron-withdrawing group (Cl^-) is incorporated into a phenyl(chalcogenolate) cluster, the λ_{em} is red shifted.[11] As seen with [(TPA)Au(SC_6H_5)] **(III.XIII)**, [(TPA)Au(SC_6H_4(m-Cl))] **(III.XIV)** and [(TPA)Au(SC_6H_4(p-Cl))] **(III.XV)**, it can be argued that with the incorporation of electron-withdrawing groups on the phenyl ring (as with compound **(3.4)** and **(3.5)**) could result in a

bathochromic shift of the emission into the IR region.[11] However, to confirm this hypothesis, more emission studies (near-IR) would need to be conducted.

Similarly, the PL and PLE of **(3.5)** recount a similar story; the λ_{exc} of **(3.5)** is determined to be 287 nm. The excitation spectrum of **(3.5)** shows no emission in the visible range (aside from the artifact two times the excitation wavelength). Again, the emission of **(3.5)** could be near the infrared region, in which, near IR emission studies would be required to confirm this hypothesis.

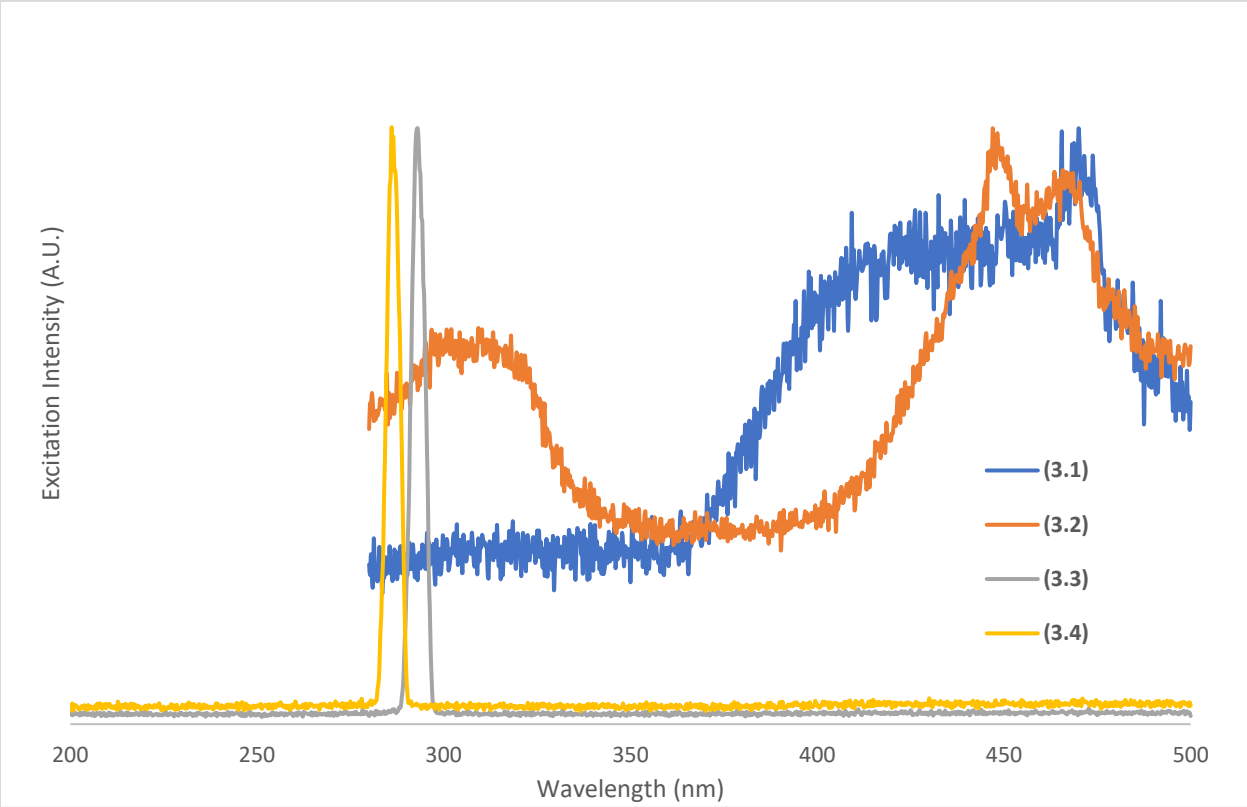

*Figure 3.10: Excitation spectra of **(3.2), (3.3), (3.4)** and **(3.5)** in the solid state at room temperature.*

3.3 Experimental

3.3.1 General Considerations

All experiments were carried out under an inert atmosphere of high purity, dried nitrogen using standard Schlenk line techniques on a double manifold vacuum line. All solvents used were either distilled over the appropriate desiccant under nitrogen or were dried using a commercial Mbraun

MB-SP series solvent purification system. Celite® was dried under dynamic vacuum at 220 °C for 24 hours and stored under nitrogen in a sealed flask.

Dibenzofuran was purchased from TCI American and was used without further purifications. 2,3,4,5,6-Pentafluorophenol thiol was purchased from Sigma Aldrich and used without further purification. Copper (I) chloride was purified by a colleague and used without further purification. Triethylamine was refluxed over CaH_2 for three hours and distilled under nitrogen according to literature procedure.[22] Chlorodiphenylphosphine and n-butyllithium (1.6 M in hexanes) were purchased and used without further purification. Tetramethylethylenediamene (TMEDA) was refluxed with KOH pellets for three hours and distilled under nitrogen according to literature procedure.[22] Phenyl(trimethylsilyl)sulfide and phenyl(trimethylsilyl)selenide were synthesized by a colleague using literature procedures and used without further purification.[23] 4,6-*bis*(diphenylphosphino)dibenzofuran (DBFDP) was synthesized by incorporating two literature procedures with few modifications.[24,25]

^{1}H, $^{31}P\{^{1}H\}$, $^{13}C\{^{1}H\}$, ^{19}F NMR spectra were recorded on the Bruker AvanceIII HD 400 (B400) with frequencies of 400.130 MHz, 161.976 MHz, 100.613 MHz, and 56.76 MHz respectively. The ^{1}H NMR spectra were referenced to residual proton solvent in $CDCl_3$. The $^{13}C\{^{1}H\}$ NMR spectra were referenced to the carbon atoms in $CDCl_3$. The $^{31}P\{^{1}H\}$ NMR spectra were referenced to 85 % H_3PO_4. Attenuated Total Reflectance Infrared (ATR-IR) spectra of samples of **(3.2)**, **(3.3)**, **(3.4)** and **(3.5)** were obtained using Bruker Alpha II Spectrometer. The data were analyzed using OPUS – Operator Default Software. Melting points of samples **(3.2) - (3.5)** were recorded on a Gallenkamp melting point apparatus under N_2 atmosphere. Samples for elemental analysis were prepared under N_2 atmosphere. Samples are currently awaiting elemental analysis at the Centre for Environmental Analysis and Remediation by Patricia Granados at Saint Mary's University in Halifax, Nova Scotia.

Single crystal X-ray data collection were completed by Dr. John F. Corrigan, Dr. Jalil Assoud and Nils Vogeler on a Bruker Kappa Axis Apex 2 diffractometer at a temperature of 110 K. The sample was placed on a MiTeGen polyimide micromount with a small amount of Paratone N oil. The raw data were scaled, and absorption corrected using SADABS and the frame integration was done by SAINT.[26,27] SHELXT program was used to solve the structure.[28] All non-hydrogen atoms were obtained from the initial solution, introduced at idealized positions, and were allowed to ride on

the parent atom. The structural model was fit to the data by full matrix least squares based on F2. The structure was further refined using the SHELXL program from the SHELXTL suite of crystallographic software.[29]

In the collection of the solid photoluminescence, crystalline samples of **(3.2)**, **(3.3)**, **(3.4)** and **(3.5)** were adhered to 2-sided Scotch tape (410B, 3M, Saint Paul, MN) on a custom-made platform with a 45-degree angle between the excitation beam and emission detector. The emission and excitation slit widths were optimized for the signal strength. The 2-sided tape was chosen due to its low PL signal. The powder was spread over the tape via spatula in a thin layer to prevent excitation of the tape via the excitation beam. The data was analyzed by the FelixGX version 2 software by Photon Technology International (PTI).

3.3.2 Synthesis of [(AuOAc)$_2$(dbfdp)] (3.1)

For synthesis of compound **(3.1)**, refer to ***Chapter 2.3.1. Synthesis of[(AuOAc)$_2$(dbfdp)]*** in the thesis '*Luminescent Group 11 Metal (I) Chalcogen Clusters with a Conjugated Diphosphine Ligand'.*

3.3.3 Synthesis of [(AuSPh)$_2$(dbfdp)] (3.2)

Compound **(3.1)** (0.050 g, 0.048 mmol, 1 equiv.) was dissolved in 10 mL of THF and stirred for 15 minutes. Phenyl(trimethylsilyl)sulfide (0.020 mL, 0.095 mmol, 2 equiv.) was added while stirring at -78 °C. The solution was warmed over 2 hours to room temperature and stirred overnight. The solution was layered with heptane and colourless crystals of **(3.2)** were observed after 2-3 days. Yield = 53 % based on **(3.1)**). $^{31}P\{^{1}H\}$ NMR (161 MHz, $CDCl_3$, 23.5 °C): δ = 30.2. m.p. = 173 °C$_{decomp}$. Crystal structure data, bond angles and bond lengths are attached in the **Appendix** in *Tables S3.1, S3.2* and *S3.3*. $^{31}P\{^{1}H\}$ NMR and ^{1}H NMR spectra are attached in the **Appendix** in *Figures S3.1* and *S3.2.*

3.3.4 Synthesis of [(AuSePh)$_2$(dbfdp)] (3.3)

Compound **(3.1)** (0.050 g, 0.048 mmol, 1 equiv.) was dissolved in 10 mL THF and stirred for 15 minutes. Phenyl(trimethylsilyl)selenide (0.020 mL, 0.095 mmol, 2 equiv.) was added while stirring at -78 °C. The solution was warmed over 2 hours to room temperature and stirred overnight. The solution was layered with heptane and colourless crystals of **(3.3)** were observed after 2-3 days. Yield = 48 % (based on **(3.1)**). $^{31}P\{^{1}H\}$ NMR (161 MHz, $CDCl_3$, 23.5 °C): δ =

27.6. m.p. = 194 °C_{decomp}. Crystal structure data, bond angles and bond lengths are attached in the **Appendix** in *Tables S3.4, S3.5* and *S3.6*. $^{31}P\{^{1}H\}$ NMR and ^{1}H NMR spectra are attached in the **Appendix** in *Figures S3.3* and *S3.4.*

3.3.5 Synthesis of [(AuSC$_6$F$_5$)$_2$(dbfdp)] (3.4)

DBFDP (0.040 g, 0.075 mmol, 1 equiv.) and Au(tht)Cl (0.048 g, 0.150 mmol, 2.0 equiv.) were dissolved in 10 mL of DCM stirred for 15 minutes. 2,3,4,5-pentafluorophenyl thiol (0.02 mL, 0.15 mmol, 2.0 equiv.) was added alongside triethylamine (0.023 mL, 0.15 mmol, 2.2 equiv.) at -78 °C. The solution was warmed to room temperature over 2 hours and DCM was removed *in vacuo*. The solids were then solubilized with 10 mL of toluene and filtered over Celite®. The resulting filtrate was layered with hexanes to yield compound **(3.4)** as colourless plates after 2-3 days. Yield = 68 %. $^{31}P\{^{1}H\}$ NMR (161 MHz, $CDCl_3$, 23.5 °C): δ = 25.6. m.p. = 202 °C_{decomp}. Crystal structure data, bond angles and bond lengths are attached in the **Appendix** in *Tables S3.7, S3.8* and *S3.9*. $^{31}P\{^{1}H\}$ NMR and ^{1}H NMR spectra are attached in the **Appendix** in *Figures S3.5* and *S3.6.*

3.3.6 Synthesis of [Cu$_4$(SC$_6$F$_5$)$_4$(dbfdp)$_2$] (3.5)

DBFDP (0.040 g, 0.075 mmol, 1 equiv.) and CuCl (0.015 g, 0.15 mmol, 2.0 equiv.) was dissolved in 10 mL of DCM stirred for 30 minutes. Following dissolution, 2,3,4,5-Pentafluorophenyl thiol (0.02 mL, 0.015 mmol, 2.0 equiv.) was added alongside triethylamine (0.023 mL, 0.015 mmol, 2.2 equiv.) at -78 °C. The solution was warmed to room temperature over 2 hours and DCM was removed *in vacuo*. The solids were then solubilized with 10 mL of toluene and filtered over Celite®. The resulting filtrate was layered with hexanes to yield compound **(3.5)** as colourless plates after 2-3 days. Yield = 73 %. $^{31}P\{^{1}H\}$ NMR (161 MHz, $CDCl_3$, 23.5 °C): δ = -17.0. m.p. = 215 °C_{decomp}. Crystal structure data, bond angles and bond lengths are attached in the **Appendix** in *Tables S3.10, S3.11* and *S3.12*. $^{31}P\{^{1}H\}$ NMR and ^{1}H NMR spectra are attached in the **Appendix** in *Figures S3.7* and *S3.8.*

3.4 Conclusions

In summary, the addition of $PhESiMe_3$ (E = S, Se) to $[(AuOAc)_2(\mu\text{-dbfdp})]$ resulted in dinuclear gold chalcogenolate complexes with terminal chalcogenolate ligands and bridging DBFDP. $[(AuSPh)_2(dbfdp)]$ **(3.2)** and $[(AuSePh)_2(dbfdp)]$ **(3.3)** were confirmed to be emissive and both displayed a green-yellow emission in the solid state at room temperature with a λ_{em} of 552 nm for **(3.2)** and λ_{em} of 513 nm for **(3.3)**. Structurally, compounds **(3.2)** and **(3.3)** are dinuclear gold complexes. Upon analysis of **(3.2)** and **(3.3)**, compound **(3.2)** had no suggested aurophilic interactions, whereas compound **(3.2)** demonstrated an interaction between the two gold atoms. Complexes **(3.2)** and **(3.3)** are consistent with other phosphine ligated gold chalcogenolate clusters reported in literature.[11,12,16] These complexes are generally for a linear for a monodentate phosphine such as PPh_3, whereas for bidentate phosphine results in a smaller complexes with a terminal chalcogenolate ligand.[11,12,16]

Following a different synthetic pathway used for **(3.2)** and **(3.3)**, $[(AuCl)_2(dbfdp)]$ **(III.IV)** and $[(CuCl)_2(dbfdp)]$ were reacted with 2 equivalents of $(C_6F_5)SH$ and 2 equivalents of NEt_3 to yield complexes $[(AuSC_6F_5)_2(dbfdp)]$ **(3.4)** and $[Cu_4(SC_6F_5)_4(dbfdp)_2]$ **(3.5)**. Compounds **(3.4)** and **(3.5)** were confirmed to be non-emissive in the visible region. Structurally, the incorporation of an electron withdrawing groups on the R group of the chalcogenolate ($C_6F_5S^-$) does result in many differences between the parent phenyl thiolate Cu (I) and Au (I) clusters.[15] Interestingly, the incorporation of the perfluorinated phenyl ring in the complexes resulted in indications of π-interactions, however further computational studies are required to confirm such.

3.5 References

(1) Fuhr, O.; Dehnen, S.; Fenske, D. Chalcogenide Clusters of Copper and Silver from Silylated Chalcogenide Sources. *Chem. Soc. Rev.* **2013**, *42* (4), 1871–1906. https://doi.org/10.1039/C2CS35252D.

(2) Veselska, O.; Demessence, A. D10 Coinage Metal Organic Chalcogenolates: From Oligomers to Coordination Polymers. *Coord. Chem. Rev.* **2018**, *355*, 240–270. https://doi.org/10.1016/j.ccr.2017.08.014.

(3) Hu, B.; Su, C. Y.; Fenske, D.; Fuhr, O. Synthesis, characterization and optical properties of a series of binuclear copper chalcogenolato complexes. *Inorganica Chim. Acta* **2014**, *419* (August), 118. https://doi.org/10.1016/j.ica.2014.05.009.

(4) Langer, R.; Yadav, M.; Weinert, B.; Fenske, D.; Fuhr, O. Luminescence in Functionalized Copper Thiolate Clusters – Synthesis and Structural Effects. *Eur. J. Inorg. Chem.* **2013**, *2013* (21), 3623–3631. https://doi.org/10.1002/ejic.201300155.

(5) DeGroot, M. W.; Corrigan, J. F. Coordination Complexes of Zinc with Reactive ESiMe3 (E = S, Se, Te) Ligands. *Organometallics* **2005**, *24* (14), 3378–3385. https://doi.org/10.1021/om050088v.

(6) DeGroot, M. W.; Corrigan, J. F. Polynuclear Bismuth Selenolates: Rings En Route to Clusters. *J. Chem. Soc. Dalton Trans.* **2000**, No. 8, 1235–1236. https://doi.org/10.1039/B001417F.

(7) Duan, T.; Zhang, X.-Z.; Zhang, Q.-F. Synthesis and Crystal Structure of a Polynuclear Copper-Selenide Cluster [CuI36(CuIICl)2Se13(SePh)12(Dppe)6] · 3EtOH. *Z. Für Naturforschung B* **2008**, *63* (8), 941–944. https://doi.org/10.1515/znb-2008-0804.

(8) Dehnen, S.; Eichhöfer, A.; Corrigan, J. F.; Fuhr, O.; Fenske, D. *Synthesis and characterization of Ib-VI nanoclusters*. https://publikationen.bibliothek.kit.edu/150081429 (accessed 2023-06-12).

(9) Dehnen, S.; Eichhöfer, A.; Fenske, D. Chalcogen-Bridged Copper Clusters. *Eur. J. Inorg. Chem.* **2002**, *2002* (2), 279–317. https://doi.org/10.1002/1099-0682(20022)2002:2<279::AID-EJIC279>3.0.CO;2-H.

(10) Li, Y.-L.; Zhang, W.-M.; Wang, J.; Tian, Y.; Wang, Z.-Y.; Du, C.-X.; Zang, S.-Q.; Mak, T. C. W. Photoluminescence Modulation of an Atomically Precise Silver(I)–Thiolate Cluster via Site-Specific Surface Engineering. *Dalton Trans.* **2018**, *47* (42), 14884–14888. https://doi.org/10.1039/C8DT03165G.

(11) Forward, J. M.; Bohmann, D.; Fackler, J. P.; Staples, R. J. Luminescence Studies of Gold(I) Thiolate Complexes. *Inorg. Chem.* **1995**, *34* (25), 6330–6336. https://doi.org/10.1021/ic00129a019.

(12) Yam, V. W.-W.; Chan, C.-L.; Li, C.-K.; Wong, K. M.-C. Molecular Design of Luminescent Dinuclear Gold(I) Thiolate Complexes: From Fundamentals to Chemosensing. *Coord. Chem. Rev.* **2001**, *216–217*, 173–194. https://doi.org/10.1016/S0010-8545(01)00310-1.

(13) Sladek, A.; Angermaier, K.; Schmidbaur, H. Gold Clustering at the Methylthiolate Anion. *Chem. Commun.* **1996**, No. 16, 1959. https://doi.org/10.1039/cc9960001959.

(14) Bumbu, O.; Ceamanos, C.; Crespo, O.; Gimeno, M. C.; Laguna, A.; Silvestru, C.; Villacampa, M. D. Unprecedented Gold−Tellurolate Clusters [Au8(μ-TeR)8(PR‘3)4]. *Inorg. Chem.* **2007**, *46* (26), 11457–11460. https://doi.org/10.1021/ic7013545.

(15) Nayyar, M. Luminescent Group 11 Metal Chalcogen Clusters with Bidentate Phosphine Ligands, The University of Western Ontario, London, 2021.

(16) Yam, V. W.-W.; Chan, C.-L.; Cheung, K.-K. Synthesis and Photophysics of Dinuclear Gold(I) Thiolates of Bis(Diphenylphosphino)-Alkyl- and -Aryl-Amines. Crystal Structure of [Au2{Ph2PN(C6H11)PPh2}(SC6H4F-p)2]. *J. Chem. Soc. Dalton Trans.* **1996**, No. 20, 4019. https://doi.org/10.1039/dt9960004019.
(17) Bonasia, P. J.; Gindelberger, D. E.; Arnold, J. Synthesis and Characterization of Gold(I) Thiolates, Selenolates, and Tellurolates: X-Ray Crystal Structures of Au4[TeC(SiMe3)3]4, Au4[SC(SiMe3)3]4, and Ph3PAu[TeC(SiMe3)3]. *Inorg. Chem.* **1993**, *32* (23), 5126–5131. https://doi.org/10.1021/ic00075a031.
(18) Jones, P. G.; Thöne, C. Gold Complexes with Selenium Ligands, I. Preparation and Crystal Structures of Phenylselenolato-gold(I) Complexes. *Chem. Ber.* **1990**, *123* (10), 1975–1978. https://doi.org/10.1002/cber.19901231008.
(19) Martinez, C. R.; Iverson, B. L. Rethinking the Term "Pi-Stacking." *Chem. Sci.* **2012**, *3* (7), 2191. https://doi.org/10.1039/c2sc20045g.
(20) Harisomayajula, N. V. S.; Makovetskyi, S.; Tsai, Y. Cuprophilic Interactions in and between Molecular Entities. *Chem. – Eur. J.* **2019**, *25* (38), 8936–8954. https://doi.org/10.1002/chem.201900332.
(21) Hunter, C. A.; Sanders, J. K. M. The Nature of .Pi.-.Pi. Interactions. *J. Am. Chem. Soc.* **1990**, *112* (14), 5525–5534. https://doi.org/10.1021/ja00170a016.
(22) Armarego, W. L. F. *Purification of Laboratory Chemicals: Part 2 Inorganic Chemicals, Catalysts, Biochemicals, Physiologically Active Chemicals, Nanomaterials*; Butterworth-Heinemann, 2022.
(23) So, J.-H.; Boudjouk, P. Convenient Syntheses of Hexamethyldisilathiane and Tetramethyldisilathiane. *Synthesis* **1989**, *1989* (04), 306–307. https://doi.org/10.1055/s-1989-27235.
(24) Kranenburg, M.; van der Burgt, Y. E. M.; Kamer, P. C. J.; van Leeuwen, P. W. N. M.; Goubitz, K.; Fraanje, J. New Diphosphine Ligands Based on Heterocyclic Aromatics Inducing Very High Regioselectivity in Rhodium-Catalyzed Hydroformylation: Effect of the Bite Angle. *Organometallics* **1995**, *14* (6), 3081–3089. https://doi.org/10.1021/om00006a057.
(25) Xie, M.; Han, C.; Zhang, J.; Xie, G.; Xu, H. White Electroluminescent Phosphine-Chelated Copper Iodide Nanoclusters. *Chem. Mater.* **2017**, *29* (16), 6606–6610. https://doi.org/10.1021/acs.chemmater.7b01443.
(26) Bruker-AXS, SADABS Version 2012.1, 2012, Bruker-AXS, Madison WI 53711, USA.
(27) Bruker-AXS, SAINT Version 2013.8, 2013, Bruker-AXS, Madison WI53711, USA.
(28) Sheldrick, G. M. SHELXT – Integrated Space-Group and Crystal-Structure Determination. *Acta Crystallogr. Sect. Found. Adv.* **2015**, *71* (1), 3–8. https://doi.org/10.1107/S2053273314026370.
(29) Sheldrick, G. M. Crystal Structure Refinement with SHELXL. *Acta Crystallogr. Sect. C Struct. Chem.* **2015**, *71* (1), 3–8. https://doi.org/10.1107/S2053229614024218.

Chapter 4

4.0 Conclusions and Outlook

4.1 Summary and Conclusions

The work in this thesis discusses the preparation and analysis of Group 11 Gold/Copper Chalcogen Clusters with a Rigid and Conjugated Bidentate Phosphine Ligand.

Gold (I) chalcogenide clusters are synthesized by forming the precursors $[(AuOAc)_2(dbfdp)]$ **(2.1)** and $[(AuOTf)_2(\mu\text{-}dbfdp)]$) **(2.2)**. Compound **(2.1)** was further reacted with chalcogen reagents with ($E(SiMe_3)_2$; E = S, Se) at lower temperatures to form dinuclear $[(Au_2S)(dbfdp)]$ **(2.3 S)** and $[(Au_2Se)(dbfdp)]$ **(2.3 Se)**. These were used in subsequent synthesis of higher nuclearity gold clusters together with $[(AuOTf)_2(\mu\text{-}dbfdp)]$) **(2.2)** or Cu(I)OTf, to form $[Au_4(\mu_4\text{-}S)(\mu\text{-}dbfdp)_2](OTf)_2$ **(2.4 S)**, $[Au_4(\mu_4\text{-}Se)(\mu\text{-}dbfdp)_2](OTf)_2$ **(2.4 Se)**, $[Au_6(\mu_3\text{-}S)_2(\mu\text{-}dbfdp)_3](OTf)_2$ **(2.5 S)** and $[Au_6(\mu_3\text{-}Se)_2(\mu\text{-}dbfdp)_3](OTf)_2$ **(2.5 Se)**. Compounds **(2.3 S)** and **(2.3 Se)** are phosphine protected dinuclear gold compounds, bridged by a chalcogen and analogous in structure, differing only in the chalcogen used. The tetranuclear **(2.4 S)** and **(2.4 Se)** and hexanuclear **(2.5 S)** and **(2.5 Se)** are also analogous in structure to each other, aside from the chalcogenide. The chalcogenide in these clusters range from μ_2-μ_4 while the metal atoms present in these clusters range from 2-6 atoms.

The overarching theme for this thesis is the phosphine ligand bridging two metal centres together. It was observed that for compounds **(2.3 S)** and **(2.3 Se)**, the complexes are dinuclear, regardless of the chalcogen used. As observed, $[(Au_2S)(dbfdp)]$ **(2.3 S)** and $[(Au_2Se)(dbfdp)]$ **(2.3 Se)** slightly differ via the chalcogen-metal bond, however resemble the same general shape of two metal centres bridged by the DBFDP and the chalcogen atom. The larger gold-chalcogen bond distance is likely attributed to the larger chalcogen size (S = 88 pm vs Se = 103 pm)[1] as when we compare **(2.3 S)** and **(2.3 Se),** the Au-Se bond is longer than the Au-S bond, despite their similar structures. Additionally, for complexes **(2.3 S/Se)-(2.5 S/Se)**, all clusters have possible aurophilic interactions with Au···Au distances falling within the generally accepted 2.5-3.5 Å threshold.[2,3] As for the higher nuclearity clusters, **(2.4 S/Se)** and **(2.5 S/Se)**, the same trend exists whereby the larger

chalcogen provides a longer gold-chalcogen bond. For compounds **(2.4 S)** and **(2.4 Se)**, the Au:E ratios are 1:4 where the chalcogen assumes a μ_4 bonding mode. For compounds **(2.5 S)** and **(2.5 Se)**, it was determined that their molecular structure contains Au_3S subunits, which are characteristic of certain gold (I) chalcogenide clusters as shown by Yam and co-workers.[4] These two clusters, **(2.5 S)** and **(2.5 Se**), exhibit aurophilic interactions and the two Au_3S subunits are held together via these gold-gold interactions and the bidentate phosphine. Interestingly, the Au:E ratio of these clusters is increased to a 3:1 ratio as compared to their precursors **(2.3 S)** and **(2.3 Se)**.

As observed with the reported compounds, the photophysical properties of **(2.3 S)** and **(2.3 Se)** depended on the identity of the chalcogen. Compound **(2.3 S)** had a λ_{em} of 514 nm whereas compound **(2.3 Se)** had a λ_{em} of 438 nm. By changing the chalcogen, a hypsochromic shift in emission wavelength was observed. Surprisingly, with the increase in nuclearity size, the loss of emissive properties in both S and Se clusters were observed.

Furthermore, when the emission spectra of **(2.3 S)** and **(2.3 Se)** were compared to $[Au_6\{\mu\text{-}Ph_2PN(p\text{-}CH_3C_6H_4)PPh_2\}_3(\mu_3\text{-}S)_2](ClO_4)_2$ **(IV.I)** reported by Yam and co-workers, **(IV.I)** had a hypsochromic shift compared to both compounds **(2.3 S)** and **(2.3 Se)**.[4] This indicates that the phosphine ligand could play a large role in modulating the structure of the cluster core, which in turn allows future modulation of the photophysical properties exhibited by gold chalcogenide clusters.[4]

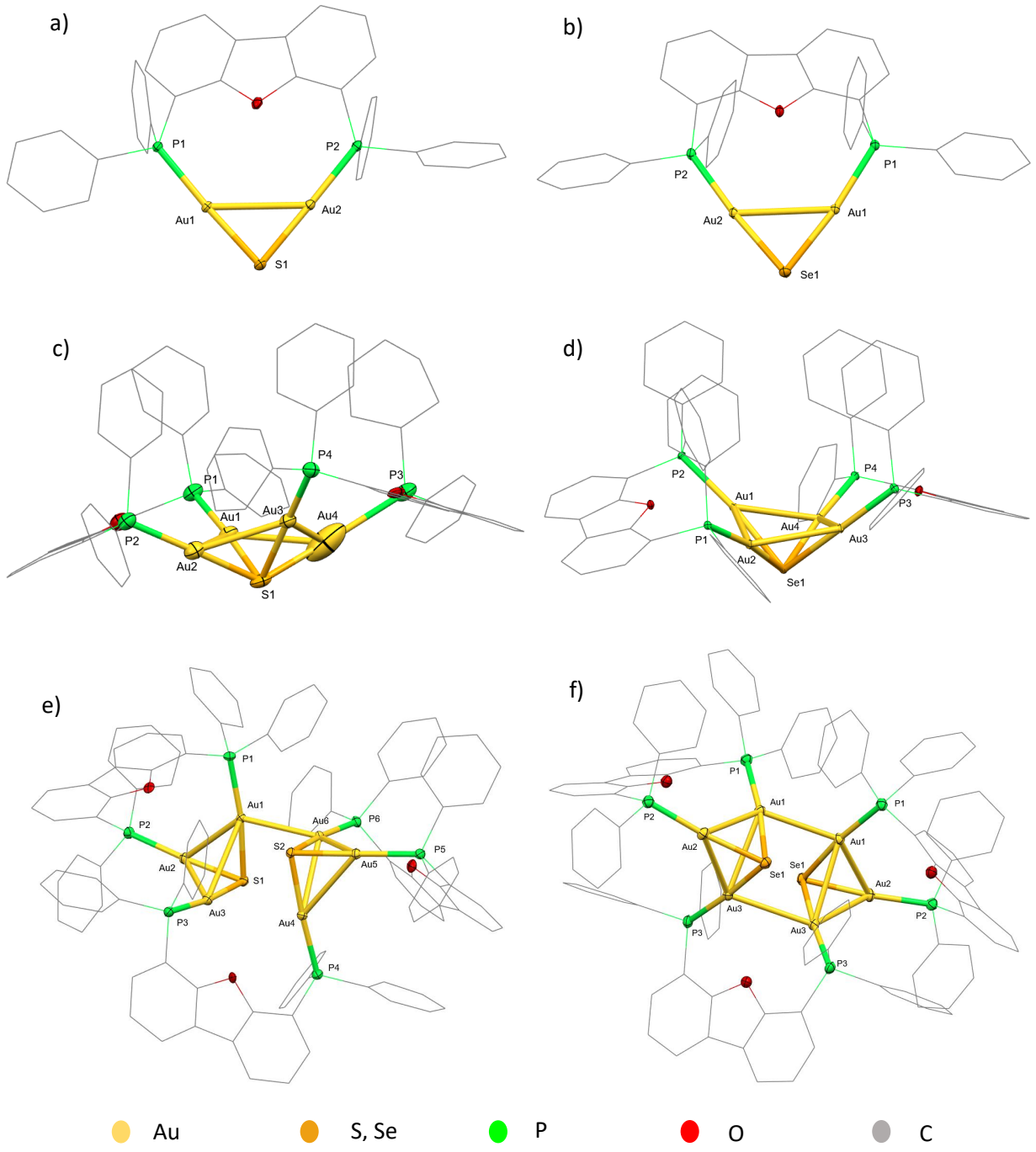

Figure 4.1: (a) Molecular structure of [(Au_2S)(μ-dbfdp)] ***(2.3 S)*** *(b) [(Au_2Se)(μ-dbfdp)]* ***(2.3 Se)*** *(c) [Au_4(μ$_4$-S)(μ-dbfdp)$_2$]$^{2+}$ unit in* ***(2.4 S)****, (d) [Au_4(μ$_4$-Se)(μ-dbfdp)$_2$]$^{2+}$ unit in* ***(2.4 Se)****, (e) [Au_6(μ$_3$-Se)$_2$(μ-dbfdp)$_3$]$^{2+}$ unit in* ***(2.5 S)****, (f) [Au_6(μ$_3$-Se)$_2$(μ-dbfdp)$_3$]$^{2+}$ unit in* ***(2.5 Se)****. (H atoms are omitted for clarity).*

Previously, it has also been reported that luminescent group 11 metal chalcogenolate clusters with DBFDP were prepared and characterized.[5] As seen with the lighter group 11 metals, it was hypothesized that the chalcogenolates in combination with gold can also act as bridging ligands and form higher nuclearity clusters. Moreover, it was of interest to study the effects of adding an electron-withdrawing group on the chalcogenolate and study the effects on photophysical properties. The incorporation of the previously used phenylchalcogenolate proved to be successful and produced complexes **(3.1)** and **(3.2)**. These complexes, unlike their copper and silver counterparts, contain only 2 metal atoms bridged by a phosphine ligand and have terminal chalcogenolate ligands. The thiolate complex **(3.1)** does not exhibit evidence of aurophilic interactions, however, the selenolate complex **(3.2)** exhibits evidence of aurophilic interactions between the two gold atoms, increasing stability within the gold (I) complex. When the electron-withdrawing groups (F^-) are added to the aryl ring of the thiolate, complex **(3.3)** remains fairly similar to the parent complex **(3.1)**. Complex **(3.3)** resembles that of complex **(3.1**), however contains evidence of intramolecular and intermolecular π interactions. As another point of comparison, to study the effect of the metal and electron-withdrawing groups on the aryl ring, the metal was swapped to Cu when synthesizing compound **(3.4)**. Compound **(3.4)** contains a cluster core of Cu:S ratio of 1:1 with bridging thiolates similar to the cluster core of $[(Cu_5(SPh)_4Cl(dbfdp)_2]$ **(IV.II)** as documented by Corrigan and co-workers.[5] As observed in complex **(3.3)**, compound **(3.4)** also exhibits evidence of π interactions between the phenyl rings of the ligand and the C_6F_5 ring, and the C_6F_5 ring and the dibenzofuran backbone. It was hypothesized that these π interactions could play a role in structural rigidity which could affect the emission-excitation spectra.

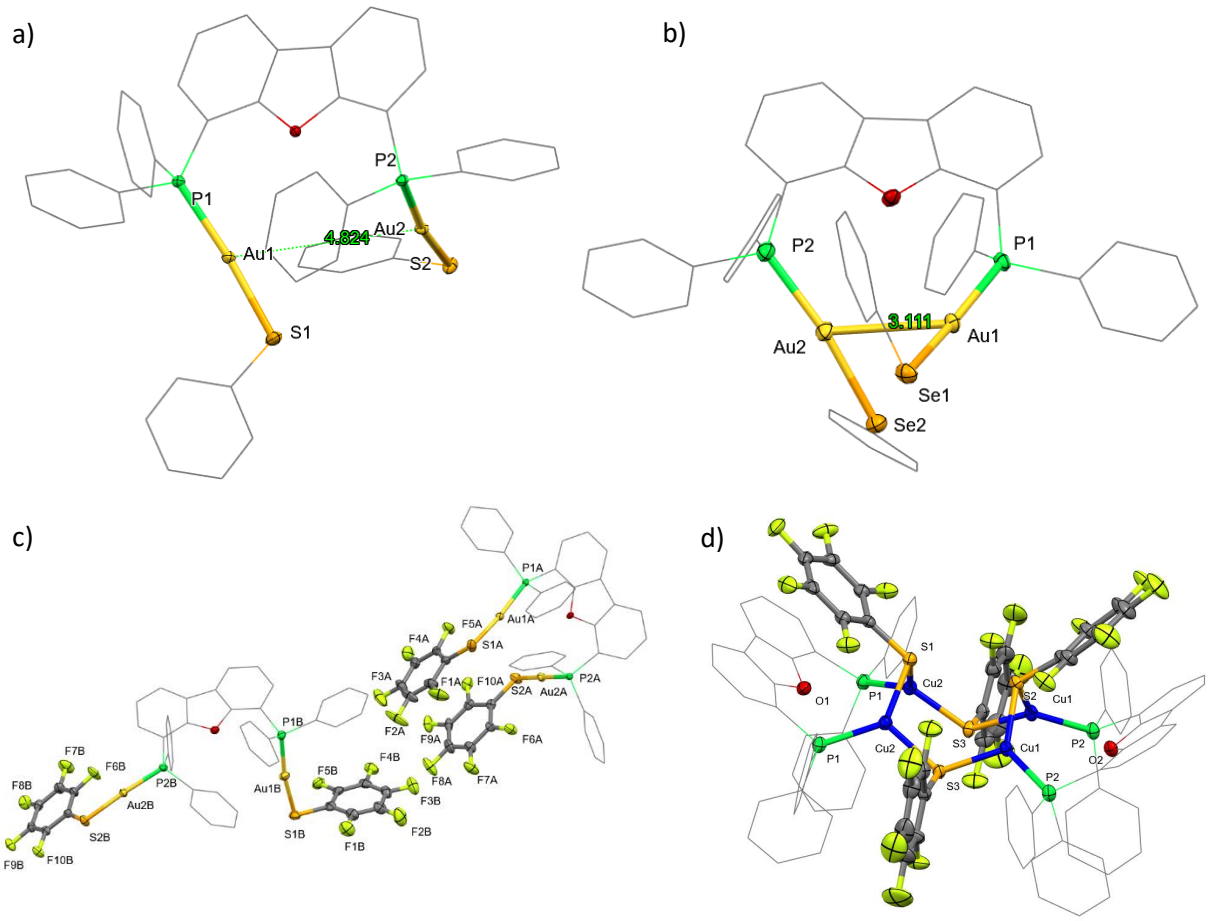

Figure 4.2: (a) Molecular structure of [(AuSPh)$_2$(μ-dbfdp)] ***(3.2)*** *(b) [(AuSePh)$_2$(μ-dbfdp)]* ***(3.2)*** *(c) [(AuSC$_6$F$_5$)$_2$(μ-dbfdp)]* ***(3.4)*** *and (d) [(Cu$_4$(SC$_6$F$_5$)$_4$(μ-dbfdp)$_2$]* ***(3.5)****. (H atoms are omitted for clarity).*

In terms of luminescent properties, the crystals of **(3.1)** and **(3.2)** are green-yellow and green emissive, respectively. Quantitatively, **(3.1)** was determined to have a λ_{em} of 552 nm when excited at 470 nm. Alternatively, when the larger chalcogen (Se) is introduced which forms complex **(3.2)**, the emission experiences a hypsochromic shift with a λ_{em} of 513 nm when excited at 447 nm. As a comparison between the two, the introduction of an aurophilic interaction (present in **(3.2)** and absent in **(3.1)**) increases the emission intensity of the complexes. Compound **(3.3)** and **(3.4)** were not observed to be visually emissive and was subsequently confirmed by excitation and emission spectroscopy. The λ_{exc} for both compounds **(3.3)** and **(3.4)** are quite similar at 293 nm and 287 nm, respectively.

The incorporation of DBFDP resulted in two minimally emissive gold (I) protected phenylchalcogenolate complexes (SPh and SePh) and two non-emissive d^{10} metal (I) protected C_6F_5 thiolate complexes. The molecular structure of these metal chalcogenolate complexes for gold have a linear coordination geometry, with two gold centres per complex. When the chalcogen is changed from S to Se in the chalcogenolate complex, the molecular structure remains isostructural between **(3.1)** and **(3.2)**. The copper complex possesses a core with a 1:1 ratio of Cu:S, with more copper centres than the gold analogue, when employing the same chalcogenolate. Despite differences in number of metal centres, a key similarity remains between the two types of chalcogenolates in that the phosphine ligand bridge two metal centres.

4.2 Outlook – Luminescent Gold (I) Chalcogenide Clusters with a Conjugated Diphosphine Ligand

Future work in this vein of research would include the incorporation of the heavier chalcogen Te. This can be explored to investigate how the changes in emission properties of the gold (I) chalcogenide clusters are affected by an even larger chalcogen than S and Se. By introducing $Te(SiMe_3)_2$, the aim is to synthesize tellurium analogues of **(2.3 S)** and **(2.3 Se)** with fine tunable emission properties, with the hypothesis that the addition of the heavier chalcogen will change the HOMO-LUMO gap.

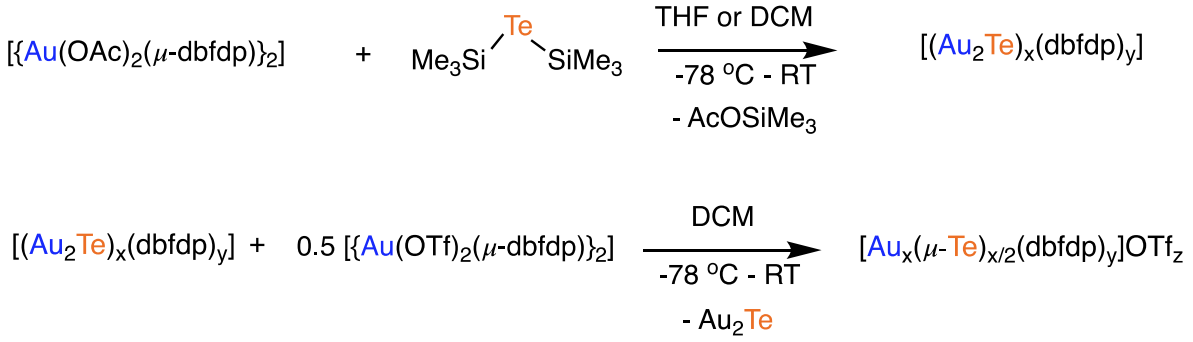

Scheme 4.1:Proposed synthetic scheme for metal chalcogenide clusters employing $Te(SiMe_3)_2$.

By using the proposed [(Au_2Te)(dbfdp)] complexes, analogues of **(2.4 S/Se)** and **(2.5 S/Se)** could be synthesized resulting in large nuclearity clusters with a proposed Au_2Te core protected by peripheral DBFDP ligands.

Moreover, the change of the substituents on the DBFDP ligand may also alter the HOMO-LUMO gap which may in turn change the wavelength of emission. Previously, it has been demonstrated that the incorporation of different organic substituents on the dibenzofuran backbone can change PLQYs in other metal chalcogenide clusters (ex. Cu). This may be of interest to gather a deeper understanding of how to fine tune organic moieties which can affect the structure-property relationships, in turn, altering the emission and excitation properties.

4.3 Outlook – Luminescent Gold (I) Chalcogenolate Clusters with a Conjugated Diphosphine Ligand

Further investigation of this topic would include obtaining computational calculations on compounds **(3.3)** and **(3.4)**. By obtaining these computational studies, the π-interactions of those select compounds can be provided. Moreover, near-infrared emission spectra of those compounds should also be gathered to determine if emissions were to occur in that region. Previously, Yam has demonstrated that with the addition of electron-withdrawing substituent groups on chalcogenolate ligands, the emission profiles of dinuclear gold (I) complexes will experience a bathochromic shift, indicated by a larger HOMO-LUMO band gap.[6]

Further work in this field of work could include the introduction of other chalcogenolates. The addition of additional electron-withdrawing groups or electron-donating groups (*t*-butyl, methoxy) could be of interest to study the effects that such substituents would have on the electronic properties of these complexes.

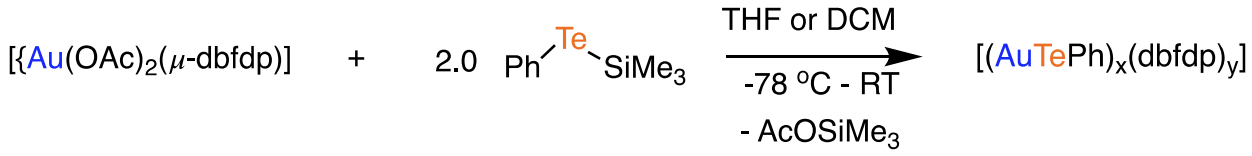

Scheme 4.2: Proposed synthetic scheme for gold (I) tellurolate clusters employing $TePh(SiMe_3)_2$.

Previous studies have demonstrated a higher nuclearity cluster employing phenyltellurolate incorporated into gold (I) phosphine protected clusters. By incorporating the larger chalcogen, it has been demonstrated that a larger cluster can be achieved in $[Au_8(\mu\text{-}TePh)_8(PPh_3)_4]$ reported by Villacampa and co-workers.[7] By incorporating DBFDP instead of PPh_3, a different cluster can be

achieved to further gather an understanding of structure property relationships in gold (I) phosphine protected clusters.

4.4 References

(1) Clementi, E.; Raimondi, D. L.; Reinhardt, W. P. Atomic Screening Constants from SCF Functions. II. Atoms with 37 to 86 Electrons. *J. Chem. Phys.* **1967**, *47* (4), 1300–1307. https://doi.org/10.1063/1.1712084.

(2) Schmidbaur, H. Is Gold Chemistry a Topical Field of Study? *Angew. Chem. Int. Ed. Engl.* **1976**, *15* (12), 728–740. https://doi.org/10.1002/anie.197607281.

(3) Schmidbaur, H.; Graf, W.; Müller, G. Weak Intramolecular Bonding Relationships: The Conformation-Determining Attractive Interaction between Gold(I) Centers. *Angew. Chem. Int. Ed. Engl.* **1988**, *27* (3), 417–419. https://doi.org/10.1002/anie.198804171.

(4) Yam, V. W.-W.; Cheng, E. C.-C.; Zhu, N. A Novel Polynuclear Gold–Sulfur Cube with an Unusually Large Stokes Shift. *Angew. Chem. Int. Ed.* **2001**, *40* (9), 1763–1765. https://doi.org/10.1002/1521-3773(20010504)40:9<1763::AID-ANIE17630>3.0.CO;2-O.

(5) Nayyar, M. Luminescent Group 11 Metal Chalcogen Clusters with Bidentate Phosphine Ligands, The University of Western Ontario, London, 2021.

(6) Yam, V. W.-W.; Chan, C.-L.; Cheung, K.-K. Synthesis and Photophysics of Dinuclear Gold(I) Thiolates of Bis(Diphenylphosphino)-Alkyl- and -Aryl-Amines. Crystal Structure of [Au2{Ph2PN(C6H11)PPh2}(SC6H4F-p)2]. *J. Chem. Soc. Dalton Trans.* **1996**, No. 20, 4019. https://doi.org/10.1039/dt9960004019.

(7) Bumbu, O.; Ceamanos, C.; Crespo, O.; Gimeno, M. C.; Laguna, A.; Silvestru, C.; Villacampa, M. D. Unprecedented Gold−Tellurolate Clusters [Au8(μ-TeR)8(PR‘3)4]. *Inorg. Chem.* **2007**, *46* (26), 11457–11460. https://doi.org/10.1021/ic7013545.

Appendices

Appendix 1.0 Permission to Reuse Copyright Material

CCC Marketplace

This is a License Agreement between Kai Yu Jeffrey Li ("User") and Copyright Clearance Center, Inc. ("CCC") on behalf of the Rightsholder identified in the order details below. The license consists of the order details, the Marketplace Permissions General Terms and Conditions below, and any Rightsholder Terms and Conditions which are included below.

All payments must be made in full to CCC in accordance with the Marketplace Permissions General Terms and Conditions below.

Order Date	17-Dec-2023	Type of Use	Republish in a thesis/dissertation
Order License ID	1428425-1	Publisher	WILEY - V C H VERLAG GMBH & CO. KGAA
ISSN	0947-6539	Portion	Chart/graph/table/figure

LICENSED CONTENT

Publication Title	Chemistry : a European journal	Rightsholder	John Wiley & Sons - Books
Article Title	Adamantyl- and Furanyl-Protected Nanoscale Silver Sulfide Clusters.	Publication Type	Journal
		Start Page	9933
Author/Editor	GESELLSCHAFT DEUTSCHER CHEMIKER.	End Page	9937
Date	01/01/1995	Issue	29
Language	English, Multiple languages	Volume	22
Country	Germany		

REQUEST DETAILS

Portion Type	Chart/graph/table/figure	Distribution	Worldwide
Number of Charts / Graphs / Tables / Figures Requested	2	Translation	Original language of publication
		Copies for the Disabled?	No
Format (select all that apply)	Print, Electronic	Minor Editing Privileges?	No
Who Will Republish the Content?	Academic institution	Incidental Promotional Use?	No
Duration of Use	Life of current edition	Currency	CAD
Lifetime Unit Quantity	Up to 499		
Rights Requested	Main product		

NEW WORK DETAILS

Title	Luminescent Group 11 Metal (I) Chalcogen Clusters with a Conjugated Diphosphine Ligand	Institution Name	Western University
		Expected Presentation Date	2024-01-22
Instructor Name	John Corrigan		

ADDITIONAL DETAILS

The Requesting Person / Organization to Appear on the License	Kai Yu Jeffrey Li

REQUESTED CONTENT DETAILS

Title, Description or Numeric Reference of the Portion(s)	Figure 2. S-substructure of 1 consisting of a S13-core composed of S2 ions (orange) that is surrounded by 32 thiolates (yellow) in a distorted icosahedral fashion. Lines between S atoms are nonbinding and solely illustrate the geometric arrangement.	Title of the Article / Chapter the Portion Is From	Adamantyl- and Furanyl-Protected Nanoscale Silver Sulfide Clusters.
		Author of Portion(s)	Dr., Bestgen, Sebastian; Dr., Yang, Xiaoxun; Dr., Issac, Ibrahim; Dr., Fuhr, Olaf; Prof. Dr., Roesky, Peter W.; Prof. Dr., Fenske, Dieter
		Publication Date of Portion	2016-07-11
Editor of Portion(s)	Dr., Bestgen, Sebastian; Dr., Yang, Xiaoxun; Dr., Issac, Ibrahim; Dr., Fuhr, Olaf; Prof. Dr., Roesky, Peter W.; Prof. Dr., Fenske, Dieter		
Volume / Edition	22		
Page or Page Range of Portion	9933-9937		

Chapter 1, *Figure 1.2* – John Wiley & Sons Reproduction Permission

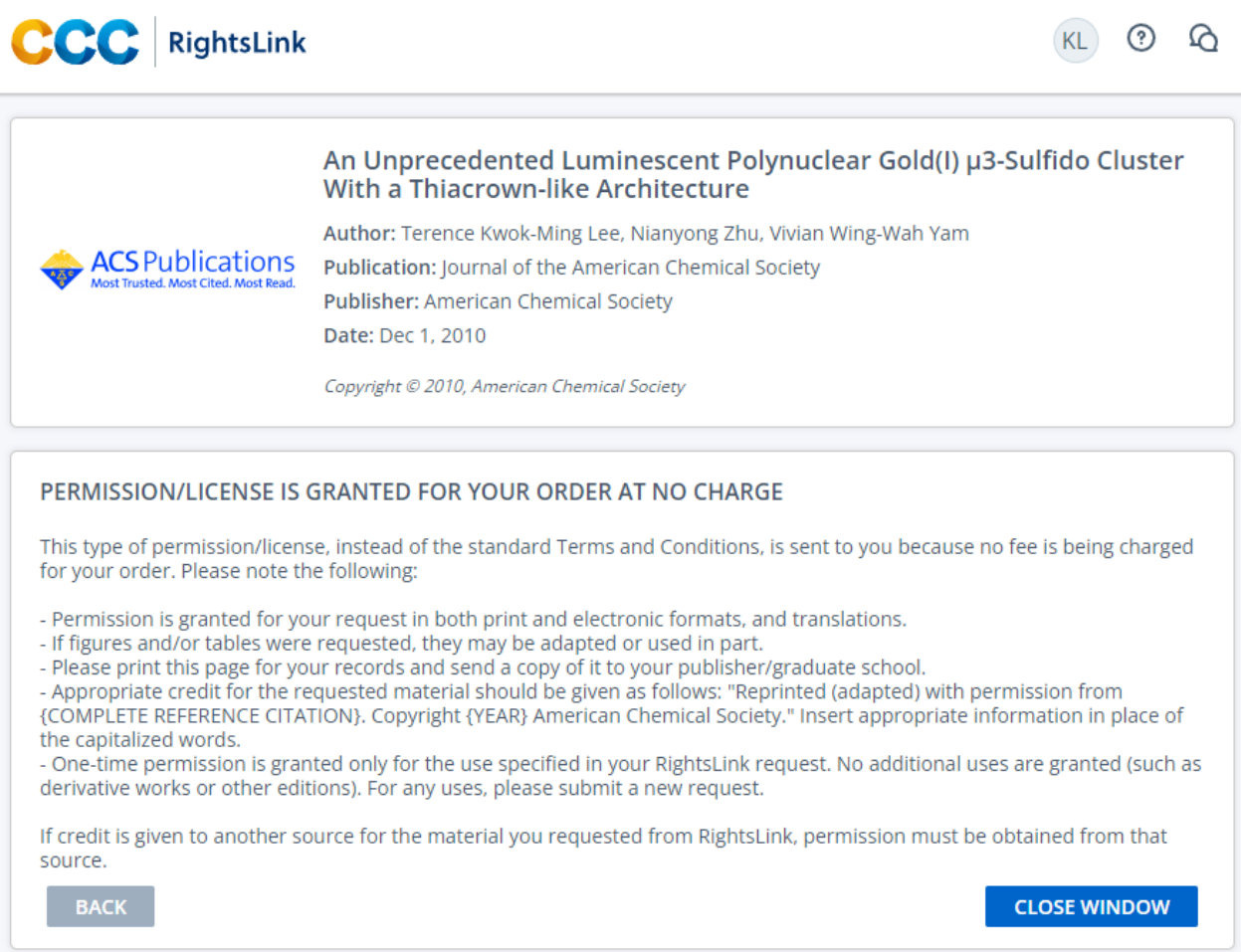

Chapter 1, *Figure 1.3 (b)* – American Chemical Society Reproduction Permission

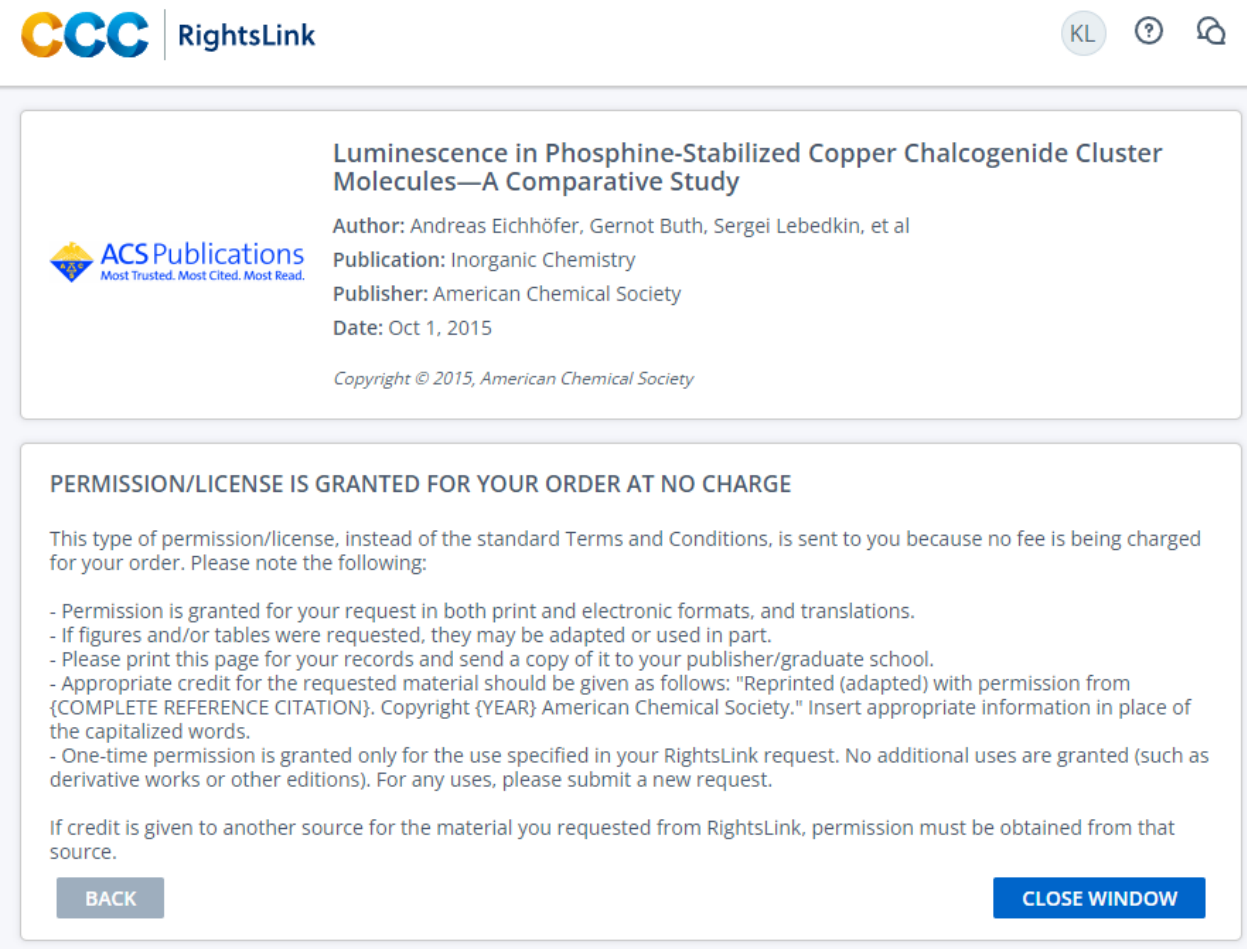

Chapter 1, *Figure 1.9* – American Chemical Society Reproduction Permission

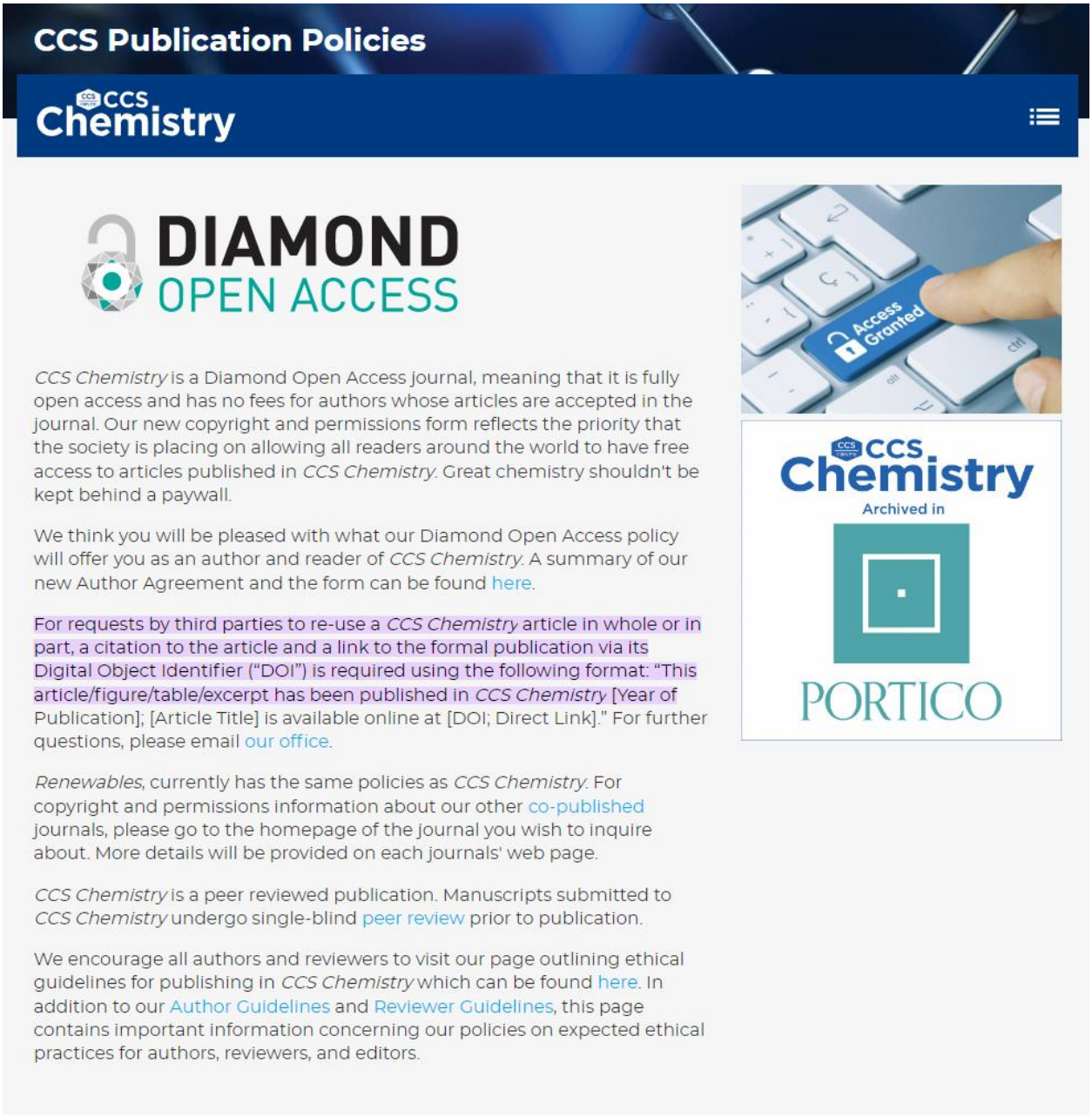

Chapter 1, *Figure 1.10* – Chinese Chemical Society Reproduction Permission

Appendix 2.0 Supporting Information for Chapter 2

Appendix 2.1: NMR Data for Compounds (2.1) – (2.5 Se)

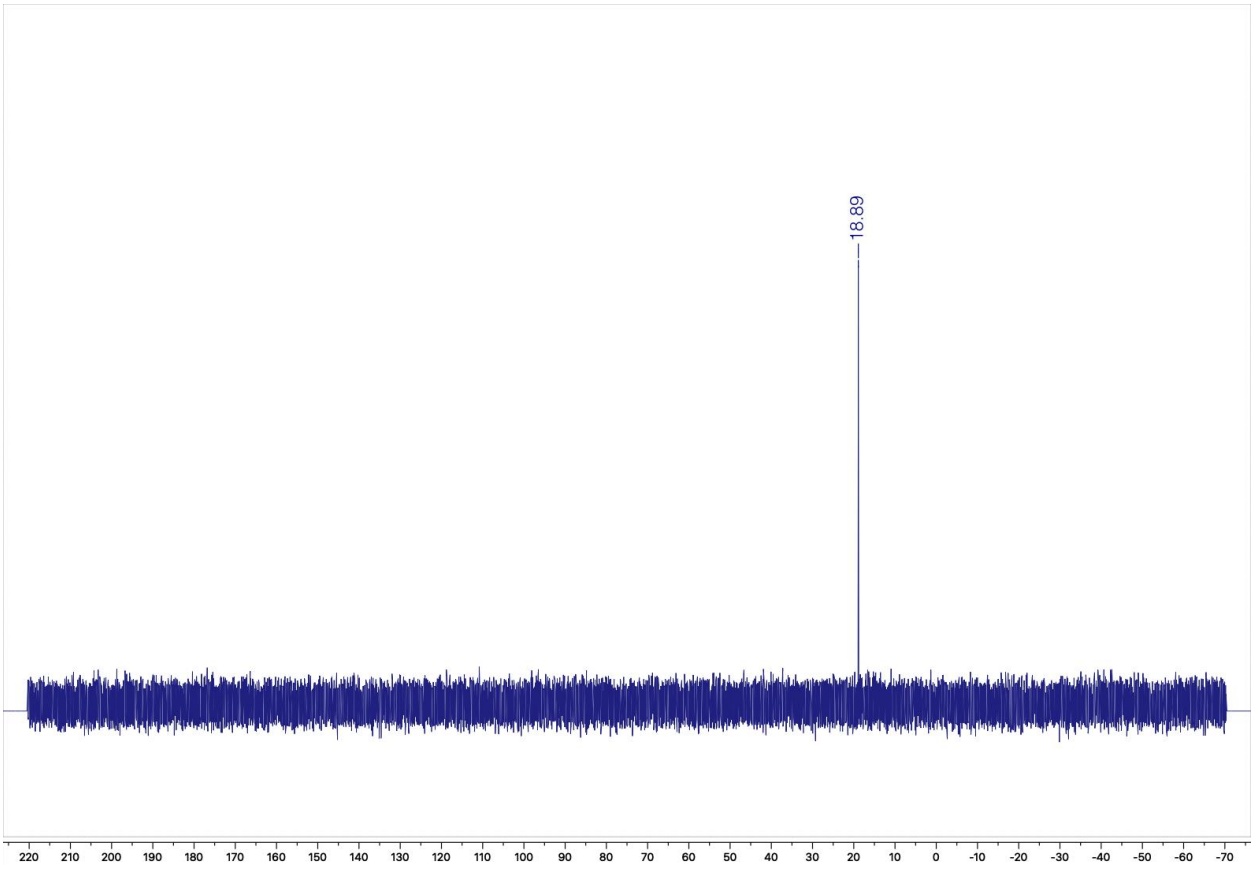

*Figure S2.1: $^{31}P\{^{1}H\}$ NMR spectrum in $CDCl_3$ (298K) of $[(AuOAc)_2(dbfdp)]$ (**2.1**)*

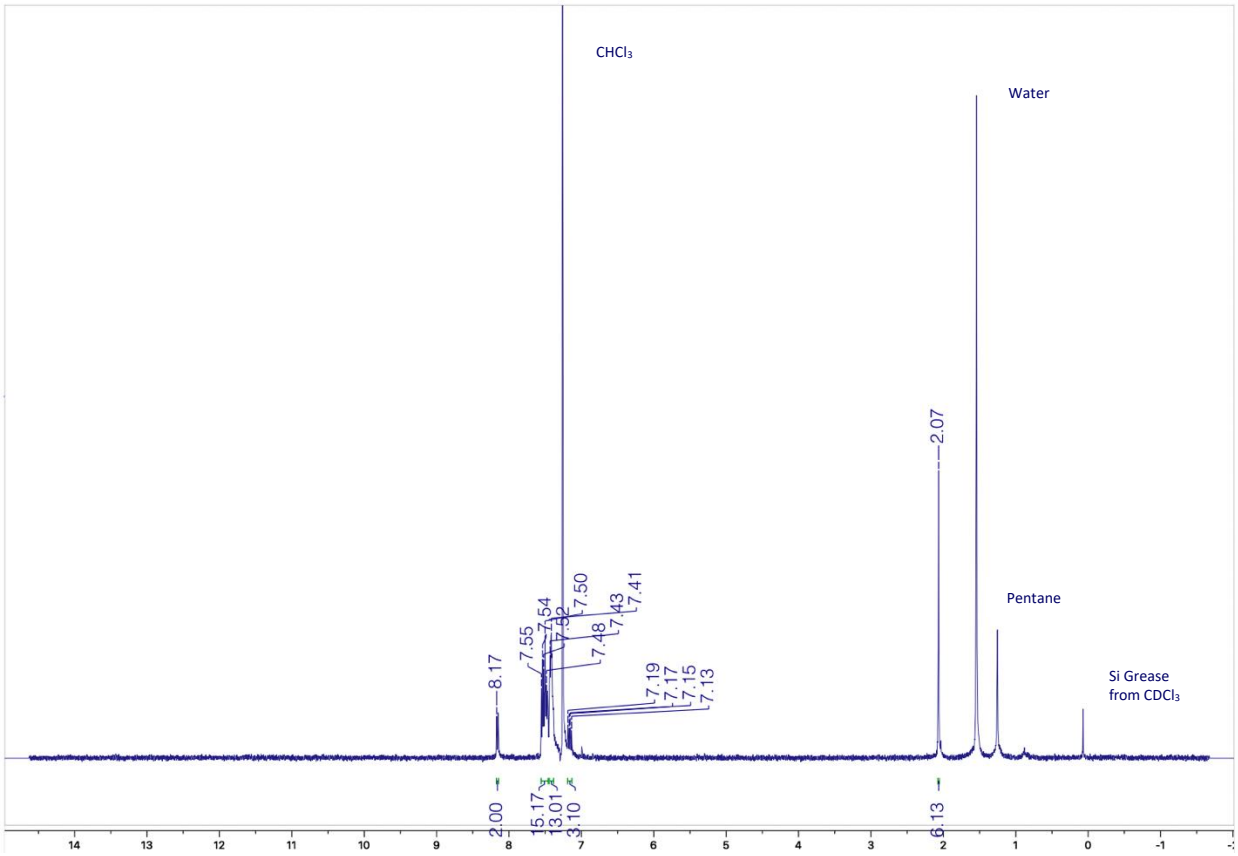

*Figure S2.2: ^{1}H NMR spectrum in $CDCl_3$ (298K) of $[(AuOAc)_2(dbfdp)]$ (**2.1**)*

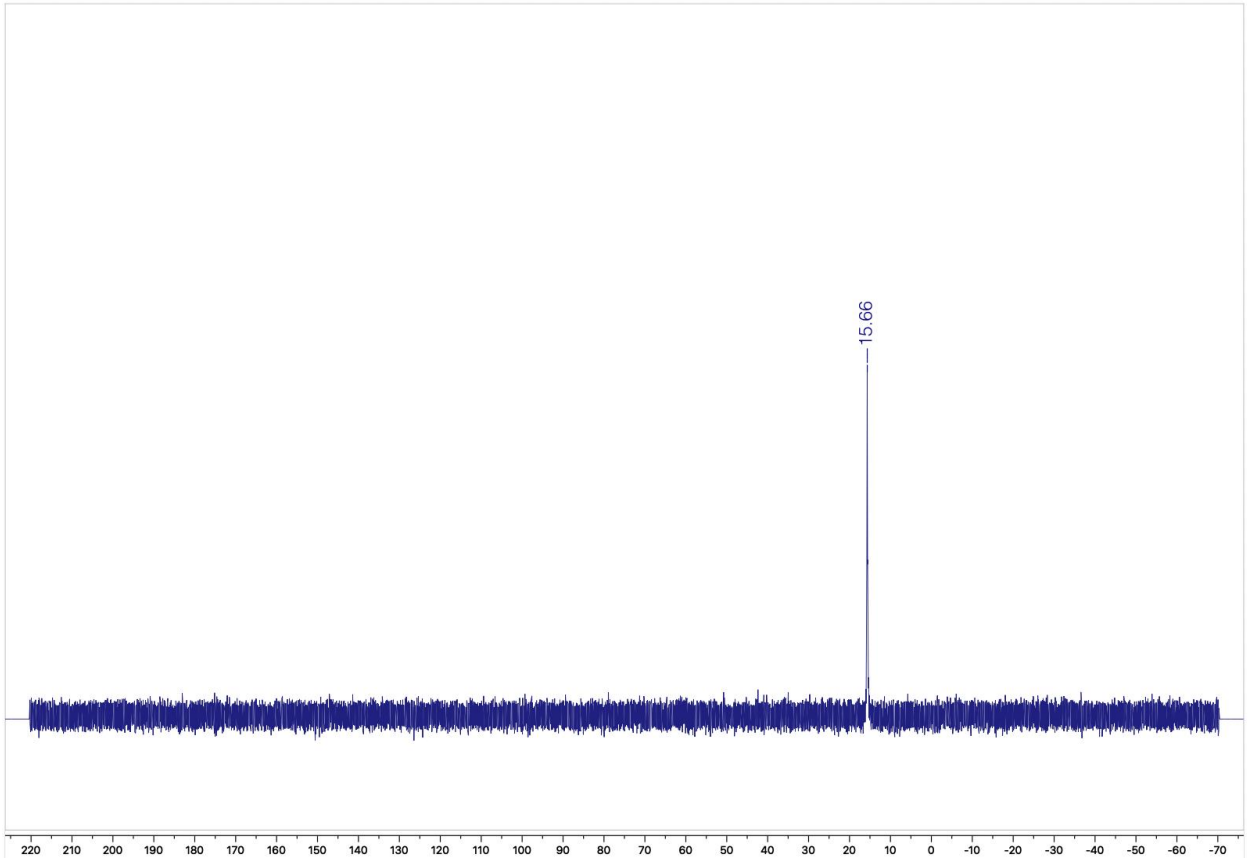

*Figure S2.3: $^{31}P\{^{1}H\}$ NMR spectrum in CD_2Cl_2 (298K) of $[(AuOTf)_2(dbfdp)]$ (**2.2**)*

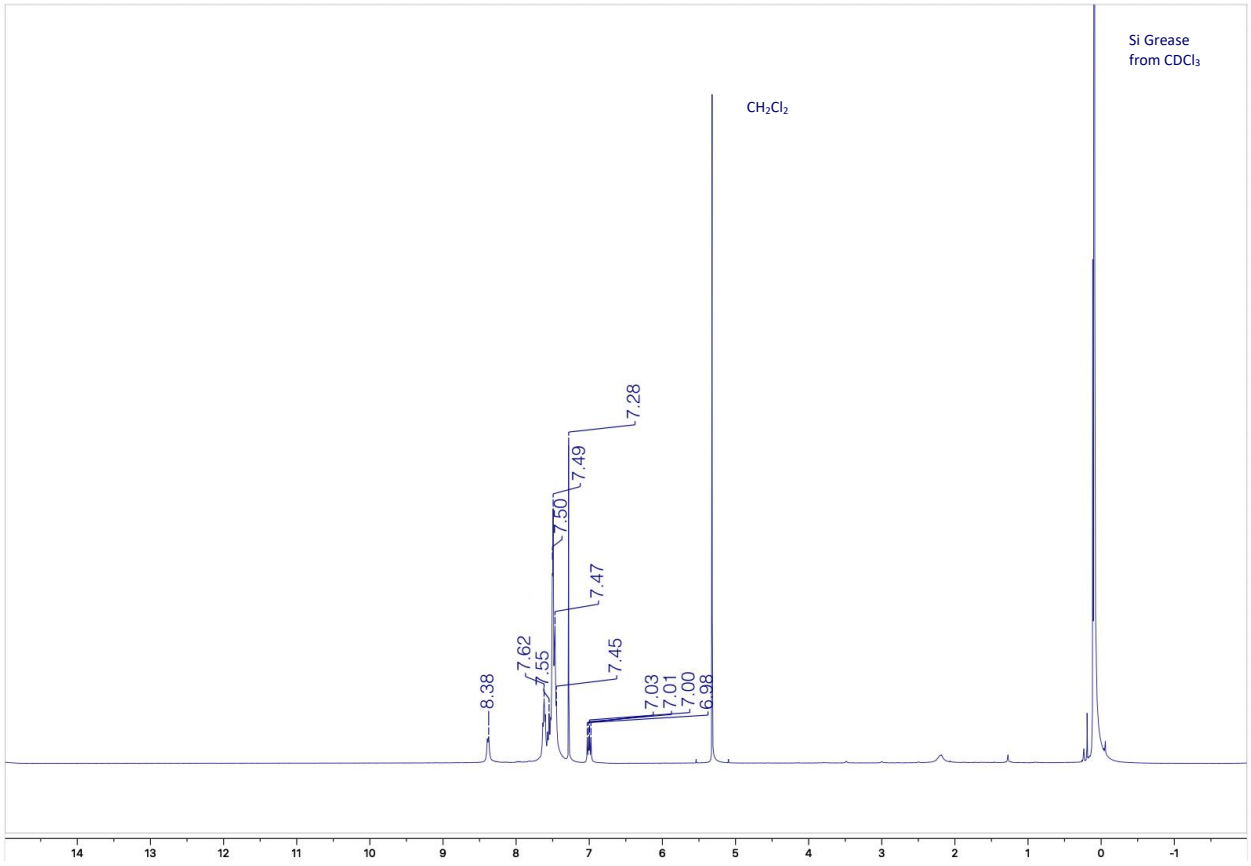

*Figure S2.4: ^{1}H NMR spectrum in CD_2Cl_2 (298K) of $[(AuOTf)_2(dbfdp)]$ (**2.2**)*

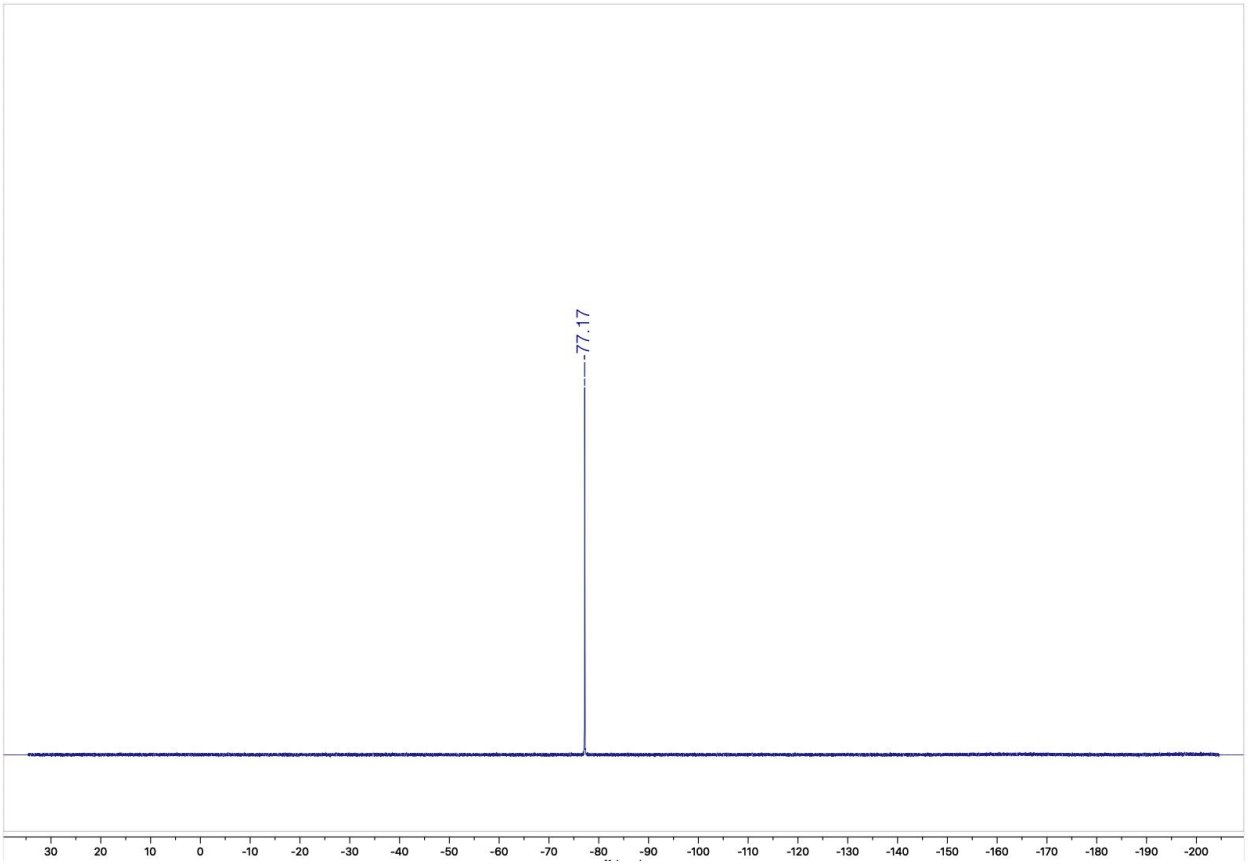

*Figure S2.5: $^{19}F\{^{1}H\}$ NMR spectrum in CD_2Cl_2 (298K) of $[(AuOTf)_2(dbfdp)]$ (**2.2**)*

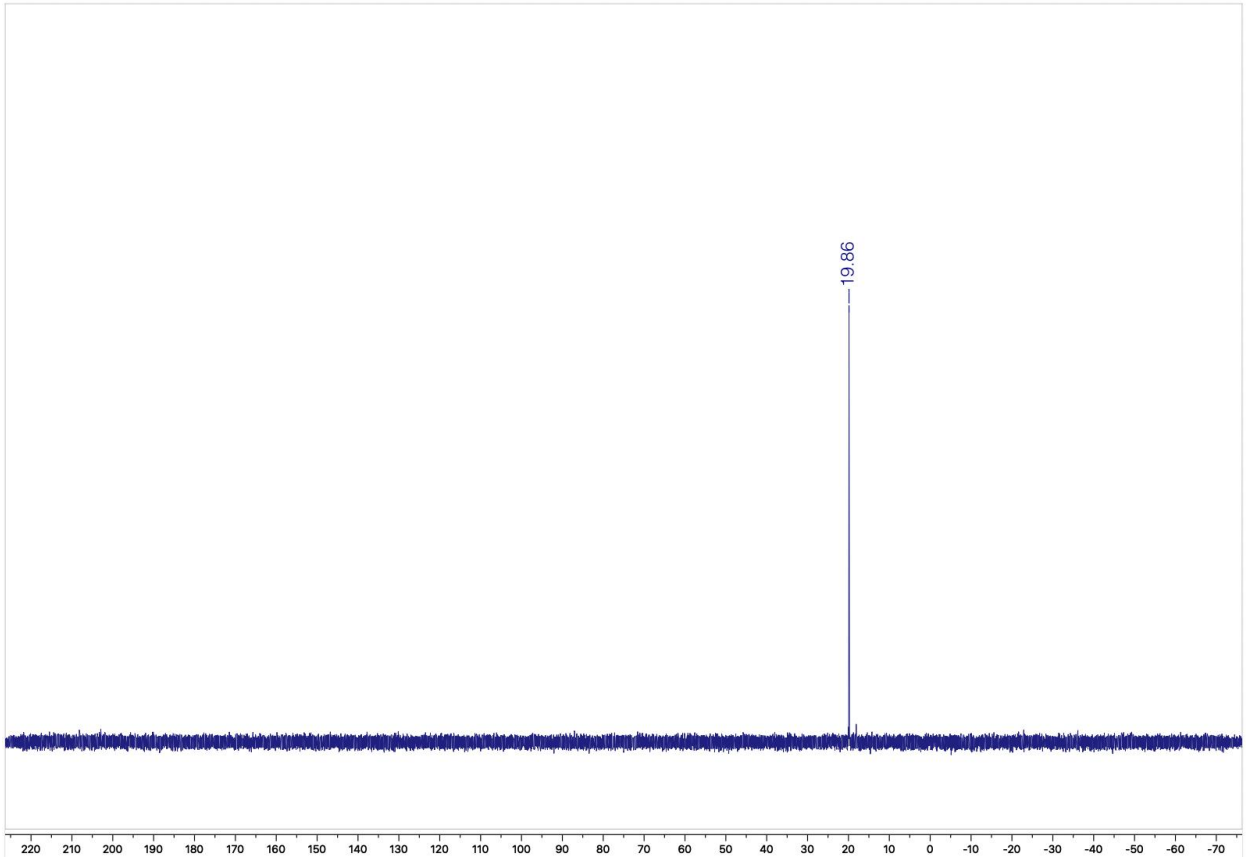

*Figure S2.6: $^{31}P\{^{1}H\}$ NMR spectrum in CD_2Cl_2 (298K) of [(Au_2S)(dbfdp)] (**2.3 S**)*

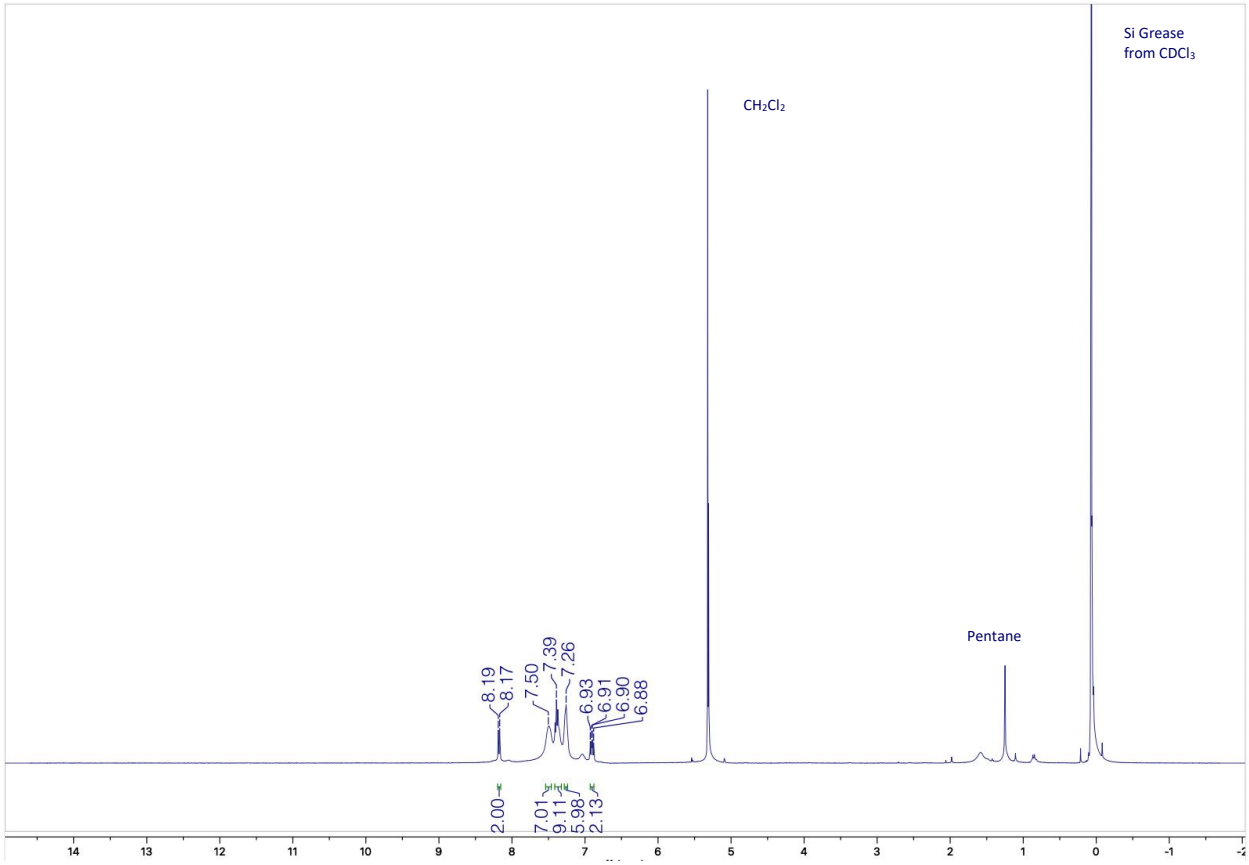

*Figure S2.7: ^{1}H NMR spectrum in CD_2Cl_2 (298K) of [(Au_2S)(dbfdp)] (**2.3 S**)*

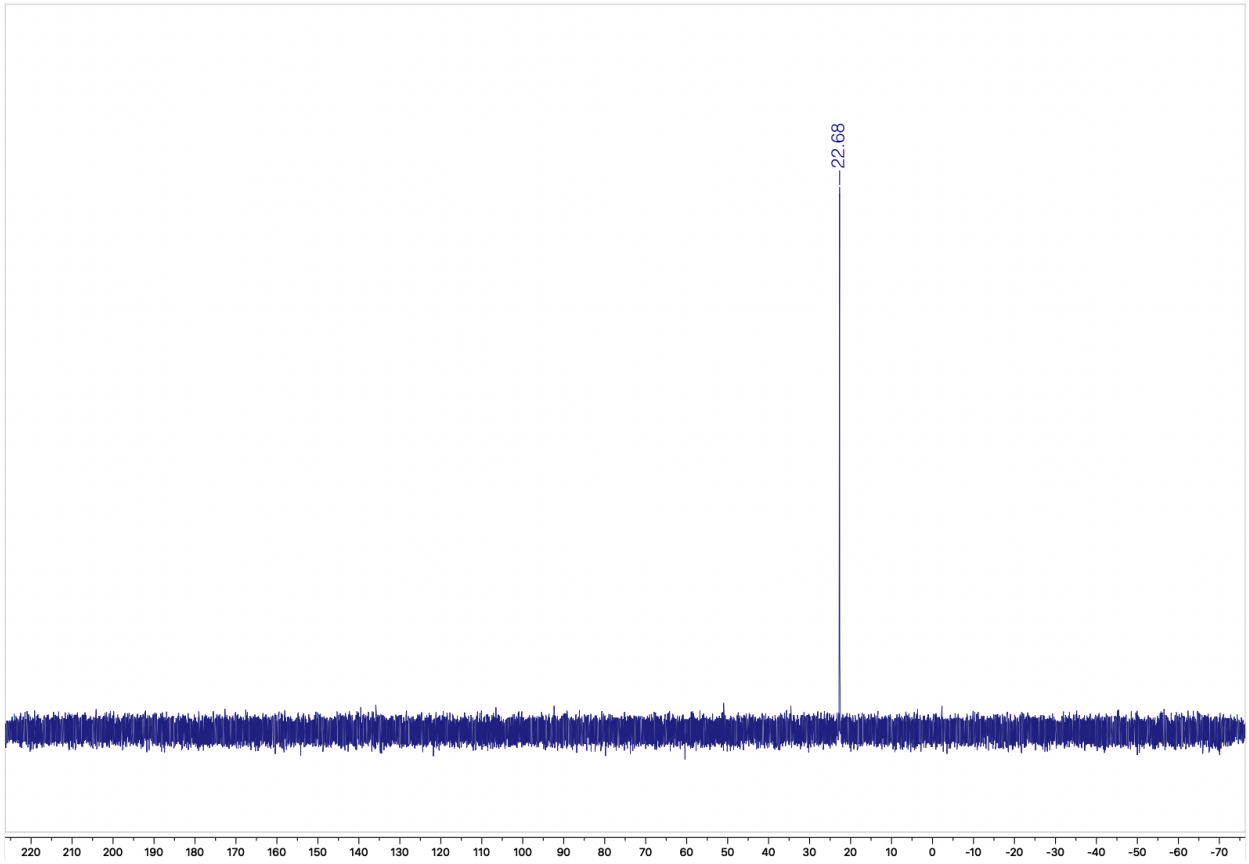

*Figure S2.8: $^{31}P\{^{1}H\}$ NMR spectrum in CD_2Cl_2 (298K) of [(Au_2Se)(dbfdp)] (**2.3 Se**)*

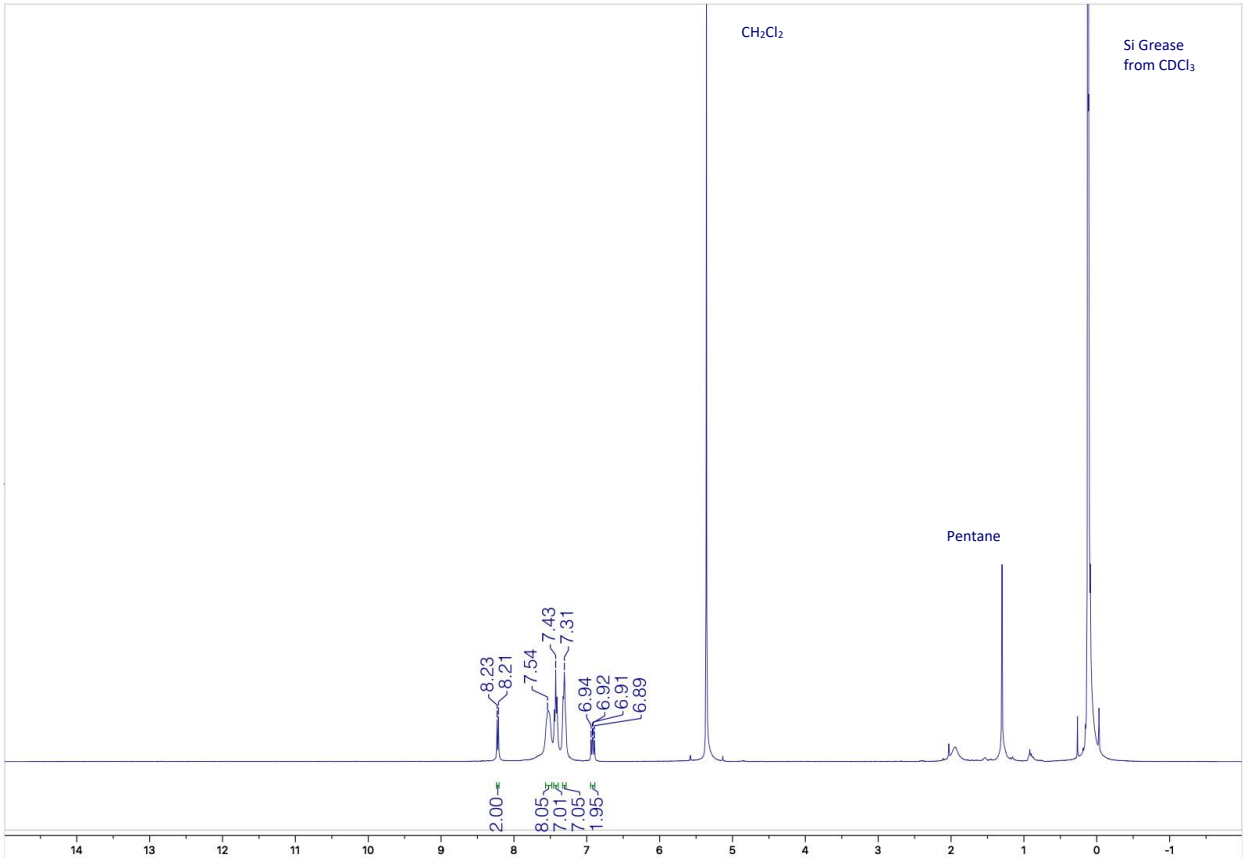

*Figure S2.9: ^{1}H NMR spectrum in CD_2Cl_2 (298K) of [(Au_2Se)(dbfdp)] (**2.3 Se**)*

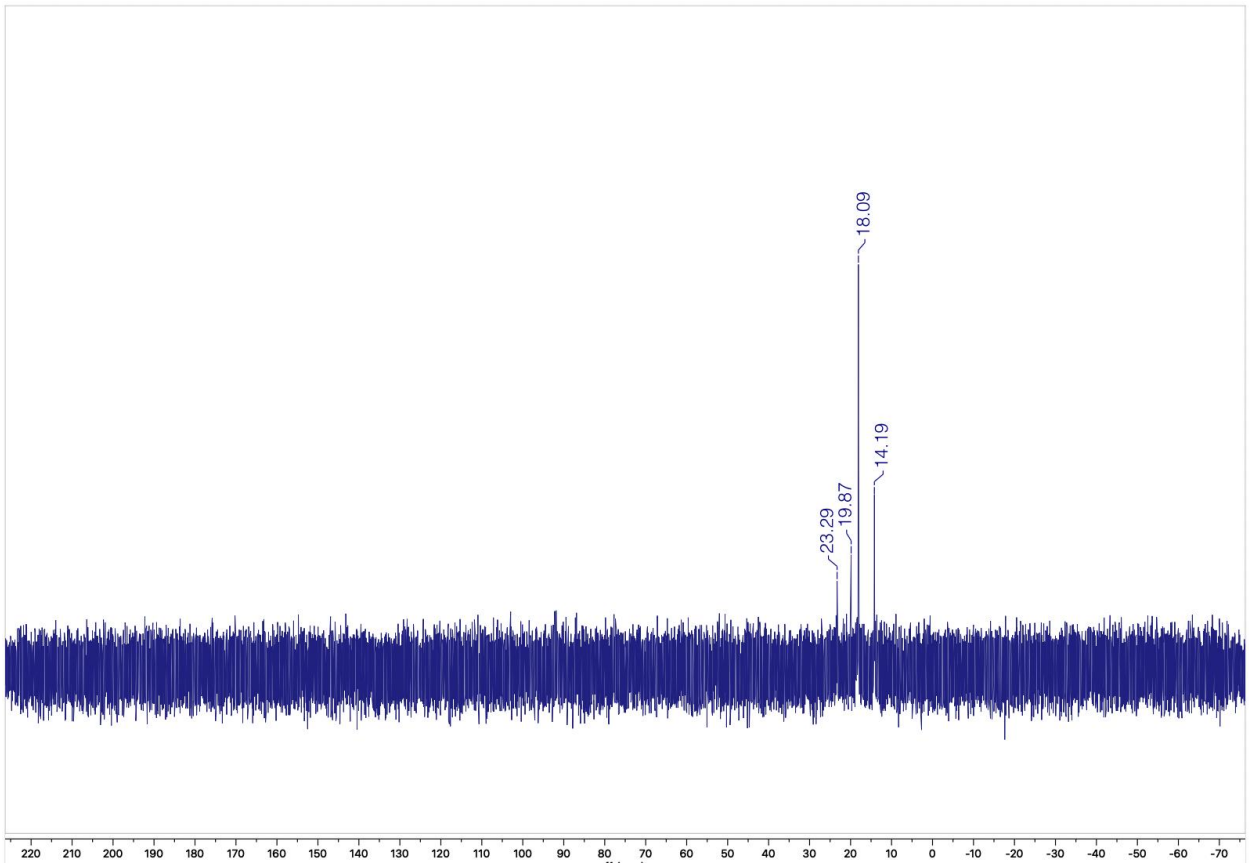

*Figure S2.10: $^{31}P\{^{1}H\}$ NMR spectrum in CD_2Cl_2 (298K) of mixture of **(2.4 S)** and **(2.5 S)***

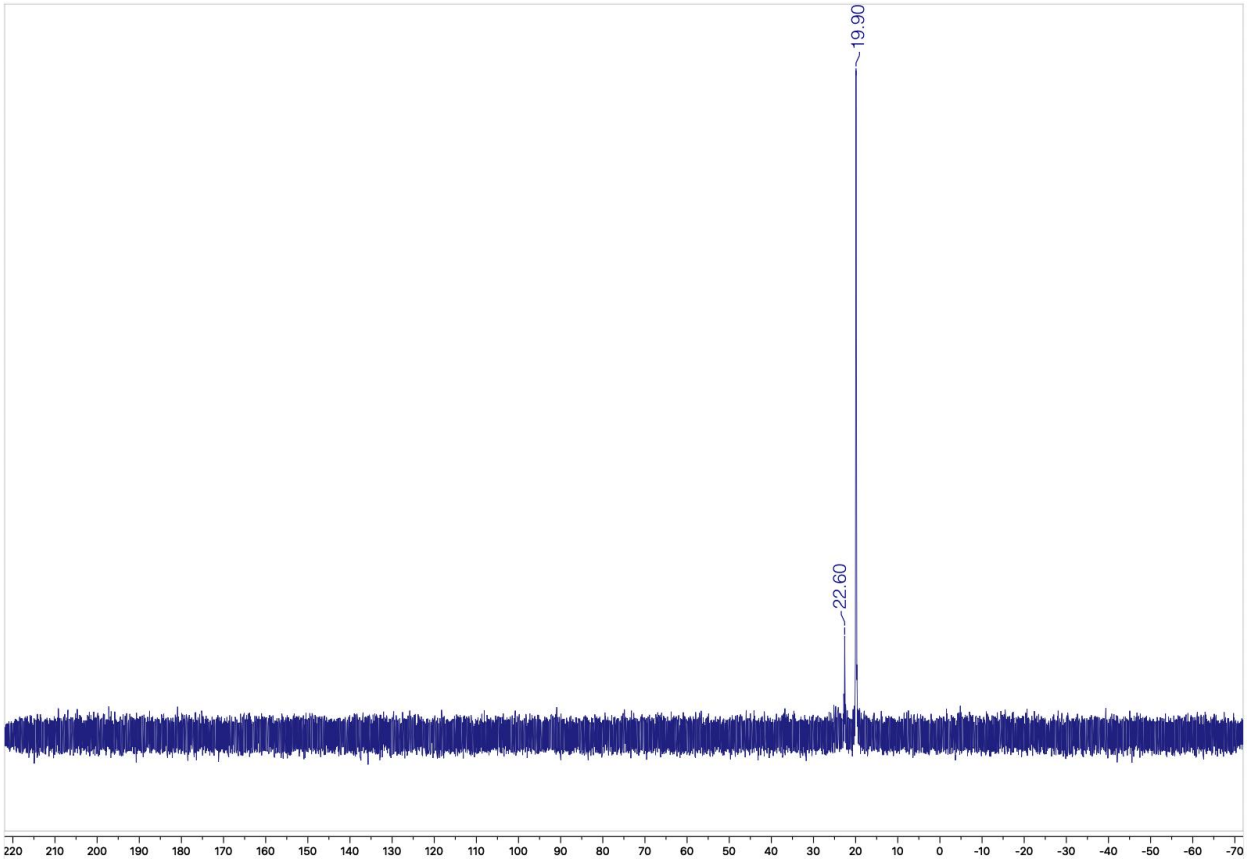

*Figure S2.11: $^{31}P\{^{1}H\}$ NMR spectrum in CD_2Cl_2 (298K) of **(2.4 Se)** and **(2.5 Se)***

Appendix 2.2: Mass Spectrometry and EDX Data for Chapter 2

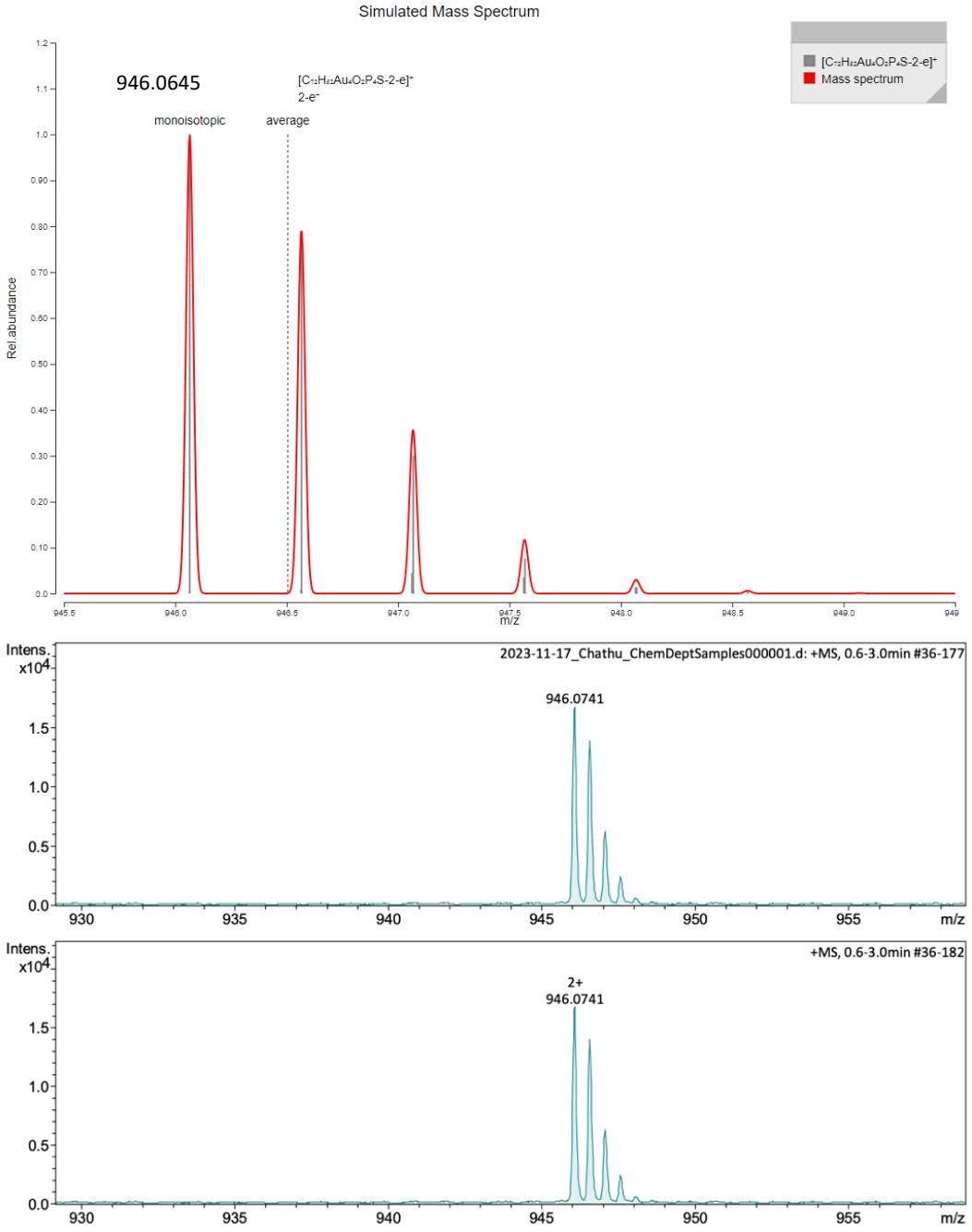

*Figure S2.12: Predicted mass spectrum of **(2.4 S)** (top) and expanded experimental mass spectrum of **(2.4 S)** (bottom)*

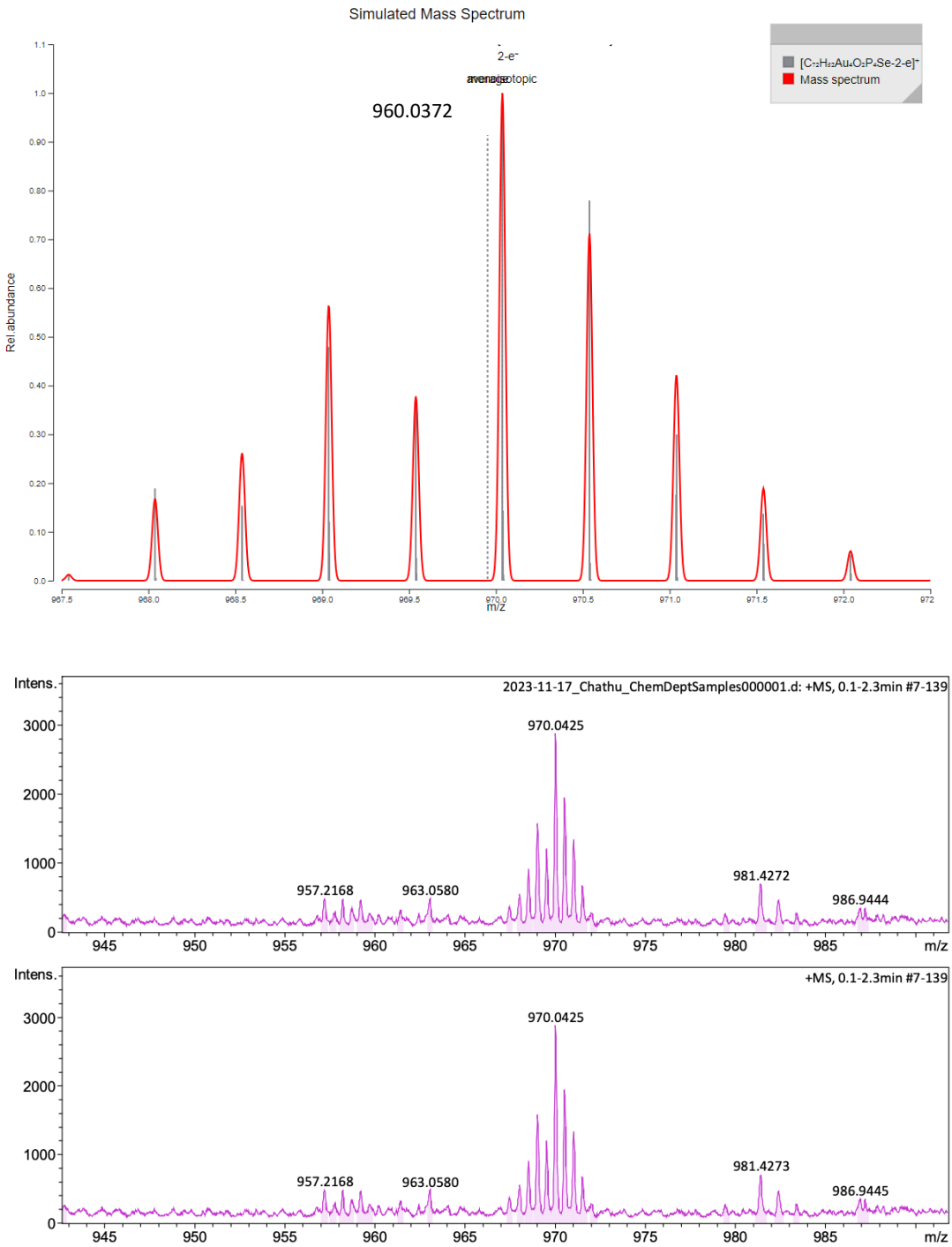

*Figure S2.13: Predicted mass spectrum of **(2.4 Se)** (top) and expanded experimental mass spectrum of **(2.4 Se)** (bottom)*

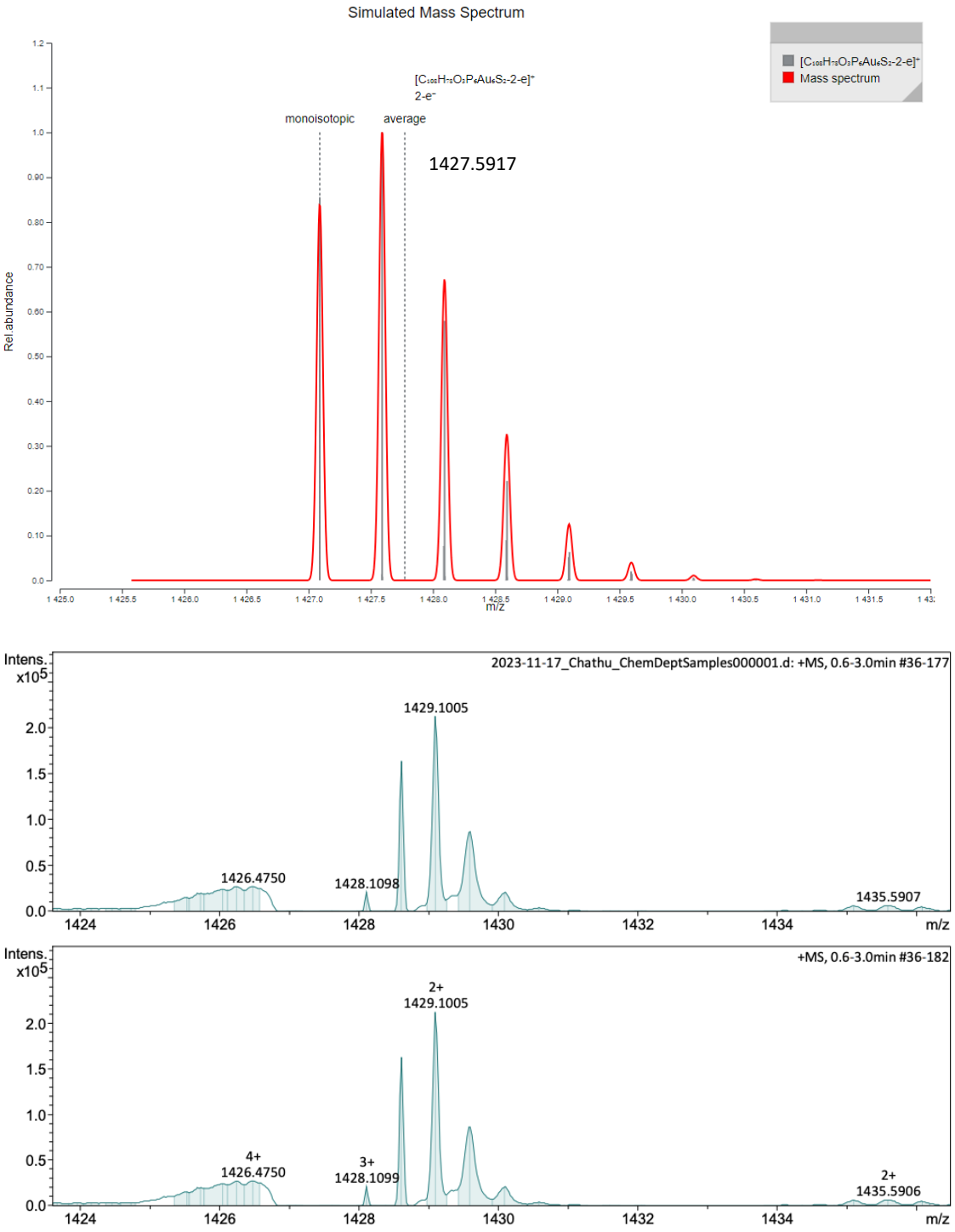

*Figure S2.14: Predicted mass spectrum of **(2.5 S)** (top) and expanded experimental mass spectrum of **(2.5 S)** (bottom)*

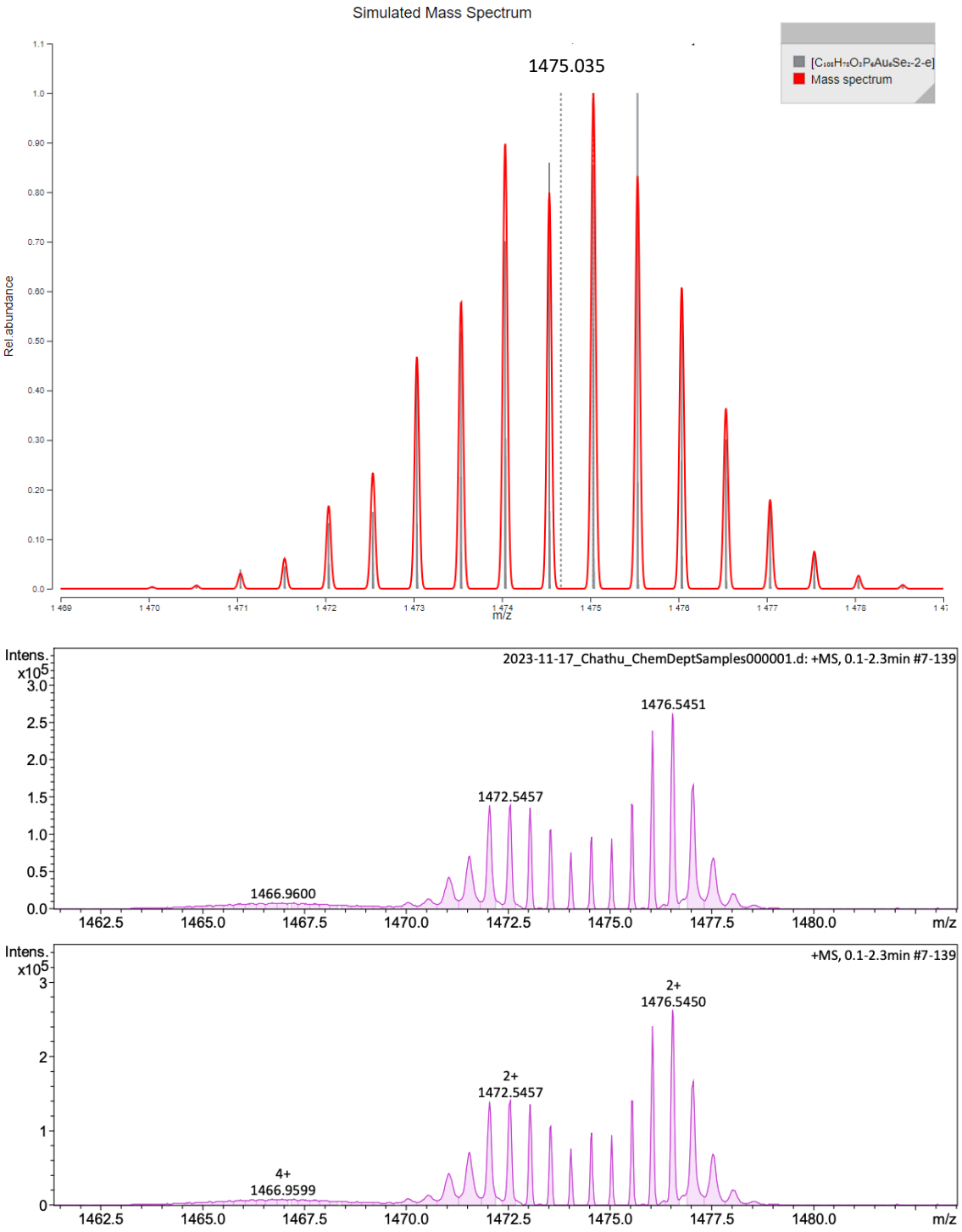

*Figure S2.15: Predicted mass spectrum of **(2.5 Se)** (top) and expanded experimental mass spectrum of **(2.5 Se)** (bottom)*

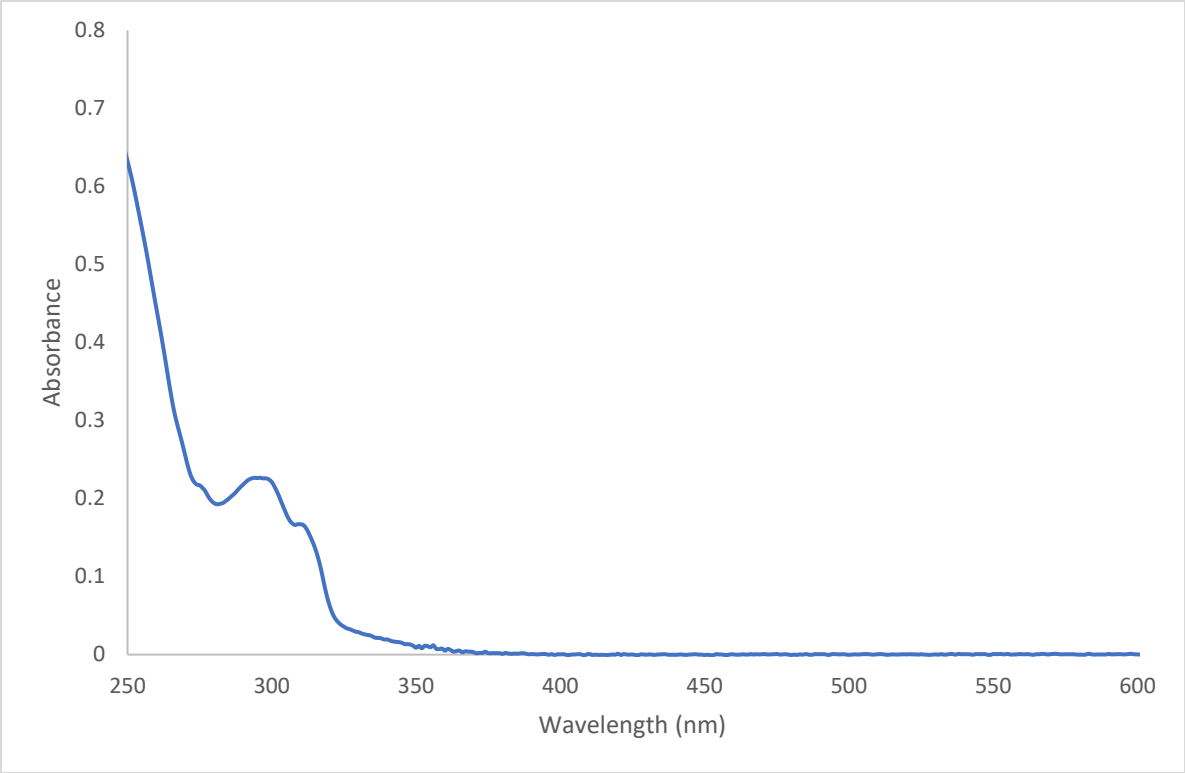

*Figure S2.16: UV-Vis Absorption Spectrum for **(2.3 S)** at 2.07 x 10^{-4} M from 200 nm to 600 nm*

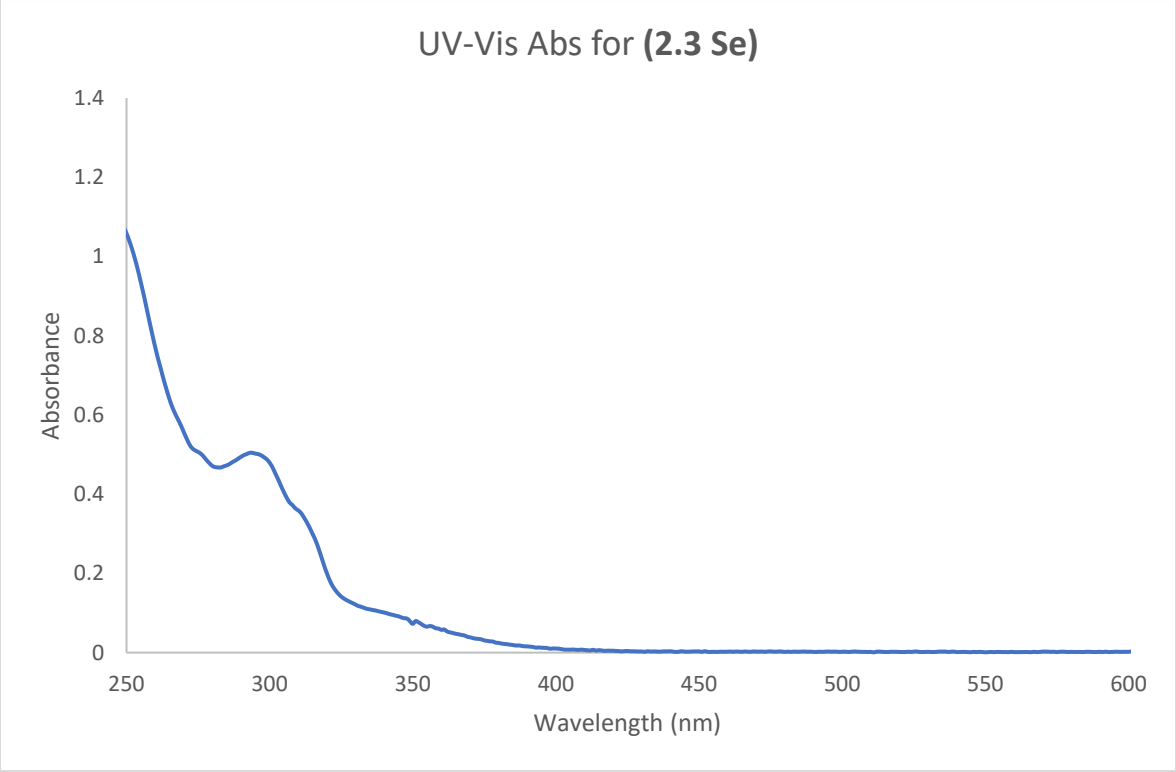

*Figure S2.17: UV-Vis Absorption Spectrum for **(2.3 Se)** at 1.9 x 10^{-4} M from 225 nm to 600 nm*

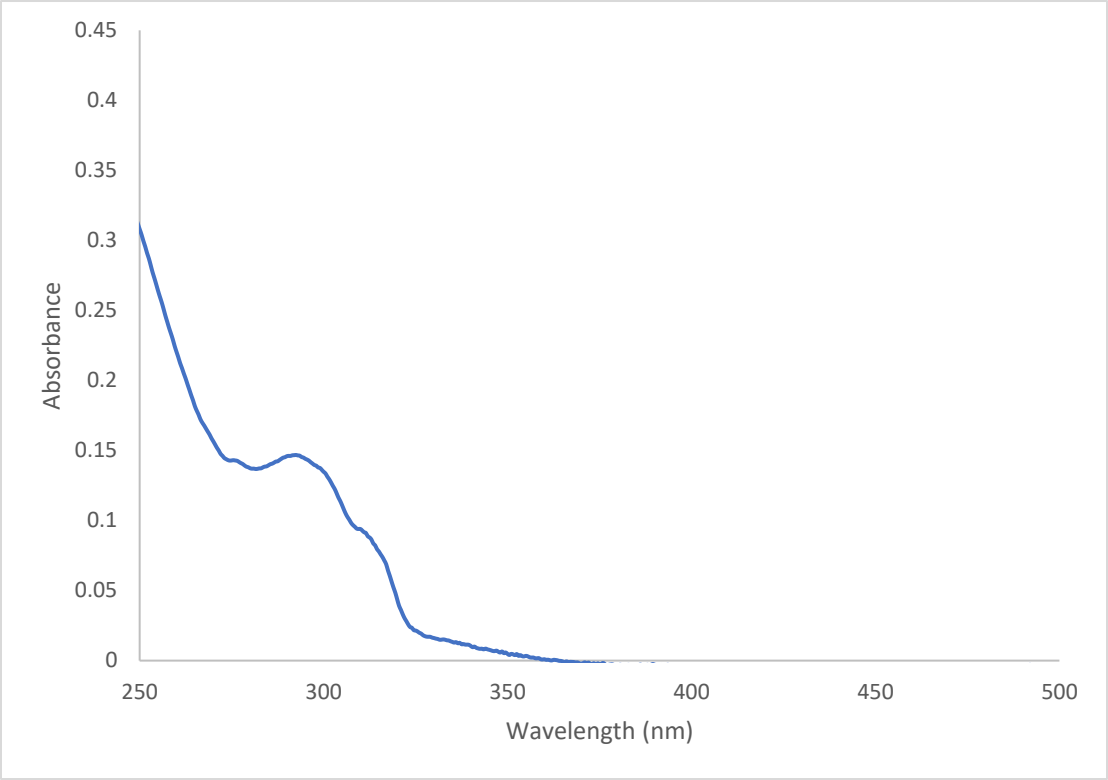

Figure S2.18: UV-Vis Absorption Spectrum for ***(2.4 S/2.5 S)*** mixture *from 200 nm to* 500 *nm*

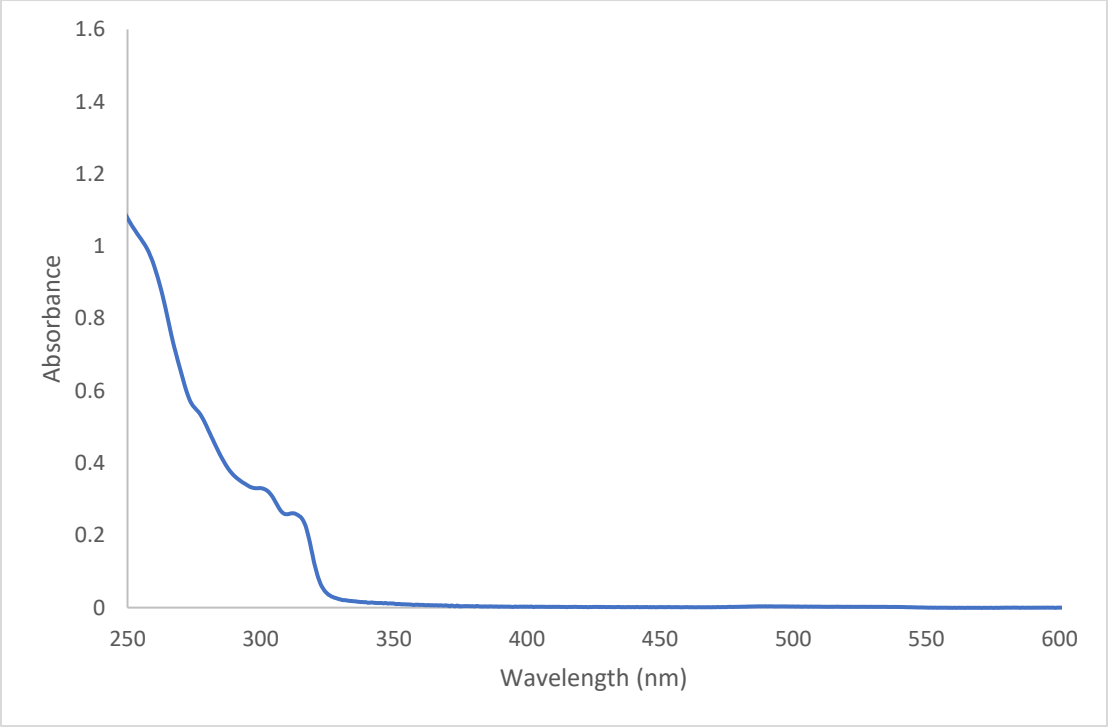

Figure S2.19: *UV-Vis Absorption Spectrum for* ***(2.4 Se/2.5 Se)*** *mixture from 200 nm to 600 nm*

Appendix 2.3: X-ray Structure Analysis and Data for Compounds (2.1) – (2.5 Se)

*Table S2.1: Crystal data and structure refinement of [(AuOAc)$_2$(dbfdp)] (**2.1**)*

Empirical formula	$C_{41}H_{33}Cl_3O_5P_2Au_2$	
Formula weight	1167.89	
Temperature	200(2) K	
Wavelength	0.71073 Å	
Crystal system	Triclinic	
Space group	*P*-1	
Unit cell dimensions	a = 11.343(6) Å	α = 93.417(13)°.
	b = 11.668(6) Å	β = 98.733(12)°.
	c = 17.094(9) Å	γ = 118.252(11)°.
Volume	1947.3(17) Å^3	
Z	2	
Density (calculated)	1.992 g/cm^3	
Absorption coefficient	7.858 mm^{-1}	
F(000)	1116	
Crystal size	0.220 x 0.160 x 0.040 mm^3	
Theta range for data collection	2.082 to 28.000°.	
Index ranges	-14<=h<=14, -15<=k<=15, -22<=l<=22	
Reflections collected	33155	
Independent reflections	9222 [R(int) = 0.0371]	
Completeness to theta = 25.242°	98.3 %	
Absorption correction	Semi-empirical from equivalents	
Max. and min. transmission	0.7460 and 0.4794	
Refinement method	Full-matrix least-squares on F^2	
Data / restraints / parameters	9222 / 0 / 481	
Goodness-of-fit on F^2	1.552	
Final R indices [I>2sigma(I)]	R1 = 0.0330, wR2 = 0.1101	
R indices (all data)	R1 = 0.0407, wR2 = 0.1197	
Extinction coefficient	0.0013(2)	
Largest diff. peak and hole	1.925 and -2.843 e.Å^{-3}	

*Table S2.2: Selected bond lengths of [(AuOAc)$_2$(dbfdp)] (**2.1**)*

Bond Length	Å	Bond Length	Å
Au(1)-P(1)	2.1988(16)	Au(2)-P(2)	2.2037(16)

*Table S2.3: Selected bond angles of [(AuOAc)$_2$(dbfdp)] (**2.1**)*

Bond angle	(°)	Bond angle	(°)
O(38)-Au(1)-P(1)	175.80(14)	C(32)-P(2)-C(26)	106.5(2)
O(42)-Au(2)-P(2)	174.39(13)	C(13)-P(2)-Au(2)	116.53(17)
C(1)-P(1)-C(14)	105.3(2)	C(32)-P(2)-Au(2)	110.13(17)
C(1)-P(1)-C(20)	103.6(2)	C(26)-P(2)-Au(2)	113.78(18)
C(14)-P(1)-C(20)	106.9(2)	C(2)-C(1)-C(6)	115.8(5)
C(1)-P(1)-Au(1)	110.07(17)	C(2)-C(1)-P(1)	125.7(4)

Table S2.4: Crystal data and structure refinement of [(Au_2S)(dbfdp)] ***(2.3 S)***

Formula	$C_{37}H_{28}Au_2Cl_2OP_2S$
Formula Weight (*g/mol*)	1047.43
Crystal Dimensions (*mm*)	0.211 × 0.147 × 0.059
Crystal Color and Habit	colourless plate
Crystal System	monoclinic
Space Group	C 2/c
Temperature, K	110
a, Å	30.833(4)
b, Å	13.3525(18)
c, Å	20.206(3)
α,°	90
β,°	126.537(2)
γ,°	90
V, $Å^3$	6683.9(16)
Number of reflections to determine final unit cell	9882
Min and Max 2θ for cell determination, °	4.82, 61.2
Z	8
F(000)	3968
ρ (*g/cm*)	2.082
λ, Å, (MoKα)	0.71073
μ, (cm^{-1})	9.119
Diffractometer Type	Bruker Kappa Axis Apex2
Scan Type(s)	phi and omega scans
Max 2θ for data collection, °	61.286
Measured fraction of data	0.999
Number of reflections measured	70307
Unique reflections measured	10293
R_{merge}	0.0659
Number of reflections included in refinement	10293
Cut off Threshold Expression	I > 2sigma(I)
Structure refined using	full matrix least-squares using F^2
Weighting Scheme	$w=1/[sigma^2(Fo^2)+(0.0446P)^2]$ where $P=(Fo^2+2Fc^2)/3$
Number of parameters in least-squares	406
R_1	0.0321
wR_2	0.0741
R_1 (all data)	0.0483
wR_2 (all data)	0.0814
GOF	1.029
Maximum shift/error	0.002
Min & Max peak heights on final ΔF Map (e^-/Å)	-1.907, 3.050

Where:

$R_1 = \Sigma | |F_o| - |F_c| | / \Sigma F_o$

$wR_2 = [\Sigma(w(F_o^2 - F_c^2)^2) / \Sigma(w F_o^4)]^{½}$
$GOF = [\Sigma(w(F_o^2 - F_c^2)^2) / (\text{No. of reflns.} - \text{No. of params.})]^{½}$

Table S2.5: Selected bond lengths of [(Au_2S)(dbfdp)] ***(2.3 S)***

Bond Length	Å	Bond Length	Å
Au1-P1	2.2533(11)	Au2-P2	2.2540(12)
Au1-S1	2.2981(11)	Au2-S1	2.2989(12)
Au1-Au2	2.9557(3)	P1-C13	1.813(4)

Table S2.6: Selected bond angles of [(Au_2S)(dbfdp)] ***(2.3 S)***

Bond angle	(°)	Bond angle	(°)
P1-Au1-S1	175.85(4)	C13-P1-C19	102.36(19)
P1-Au1-Au2	127.72(3)	C13-P1-C1	102.80(19)
S1-Au1-Au2	50.00(3)	C19-P1-C1	106.50(19)
P2-Au2-S1	178.08(4)	C13-P1-Au1	118.11(14)
P2-Au2-Au1	128.89(3)	C19-P1-Au1	114.30(14)
S1-Au2-Au1	49.97(3)	C1-P1-Au1	111.46(13)

Table S2.7: Crystal data and structure refinement of [(Au_2Se)(dbfdp)] ***(2.3 Se)***

Formula	$C_{37.50}H_{29}Au_2Cl_3OP_2Se$
Formula Weight (*g/mol*)	1136.79
Crystal Dimensions (*mm*)	0.308 × 0.224 × 0.107
Crystal Color and Habit	colourless block
Crystal System	triclinic
Space Group	P -1
Temperature, K	110
a, Å	11.5528(6)
b, Å	13.4362(7)
c, Å	13.6365(7)
α,°	67.1020(10)
β,°	77.592(2)
γ,°	65.6750(10)
V, $Å^3$	1773.06(16)
Number of reflections to determine final unit cell	9394
Min and Max 2θ for cell determination, °	5.22, 66.48
Z	2
F(000)	1070
ρ (*g/cm*)	2.129
λ, Å, (MoKα)	0.71073
μ, (cm^{-1})	9.638
Diffractometer Type	Bruker Kappa Axis Apex2
Scan Type(s)	phi and omega scans
Max 2θ for data collection, °	66.592
Measured fraction of data	0.999
Number of reflections measured	99914
Unique reflections measured	13649
R_{merge}	0.0297
Number of reflections included in refinement	13649
Cut off Threshold Expression	I > 2sigma(I)
Structure refined using	full matrix least-squares using F^2
Weighting Scheme	$w=1/[sigma^2(Fo^2)+(0.0165P)^2+1.5382P]$ where $P=(Fo^2+2Fc^2)/3$
Number of parameters in least-squares	433
R_1	0.0168
wR_2	0.0393
R_1 (all data)	0.0208
wR_2 (all data)	0.0403
GOF	1.088
Maximum shift/error	0.002
Min & Max peak heights on final ΔF Map (e^-/Å)	-1.630, 1.924

Where:

$R_1 = \Sigma(|F_o| - |F_c|) / \Sigma F_o$

$wR_2 = [\Sigma(w(F_o^2 - F_c^2)^2) / \Sigma(w F_o^4)]^{½}$
$GOF = [\Sigma(w(F_o^2 - F_c^2)^2) / (\text{No. of reflns.} - \text{No. of params.})]^{½}$

Table S2.8: Selected bond lengths of [(Au_2Se)(dbfdp)] ***(2.3 Se)***

Bond Length	Å	Bond Length	Å
Au1-P1	2.2647(5)	Au2-P2	2.2639(5)
Au1-Se1	2.4085(2)	Au2-Se1	2.4152(2)
Au1-Au2	2.97466(15)	P1-C1	1.8109(19)

Table S2.9: Selected bond angles of [(Au_2Se)(dbfdp)] ***(2.3 Se)***

Bond angle	(°)	Bond angle	(°)
P1-Au1-Se1	173.744(13)	C1-P1-C19	103.26(9)
P1-Au1-Au2	122.078(12)	C1-P1-C13	105.94(9)
Se1-Au1-Au2	52.027(5)	C19-P1-C13	105.61(9)
P2-Au2-Se1	175.182(13)	C1-P1-Au1	110.38(6)
P2-Au2-Au1	123.359(13)	C19-P1-Au1	114.22(7)
Se1-Au2-Au1	51.825(6)	C13-P1-Au1	116.31(6)

Table S2.10: Crystal data and structure refinement of $[Au_4(\mu_4\text{-}S)(\mu\text{-}dbfdp)_2]OTf_2$ ***(2.4 S)***

Empirical formula	$C_{76}H_{56}Cl_4F_6O_8P_4S_3Au4$	
Formula weight	2360.93	
Temperature	200(2) K	
Wavelength	0.71073 Å	
Crystal system	Triclinic	
Space group	*P*-1	
Unit cell dimensions	*a* = 12.216(6) Å	α = 74.284(14)°
	b = 18.460(9) Å	β = 74.920(14)°
	c = 18.700(9) Å	γ = 76.208(14)°
Volume	3855(3) $Å^3$	
Z	2	
Density (calculated)	2.034 g/cm^3	
Absorption coefficient	7.960 mm^{-1}	
F(000)	2244	
Crystal size	0.340 x 0.020 x 0.010 mm^3	
Theta range for data collection	1.165 to 27.999°.	
Index ranges	-16<h<15, -24<k<24, -24<l<24	
Reflections collected	18574	
Independent reflections	18574 [R(int) = 0.0879]	
Completeness to theta = 25.242°	99.9 %	
Refinement method	Full-matrix least-squares on F^2	
Data / restraints / parameters	18574 / 0 / 933	
Goodness-of-fit on F^2	1.244	
Final R indices [I>2sigma(I)]	R1 = 0.1352, wR2 = 0.3037	
R indices (all data)	R1 = 0.2224, wR2 = 0.3439	
Extinction coefficient	0.0058(2)	
Largest diff. peak and hole	5.169 and -4.594 $e.Å^{-3}$	

Table S2.11: Selected bond lengths of [$Au_4(\mu_4\text{-}S)(\mu\text{-}dbfdp)_2]OTf_2$ ***(2.4 S)***

Bond Length	Å	Bond Length	Å
Au(1)-P(1)	2.268(4)	Au(3)-P(4)	2.261(4)
Au(1)-S(1)	2.351(3)	Au(3)-S(1)	2.375(4)
Au(1)-Au(2)	2.9340(14)	Au(3)-Au(4)	2.777(2)
Au(1)-Au(4)	2.9439(19)	Au(4)-O(3B)#1	2.337(14)
Au(2)-P(2)	2.293(4)	Au(4)-S(1)	2.484(4)
Au(2)-S(1)	2.412(4)	Au(4)-P(3)	2.860(5)
Au(2)-Au(3)	2.9190(13)	C(1)-C(2)	1.35(2)

Table S2.12: Selected bond angles of [$Au_4(\mu_4\text{-}S)(\mu\text{-}dbfdp)_2]OTf_2$ ***(2.4 S)***

Bond angle	(°)	Bond angle	(°)
P(1)-Au(1)-S(1)	176.65(13)	P(2)-Au(2)-S(1)	173.28(13)
P(1)-Au(1)-Au(2)	125.33(10)	P(2)-Au(2)-Au(3)	132.35(11)
S(1)-Au(1)-Au(2)	52.93(9)	S(1)-Au(2)-Au(3)	51.85(9)
P(1)-Au(1)-Au(4)	128.58(10)	P(2)-Au(2)-Au(1)	123.09(10)
S(1)-Au(1)-Au(4)	54.57(10)	S(1)-Au(2)-Au(1)	51.04(8)
Au(2)-Au(1)-Au(4)	98.53(5)	Au(3)-Au(2)-Au(1)	73.88(4)
P(4)-Au(3)-S(1)	172.00(12)	P(4)-Au(3)-Au(2)	123.77(9)
P(4)-Au(3)-Au(4)	129.49(10)	S(1)-Au(3)-Au(2)	53.02(9)
S(1)-Au(3)-Au(4)	57.01(10)	Au(4)-Au(3)-Au(2)	102.84(5)
O(3B)#1-Au(4)-S(1)	89.7(3)	Au(3)-Au(4)-P(3)	114.60(12)
O(3B)#1-Au(4)-Au(3)	140.8(3)	O(3B)#1-Au(4)-Au(1)	90.9(3)
S(1)-Au(4)-Au(3)	53.32(9)	S(1)-Au(4)-Au(1)	50.47(8)
O(3B)#1-Au(4)-P(3)	100.6(3)	Au(3)-Au(4)-Au(1)	75.81(5)
Au(1)-S(1)-Au(3)	96.19(13)	Au(1)-S(1)-Au(4)	74.96(11)

Au(1)-S(1)-Au(2)	76.03(10)	Au(3)-S(1)-Au(4)	69.68(10)
Au(3)-S(1)-Au(2)	75.14(11)	Au(2)-S(1)-Au(4)	130.91(15)

Table S2.13: Crystal data and structure refinement of $[Au_4(\mu_4\text{-}Se)(\mu\text{-}dbfdp)_2](OTf)_2$ ***(2.4 Se)***

Empirical formula		
Formula weight		
Temperature	100.00 K	
Wavelength		
Crystal system		
Space group	$P\bar{1}$	
Unit cell dimensions	a = 12.2213(1) Å	α = 73.754(1) °.
	b = 17.5601(2) Å	β = 74.616(1) °
	c = 19.0426(2) Å	γ = 75.895(1) °.
Volume	3718.97 Å^3	
Z		
Density (calculated)		
Absorption coefficient		
F(000)		
Crystal size		
Theta range for data collection		
Index ranges		
Reflections collected		
Independent reflections		
Completeness to theta = 25.242°		
Absorption correction		
Refinement method		
Data / restraints / parameters		
Goodness-of-fit on F^2		
Final R indices [I>2sigma(I)]		
R indices (all data)		
Extinction coefficient		
Largest diff. peak and hole		

Table S2.14: Selected bond lengths of [$Au_4(\mu_4\text{-}Se)(\mu\text{-}dbfdp)_2](OTf)_2$ ***(2.4 Se)***

Bond Length	Å	Bond Length	Å
Au(1)-Au(2)	2.8831	Au(2)-Au(3)	2.9399
Au(1)-Au(4)	2.8667	Au(3)-Au(4)	2.9482
Au(2)-P(1)	2.2627	Au(1)-P(1)	2.2627
Au(1)-Se(1)	2.4968	Au(2)-Se(1)	2.4959
Au(3)-Se(1)	2.4720	Au(4)-Se(1)	2.4904

Table S2.15: Selected bond angles of [$Au_4(\mu_4\text{-}Se)(\mu\text{-}dbfdp)_2](OTf)_2$ ***(2.4 Se)***

Bond angle	(°)	Bond angle	(°)
Au(2)-Au(1)-Au(4)	99.01	Au(4)-Au(1)-P(2)	128.51
Au(2)-Au(1)-P(2)	126.37	Au(4)-Au(1)-Se(1)	54.81
Au(2)-Au(1)-Se(1)	54.71	P(2)-Au(1)-Se(1)	173.17
Au(1)-Au(2)-Au(3)	79.80	Au(1)-Au(2)-P(1)	120.89
Au(1)-Au(2)-Se(1)	54.74	Au(3)-Au(2)-P(1)	136.29

Table S2.16: Crystal data and structure refinement of $[Au_6(\mu_3\text{-}S)_2(\mu\text{-}dbfdp)_3](OTf)_2$ ***(2.5 S)***

Empirical formula	$C_{122.24}H_{104.47}Cl_3F_6O_{9.30}P_6S_4Au_6$	
Formula weight	3438.34	
Temperature	100.00 K	
Wavelength	0.71073 Å	
Crystal system	Monoclinic	
Space group	$P\ 2_1/c$	
Unit cell dimensions	a = 14.7619(4) Å	α = 90°.
	b = 39.5014(14) Å	β = 92.7730(10)°
	c = 21.0695(8) Å	γ = 90°.
Volume	12271.6(7) Å^3	
Z	4	
Density (calculated)	1.861 g/cm^3	
Absorption coefficient	7.422 mm^{-1}	
F(000)	6581	
Crystal size	0.18 x 0.16 x 0.08 mm^3	
Theta range for data collection	1.726 to 29.719°.	
Index ranges	-20<=h<=19, -51<=k<=51, -29<=l<=29	
Reflections collected	87450	
Independent reflections	28769 [R(int) = 0.1536]	
Completeness to theta = 25.242°	98.7 %	
Absorption correction	None	
Refinement method	Full-matrix least-squares on F^2	
Data / restraints / parameters	28769 / 0 / 1387	
Goodness-of-fit on F^2	0.949	
Final R indices [I>2sigma(I)]	R1 = 0.0623, wR2 = 0.1539	
R indices (all data)	R1 = 0.1368, wR2 = 0.2011	
Extinction coefficient	n/a	
Largest diff. peak and hole	2.458 and -2.837 e.Å^{-3}	

Table S2.17: Selected bond lengths of $[Au_6(\mu_3\text{-}S)_2(\mu\text{-}dbfdp)_3](OTf)_2$ ***(2.5 S)***

Bond Length	Å	Bond Length	Å
Au(1)-Au(2)	2.9697(7)	Au(2)-P(2)	2.251(4)
Au(1)-Au(6)	2.9241(7)	Au(6)-Au(4)	3.0739(8)
Au(1)-Au(3)	3.1768(8)	Au(6)-Au(5)	2.9903(8)
Au(1)-S(1)	2.360(4)	Au(6)-S(2)	2.363(4)
Au(1)-P(1)	2.277(4)	Au(6)-P(6)	2.265(4)
Au(2)-Au(3)	3.1218(8)	Au(4)-Au(5)	3.1118(8)
Au(2)-S(1)	2.337(4)	Au(4)-S(2)	2.316(4)
Au(4)-P(4)	2.248(4)	Au(5)-S(2)	2.332(3)
Au(3)-S(1)	2.301(4)	Au(5)-P(5)	2.254(4)
Au(3)-P(3)	2.251(4)	P(2)-C(00P)	1.823(13)

Table S2.18: Selected bond angles of $[Au_6(\mu_3\text{-}S)_2(\mu\text{-}dbfdp)_3](OTf)_2$ ***(2.5 S)***

Bond angle	(°)	Bond angle	(°)
Au(2)-Au(1)-Au(3)	60.936(18)	P(2)-Au(2)-Au(1)	125.99(10)
Au(6)-Au(1)-Au(2)	133.91(3)	P(2)-Au(2)-Au(3)	134.23(10)
Au(6)-Au(1)-Au(3)	93.04(2)	P(2)-Au(2)-S(1)	176.67(14)
S(1)-Au(1)-Au(2)	50.44(8)	Au(1)-Au(6)-Au(4)	98.78(2)
S(1)-Au(1)-Au(6)	83.76(9)	Au(1)-Au(6)-Au(5)	135.90(3)
S(1)-Au(1)-Au(3)	46.27(9)	Au(5)-Au(6)-Au(4)	61.729(18)
P(1)-Au(1)-Au(2)	120.54(10)	S(2)-Au(6)-Au(1)	86.89(8)
P(1)-Au(1)-Au(6)	105.18(10)	S(2)-Au(6)-Au(4)	48.27(9)
P(1)-Au(1)-Au(3)	132.61(10)	S(2)-Au(6)-Au(5)	49.99(8)
P(1)-Au(1)-S(1)	170.98(13)	P(6)-Au(6)-Au(1)	102.52(10)
Au(1)-Au(2)-Au(3)	62.809(18)	P(6)-Au(6)-Au(4)	130.39(11)
S(1)-Au(2)-Au(1)	51.12(9)	P(6)-Au(6)-Au(5)	120.43(10)

S(1)-Au(2)-Au(3)	47.22(9)	P(6)-Au(6)-S(2)	170.41(13)
Au(6)-Au(4)-Au(5)	57.814(17)	Au(2)-Au(3)-Au(1)	56.255(17)
S(2)-Au(4)-Au(6)	49.60(9)	S(1)-Au(3)-Au(1)	47.81(9)
S(2)-Au(4)-Au(5)	48.20(8)	S(1)-Au(3)-Au(2)	48.19(9)
P(4)-Au(4)-Au(6)	126.73(11)	P(3)-Au(3)-Au(1)	126.65(10)
P(4)-Au(4)-Au(5)	128.92(10)	P(3)-Au(3)-Au(2)	127.22(10)
P(4)-Au(4)-S(2)	175.74(14)	P(3)-Au(3)-S(1)	173.54(14)

Table S2.19: Crystal data and structure refinement of $[Au_6(\mu_3\text{-}Se)_2(\mu\text{-}dbfdp)_3](OTf)_2$ ***(2.5 Se)***

Empirical formula	$C_{56}H_{42}Cl_2F_3O_{4.50}P_3SSeAu_3$	
Formula weight	1709.62	
Temperature	200(2) K	
Wavelength	0.71073 Å	
Crystal system	Monoclinic	
Space group	*C*2/*c*	
Unit cell dimensions	*a* = 11.590(2) Å	α = 90°
	b = 38.869(6) Å	β = 96.338(9)°
	c = 26.224(4) Å	γ = 90°
Volume	11742(3) Å^3	
Z	8	
Density (calculated)	1.934 g/cm^3	
Absorption coefficient	8.360 mm^{-1}	
F(000)	6456	
Crystal size	0.540 x 0.040 x 0.010 mm^3	
Theta range for data collection	1.048 to 23.697°.	
Index ranges	-12<=h<=11, -43<=k<=43, -29<=l<=28	
Reflections collected	64128	
Independent reflections	8169 [R(int) = 0.0354]	
Completeness to theta = 23.697°	91.9 %	
Absorption correction	Semi-empirical from equivalents	
Max. and min. transmission	0.7450 and 0.5486	
Refinement method	Full-matrix least-squares on F^2	
Data / restraints / parameters	8169 / 0 / 663	
Goodness-of-fit on F^2	1.276	
Final R indices [I>2sigma(I)]	R1 = 0.0352, wR2 = 0.0822	
R indices (all data)	R1 = 0.0498, wR2 = 0.0886	
Extinction coefficient	n/a	
Largest diff. peak and hole	1.695 and -1.401 e.Å^{-3}	

Table S2.20: Selected bond lengths of $[Au_6(\mu_3\text{-}Se)_2(\mu\text{-}dbfdp)_3](OTf)_2$ ***(2.5 Se)***

Bond Length	Å	Bond Length	Å
Au(1)-P(1)	2.269(3)	Au(2)-Au(3)	3.1845(7)
Au(1)-Se(1)	2.4771(11)	Au(3)-P(3)	2.257(3)
Au(1)-Au(2)	3.0474(7)	Au(3)-Se(1)	2.4319(11)
Au(1)-Au(1)#1	3.0511(9)	Au(3)-Au(3)#1	3.2135(9)
Au(1)-Au(3)	3.0758(7)	P(1)-C(1)	1.811(10)
Au(2)-P(2)	2.264(3)	P(1)-C(27)	1.812(10)
Au(2)-Se(1)	2.4317(11)	P(1)-C(21)	1.817(10)

Table S2.21: Selected bond angles of $[Au_6(\mu_3\text{-}Se)_2(\mu\text{-}dbfdp)_3](OTf)_2$ ***(2.5 Se)***

Bond angle	(°)	Bond angle	(°)
P(1)-Au(1)-Se(1)	170.46(7)	P(3)-Au(3)-Se(1)	174.57(7)
P(1)-Au(1)-Au(2)	119.71(7)	P(3)-Au(3)-Au(1)	127.73(7)
Se(1)-Au(1)-Au(2)	50.96(3)	Se(1)-Au(3)-Au(1)	51.86(3)
P(1)-Au(1)-Au(1)#1	103.71(7)	P(3)-Au(3)-Au(2)	125.54(7)
Se(1)-Au(1)-Au(1)#1	85.60(3)	Se(1)-Au(3)-Au(2)	49.10(3)
Au(2)-Au(1)-Au(1)#1	136.558(17)	Au(1)-Au(3)-Au(2)	58.227(13)
P(1)-Au(1)-Au(3)	129.98(7)	P(3)-Au(3)-Au(3)#1	106.34(7)
Se(1)-Au(1)-Au(3)	50.55(3)	Se(1)-Au(3)-Au(3)#1	79.07(3)
Au(2)-Au(1)-Au(3)	62.672(14)	Au(1)-Au(3)-Au(3)#1	88.343(10)
Au(1)#1-Au(1)-Au(3)	91.361(10)	Au(2)-Au(3)-Au(3)#1	127.940(17)
P(2)-Au(2)-Se(1)	173.84(7)	Au(2)-Se(1)-Au(3)	81.80(3)
P(2)-Au(2)-Au(1)	127.23(7)	Au(2)-Se(1)-Au(1)	76.74(3)
Se(1)-Au(2)-Au(1)	52.30(3)	Au(3)-Se(1)-Au(1)	77.59(3)
P(2)-Au(2)-Au(3)	136.89(7)	C(1)-P(1)-C(27)	104.5(5)
Se(1)-Au(2)-Au(3)	49.10(3)	Au(1)-Au(2)-Au(3)	59.101(16)

Appendix 2.4: Additional Emission Spectra for Chapter 2

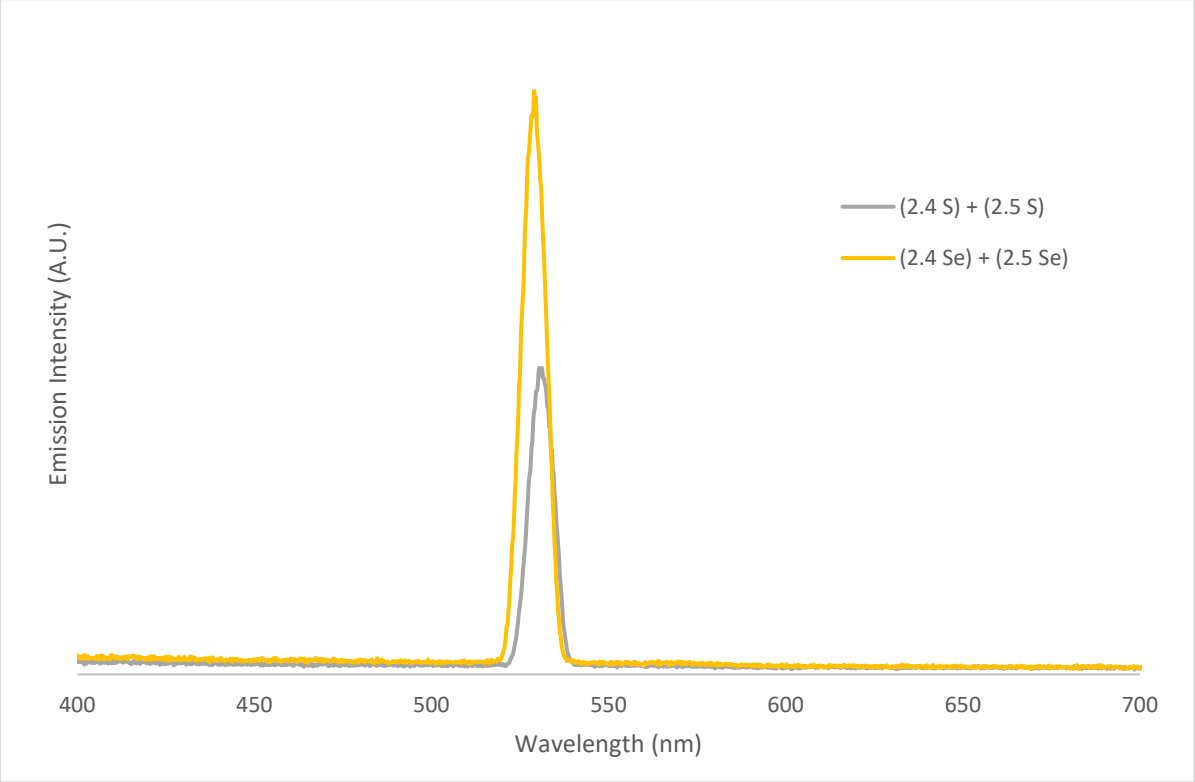

Figure S2.20: Emission spectra of crystalline solids of mixtures of ***(2.4 S)/(2.5 S)*** *and* ***(2.4 Se)/(2.5 Se)*** *in the solid state at room temperature. (λ_{exc} = 264 nm* ***(2.4 S)/(2.5 S)****, λ_{exc} = 264 nm* ***(2.4 Se)/(2.5 Se)****). The maxima at 528 nm are attributed to an artifact 2 times the excitation wavelength.*

Appendix 3.0 Supporting Information for Chapter 3

Appendix 3.1: NMR Data for Compounds (3.2) – (3.4)

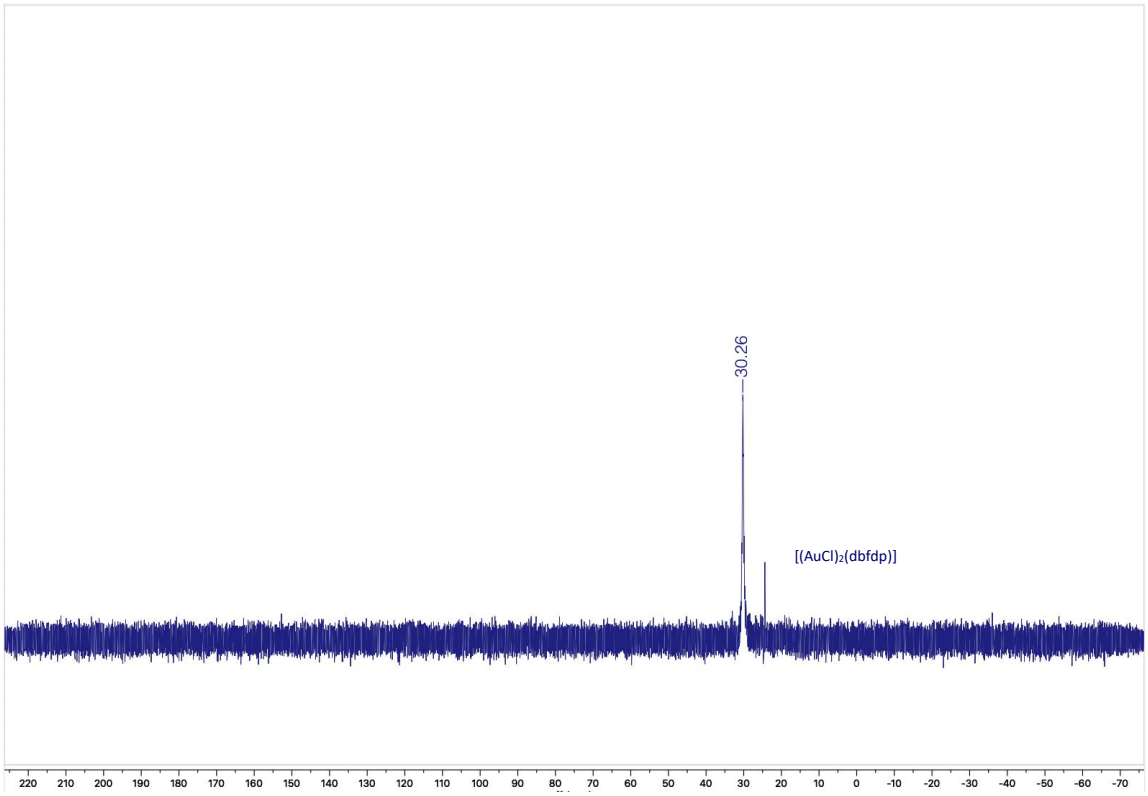

Figure S3.1: $^{31}P\{^{1}H\}$ NMR spectrum in $CDCl_3$ (298K) of $[(AuSPh)_2(\mu\text{-dbfdp})]$ ***(3.2)***

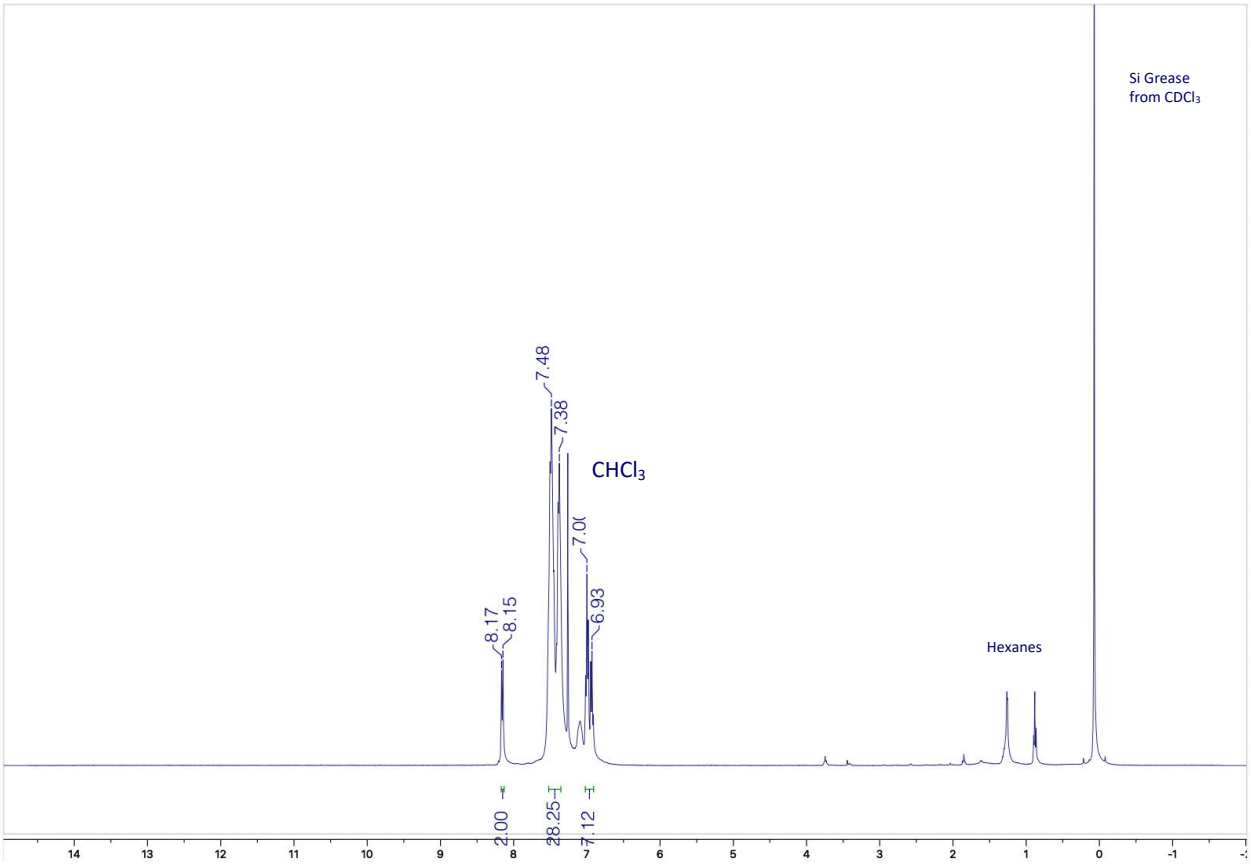

Figure S3.2: ^{1}H NMR spectrum in $CDCl_3$ (298K) of [$(AuSPh)_2$(μ-dbfdp)] ***(3.2)***

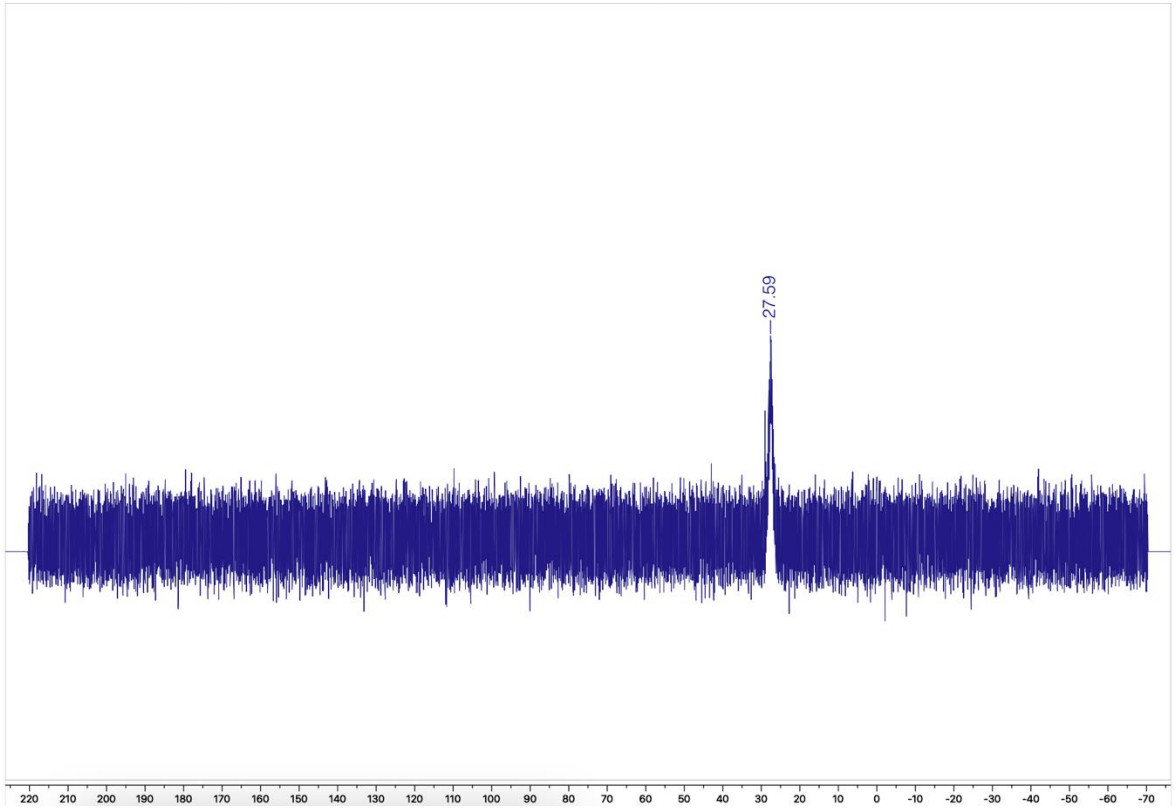

Figure S3.3: $^{31}P\{^{1}H\}$ NMR spectrum in $CDCl_3$ (298K) of $[(AuSePh)_2(\mu\text{-dbfdp})]$ ***(3.3)***

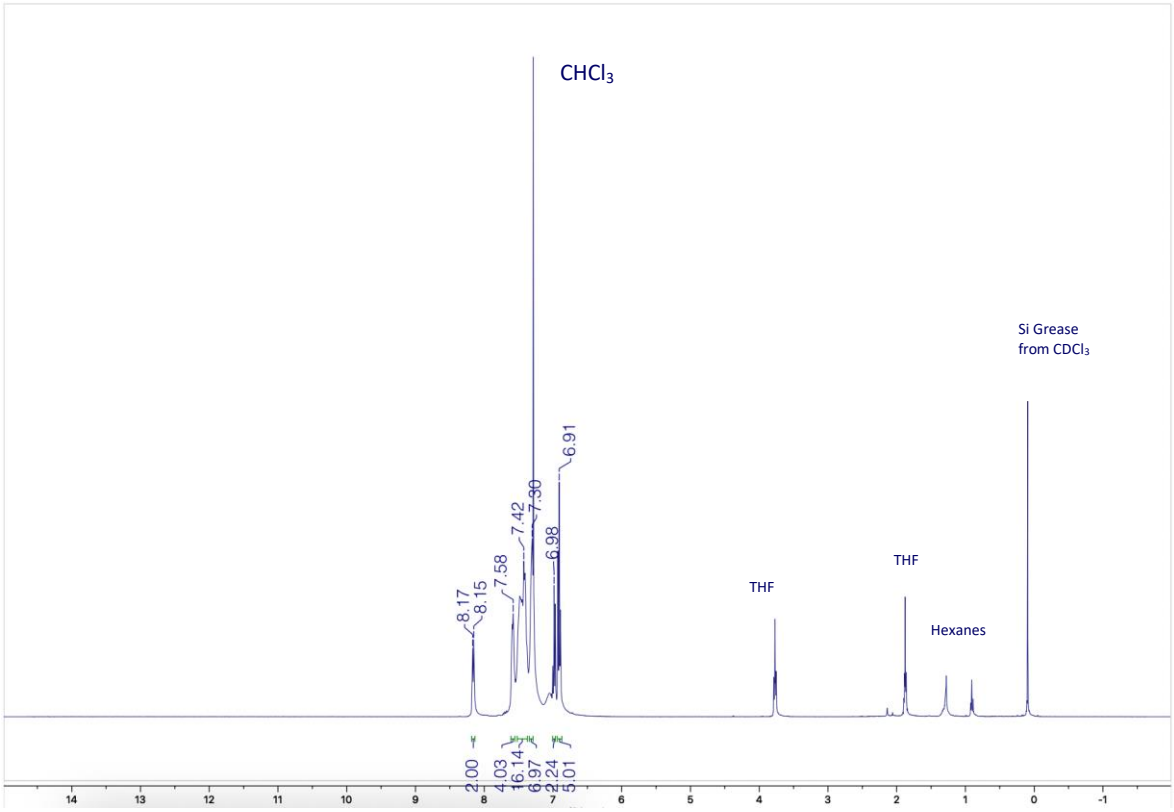

Figure S3.4: ^{1}H NMR spectrum in $CDCl_3$ (298K) of $[(AuSePh)_2(\mu\text{-dbfdp})]$ ***(3.3)***

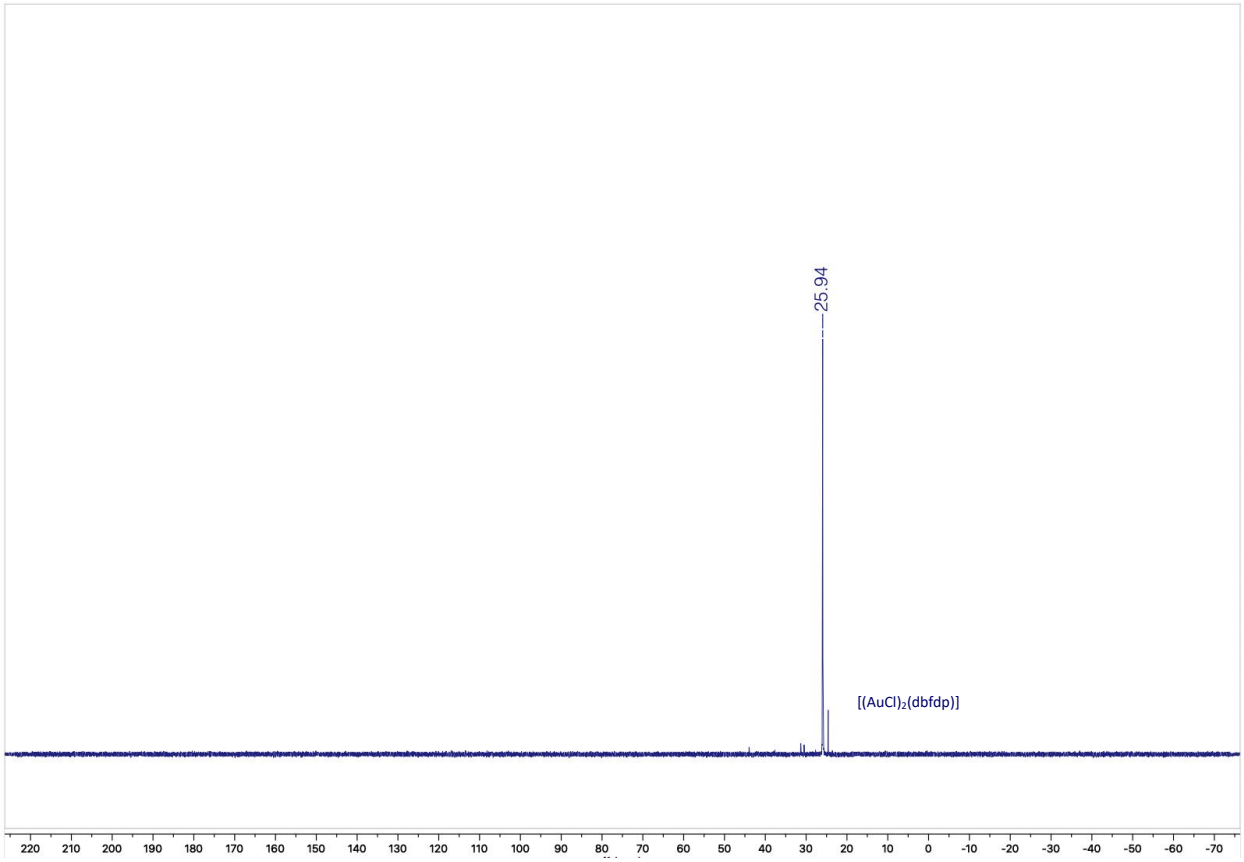

Figure S3.5: ^{31}P NMR spectrum in CD_2Cl_2 (298K) of $[(AuSC_6F_5)_2(dbfdp)]$ ***(3.4)***

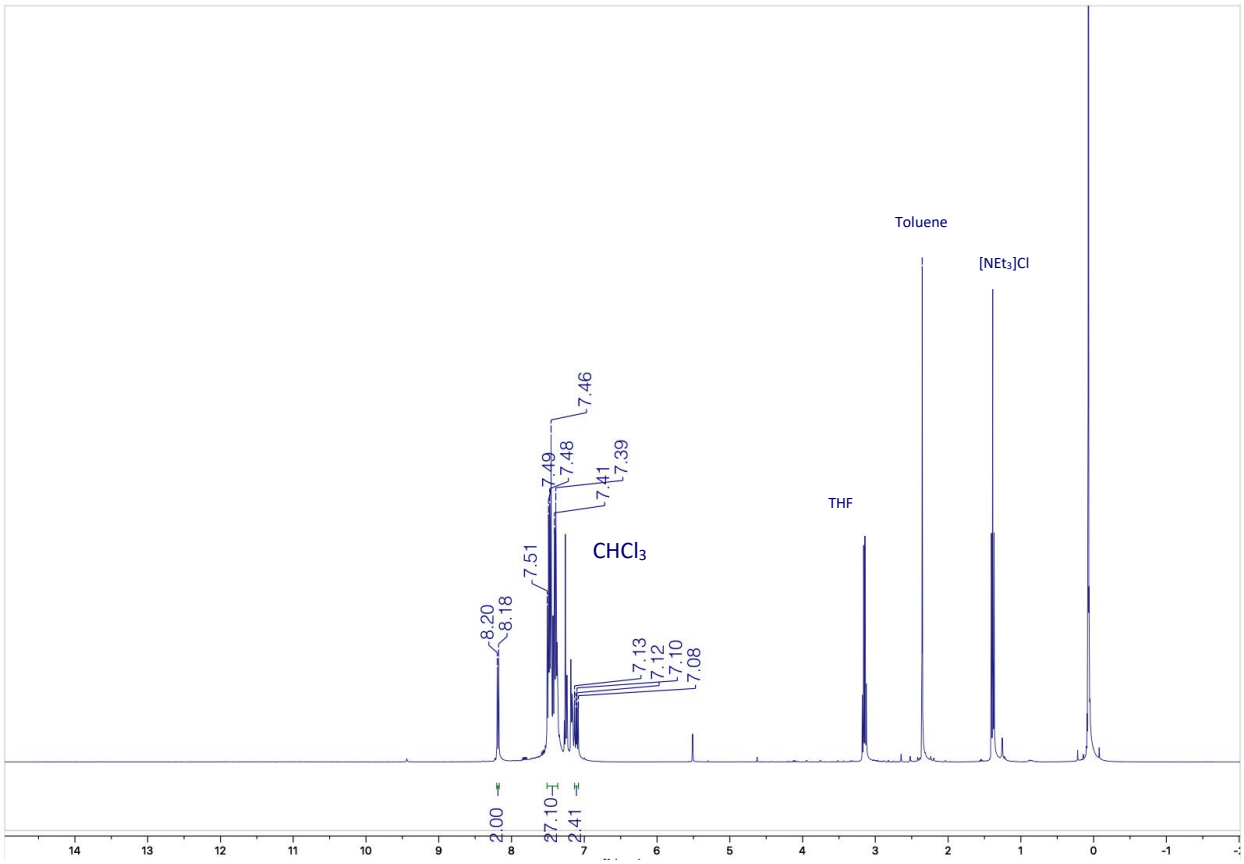

Figure S3.6: ^{1}H NMR spectrum in $CDCl_3$ (298K) of $[(AuSC_6F_5)_2(dbfdp)]$ ***(3.4)***

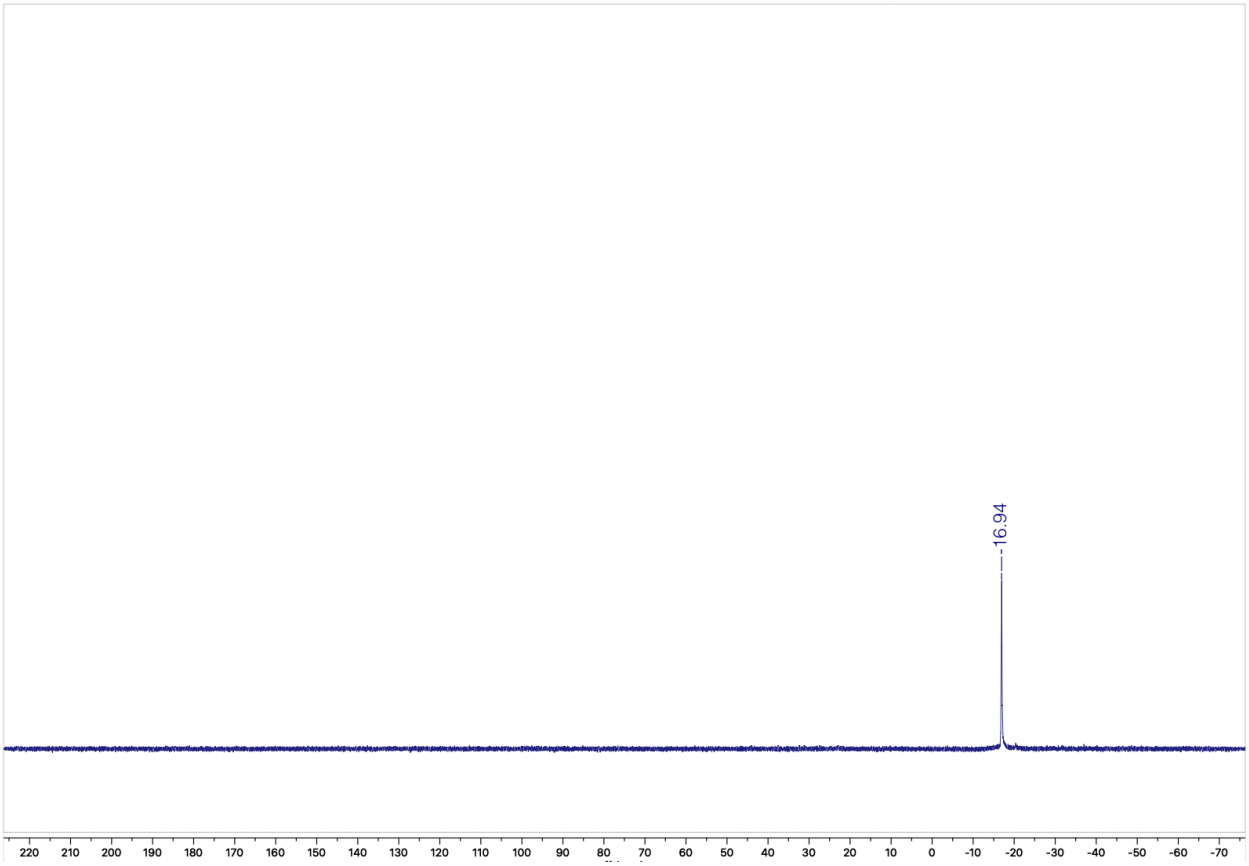

Figure S3.7: $^{31}P\{^{1}H\}$ NMR spectrum in CD_2Cl_2 (298K) of $[Cu_4(\mu_2\text{-}SC_6F_5)_4(\mu\text{-dbfdp})_2]$ ***(3.5)***

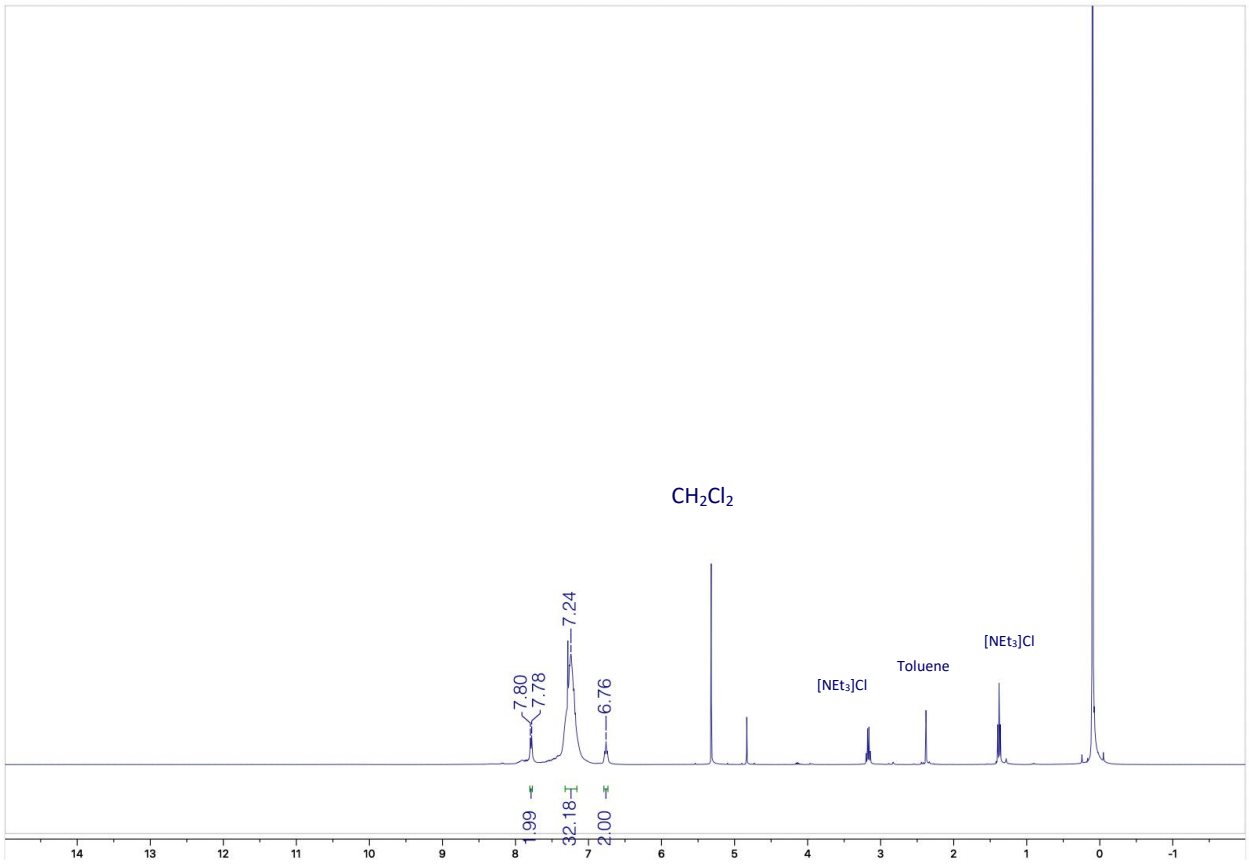

Figure S3.8: ^{1}H NMR spectrum in CD_2Cl_2 (298K) of $[Cu_4(\mu_2\text{-}SC_6F_5)_4(\mu\text{-}dbfdp)_2]$ ***(3.5)***

Appendix 2.2: X-ray Structure Analysis and Data for Compounds (3.2) - (3.5)

Table S3.1: Crystal data and structure refinement of [(AuSPh)$_2$(dbfdp)] ***(3.2)***

Empirical formula	$C_{48}H_{36}OP_2S_2Au_2$	
Formula weight	1148.76	
Temperature	110.15 K	
Wavelength	0.71073 Å	
Crystal system	Monoclinic	
Space group	$P2_1/c$	
Unit cell dimensions	a = 11.0566(5) Å	α = 90°
	b = 40.074(2) Å	β = 104.1680(10)°
	c = 10.3355(4) Å	γ = 90°
Volume	4440.2(3) Å^3	
Z	4	
Density (calculated)	1.718 g/cm^3	
Absorption coefficient	6.801 mm^{-1}	
F(000)	2208	
Crystal size	0.257 x 0.085 x 0.036 mm^3	
Theta range for data collection	1.966 to 33.258°.	
Index ranges	-16<=h<=17, -61<=k<=61, -15<=l<=15	
Reflections collected	253765	
Independent reflections	16980 [R(int) = 0.0866]	
Completeness to theta = 25.242°	100.0 %	
Absorption correction	None	
Max. and min. transmission	0.6956 and 0.4397	
Refinement method	Full-matrix least-squares on F^2	
Data / restraints / parameters	16980 / 0 / 509	
Goodness-of-fit on F^2	1.027	
Final R indices [I>2sigma(I)]	R1 = 0.0335, wR2 = 0.0630	
R indices (all data)	R1 = 0.0461, wR2 = 0.0663	
Extinction coefficient	0.00012(2)	
Largest diff. peak and hole	1.214 and -1.225 e.Å^{-3}	

Table S3.2: Selected bond lengths of [(AuSPh)$_2$(dbfdp)] ***(3.2)***

Bond Length	Å	Bond Length	Å
Au(1)-S(1)	2.2934(9)	S(1)-C(49)	1.770(5)
Au(1)-P(1)	2.2496(8)	S(2)-C(58)	1.777(3)
Au(2)-S(2)	2.3043(7)	P(1)-C(13)	1.812(3)
Au(2)-P(2)	2.2661(7)	P(1)-C(19)	1.818(3)

Table S3.3: Selected bond angles of [(AuSPh)$_2$(dbfdp)] ***(3.2)***

Bond angle	(°)	Bond angle	(°)
P(1)-Au(1)-S(1)	175.32(3)	C(58)-S(2)-Au(2)	103.49(10)
P(2)-Au(2)-S(2)	170.67(3)	C(13)-P(1)-Au(1)	110.52(11)
C(49)-S(1)-Au(1)	106.00(15)	C(13)-P(1)-C(19)	106.81(16)

Table S3.4: Crystal data and structure refinement of [(AuSePh)$_2$(dbfdp)] ***(3.3)***

Empirical formula	$C_{48}H_{36}OP_2Se_2Au_2$	
Formula weight	1242.56	
Temperature	200(2) K	
Wavelength	0.71073 Å	
Crystal system	Triclinic	
Space group	*P*-1	
Unit cell dimensions	a = 10.147(4) Å	α = 104.043(10)°
	b = 10.557(4) Å	β = 92.548(10)°
	c = 20.523(7) Å	γ = 103.126(9)°
Volume	2065.5(13) Å^3	
Z	2	
Density (calculated)	1.998 g/cm^3	
Absorption coefficient	8.971 mm^{-1}	
F(000)	1176	
Crystal size	0.130 x 0.060 x 0.010 mm^3	
Theta range for data collection	2.409 to 27.999°.	
Index ranges	-13<=h<=13, -13<=k<=13, -27<=l<=27	
Reflections collected	45268	
Independent reflections	9950 [R(int) = 0.1201]	
Completeness to theta = 25.242°	99.8 %	
Absorption correction	Semi-empirical from equivalents	
Max. and min. transmission	0.7460 and 0.4983	
Refinement method	Full-matrix least-squares on F^2	
Data / restraints / parameters	9950 / 0 / 498	
Goodness-of-fit on F^2	1.286	
Final R indices [I>2sigma(I)]	R1 = 0.0579, wR2 = 0.1038	
R indices (all data)	R1 = 0.1133, wR2 = 0.1146	
Extinction coefficient	0.00296(18)	
Largest diff. peak and hole	2.290 and -3.784 e.Å^{-3}	

Table S3.5: Selected bond lengths of [(AuSePh)$_2$(dbfdp)] ***(3.3)***

Bond Length	Å	Bond Length	Å
Au(1)-P(1)	2.283(2)	Au(2)-Se(2)	2.4297(13)
Au(1)-Se(1)	2.4519(14)	C(1)-C(2)	1.390(13)
Au(1)-Au(2)	3.1112(10)	C(1)-C(6)	1.396(12)
Au(2)-P(2)	2.267(3)	C(1)-P(1)	1.825(10)

Table S3.6: Selected bond angles of [(AuSePh)$_2$(dbfdp)] ***(3.3)***

Bond angle	(°)	Bond angle	(°)
P(1)-Au(1)-Se(1)	166.70(7)	P(2)-Au(2)-Se(2)	167.06(8)
P(1)-Au(1)-Au(2)	106.62(7)	P(2)-Au(2)-Au(1)	121.96(7)
Se(1)-Au(1)-Au(2)	81.39(3)	Se(2)-Au(2)-Au(1)	69.12(4)

Table S3.7: Crystal data and structure refinement of [(AuSC$_6$F$_5$)$_2$(dbfdp)] ***(3.4)***

Empirical formula	$C_{48}H_{26}F_{10}OP_2S_2Au_2$	
Formula weight	1328.68	
Temperature	200(2) K	
Wavelength	0.71073 Å	
Crystal system	Triclinic	
Space group	*P*-1	
Unit cell dimensions	*a* = 10.862(4) Å	α = 99.194(10)°
	b = 14.707(5) Å	β = 91.884(11)°
	c = 28.754(11) Å	γ = 105.235(10)°
Volume	4362(3) Å^3	
Z	4	
Density (calculated)	2.023 g/cm^3	
Absorption coefficient	6.970 mm^{-1}	
F(000)	2528	
Crystal size	0.125 x 0.120 x 0.010 mm^3	
Theta range for data collection	1.457 to 28.000°.	
Index ranges	-14<=h<=14, -19<=k<=19, -37<=l<=37	
Reflections collected	81572	
Independent reflections	21048 [R(int) = 0.0583]	
Completeness to theta = 25.242°	100.0 %	
Absorption correction	Semi-empirical from equivalents	
Max. and min. transmission	0.7460 and 0.5285	
Refinement method	Full-matrix least-squares on F^2	
Data / restraints / parameters	21048 / 0 / 1171	
Goodness-of-fit on F^2	1.188	
Final R indices [I>2sigma(I)]	R1 = 0.0431, wR2 = 0.0836	
R indices (all data)	R1 = 0.0679, wR2 = 0.0907	
Extinction coefficient	n/a	
Largest diff. peak and hole	2.109 and -2.068 e.Å^{-3}	

Table S3.8: Selected bond lengths of [(AuSC$_6$F$_5$)$_2$(dbfdp)] ***(3.4)***

Bond Length	Å	Bond Length	Å
Au(1A)-P(1A)	2.2632(18)	P(1A)-C(26A)	1.821(6)
Au(1A)-S(1A)	2.312(2)	P(1A)-C(32A)	1.828(6)
Au(2A)-P(2A)	2.2656(17)	P(1A)-C(1A)	1.829(6)
Au(2A)-S(2A)	2.3135(19)	P(2A)-C(11A)	1.813(6)

Table S3.9: Selected bond angles of [(AuSC$_6$F$_5$)$_2$(dbfdp)] ***(3.4)***

Bond angle	(°)	Bond angle	(°)
P(1A)-Au(1A)-S(1A)	172.11(7)	C(26A)-P(1A)-C(1A)	105.9(3)
P(2A)-Au(2A)-S(2A)	175.20(7)	C(32A)-P(1A)-C(1A)	103.1(3)
C(26A)-P(1A)-C(32A)	103.9(3)	C(26A)-P(1A)-Au(1A)	111.4(2)

Table S3.10: Crystal data and structure refinement of $[Cu_4(SC_6F_5)_4(dbfdp)_2]$ ***(3.5)***

Empirical formula	$C_{48}H_{26}F_{10}OP_3SCu_2$	
Formula weight	1060.74	
Temperature	200(2) K	
Wavelength	0.71073 Å	
Crystal system	Orthorhombic	
Space group	$Cmc2_1$	
Unit cell dimensions	a = 24.965(13) Å	α = 90°
	b = 17.763(9) Å	β = 90°
	c = 22.292(12) Å	γ = 90°
Volume	9886(9) $Å^3$	
Z	8	
Density (calculated)	1.425 g/cm^3	
Absorption coefficient	1.071 mm^{-1}	
F(000)	4248	
Crystal size	0.210 x 0.110 x 0.060 mm^3	
Theta range for data collection	1.407 to 27.999°.	
Index ranges	-31<=h<=32, -21<=k<=23, -28<=l<=29	
Reflections collected	55823	
Independent reflections	11979 [R(int) = 0.0682]	
Completeness to theta = 25.242°	99.9 %	
Refinement method	Full-matrix least-squares on F^2	
Data / restraints / parameters	11979 / 1 / 603	
Goodness-of-fit on F^2	1.353	
Final R indices [I>2sigma(I)]	R1 = 0.0448, wR2 = 0.1021	
R indices (all data)	R1 = 0.0746, wR2 = 0.1126	
Absolute structure parameter	0.298(17)	
Extinction coefficient	0.00029(8)	
Largest diff. peak and hole	0.533 and -0.696 $e.Å^{-3}$	

Table S3.11: Selected bond lengths of [$Cu_4(SC_6F_5)_4(dbfdp)_2$] ***(3.5)***

Bond Length	Å	Bond Length	Å
Cu(1)-P(1A)	2.2379(19)	P(1A)-C(14A)	1.823(7)
Cu(1)-S(20A)	2.2491(19)	P(1A)-C(8A)	1.823(6)
Cu(1)-P(3C)	2.2908(19)	C(1A)-C(2A)	1.386(9)
P(1A)-C(1A)	1.819(6)	C(1A)-C(6A)	1.393(9)

Table S3.12: Selected bond angles of [$Cu_4(SC_6F_5)_4(dbfdp)_2$] ***(3.5)***

Bond angle	(°)	Bond angle	(°)
P(1A)-Cu(1)-S(20A)	131.78(8)	C(14A)-P(1A)-C(8A)	104.1(3)
P(1A)-Cu(1)-P(3C)	118.58(6)	C(1A)-P(1A)-Cu(1)	113.3(2)
S(20A)-Cu(1)-P(3C)	109.57(7)	C(14A)-P(1A)-Cu(1)	113.2(2)
C(1A)-P(1A)-C(14A)	104.0(3)	C(8A)-P(1A)-Cu(1)	119.2(2)
C(1A)-P(1A)-C(8A)	101.4(3)	C(2A)-C(1A)-C(6A)	114.8(6)

Appendix 3.3: Additional Emission Spectra for Chapter 3

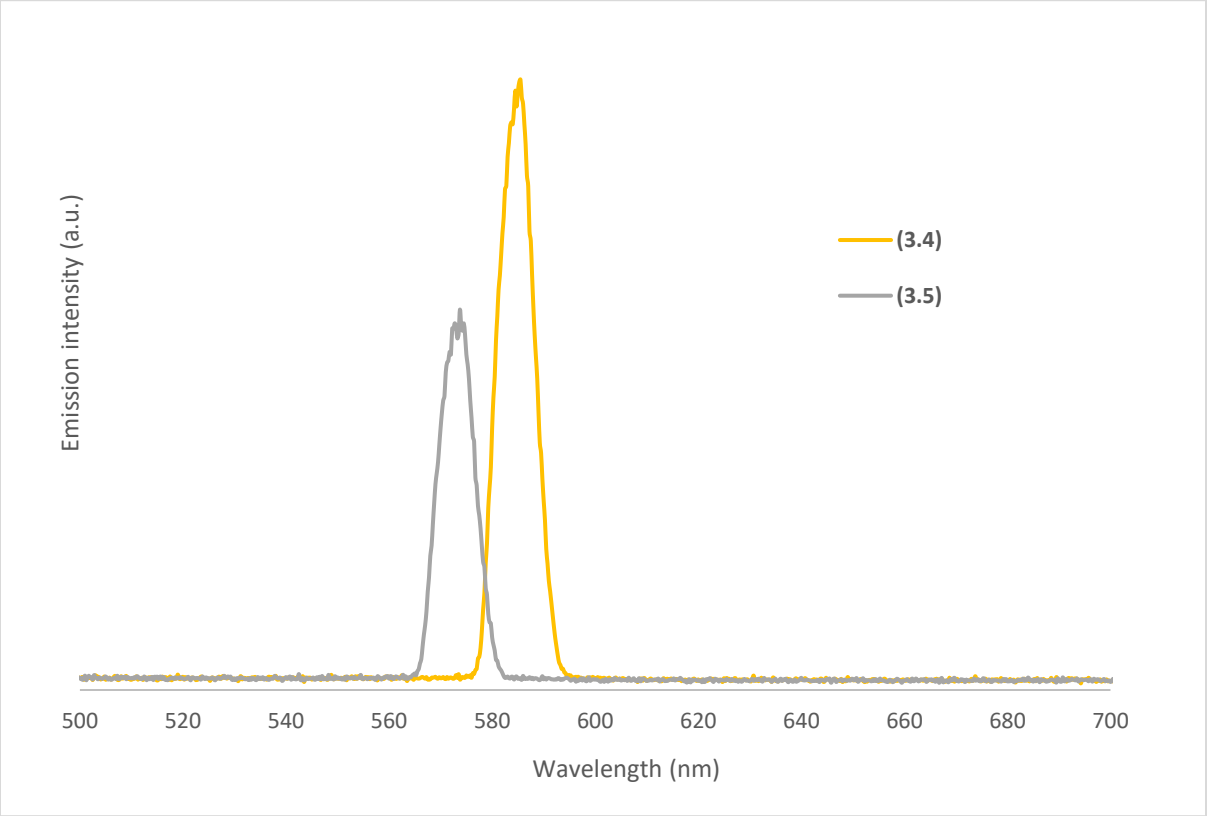

*Figure S3.9: Emission spectra of **(3.4)** and **(3.5)** in the solid state at room temperature. (λ_{exc} = 293 nm **(3.4)**, λ_{exc} = 287 nm **(3.5)**). The maxima at 586 nm for **(3.4)** and at 574 nm **(3.5)** is attributed to an artifact 2 times the excitation wavelength.*

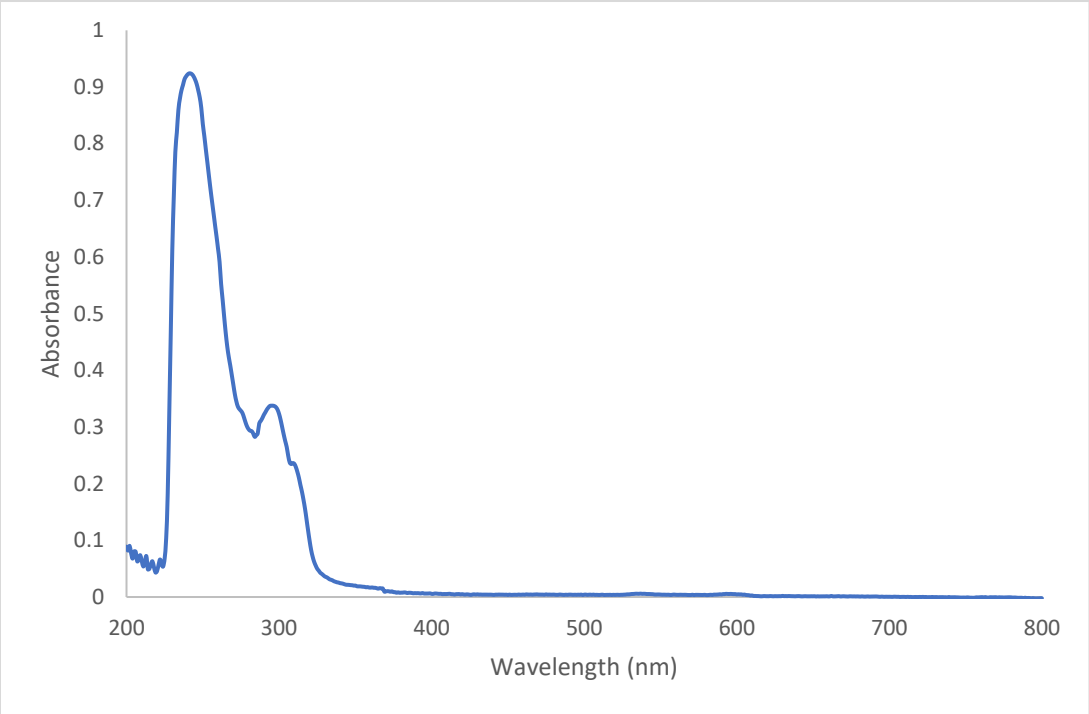

Figure S3.10: Absorption spectra of ***(3.4)*** *from 200 nm to 800 nm.* ***(3.4)*** *has a* λ_{max} *of 242 nm and a local maxima at 293 nm.*

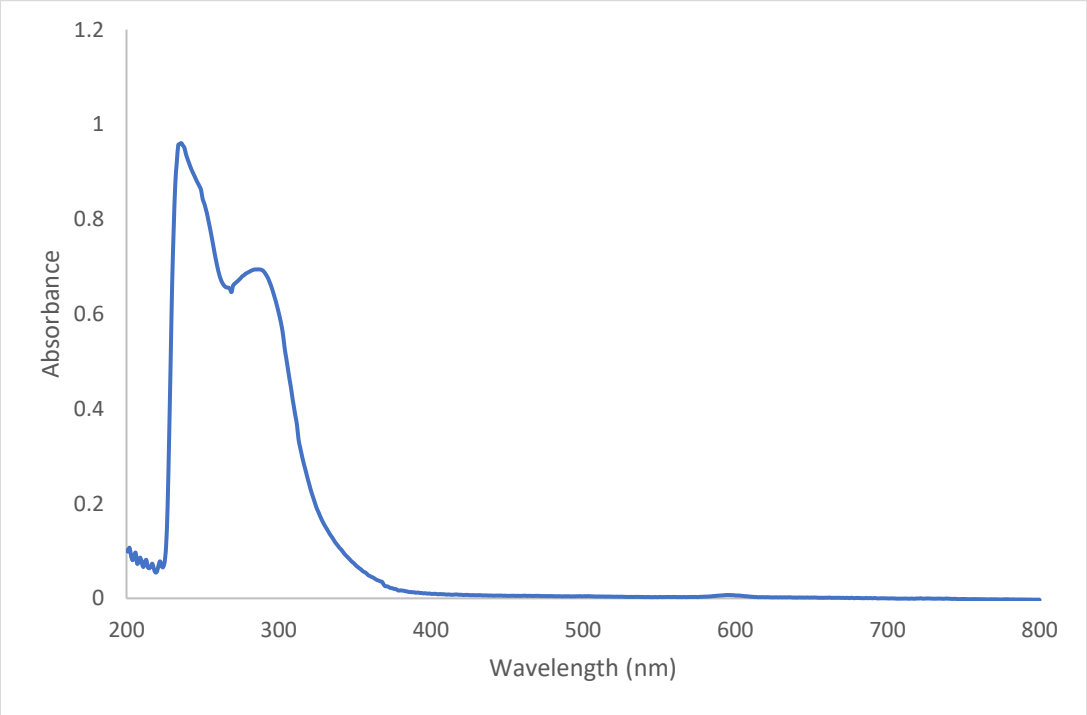

Figure S3.11: Absorption spectra of ***(3.5)*** *from 200 nm to 800 nm.* ***(3.4)*** *has a* λ_{max} *of 236 nm and a local maxima at 287 nm.*

Curriculum Vitae

Kai Yu Jeffrey Li

Education

- M.Sc. The University of Western Ontario (Sept 2021 – present), "Luminescent Gold Chalcogenide/Chalcogenolate Clusters", supervised by Dr. John F. Corrigan
    - Courses taken:
        - CHEM 9621A (Methods of Inorganic Chemistry)
        - CHEM 9541B (Crystallography I)
- Honours B.Sc. The University of Western Ontario (Sept 2016 – April 2021), Honours Specialization in Chemistry

Publications and Presentations

- Canadian Chemistry Conference and Exhibition 2023 (In Person, June 2023): "Luminescent Group (I) Chalcogenide and Chalcogenolate Clusters" (poster)
- 53rd Annual Inorganic Discussion Weekend (In Person, November 2022): "Luminescent Gold (I) Chalcogen Clusters" (presentation)
- 49th Southern Ontario Undergraduate Student Chemistry Conference (Virtual, March 2021): "Ligand Controlled Luminescence in Silver and Gold-Chalcogenide Clusters" (presentation)

Certifications

- WHMIS, The University of Western Ontario, Jan 2022
- Laboratory Safety and Waste Management, The University of Western Ontario, Sept 2020
- Worker Health and Safety Awareness, The University of Western Ontario, Sept 2020

Teaching Experience

- Teaching Mentor: Supervised and taught laboratory techniques to one 4491E student (fall 2021)
- Teaching Assistant: Instructed and supervised second year chemistry student laboratories (fall 2021 – winter 2023)

Laboratory Skills

- Organic and inorganic synthetic skills: Schlenk techniques, glove box, titration, TLC, flash column chromatography, distillation under inert conditions and crystallization
- Analysis and characterization skills: NMR Spectroscopy, ATR-IR Spectroscopy, UV – Vis Spectroscopy (also solid-state UV – Vis), Mass Spectrometry, Atomic Absorption Spectroscopy, Emission and Excitation Spectrofluorometry
- Proficient in Chem Draw and Mestre Nova